SEISMIC POUNDING OF ADJACENT MULTIPLE-STOREY BUILDINGS CONSIDERING SOIL-STRUCTURE INTERACTION AND THROUGH-SOIL COUPLING

A Thesis
Submitted in Partial Fulfilment
of
the Requirements for the Degree
of
Doctor of Philosophy in Civil Engineering
at the
University of Canterbury
Christchurch
NEW ZEALAND

by

Amar Mahmood Rahman

1999

DEDICATION

No words can express the gratitude I feel towards my parents and my brother for the support, encouragement and motivation with which they have provided me. I will remain forever indebted to them for the sacrifices they have made.

During the course of this project I have faced many personal challenges and difficulties. I would like to thank my wife, Susanne, who supported, advised and encouraged me during this trying time. Her love, patience and strength were inspirational.

To them I dedicate this work.

ABSTRACT

Structural pounding may be defined as the collisions occurring between adjacent dynamically excited structures which lack a sufficient separation gap between them. Extensive theoretical and experimental studies have been conducted to investigate this phenomenon. However, the majority, if not all, of these studies fail to consider the flexibility of the soil upon which these structures are constructed. This study aims to investigate the degree of approximation inherent in previous pounding studies which neglected this important feature. In this study, two aspects of soil flexibility effects on dynamic structural response were investigated: the influence of the supporting soil properties on the individual structures (soil-structure interaction) and the through-soil interaction between the foundations of the adjacent structures.

Two structural configurations of reinforced concrete moment-resistant frames were considered: the case of two adjacent twelve-storey frames and the pounding of a twelve- and six-storey frames. Four cases of external excitation were investigated: two actual earthquake records applied from two directions each. A nonlinear inelastic dynamic analysis software package developed at the University of Canterbury has been utilized in this study. Suitable numerical models were developed for the through-soil interaction phenomenon and for the structures, which were designed in accordance to the relevant New Zealand design codes. Soil-structure interaction was represented by means of existing models available in the literature. Various separation gaps were provided and the results were compared with the no pounding case. Storey-level impacts only were considered. The pounding response in which soil flexibility was accounted for was compared to the fixed base response for each of the separation gaps incorporated in this study.

A high variation in the results was witnessed, indicating the significance of consideration of soil flexibility effects. In addition, the importance of excitation direction was highlighted in this study. The relative storey accelerations were more dependent on the characteristics of the excitation rather than on the magnitudes of the impact forces. Recommendations were proposed which aim towards the generalization of the results of this study.

ACKNOWLEDGEMENT

The research presented in this thesis was conducted at the Department of Civil Engineering, University of Canterbury, Christchurch, New Zealand, under the supervision of Dr. Athol James Carr (Reader) and Associate Professor Peter James Moss. I extend my heartfelt gratitude to the Department for its support and encouragement.

I am extremely indebted to my supervisors, Dr. Athol J. Carr and Dr. Peter J. Moss, for their support, patience and assistance, without which this project would not have been completed.

The assistance of the New Zealand Society for Earthquake Engineering provided moral and financial incentive in completing this work and is gratefully acknowledged. In addition, a Royal Society of New Zealand grant assisted the author in presenting this project at the 2nd Asia-Pacific Conference on Shock and Impact Loads on Structures (Melbourne, 1997).

I also wish to thank the staff, academic and secretarial, of the Department for their assistance, in particular Professor Emeritus T. Paulay, Dr. K. McMannus, Dr. J. Restrepo and Mr. D. Bull for their technical advice, unlimited support and cheerfulness. The kind assistance and helpful comments of Professor D.L. Karabalis of the Department of Civil Engineering, University of Patras, Greece, are also gratefully acknowledged. I would like to thank the Civil Engineering technical staff, Messrs. B. Hutchinson and P. Coursey, for their assistance. I also wish to thank the staff of the Engineering Library at the University of Canterbury, whose patience and assistance knew no bounds.

Finally, I wish to thank my fellow post-graduate students who have made easier the many difficult times I have gone through in the process of completing this work, particularly: Dr. F.J. Crisafulli, Dr. Widodo, Miss Erica Dalziell, Mr. E. Christoforou, Mr. I. Satyarno and Mr. J. Zhang.

TABLE OF CONTENTS

1. INTRODUCTION

Even though structural pounding was recognized as early as 1926 in what may be considered to be the first text on aseismic design and construction [F5], it was not until the Mexico City Earthquake of 1985 that the damage potential of structural pounding came to be fully appreciated. This was due to the large number of buildings in which structural pounding was identified as the main cause of serious damage and/or collapse [B3]. Despite the recommendation of minimum separation gaps in the relevant codes in force at the time, these provisions were seldom implemented for various reasons, technical and non-technical. The Mexico City event spurred the engineering community into conducting extensive research to further understand this phenomenon from all its aspects. As a result, many studies pertaining to structural pounding have been conducted over the past 25 years. These investigations covered case studies of structural pounding which had occurred during seismic events [B3,G7,H1,K3,K4,M8,N4,T1,W1] and the analytical investigation of these cases [K5,M1], analytical studies pertaining to the impact problem [D1,J4,J5,L13], experimental studies [F3,P3] and the development of pounding mitigation methods [F1,J2,K6].

Many simplifying assumptions were applied in the formulation and development of analytical and numerical solutions in these studies. The most significant assumptions pertaining to the foundation conditions are the following:

- A rigid base connection between the impacting structures and the foundation soils upon which they rest.
- The absence of through-soil interaction between these structures.

The former assumption implies a very stiff foundation soil. This may be true in the case of low structure mass to soil stiffness ratio but is not valid for cases of heavy structures constructed on soft soils. Besides changing the characteristics of the impinging seismic waves, the dynamic properties and consequently the response of the vibrating systems will be affected. The latter assumption implies the complete isolation of the oscillating structures from the soil environment in which they are constructed. Obviously this is a gross simplification as there is a significant degree of interaction between adjacent structures at foundation level due to the effects of the outward-propagating waves. These waves alter the properties of the soil between the

adjacent foundations in addition to transmitting a portion of the energy that is not dissipated in the soil medium. The extent of this effect is influenced by the soil properties, foundation dimensions, the predominant modes of response of the adjacent structures, the characteristics of the excitation, in addition to other factors.

Even though the effects of structural pounding, soil-structure interaction and through-soil coupling (or structure-soil-structure interaction as it is also known) on structural response have been investigated separately, the only pounding study which considers soil-structure interaction is that by Schmid and Chouw [S2]. Their investigation, however, did not account for the effects of through-soil coupling.

It is the purpose of this study to investigate the combined effects of soil flexibility on the dynamic response of adjacent structures subjected to storey-level pounding. Inelastic time-history analyses are conducted for various cases of excitation and structural configurations. RUAUMOKO [C1], a software package developed at the University of Canterbury, is utilized in this study. A through-soil foundation coupling model has been developed and incorporated into RUAUMOKO for the purposes of this study. Two structural configurations were considered: the first involving two twelve-storey structures, while the second consists of a twelve- and a six-storey building. All structures are reinforced concrete moment-resistant frames designed in accordance with the relevant New Zealand codes [N5,N6]. Details of these frames, in addition to the assumptions implemented in the numerical modelling, are presented in Chapter 5. The first fifteen seconds of two different earthquake records were incorporated as the excitations: the N-S component of the 1940 El Centro earthquake (peak ground acceleration PGA=0.348g) and the S-14^0-W component of the 1971 Pacoima Dam earthquake (PGA=1.23g). In addition to the fifteen second excitation, a free-vibration phase of five second duration was allowed at the termination of the seismic excitation. The effect of excitation from different directions was also investigated.

Each of the following three chapters discusses various aspects of one of the phenomena presented above, i.e. structural pounding (Chapter 2), soil-structure interaction (Chapter 3) and through-soil coupling (Chapter 4). The parameter studies that have been conducted to investigate the sensitivity of the various assumptions incorporated in the numerical modelling are presented in Chapter 5 and Appendix A. In addition, the results of the simulations involving the above configurations and excitations and the discussions thereof are presented in the same chapter. Additional results pertaining to the response of each of the frames and the influence of various factors on the impact forces are presented in Appendices B-E. The details of the

structural models incorporated in this study are outlined in Appendix F while Appendix G presents analytical verification of the through-soil interaction model developed herein.

2. STRUCTURAL POUNDING

2.1 Introduction

The burgeoning urban population witnessed by many countries in recent years has prompted owners and developers towards the optimal utilization of available property. This, in addition to the rapidly increasing value of real-estate, has led to an increase not only in the overall heights (number of stories) of buildings but also in their floor areas. Many modern multi-storey buildings are now constructed up to their property lines with limited, and in some cases no, separation between adjacent structures. These trends may also be observed in many older buildings which, due to settlement, accumulation of debris over the years, or construction methods prevalent at the time, are in direct contact with neighbouring structures.

The difference in dynamic properties of adjacent structures, vis-a-vis mass, stiffness and strength, besides differing foundation properties, result in an out-of-phase oscillation of the vibrating systems. This out-of-phase motion may result in the collision of the adjacent structures if sufficient separation is not provided. Valles and Reinhorn [V1] have suggested the following six parameters that affect the pounding response of adjacent structures: characteristics of earthquake excitation, fundamental periods of structures, damping and hysteretic characteristics, mass of colliding elements, the actual gap as a fraction of critical separation gap (calculated by means of a method developed by the authors) and the inelastic behaviour at the impact interface.

Structural pounding may occur in parts of the same building such as at expansion or construction joints [M8, T1, and W1] or between nonstructural and structural components [H1]. Pedestrian bridges may also pose a potential pounding risk as they may collide against the structures that they connect as was witnessed during the Hyogo-ken-Nanbu (Kobe) earthquake of 1995 [N4].

Substantial damage due to pounding may be sustained by adjacent buildings of differing storey heights. In this case, the column of one building may experience repeated impacts along its height from the slab of the adjacent building. This will result in local damage and may even lead to partial collapse of the storey [G7]. The high-amplitude local acceleration induced by pounding has been found to cause extensive damage of appurtenances at the level of pounding [K2].

Storey-level pounding between adjacent multi-storey structures only will be examined in this study. Some important aspects of the structural pounding phenomenon, as well as research conducted in this field, will be elaborated upon in some detail in this chapter. This will hopefully elucidate the reasons for the growing realization within the engineering community of the significance of structural pounding.

2.2 Historical Preview

Many cases of structural pounding witnessed subsequent to major seismic events in recent times have been described in the literature. The extent of damage resulting from structural pounding varied in the incidents reported from cosmetic or light [M1,B2] to severe [N2,H1] and in some cases ensued in total collapse [B3,G7].

Ford [F5] alluded to structural pounding in what is considered to be the first text devoted to the design of earthquake resistant structures. His recommendations related to pounding between non-structural components and the structural elements of a building.

To illustrate the damage potential of structural pounding, a brief synopsis of pounding cases reported from previous earthquakes is presented below.

- Pounding sustained by three collapsed stairways of the Olive View Hospital against the main building during the 1971 San Fernando Earthquake [B2]. The extent of damage due to structural pounding varied in severity in the three staircases but was not the main cause of failure. Pounding was in evidence in the fourth, uncollapsed, staircase as well. The main building also sustained some pounding damage as a result of impacting against an adjacent retaining wall and a warehouse due to insufficient seismic gaps.
- The May 1976 Friuli Earthquake in Italy in which a tall prefabricated storage shed pounded against a single storey brick annex at the mid-height of the shed [G7]. The annex collapsed completely due to shear failure in the columns while the shed was almost undamaged except for some indentations in the exterior panelling. This was due to the damping provided by the joint material between the exterior panels covering the frames of the prefabricated shed.
- Significant damage at the construction joint between the main part of a hotel and its entrance annex during the March 1977 Romanian Earthquake [T1].
- The Mexico City Earthquake of September 1985 provided the stimulus for research into structural pounding. This was due to the extensive damage

sustained by a large number of buildings as a direct cause of structural pounding. Pounding occurred in over 40% of the 330 buildings which had collapsed or sustained severe damage and was identified as the primary cause of collapse in at least 15% [B3].

- Pounding of the deck of the cable-stayed Shipshaw Bridge, spanning the Saguenay River in Quebec, against both its abutments as a result of longitudinal motion during the 1988 Saguenay earthquake [F2]. Cracking of the concrete cover of the abutments, local buckling of the deck's horizontal bracing members and complete failure of one of four anchorage plates connecting the deck to one abutment resulted directly from the repeated collisions.
- Significant damage due to pounding was identified in buildings 90km distant from the epicenter of the 1989 Loma Prieta earthquake (M_L=7.1) [K4]. Had the epicenter been closer the extent of pounding-related damage would most certainly have been more pronounced.
- Malhotra et al. [M8] reported the presence of spikes in the strong-motion acceleration records mounted on a box-bridge girder bridge during the 1992 Big Bear and Landers earthquakes in California. One of the three mechanisms they identified as the cause for these spikes was pounding between the bridge segments at the expansion joints.
- High-frequency spikes were detected in the accelerograms of a base-isolated building after the 1994 Northridge earthquake [M14]. The cause was determined to be the impact of the structure against its stops after the lateral seismically-induced displacements had exceeded the separation gap provided.
- The horizontal displacement of a base-isolated structure, exceeding the provided isolation gap, resulted in pounding of the building against its stops during the 1994 Northridge earthquake [T3].

Other notable events where cases of pounding were reported are the Alaska 1964 [N2], the Venezuela 1967 [H1], the Philippine 1976 [E1], the Miyagi-ken-Oki 1978 [E2], and the 1981 Central Greece [E3] earthquakes, to name but a few.

2.3 Effects of Pounding

Impacts due to structural pounding transmit short duration, high amplitude forces to the impacting structures and may occur at any level of the colliding structures and at any location along the impacting levels (in the case of slab-column impacts). The detrimental effects of these forces may be enumerated as follows:

- High-amplitude, short duration local accelerations which are generally not accounted for in design [F1].
- Localized degradation of stiffness, and/or strength in impacting members. In addition to the adverse effects this will entail on the strength of the members, the distribution of shear and flexural forces will also be affected. Since the code design of earthquake resistant structures is based upon the capacity design method [P4], this is an especially significant factor that must be accounted for when assuming plastic hinge locations.
- Modification to the overall dynamic response of structures. Either an amplification or de-amplification of response will be sustained by structures, depending on the relative dynamic characteristics of the impacting structures on one hand and the supporting medium on the other, in addition to the characteristics of the seismic excitation. Modes of response not accounted for in design may be introduced, for example torsion [L6].

Cases have been reported where pounding has had a beneficial effect. Pounding was believed to have altered the direction of collapse of one of the staircases of the Olive View Hospital away from the main building during the San Fernando earthquake [B2]. Also, contact of the main building with the adjacent structures supported the soft-storey that formed at the level of contact [M1].

2.4 Structural Pounding Studies

Extensive analytical, numerical and experimental studies have been conducted to shed light on the pounding phenomenon. Various aspects of pounding have been investigated, such as the vibro-impact problem, the dynamics of pounding and of contact of the impacting bodies and numerical solutions to the impacting of oscillating single-degree-of-freedom (SDOF) and multi-degree-of-freedom (MDOF) systems.

2.4.1 Analytical Studies of Pounding as a Vibro-Impact Problem

An analytical study of the nonlinear contact problem was conducted by Jing and Young [J4]. A closed-form solution of the impact of a SDOF system subjected to white-noise excitation against an elastic constraint with Hertzian force-displacement characteristics was effected. The influences of clearance size and contact stiffness were investigated. It was found that the variations in the response decreased with increasing separation gap. In addition, if the separation exceeded twice the root of the mean square response of the corresponding linear system, the effects of pounding may be ignored. Also, the frequency of response changed with separation gap and contact stiffness. It is worth noting that this study [J4] is an extension of the study by Jing and Sheu [J5], who were the first to obtain the closed-form solution of impacting SDOF systems with Hertzian contact law subjected to white noise excitation.

Davis [D1] investigated the impact of a damped SDOF oscillator against, both, a moving and a stationary barrier. The excitation was in the form of a constant acceleration amplitude for the former case and a constant displacement amplitude (the displacement of the barrier was equal to the ground motion) for the latter. This is representative of the upper- and lower-bound cases of a flexible long-period structure and a stiff short-period one, respectively. Two forms of impact models were implemented: a nonlinearly elastic Hertzian model, and an inelastic coefficient-of-restitution model. The solution was presented in the form of a response spectra between the impact velocity of the SDOF oscillator and the excitation period. The influence of separation distance was also examined. The following observations were noted in this study:

- The maximum impact velocity of an elastic structure was attained at a period of excitation equal to one-half the natural period of an equivalent non-impacting oscillator. This implies that the natural period of the colliding oscillator reduces to half of its value in the no-pounding case.
- Cut-off frequencies were identified below which continuous impacts do not occur, providing some insight as to the required separation gap.

2.4.2 Multiple-Sided Pounding of SDOF Systems

One- and two-sided impacts of damped SDOF systems was investigated by Wolf et al. [W5]. Impacts were modelled by a linearly elastic spring in parallel with a dashpot. It was found that the response of a very flexible oscillator increases as a result of pounding, while for a stiff structure slight decreases may be detected. Due to the restriction of impacts within a small area, high frequency modes are excited.

Amplifications in the displacement response spectrum for the zero separation gap case were found to be dependent on the stiffness of the contact element and the ratio of frequency of excitation to the natural frequency of the structure.

The effects of one- and two-sided pounding of structures modelled as SDOF oscillators was also investigated by Anagnostopoulos [A1] and Athanassiadou et al. [A5]. In the former study, a series of buildings, modelled as SDOF damped oscillators with bilinear force-displacement characteristics, were excited by scaled earthquake records. Impacts were simulated by means of viscoelastic contact elements, the stiffness of which was assigned a value equal to twenty times the stiffness of the stiffer SDOF system in the colliding pair. The damping coefficient was related to the coefficient of restitution. Parameter studies revealed the insensitivity of the system displacement response to impact element properties.

It was observed that the displacements of the exterior structures may be appreciably amplified, while interior structures may experience either amplification or deamplification, depending on the ratio of natural periods. In addition, it was shown that elastic and inelastic structures behaved similarly when subjected to pounding, with more serious repercussions, however, on the latter. In addition, no clear dependence was determined between yield level and response amplification due to pounding. One of the important factors on the pounding response was the mass ratio of the adjacent oscillators. The system with the smaller mass exhibited larger increases.

The aforementioned study by Athanassiadou et al. [A5] developed the previous study of Anagnostopoulos [A1} by including travelling wave effects. Inelastic force-displacement behaviour of the SDOF oscillators was represented by the modified Clough hysteresis model. A phase lag in the excitation of each successive SDOF oscillator was applied based on the average velocity of seismic wave propagation and the distance of the structures from each other. Impacts were modelled by means of a coefficient of restitution. In addition to the corroboration of the findings of the previous study [A1], the following observations were also noted:

- The effects of pounding increase with the relatively large increase of the phase difference in the starting time of the excitation between the first and last buildings in the row.
- For the case of adjacent structures of differing natural periods, pounding adversely affects the rigid buildings, especially when located at the end of the row.

- When the difference in periods of adjacent structures is mainly due to differences in stiffness rather than mass, then pounding response is insensitive to the strength, coefficient of restitution of impact elements and relative mass of impacting structures.

2.4.3 Pounding of MDOF Systems

The preceding studies pertaining to pounding of SDOF, while providing valuable insight on the overall pounding response, do not assist in the clear understanding of the response of impacting MDOF systems and the ensuing effects on structural elements.

Extensive numerical and analytical studies have been conducted on MDOF systems recently due to advances in computer technology and numerical solution methods.

The pounding of a flexible15-storey steel moment-resistant frame and an adjacent rigid 8-storey structure was investigated by Maison and Kasai [M3]. Limitations to the numerical models include the assumption of in-plane rigid diaphragms and single point pounding (at the top level of the shorter building). The impact element stiffness was based on the in-plane axial stiffness of the concrete floor system. Excitations were in the form of actual earthquake records, in addition to a snap-back free-vibration analysis. It was found that neglect of pounding would result in the unconservative design of the structural elements, especially in the stories above the pounding level. This was attributed to the marked increase in storey drifts, shears and overturning moments. Reflections of the impact forces propagating from the level of impact to the fixed base resulted in large shear gradients towards the building base. It was postulated that these gradients are due to the shear wave reflections at the base which augment the incident shear waves. The results of a snap-back analysis provided an indication of the general response trends due to a seismic excitation. The trends exhibited by the pounding structures in this study are exclusive to structural configurations similar to those of the study and caution was advised in extrapolating the results to other situations.

The pounding response of two flexible buildings was also examined by Maison and Kasai [M6] as a development on their previous study. The same configuration was implemented as in the previous study [M3] and actual and artificial earthquake records were the assumed excitations. The adverse effects of pounding were found to increase in the building with the lesser mass. Building mid-height pounding results in an increase in storey response envelopes over the entire building height. On the other hand, top level pounding may result in a decrease of the response envelopes, except

for the storeys in the vicinity of impacts. The observations noted in the previous study applied in this case also.

Anagnostopoulos et al. [A2] investigated the pounding of buildings in series modelled as lumped-mass shear beam type MDOF inelastic (bilinear) systems excited by actual earthquake records. Soil-structure interaction was accounted for through the implementation of a spring-dashpot system at the base of the structures. Impacts were simulated by viscoelastic elements located along the heights of the structures. The insensitivity of the response to the properties of the impact elements, observed in the aforementioned studies, was confirmed. The impact element stiffnesses were such that the local periods of the mass-impact springs were below the lowest translational periods of the adjacent buildings. Various configurations of three buildings were considered, with respect to fundamental natural periods. It was observed that the effect of pounding on the response of a structure is a function of the mass and period ratio with respect to the adjacent building(s). When the masses of the adjacent buildings are similar, pounding amplified the response of the stiffer building. This amplification increased with decreasing period ratio and with increasing stiffness of the building under consideration. For buildings with large differences in mass ratios, pounding results in high overstresses in the building with the smaller mass.

Nonlinear time-history analyses of various configurations of impacting steel buildings (3- and 8-storey) were investigated by Filiatrault et al. [F2]. Storey-to-storey, as well as storey-to-column, pounding was investigated under various actual and artificial excitations with Hertzian contact elements located at potential impact nodes. Code-specified recommendations with respect to required separation gap were found to be excessive. An alternative formulation was proposed, similar to Eq. 2.2, which would provide a realistic separation gap. It was observed that the time between successive impacts corresponds to about one-half the mean period of the buildings. Therefore, provision of even a small gap would substantially reduce the number of impacts, as was also recommended by Athanassiadou et al. [A5]. The detrimental repercussions of floor-to-column pounding were highlighted in this study.

The study by Schmid and Chouw [S2] was the only study which considered the direct effects of soil-structure interaction on the response of pounding structures in some detail. The structures (which were of unequal total heights) were modelled as beam elements with distributed mass and a Laplace transform was applied to the relevant equations of motion. The continuous half-space representing the soil was modelled by

a boundary-element mesh. A semi-analytical method was adopted in formulating and solving the equations of motion.

The following assumptions were applied in this study:

- Contact was predetermined at the top level of the shorter building.
- Surface foundations.
- The soil was a continuous half-space with no material damping.

Despite the above simplifying assumptions it was found that inclusion of soil-structure interaction effects had a profound influence on post-impact behaviour which cannot be extrapolated from a fixed-base analysis.

Investigations into other aspects of pounding response, such as P-Δ effects [L12] and eccentric pounding [L5-L7], have also been conducted.

2.4.4 Experimental Pounding Studies

The validation of analytical and numerical studies through experimental investigations has been carried out by a number of researchers. A shake-table pounding test of adjacent eight- and three-storey steel frames was conducted by Filiatrault et al. [F3]. In addition to floor-to-floor contacts, impacting of slabs with columns was also investigated. An excitation equal to 0.15 g of the 1940 El Centro event was implemented. Floor-to-floor pounding verified earlier analytical studies [K2] with respect to the effect of pounding on peak floor accelerations, namely, the insensitivity of these accelerations to the initial separation gap magnitudes. In addition, peak floor accelerations fluctuated dramatically (rapid increase followed by a rapid decrease) at pounding level in the tall building. It was also found that the maximum impact force was independent of the initial separation gap. This distance, however, had a major influence on the number of impacts recorded.

Suitable models for implementation into existing computer software were prepared and calibrated with results obtained from quasi-static tests on the structures. Unlike earlier software, the non-linear time-history analysis software used in this study (PC-ANSR [M7]) allowed the modelling of impact at all levels and not only at roof level of the shorter building. Conventional uni-axial contact elements were not able to accurately represent the relative rotations occurring at the contact points. In the selection of suitable damping ratios for the contact elements implemented in the PC-ANSR software, it was found that the assumption of negligible damping resulted in values comparable to those obtained experimentally. However, the authors advised against extrapolating these results to other pounding cases.

The experimental results of the above investigation were utilized to compare the performance of a number of existing dynamic structural analysis software [C6]. RUAUMOKO [C1] displayed the most favourable execution time. In addition, the results compared well with those obtained experimentally.

Papadrakakis et al. [P3] compared the experimental results of the pounding of two concrete two-storey frames with a numerical study that modelled the impacts based on a Lagrange multiplier approach [P2]. Storey level impacts only were considered and two forms of excitations were used: sinusoidal and random acceleration.

- Pounding had a beneficial effect on the flexible structure (and on the system as a whole) as was noted from the reduction in the input energy demand. However, the increase in separation distance due to local pounding-induced damage reduced this beneficial effect.
- For the stiff structure, pounding amplified the input energy when the system was subjected to an excitation close to the resonance of the flexible building. This increase was also noted when compared with the energy developed during the resonance of the stiffer building. The extent of amplification is dependent on the characteristics of the ground motion.
- It was shown that the large accelerations occurring due to pounding at a particular level do not affect the corresponding accelerations at adjacent levels. These accelerations have a significant effect on equipment and appurtenances at the level of pounding and do not influence the total displacements in the structure. This is due to the short duration of the impulsive forces induced by pounding and the resistance of the slab inertia.
- The above observations were corroborated by the results of an analytical pounding study of adjacent 5-storey reinforced concrete buildings. It was concluded that increasing the flexibility of the stiff structure would be more beneficial than increasing the stiffness of the flexible structure.

2.5 Prevention of Structural Pounding

2.5.1 Code Provisions

A number of codes have recognized the latent threat of structural pounding and have attempted to mitigate this threat. None, however, outline a suitable method to quantify pounding effects. Although many pounding mitigation techniques have been proposed (such as link elements, dampers, etc.), most codes recommend a minimum separation

distance to be provided between adjacent buildings or between the building of interest and its property line. These requirements, however, are not strictly enforced by the authorities nor is their implementation adhered to by developers or the engineering community at large. The reasons for this noncompliance may be enumerated as follows:

- The late inception of such requirements in some codes as the potential hazard and repercussions of pounding has only recently been recognized.
- Developers and contractors have exhibited a reticence in the application of these requirements due to economic considerations and other non-technical factors.
- The implementation of minimum separation gap requirements may result in impracticably wide expansion joints between units of the same building [J1].
- Unfamiliarity with the properties of the adjacent structures (most often owned by another party), hindering the development of accurate numerical models for implementation in dynamic time-history analyses.

Code equations defining the recommended minimum separation gap often ignore the changes in the dynamic properties of the vibrating systems (e.g. stiffness, damping, etc.) resulting from the large inelastic deformations which may be required of these systems. Code requirements pertaining to maximum allowable interstorey drifts are imposed to limit excessive ductility demands on the members and not with the prevention of structural pounding in mind. The only parameters which are accounted for in code separation gap equations are the maximum elastic displacements attained in the top stories of the adjacent structures due to the code seismic design forces [N3,N5,U1]. Some codes consider building height as well as a "response reduction factor", also known as a "behaviour factor" [E7], in addition to elastic displacements. As a result of the above, design code recommendations pertaining to separation gap requirements tend to be unrealistically excessive, further discouraging the implementation of code requirements. Valles et al. [V1] present a comprehensive review of the separation gap requirements from various building codes, in addition to other pounding mitigation techniques.

Section 2.5.4.2 of the 1992 New Zealand Loadings Code [N5] requires the separation distance between adjacent structures to be equal to the sum of their maximum design lateral displacements for the ultimate limit state (implying inelastic displacements).

One suggestion [A2] has been to impose limitations other than separation gaps between buildings, such as special detailing and placing of impact absorbing elements

at locations where pounding is expected to occur (as recommended in the Greek code).

Though these code-specified requirements may provide some degree of protection against potential structural pounding there remains the possibility of the occurrence of an event exceeding the "design level" earthquake. In this case, the resulting damage would undoubtedly exceed that expected from the code-specified levels of excitation.

The present study aims to determine the effects of pounding on specific structural configurations and no attempt is made to determine the critical separation gap. Nevertheless, a synopsis is presented below of the relevant studies pertaining to separation gap requirements and other pounding mitigation techniques.

2.5.2 Equations Defining the Minimum Separation Gap

One method employed in the determination of the required separation gap to preclude pounding is by means of a dynamic time-history analysis and the calculation of the relative displacements at levels of potential pounding. However, as this is a costly exercise, a number of researchers have suggested various equations to calculate minimum seismic separation requirements.

The derivation of the critical separation gap by Lin [L10] simulated the dynamics of the pounding problem as a stochastic process. The mean and standard deviation of the required separation distance was derived based on the assumption of low damped linear systems excited by a white-noise type excitation. The main requirement of this method is that the modal frequencies of the buildings are well separated. This is difficult to guarantee if soil-structure interaction is considered.

Other methods of determination of critical separation gap are based on the cross-correlation coefficient ρ_{AB} defined by Der Kiureghian [D2]:

$$\rho_{AB} = \frac{8\xi^2\left(1+T_B/T_A\right)\left(T_B/T_A\right)^{3/2}}{\left\{1-\left(T_B/T_A\right)^2\right\}^2 + 4\xi^2\left(1+\left(T_B/T_A\right)^2\right)\left(T_B/T_A\right)} \qquad (2.1)$$

where T_A, and T_B are the fundamental natural periods of buildings A and B, and ξ is the (equal) critical damping ratio for both buildings.

Jeng et al. [J2] developed the double difference combination (DDC) method to account for the phase difference of vibration between the adjacent structures by means of the above coefficient (Eq. 2.1). The relative displacement between adjacent linear elastic

MDOF systems with similar critical damping ratios and approximated by the fundamental mode of vibration was defined as:

$$u_{rel}(DDC) = \sqrt{u_A^2 + u_B^2 - 2\rho_{AB} u_A u_B} \qquad (2.2)$$

where u_A , u_B are the maximum elastic displacements at the levels where pounding is expected to occur.

The authors, recognizing the effect of inelastic behaviour of the structures on separation gap requirements, suggested modifying Eq. 2.2 to account for the expected variations in dynamic properties [K6]. This was partly accomplished by deriving the displacements u_A *and* u_B from an inelastic response spectrum. Further modifications entailed the redefinition of the cross-correlation factor ρ_{AB} (Eq. 2.1) to account for the variation in dynamic characteristics (natural periods and damping ratios). The latter was achieved through the definition of an elastic system, equivalent to the inelastic system, which simulated the inelastic phase difference between the two buildings. Expressions for the "effective period" and "effective damping" for this elastic system were statistically derived, based on exhaustive time-history analyses implementing several earthquakes, displacement ductilities, two different hysteresis rules (bilinear and stiffness degrading), vibration periods and building heights.

The proposed expressions for the "effective period" T^* were derived as:

$$T^*/T = 1 + 0.09(\mu - 1) \quad \text{(bilinear model)} \qquad (2.3)$$

$$T^*/T = 1 + 0.18(\mu - 1) \quad \text{(stiffness degrading model)} \qquad (2.4)$$

and for the "effective damping" ξ^* :

$$\xi^* = \xi + 0.084(\mu - 1)^{1.3} \quad \text{(bilinear model)} \qquad (2.5)$$

$$\xi^* = \xi + 0.160(\mu - 1)^{0.9} \quad \text{(degrading stiffness model)} \qquad (2.6)$$

where μ is the displacement ductility and ξ and T are the critical damping and initial natural period, respectively, of the elastic buildings.

The general equation for the cross-correlation factor ρ_{AB} was then formulated with respect to the above expressions for the effective period and effective damping, as follows:

$$\rho_{AB} = \frac{8\sqrt{\xi_A^* \xi_B^*}\left(\xi_B^* + \xi_A^* T_B^*/T_A^*\right)\left(T_B^*/T_A^*\right)^{3/2}}{\left[1-\left(T_B^*/T_A^*\right)^2\right]^2 + 4\xi_A^*\xi_B^*\left[1+\left(T_B^*/T_A^*\right)^2\right]\left(T_B^*/T_A^*\right) + 4\left(\xi_A^{*2} + \xi_B^{*2}\right)\left(T_B^*/T_A^*\right)^2} \tag{2.7}$$

The above expression for the cross-correlation factor was substituted into the spectral difference equation (Eq. 2.2), noting that the displacements u_A *and* u_B are to be obtained from an inelastic response spectrum, as mentioned previously.

The authors proposed a lower bound of spectral relative displacement, $u_{REL}(SPD)$, to account for the effects of biased response [N1,Y1]. This response was observed for buildings modelled as bilinear systems with displacement ductilities of 3 or more and T_B^*/T_A^* in the range of 0.8 to 1.3:

$$u_{rel}(SPD) = \sqrt{u_A^2 + u_B^2 - 2\rho_{AB} u_A u_B} \geq 0.25(u_A + u_B) \tag{2.8}$$

This limitation would also account for the approximations in the estimation of the dynamic properties of the vibrating systems, i.e. displacement ductilities and natural periods.

The proposed method, while providing more realistic estimates of separation distances than the SPD, ABS, and SRSS methods, has the following limitations:

- It does not account for higher mode effects, rendering this method unsuitable for tall buildings or for structures in which soil flexibility influences the response.
- Pounding was assumed to occur only at the upper level of the shorter building. In structures of similar stories, maximum impact forces may be developed at other locations.
- The above method was modified, through the implementation of random vibration theory and modification of Eq. 2.1, to include the effects of the time lag of the ground motion to account for travelling wave effects [J2].

A method proposed by Penzien [P8] also relies on the definition of the cross-correlation coefficient of Eq. 2.1 in developing an expression for the critical separation gap. The CQC [D2] method is employed in the formulation of the relative displacement between two buildings at the top level of the shorter building. For inelastic (bilinear) systems, an equivalent linearized system is derived. Equivalent elastic stiffness and damping ratios are obtained by means of factors which relate the characteristics of the elastic and post-yield behaviour in addition to the excitation.

The effects of travelling waves on the seismic response of buildings in series and on the required separation distance were investigated by Athanassiadou et al. [A5]. A group of four to eight buildings in series and of almost equal height was modelled as damped SDOF oscillators with inelastic force-displacement behaviour represented by the Clough hysteresis rule. The natural periods of these models ranged between values representative of actual low- to medium-rise reinforced concrete buildings (0.15 to 1.2 seconds). The structures were excited by a travelling ground motion with a time-lag corresponding to the assumed wave velocity and separation distances between the structures.

The following equation was proposed to estimate the critical separation gap for adjacent buildings with natural periods within the indicated limits:

$$d = 0.5\sqrt{(q_1 \delta_1)^2 + (q_2 \delta_2)^2} \qquad (2.10)$$

for $0.90\ sec. \leq T_1 \leq 1.50\ sec.$ and $0.45\ sec. \leq T_2 \leq 0.75\ sec.$

where:

d = Separation distance

q_1, q_2 = "Behaviour factor" accounting for inelastic behaviour as per the 1985 CEB Model Code for Seismic Design.

δ_1, δ_2 = Elastic displacements obtained from equivalent static lateral force analysis for each of the adjacent structures *1* and *2*.

T_1 , T_2 = The natural periods of buildings *1* and *2*, respectively.

This study found that variation of the separation gap by even a small amount altered the pounding response considerably.

Valles et al. [V1] developed a graphical method for determination of critical gap width, known as the Pseudo Energy Radius. In this method, the displacement is plotted on the abscissa while the velocity divided by the frequency of the structure is the ordinate. The radius of any point along the plot represents the kinetic plus potential energies, i.e. the instantaneous elastic structural energy. Therefore, the maximum displacement attained by a structure is represented by the longest Pseudo Energy Radius.

2.5.3 Other Methods of Pounding Mitigation

The implementation of the separation gaps recommended by the equations above is restricted to structures that are in the design phase. They are not applicable to existing structures that may be susceptible to pounding. In such cases, alternative

pounding mitigation techniques have been investigated. These include link elements [W3], friction elements [F1], energy dissipation devices [A1] and strengthening of structural elements at expected pounding locations [A2].

The changes in the dynamic characteristics of interconnected linear MDOF systems was analytically investigated by Westermo [W3]. The linkage system consisted of hinged beams located at levels where pounding was expected to occur. The structures analyzed were linear elastic models of equal or differing total and/or storey heights, and natural frequencies. It was found that if coupling resulted in an increase in the natural frequency of the structure, a reduction in shear at low excitation frequencies is to be expected. The presence of the linkage mechanism induced larger deflections in the stiffer of the linked structures, in addition to inducing higher modes of vibration. The forces generated in the link element were of the order of the smaller base shear of the unconnected structures.

The inelastic response of adjacent undamped steel structures connected by friction damped links was numerically investigated by Filiatrault et al. [F1]. The energy dissipation mechanism in these links is initiated when the stiffness of the link element (K_c) is exceeded and slip occurs. The amount of energy dissipated is a function of the slip load P_s along with the slip travel. As the slip travel is constant the dissipated energy is dependent on the slip load. A sensitivity study was conducted to determine the ideal values of these two parameters K_c and P_s. The effects of changing the properties of the link elements, besides the effects of linkage on the overall response, were investigated. The following findings were reported:

- The stiffness of the link element had a negligible effect on the elastic fundamental period of the linked structures, provided the link stiffness was within a practical range.
- It was found that linkage had a beneficial effect on system response if the uncoupled fundamental periods of both buildings were longer than the predominant period of the ground motion. Conversely, if the predominant period of the ground motion was longer than the fundamental period of the stiffer building, larger seismic forces would develop.
- In the case of structures of unequal height, coupling caused yielding in the upper levels of the taller, more flexible structure which behaved as a cantilever above the level of linkage. This stiffening effect of the adjacent low-rise structure must, therefore, be accounted for in the design of the taller structure.

- A single link at the roof level of the shorter building was found to be sufficient to preclude pounding.

Wolf and Skrikerud [W5] proposed the implementation of tuning devices in the form of springs either tensioned, pre-tensioned or without tension. Their numerical analyses showed a reduction in structural response in some ranges of the tuning device stiffness and of pre-load value. In addition, the high-frequency component of the response induced by pounding was eliminated by means of the tensioning.

Jeng et al. [J1,J2] suggested increasing the damping of structures in order to induce in-phase oscillations of the adjacent structures. Anagnostopoulos [A1] suggested the use of a soft viscoelastic filler in the gaps between adjacent structures to reduce the impact forces. In another study, Anagnostopoulos et al. [A2] suggested the implementation of special provisions in design codes which would aim towards the reduction of marked differences in dynamic properties (limitations imposed on heights, masses, etc. of adjacent structures). This, in conjunction with the implementation of special detailing in the structural elements, would allow the introduction of other provisions alternative to the current separation gap limitations. An example cited in their study is the Greek code which requires detailing of the columns of concrete buildings at the sides which are susceptible to pounding.

2.6 Analytical and Numerical Modelling of Pounding

Many difficulties are inherent in the mathematical modelling of the impact phenomenon, due to its highly nonlinear nature. The closed-form analytical solution of the impact phenomenon assumes the pounding structures to be oscillating as a single unit at impact. The assumed properties of the impact elements (stiffness and damping) determine the dynamic characteristics of this "post-impact" system. In addition, the amount of impact force imparted to the adjacent structure is dependent on the user-defined characteristics of the impact element.

The most common modelling method implemented in application software is the representation of impacts by means of a stiffness-based element, usually in the form of a spring-dashpot system or a truss (uni-axial) element. The behaviour of these elements may be linear or nonlinear, where some energy dissipation is effected through hysteretic damping.

Damping may also be assigned in the form of a dashpot in parallel with the spring as in the Kelvin model [A1,A2,W5]. Some hysteretic damping may also be included in this model through the incorporation of a nonlinear spring. More recently, a Hertz contact

law [G8] has been implemented in the modelling of the spring element [D1]. While most impact problems violate the basic assumptions of the original Hertz impact rule, experimental results have exhibited a strong correlation with those predicted from this rule. Although hysteretic energy dissipation may not be represented by the Hertz contact law, its nonlinear characteristics provide a more realistic representation of the increasing contact areas expected during pounding.

The Hertz impact rule is expressed mathematically as follows [G8] (see Fig. 5.1):

$$F = \beta(x - a)^{3/2} \tag{2.11}$$

where:

β = assumed stiffness of the contact element

x = relative displacement of the oscillating system

a = at-rest separation gap.

Davis [D1] showed the insensitivity of the response of a SDOF oscillator to the value (3/2) of the Hertz exponent. However, the selection of a large exponent and small stiffness factor is important for cases where separation distance is small and there is a possibility of significant penetration between the adjacent structures.

The main difficulty in the stiffness-based elements is the assignment of appropriate values for the spring and/or dashpot. While the global response has been found to be insensitive to these properties, as has been presented in the studies above, due consideration must be given in the selection of accurate values in studies of localized pounding effects and floor response spectra.

Many recommendations have been made regarding the assumption of the impact element stiffness value. A number of these recommendations are enumerated below:

- Wada et al. [W1] incorporated an impact element with a stiffness equal to the axial stiffness of the beams and slab at the impact level (5 000 t/cm). This approach was implemented in a number of later studies (Maison and Kasai [M3], Sinclair [S8]).
- Anagnostopoulos [A1] proposed an impact stiffness coefficient equal to twenty times the lateral stiffness of the more rigid equivalent SDOF system.
- Anagnostopoulos and Spiliopoulos [A2] assigned stiffnesses to the impact springs such that the local periods of the mass-impact springs were less than the lowest translational periods of the pounding buildings.

- Maison and Kasai, [M3,M6] implemented a stiffness value corresponding to the axial stiffness of the floor slab at the postulated levels of contact (50 000 kips/in or 8.755×10^6 kN/m). The contact element damping was assigned values of 5% and 20%. No noticeable effect on the displacement response was witnessed for these differing values of damping.
- Sinclair [S8] incorporated a truss element with its stiffness equal to the axial stiffness of the smaller beam (6×10^6 kN/m). Included was the axial stiffness of an area of floor slab equal in length to twelve times its thickness, with an arbitrary length of one metre (as per NZS: 3101, 1995). Two types of impact element contact rules were compared: a bi-linear with slackness hysteresis rule and a Hertz contact law.
- Filiatrault et al. [F2] assumed a value of impact element stiffness which would result in numerical convergence of the linked system. Free-vibration analyses were conducted for the linked system with various values of impact element stiffnesses.

Various researchers [A1, S8, M3] have indicated the relative insensitivity of the overall structural response to the assumed value of the impact element stiffness. Anagnostopoulos and Spiliopoulos [A2] postulated that the ductility demands are insensitive to the impact element stiffness, while some sensitivity is observed on the response from variation of the coefficient of restitution (see below). Maison and Kasai [M3,M6] noted the insensitivity of the peak displacement, drift and overturning moment to impact element stiffness, while a somewhat larger influence was observed on the maximum shears. However, the response of the shorter, stiffer building was not investigated in their study. Anagnostopoulos [A1] also noted the insensitivity of displacement response to impact spring stiffness although the influence of this factor on the local accelerations was emphasized.

Another form of impact modelling, which has been applied extensively and does not require the incorporation of gap elements, is that based on the conservation of energy (or momentum) and/or the enforcement of geometrical compatibility conditions. One of these models is the coefficient of restitution [G8]. The final velocities of centrally colliding bodies are determined based upon their initial velocities and a coefficient of restitution (e) which accounts for plasticity due to impact. The final velocities of centrally impacting bodies are determined from:

$$v'_1 = v_1 - (1 + e)\frac{m_2 (v_1 - v_2)}{m_1 + m_2} \qquad (2.12a)$$

$$v'_2 = v_2 - (1+e)\frac{m_1(v_1 - v_2)}{m_1 + m_2} \tag{2.12b}$$

where v_i and v'_i are the initial and final velocities of bodies $i = 1$ and 2, and m_i represents the masses of the bodies. The parameter e, known as the coefficient of restitution, is defined as follows:

$$e = \frac{v'_1 - v'_2}{v_2 - v_1} \tag{2.13}$$

The coefficient of restitution was originally considered to be a function of the material properties only. However, the effects of mass, shapes and relative velocities of the impacting bodies have been acknowledged. Its value is between 0.0 (perfectly plastic impact) to 1.0 (perfectly elastic impact). Traditionally, the coefficient of restitution was determined from the rebound height (h^*), which is the height attained by a sphere dropped from a height h on a massive plate of the same material:

$$e^2 = \frac{h^*}{h} \tag{2.14}$$

Anagnostopoulos [A1] proposed a relationship between the dashpot constant (linear impact model) and the coefficient of restitution (e) by means of equating the energy losses during impact as follows:

$$c_c = 2\,\xi_i \sqrt{k_c \frac{m_1 m_2}{m_1 + m_2}} \tag{2.15}$$

with $$\xi_i = \frac{-\ln e}{\sqrt{\pi^2 + (\ln e)^2}} \tag{2.16}$$

where c_c is the dashpot constant of the impact element, k_c is the stiffness of the impact element and ξ_i is the damping ratio. In Anagnostopoulos' study, the dashpot constants assumed for the viscous damping elements were assumed equivalent to a coefficient of restitution of 0.65.

Values of coefficients of restitution adopted in a number of studies are shown in Table 2.1 below.

STUDY	(e)
Anagnostopoulos [A1]	0.5
Maison and Kasai [M6]	0.53 & 0.85
Anagnostopoulos and Spiliopoulos [A2]	0.5 & 0.75
Athanassiadou,et.al. [A5]	0.2 - 0.8
Leibovich, et al. [L6-7]	0.5

Table 2.1: Values of coefficient of restitution implemented by various researchers.

Athanassiadou, et al. [A5] found that for a range of realistic values of the coefficient of restitution (0.2 to 0.8) the variations in the response were relatively minor. Anagnostopoulos et al. [A2] indicated the limited sensitivity of the ductility demand to the variation of the coefficient of restitution.

Other energy-based pounding models are the Lagrange multiplier method [P2] and modal analysis method [C4]. A mathematical method in which contact is expressed as nonconvex and nonmonotone constitutive relations [L13] allows friction at the contact nodes to be accounted for.

2.7 Summary

Based on the results of the studies presented above, the following assumptions were incorporated in the mathematical model implemented in RUAUMOKO:

- A CONTACT-type member was assumed, with a Hertz contact rule (see Fig. 5.1).
- The value of the impact element stiffness was based on the axial stiffness of the lower level (exterior) beams of the Rahman frame, to which was added an arbitrary width of slab (as per NZS 3101:1995, Section 4.3.3.7).
- As a constant damping (5%) was assumed for all modes of the system, the damping coefficient of the CONTACT member was assumed equal to zero. This is deemed to be a valid assumption due to the short duration of the impact events.
- The time-step used in the analyses is 0.001 seconds, which is comparable to the recommendations of other studies [e.g. S8, A2]. Such a small temporal increment is necessary to detect the short-duration impact events. In addition, the significance of the time-stations at which the results were saved for implementation into the postprocessor was highlighted in this study. The implications of this aspect are presented in Chapter 5.

3. SOIL-STRUCTURE INTERACTION

3.1 Introduction

The effects of soil-structure interaction on structural response were first recognized during the San Francisco earthquake of 1906. The California Earthquake Commission Report [L2] noted that "the firmer and more elastic a rock formation, the less the intensity of the earthquake shock it transmits to buildings standing on it; and there is a graduation in this quality from the firmest bed rock to the loosest gravel, sand and mud". These effects were introduced as "foundation coefficients" which represented the expected amplification of peak ground accelerations of a given site compared to a rock site. Since then, considerable analytical and experimental research has been conducted to gain more insight into the soil-structure interaction phenomenon. This research has been prompted by the developments in the atomic energy industry. With the massive size of the installations involved and the stringent safety requirements, the engineering profession has been compelled to more detailed consideration of soil-structure interaction effects. Some of the problems inherent in the investigation of soil-structure interaction have been the identification of the various parameters which influence this phenomenon, the formulation of mathematical expressions incorporating these parameters and the solution of these expressions. Another concern has been the application of these extensive research findings into a form amenable to design office implementation.

Traditional design office practice assumes a fixed connection between the structure and the supporting soil at foundation level. However, the response of a soil mass subjected to a seismic excitation is similar to that of any engineered structure with its own unique dynamic characteristics (i.e. mode shapes and natural frequencies), thereby affecting any structures the soil mass may be supporting. In general, the dynamic response characteristics of a soil mass differ from those of an engineered structure in the following respects:

- The supporting soil mass is of infinite boundaries (an unbounded domain).
- The presence of energy waves (both from the seismic event and the dynamically responding structure supported by the soil mass) propagating through the soil mass. These waves affect the properties of the soil and alter the dynamic response of the supported structure through the introduction of additional damping. In a layered soil profile, a portion of the waves emanating from the foundation-soil

interface may also be reflected from the boundaries of the underlying soil layers, returning to impinge on the foundation.

- The material properties of the soil are strain-dependent, complicating the numerical and/or analytical modelling of its behaviour.

From the above, it may be surmised that consideration of soil-structure interaction will not only affect the dynamic characteristics of the supported structure but also the nature of the input excitation. As the disparity between the dynamic properties of the structure and those of the supporting soil increases, the significance of soil-structure interaction effects increases proportionately.

Despite the importance of soil-structure interaction effects and their possible repercussions on the structural response, the consideration of soil-structure interaction in conventional design office practice is not a routine procedure. This may be attributed to many factors, among them:

- The complexity of available soil-structure interaction models, obscuring insight into the relevant parameters influencing soil-structure interaction.
- The difficulty of incorporating these models into existing commercial structural analysis software.
- The ambiguity of some building codes in defining the situations in which consideration of soil-structure interaction is requisite.

Extensive research has been conducted in the development of realistic mathematical and physical models. Many simplifying assumptions are necessary to develop a rigorous analytical or numerical solution to the equation of wave-propagation through soil (upon which soil-structure interaction models are based). These simplifications include:

- The type of seismic waves considered.
- The nature of the soil profile at the site.
- The geometric properties of the foundation.
- The assumption of perfect bond at the foundation-soil interface.
- The representation of a 3-dimensional problem by a 2-dimensional model, which is the most fundamental approximation [M10].

Advances in mathematical analysis techniques and computer technology have culminated in the development of simple easy-to-use numerical models. Despite their

ostensible simplicity, most of these models incorporate many of the important parameters that are of prime concern in a soil-structure analysis (e.g. foundation shape, embedment, condition of side-wall contact, etc.). A comprehensive review of the state-of-the-art and relevant developments has been presented by Gazetas [G2].

Verification of derived soil-structure interaction models has been conducted through observed response of existing instrumented structures [Z1, Z2], small- and large-scale tests of structures [F7, G1, W12] and foundation slabs [C5, G5, N8]. Gazetas and Stokoe [G5] have presented a brief review of a number of tests (besides those cited above) and the limitations and merits of the various methods employed in these tests.

In this study, the soil-structure interaction model presented by Wolf [W8] is implemented. These discrete-element models, representing the force-displacement response (including inertial effects) of the rigid foundations, are applied directly under the supported structure.

3.2 Effects of Soil-Structure Interaction

The effects of consideration of soil-structure interaction in a dynamic analysis are twofold. The first effect is on the free-field excitation and the second is on the response characteristics of the oscillating system.

3.2.1 Effects of Soil-Structure Interaction on Seismic Excitation

The presence of a soil layer above the bedrock will lead to a reduction in the bedrock motion due to overburden. The ground motion at the free-field will either be amplified or attenuated depending on the following:

- Characteristics of the bedrock excitation (amplitude, frequency content and duration).
- Soil profile (lateral homogeneity, layering, presence of bedrock and thickness of layers, history of formation).
- Topography of the site.
- Soil properties (for each layer shear strength modulus, Poisson's ratio, mass density).

As an example, an excitation with predominantly low frequency components will be amplified at the free-field if the waves travel through an overlying soil mass with a long fundamental period (e.g. a deep soil layer or layers with low shear modulus). Therefore, a long period structure on this site will be more adversely affected than an

adjacent short period structure on the same site. However, a level of excitation may be attained which will result in excessive soil deformations leading to a loss in soil shear strength. This limits the excitation level that a site may be capable of sustaining [P6]. Site conditions at Mexico City during the 1985 earthquake were such that elastic response was maintained to high levels of soil shear strains. As a result, and due to the fact that the predominant frequencies of the seismic excitation were close to those of the soil site, the amplification of the bedrock motions at the free-field was substantial [W4]. The strain-dependence of the soil properties renders the determination of the site response under seismic excitations a difficult exercise. This will be presented in a subsequent section.

The effects of soil-structure interaction were implicitly considered in this study through the application of the seismic excitation at the base of the soil-structure interaction models. In other words, the free-field seismic excitation was applied directly at the base nodes of the soil-structure interaction models with no modifications.

3.2.2 Effects of Soil-Structure Interaction on Structural Response

Due to the presence of the supporting soil medium, the dynamic characteristics of the structure are modified as follows:

- The introduction of a rocking vibration mode and an average horizontal translation. Base shears and moments, resulting from the dynamic response of the structure to the seismic excitation, increase the deformations at foundation level, thereby increasing these vibration modes.
- The effects of these rigid-body components of motion are to vary the inertial forces along the height of the structure due to the change in the vibration mode shapes.
- In addition, the natural periods of the structure are lengthened with repercussions on element ductility demands and overall system response.
- Waves emanating from the foundation-soil interface dissipate energy, leading to an increase in damping. This damping is effected in two forms:

  i. Through the energy transmitted by the waves (radiation or geometric damping, first recognised by Reissner [R1] in 1936).

  ii. Through material (hysteretic) damping in the soil [V2, V3].

  These waves may be reflected back into the bounded domain (structure and adjacent soil medium within the artificial boundary) in the case of a layered soil medium. The fundamental frequency of the soil layer determines the

extent of radiation damping that will occur. If the excitation frequency is less than the fundamental frequency of the soil layer (as in the case of a shallow layer underlain by bedrock), damping will not occur and only material damping is present. This property of the soil layer is known as the cutoff frequency [W8]. The method of incorporating these two types of damping (radiation and hysteretic) in the impedance function will be presented in a subsequent section. Only radiation damping was considered in this study for the reasons stated in Section 3.3.2.2.

3.3 Aspects of Soil-Structure Interaction Theory and Modelling

The soil mass responds to a dynamic excitation in a manner similar to any engineered structure. It therefore possesses damping, a fundamental natural period (in addition to higher harmonics) and will amplify excitations with natural frequencies close to those of the soil site. A structure subjected to an earthquake excitation will therefore not only respond to this (modified) excitation but also to the earthquake-induced dynamic response of the soil mass upon which it is supported. In addition to the assumptions pertaining to the modelling of the superstructure, many difficulties are also inherent in the modelling of the soil. The practical assessment and mathematical modelling of the dynamic material properties of the soil mass are quite complex. Many mathematical and mechanical (rheological) models (such as the Winkler [G2], Kelvin-Voigt [I3], and Complex Composite models [K9]) have been developed to represent soil cyclic force-displacement behaviour. In general, these rheological models comprise a spring-dashpot system in series or in parallel, respectively representing the stress-relaxation and creep characteristics of the soil. Experimental studies are imperative in order to determine the accuracy of these representations. As an example, the model postulated by Pender [P5] comprises two Kelvin-Voigt systems in series. The upper system is representative of the non-linear soil adjacent to the foundation while the linear behaviour of the deeper soil is represented by the lower Kelvin-Voigt system.

The fundamental precept of any soil-structure interaction problem is the determination of the relationship between the applied forces and the resulting displacements. The force-displacement relationship for a rigid massless foundation disk may be expressed as:

$$K_a(\omega) = \frac{R_a(\omega)}{u_a(\omega)} \tag{3.1}$$

where $K_a(\omega), R_a(\omega), u_a(\omega)$ are, respectively, the (frequency-dependent) stiffness, dynamic force (or moment) and response (translation or rotation). The subscript a refers to the mode of vibration: horizontal, vertical, rocking, torsional and coupled horizontal-rocking.

Since the force and displacement are generally not in-phase, it is more convenient to express the force-displacement relationship in complex notation:

$$K_a(\omega) = K_{a1}(\omega) + i K_{a2}(\omega) \tag{3.2}$$

where $i = \sqrt{-1}$ in the second term, which represents the (90°) out-of-phase component of the impedance function.

Roesset [R7] has drawn an analogy between the vibration of a 3-dimensional massless foundation-soil system and that of a single-degree-of-freedom (SDOF) oscillator. The equation of motion of a SDOF oscillator under a harmonic excitation $R(t) = R_o exp(i\omega t)$, assuming a harmonic response $u(t) = u_o exp(i\omega t)$ is:

$$M\ddot{u}(t) + C\dot{u}(t) + Ku(t) = R(t) \tag{3.3a}$$

$$(K - M\omega^2) + iC\omega = \frac{R_0}{u_o} \tag{3.3b}$$

where M, C and K are the mass, damping and stiffness, respectively, of the SDOF oscillator. Comparing Eqs. 3.2 and 3.3b, we note that:

$$K_{a1}(\omega) = K - M\omega^2 \tag{3.4a}$$

and $$K_{a2}(\omega) = C\omega \tag{3.4b}$$

From the above, it may be seen that the real part (K_{a1}) of the dynamic impedance (Eq. 3.2) is a function of the stiffness and mass of the oscillating system. The frequency dependence of this real part (Eq. 3.4a) is reflected in the inertia term and not in the stiffness term. The imaginary term of Eq. 3.2 is the (90° out-of-phase) frequency-dependent damping and is representative of the energy dissipation due to the radiation of waves away from the foundation-soil interface (radiation damping). It is usually represented in the form of a viscous damper for mathematical expediency. Strain-dependent material damping (due to hysteretic behaviour of the soil) may also be introduced and will be presented in a subsequent section.

The dynamic impedance function of a SDOF system may also be expressed in terms of static and dynamic components, as follows:

$$K_a(\omega) = K_a.\left\{\left(1-\frac{\omega^2}{\omega_n^2}\right)+i2\beta\frac{\omega}{\omega_n}\right\} \qquad (3.5)$$

or $$K_a(\omega) = K_a.(k_a + i\omega c_a) \qquad (3.6)$$

where $\beta = C/C_{cr}$ is the critical viscous damping ratio and $C_{cr} = 2\sqrt{KM}$ is the critical damping. The natural frequency of the oscillating system is $\omega_n = \sqrt{K/M}$. Thus, the dynamic impedance is expressed as the product of a static term K_a and a frequency-dependent dynamic term $(k_a + i\omega c_a)$.

In a soil-structure interaction problem the determination of Eq. 3.1 necessitates the solution of the equation of wave-propagation. This is due to the effect of the exciting force, which elicits a response in the form of energy waves radiating from the point of application of the force. It is assumed that energy radiates only from the foundation-soil interface (point of force application) to infinity (point of ensuing response), i.e. there are no incoming waves propagating from infinity to the foundation. This is known as the "radiation condition formulated at infinity". The dynamic stiffness coefficients, derived from the solution of the wave-propagation equation, must then be transformed into the time domain. This allows the application of these coefficients in a time-history analysis that the practicing engineer is more familiar with. In addition to familiarity, a frequency domain solution is not viable for a non-linear analysis since it requires the Fourier series expansion of the seismic excitation, the determination of the response for each term and, finally, the superposition of these terms to determine the total response.

In addition to the above, other simplifying assumptions for the foundation-soil system are implemented in order to facilitate the solution of the equation of wave-propagation. These simplifications pertain to the following aspects [G2]:

- Extent of foundation embedment.
- Foundation base and wall-soil surface contact condition.
- Foundation shape (geometry).
- Soil profile and properties.
- Foundation rigidity (which affects the stress distribution at the foundation-soil interface).

In this study, rigid square separate footings are assumed. Perfect bond is assumed to exist between these footings and the surface of the non-layered elastic homogeneous soil upon which they are supported.

Some of the main features of the dynamic impedance relationship and the difficulties intrinsic to the soil-structure interaction phenomenon are presented briefly in the following sections.

3.3.1 Boundaries of the Soil Mass

Obviously, determination of the dynamic properties of the unbounded soil domain and its representation by means of a suitable physical model are challenging tasks. This is especially true in a finite-element type of solution which necessitates the discretization of an infinite domain. Researchers have resorted to the discretization of a finite domain by defining the limits of this domain with artificial boundaries. These boundaries encompass that part of the soil that affects the characteristics of the excitation and the response of the supported structure. The limits of this bounded domain (which includes the structure) must be at such a distance that any reflections of waves (which are emanating from the foundation-soil interface) impinging from the boundaries back into the bounded domain will not affect the analysis. This satisfies the radiation condition. The dynamic stiffness relationships are thus formulated not at infinity but at these artificial boundaries. However, in order to satisfy the radiation condition, a substantial portion of the soil mass would have to be included in the bounded domain. Other difficulties inherent in the development of artificial boundaries are [R4]:

- The waves impinging on the artificial boundary are of various forms: body (in-plane and anti-plane shear, dilatational) and surface (Rayleigh, Love) and, therefore, must be treated accordingly.
- The angle of incidence of the impinging waves on the boundary must be accounted for.
- Some models are unable to deal with nonlinearities, not only those adjacent to the artificial boundary but at any location within the bounded domain. While this approximation (i.e. linear behaviour) is valid for most of the bounded domain, it is not true for that region of the soil adjacent to the foundation. In this region, significant nonlinearities may exist in the form of foundation lift-off (rocking) and high-amplitude strains.
- The definition of the end conditions of the artificial boundary (e.g. free or fixed) is dependent on the site stratigraphy [R6].

These issues will not be addressed here nor will the development of artificial boundary models. However, the two different analysis techniques that are based on the location and type of the artificial boundary are briefly summarized in the following sections.

3.3.1.1 Direct Method of Analysis

In this method the structure and adjacent soil are discretized by a suitable finite-element mesh. The properties (boundary conditions) of the artificial boundary in this case are representative of the force-displacement characteristics of the "unbounded domain", i.e. the soil mass not included within the boundary. This "transmitting boundary" does not allow the reflection of impinging waves back into the bounded domain. This is achieved by virtue of its properties and its distance from the foundation-soil interface. In a rigorous analysis the boundary conditions are temporally and spatially global. This means that to advance one time station at a specific node requires information from all other nodes over the entire boundary for the previous time stations. Approximate solutions may be obtained through the application of boundary conditions that are local in space and time; only information from adjacent nodes during the same time station or a few preceding time-steps are required. The direct method is computationally expensive in that the discretization of a considerable portion of soil adjacent to the structure as part of the bounded domain is required. This implies the introduction of a significant number of degrees-of-freedom into the analysis.

3.3.1.2 Substructure Method

The artificial boundary is applied directly at the foundation-soil interface and the structure and soil are individually modelled as separate substructures in this method. The superstructure is discretized by a suitable mesh or represented by a spring-dashpot-mass system. The force-displacement relationships (impedance functions) of the unbounded soil are derived through the solution of the relevant boundary-integral equations on the artificial boundary. These equations are derived through the application of the radiation condition formulated at infinity (Green's functions) and not at the artificial boundary as in the direct method. This is due to the nature of the artificial (transmitting) boundary which allows the energy waves to pass through it with almost no reflections.

The Green's functions applied in a boundary-element formulation correspond to the boundary conditions applied in a finite-element solution. In the latter method, application of the boundary conditions to the assumed shape functions and solution of the ensuing system equations result in the interpolation functions, which are expressed

in terms of nodal displacements. In a boundary-element solution, these boundary conditions are in the form of integral equations which represent the response to energy waves resulting from a surface excitation. Approximations are applied in the form of prescribed stress and/or displacement conditions at the foundation-soil interface and the free surface to facilitate the solution of the system equations. Special analytical and numerical methods are then applied to the resulting boundary-integral equations to obtain the dynamic impedance functions. These dynamic stiffness coefficients are temporally and spatially global and are formulated at the common nodes on the artificial boundary at which the soil-structure system was discretized. The equations of motion of the total system are then formulated at these common nodes. This is achieved through the combination of the force-displacement coefficients (dynamic impedance coefficients) of the unbounded soil with the discretized equations of motion of the structure at the aforementioned nodes. This method allows the application of different analysis and modelling techniques for each individual substructure, which is the advantage of this method over the direct method of analysis.

In either of the two methods presented above, the force-displacement characteristics of the unbounded soil domain may be represented by a spring-mass-dashpot system (also known as a discrete-element system) at the discretized nodes along the artificial boundary. The frequency-independent coefficients of this system may be derived through the application of the truncated semi-infinite cone model which will be subsequently presented.

3.3.2 Dynamic Soil Properties

The most important properties of the soil that define the dynamic response of the soil mass are the soil shear modulus (G) and material (hysteretic) damping. Since both these values are strain dependent, the determination of exact values is problematic. These soil properties are not only dependent on strain amplitude but also on strain rates, number of cycles and duration of loading [R3]. The area within the hysteresis (shear stress-shear strain) loop is a measure of the energy dissipated by hysteretic action. The characteristics of the earthquake excitation are also an important factor in determining maximum stress levels.

In general, soil tends to behave in a linear elastic manner up to certain strain amplitudes (levels of excitation) [P7]. The extreme manifestation of non-linear soil behaviour is liquefaction (saturated sand), with a reduction in free-field excitation and settlement being the more common manifestations of non-linear soil response. Due to the many parameters upon which soil behaviour is dependent, especially those

pertaining to the characteristics of the seismic excitation, the prediction of non-linear site response is onerous. Some of the parameters which may assist in the prediction of site soil behaviour have been presented by Pender [P7].

3.3.2.1 Soil Shear Modulus

The small strain shear modulus may be determined by laboratory tests (e.g. resonant column method [R2]) or *in-situ* methods (e.g. cross-hole method [S9]). The latter methods are preferred due to the difficulty of obtaining undisturbed samples and the simulation of prevalent (pre-earthquake) stress conditions in the laboratory [Y2]. The shear modulus of the soil (G_s) is determined by means of tests measuring the shear-wave velocity of the soil. The following equation is then applied:

$$G_s = \rho v_s^2 \tag{3.7}$$

where ρ and v_s are, respectively, the mass density (T/m^3) and shear-wave velocity (m/s) of the soil. Alternatively, the small strain shear modulus may be derived from the following equation:

$$G_s = \frac{E_s}{2(1+\nu_s)} \tag{3.8}$$

where the elastic (Young's) modulus (N/mm^2) and Poisson's ratio of the soil are denoted by E_s and ν_s, respectively. The application of either of the two equations above is determined by the available data.

Many factors influence the magnitude of the small strain shear modulus [R2], the most important of which are [R3]: the average confining pressure, void ratio, duration of application of load and shear strain amplitude. A number of researchers [e.g. A3, H2, H3, H4, H5, L1, L8, S4, and T2] have quantified the variation of soil properties with strain amplitudes based on laboratory and *in-situ* tests for different types of soils.

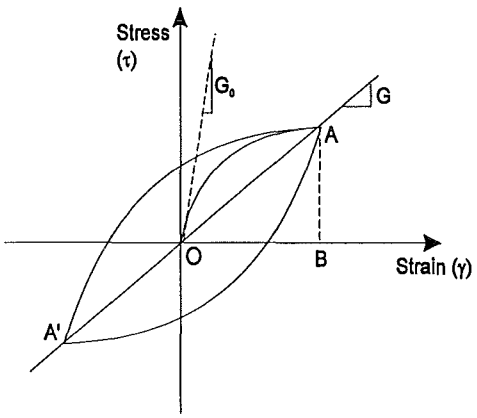

Fig. 3.1: Soil stress-strain behaviour.

3.3.2.2 Soil Damping

One of the most important features of soil-structure interaction is soil damping, which is manifested in two distinct ways:

- Material damping resulting from a hysteretic energy dissipating mechanism due to frictional contact between the soil particles (see Fig. 3.1).
- Radiation or geometric damping due to the propagation of energy waves away from the vibrating foundation. If the frequency of excitation is below the cutoff frequency, which is the fundamental frequency of the soil mass, no radiation damping occurs [W8]. The natural periods of the soil layer T of depth H is given by [D4]:

$$T_n = \frac{4H}{(2n-1)v_s} \tag{3.9}$$

where n is an integer (1, 2, 3, etc.) which relates to the mode of vibration. The fundamental period of vibration of the soil is determined from Eq. 3.9 for $n = 1$. The ability of the semi-infinite truncated cone model (implemented in this study) to simulate this feature [W8] is one of this model's most salient attributes. Radiation damping is discussed in subsequent sections while material damping is presented in the following paragraphs.

As mentioned previously, extensive laboratory and *in-situ* tests have been conducted by many researchers to determine the shear stress-shear strain relationship for various types of soils. Consequently, many types of soil hysteresis models have been developed (e.g., Ramberg-Osgood model [R3]) to represent the stress-strain characteristics of soil from a number of basic parameters. The material damping may then be derived from the area under the stress-strain curve or hysteretic model as follows:

$$\frac{\Delta W}{W} = 4\pi\zeta \tag{3.10}$$

where the various terms are defined as (see Fig.3.1):

ΔW = The area under the hysteresis curve *A-A'*, representing the total energy input into the system.

W = Area *OAB,* which is representative of the elastic energy stored in a spring subjected to the same stress-strain levels as the soil mass. This is equal to :

$$W = \frac{1}{2} K w^2 \tag{3.11}$$

where K is the static stiffness of the spring (equal to the static stiffness of the soil mass) and w is the spring displacement (soil deformation).

The hysteretic damping ratio is denoted by ζ and may be determined experimentally from the following equation:

$$\zeta = \frac{1}{2} tan\delta \tag{3.12}$$

where δ represents the experimentally derived phase angle [S4,V2] between the stress and the associated strain for the harmonically oscillating soil specimen. Expressing Eq. 3.10 in terms of Eq. 3.12 leads to a frequency-independent formulation for the material damping. Alternatively, a frequency-dependent expression may be derived through the application of a Voigt viscoelastic model [V3] as follows. Expressing Eq. 3.10 in an alternative format:

$$\frac{\Delta W}{W} = 2\pi \frac{\omega G'}{G} \tag{3.13}$$

where ω is the frequency of excitation, G' and G are the shear moduli of viscosity and elasticity, respectively. In a frequency-independent (constant hysteretic) formulation (Eq. 3.12) [D3], the parameter $\omega G'$ is a constant value and $tan\delta = \omega G'/G$ whereas, in a Voigt solid model, the constant value is G' and Eq. 3.13 is frequency-dependent. For the frequencies of interest in an analysis involving seismic excitations, the use of the constant hysteretic model (Eq. 3.10) is more appropriate. This has been corroborated by stress-strain tests conducted on soils [D3, R2,S4] which demonstrated the dependence of $\Delta W/W$ on strain amplitudes.

In the soil-structure interaction model used in this study, the incorporation of hysteretic (material) damping may be accomplished through the correspondence principle [M12, W8]. This principle allows for the changes in the elastic constants, due to the consideration of material damping, through the implementation of a complex factor $(1+2i\zeta_s)$ into the relevant elastic constants as follows:

$$\begin{aligned} G_\zeta &= G_s(1+2i\zeta_s) \\ E_{\zeta s} &= E_c(1+2i\zeta_s) \\ v_{\zeta s} &= v_s\sqrt{1+2i\zeta_s} \approx v_s(1+i\zeta_s) \\ v_{\zeta p} &= v_p\sqrt{1+2i\zeta_s} \approx v_p(1+i\zeta_s) \end{aligned} \tag{3.14a-d}$$

where the subscript ζ denotes the material-damped elastic coefficient and $i = \sqrt{-1}$. The shear modulus of the soil is denoted by G_s and the Elastic (Young's) Modulus by E. The shear and dilatational wave velocities are denoted by v_s and v_p, respectively.

The material damping ratio of the soil is denoted by ζ_s, where the subscript s designates soil. The amplitudes of the stiffness and damping coefficients of the cone model (presented in the following sections) are modified as follows:

$$\rho c_\zeta^2 = \rho v^2 (1 + 2i\zeta_s)$$
$$i\omega\rho c_\zeta = i\omega\rho v(1 + i\zeta_s) \qquad (3.15a,b)$$

where the relevant value of the wave velocity v corresponding to the mode of vibration is substituted. The mass density (kg/m^3) is denoted by ρ. Through the application of the correspondence principle, Wolf [W8] has developed linear (Voigt viscoelastic) and nonlinear (frictional) elements, representative of soil material damping, for incorporation into the discrete-elements of the semi-infinite truncated cone model. These damping elements may be implemented directly, along with the discrete-element models, in time-history analysis software. In this study, the material damping of the soil was not accounted for in the soil-structure interaction models utilized herein. This was due to the application of a constant damping model (5% damping across all modes) in the mathematical model of the structure-soil system. The assumed model was deemed to be representative of the total system damping due to the difficulty of determining and isolating the damping characteristics of the various components (moment-resistant frames, impact elements and soil mass) which comprise the total system.

3.4 The Semi-Infinite Truncated Cone Soil-Structure Interaction Model [W8]

The lumped-parameter models (LPM) which are incorporated in this study are based upon the discrete-elements derived from the cone models, as presented by Wolf [W8]. The (one-dimensional) truncated semi-infinite cone representation of the (three-dimensional) soil domain beneath a rigid massless foundation was first developed by Ehlers [E4] in 1942 for the translational degree of freedom. That for the rocking mode was derived by Meek and Veletsos [M9] in 1974.

The (frequency-independent) spring-mass-dashpot system of the LPM, derived from the cone model, incorporates many of the salient features of the soil-structure interaction phenomenon while at the same time maintaining ease of implementation into existing software. The cone model differs from existing methods, such as those based on curve-fitting techniques, in that a strength-of-materials approach is applied in the derivation of the cone properties without violating the fundamental principles of the half-space theory.

Although some attributes of the semi-infinite truncated cone model have been questioned, these reservations have been disproved [M11]. These contentions pertain to the following aspects:

- Application of a strength-of-materials approach in lieu of the rigorous half-space theory in the formulation of the system equations.
- The omission of Rayleigh waves in the wave propagation formulation.
- The validity of excluding the unbounded soil domain outside the cone region.

The ease of implementation into existing dynamic analysis software, of visualization and the range of foundation cases which it covers [M11, M12, W6, W7, W8, W9] are the main reasons for incorporating the discrete-element model derived from the cone model in this study.

3.4.1 Derivation of Semi-Infinite Truncated Cone Model

For each degree-of-freedom, the semi-infinite truncated cone represents (as a first approximation) the three-dimensional linearly elastic undamped homogeneous unlayered soil mass beneath the massless surface foundation (basemat). The extension of the cone model to other soil profiles and foundation embedment conditions is possible through the manipulation of the basic cone model (representing the homogeneous unlayered half-space) presented herein. For layered media, a layered cone model is constructed from the wave pattern resulting from the reflections and refractions of the propagating wave off the layer boundaries [W8, W9].

The system equations for any type of cone model (layered or unlayered) may be solved at the foundation-soil interface only and not for the entire soil domain within the cone. Thus, the discrete spring-mass-dashpot system derived from the cone model defines the three-dimensional force-displacement relationship of the massless footing (basemat) at the foundation-soil interface and not along the entire depth of the semi-infinite truncated cone. Similarly, if the fixed node (i.e. that which is not connected to the structure) is defined as the base node of the discrete system, then the application of a seismic excitation at this base node does not imply the excitation of the base of the cone model (bedrock layer), but the excitation of the foundation base. Thus, the dynamic excitation applied in this manner is representative of the earthquake record modified due to the presence of the soil layers (represented by the discrete-element system) and is not the free-field motion.

The dynamic impedance function, describing the dynamic force-displacement properties of the unbounded soil medium, may be expressed in terms of a static term

(K_a) and a dynamic term ($k_a + i\omega c_a$) where *a* denotes the mode of vibration (Eq. 3.6). The static stiffness component derived below expresses the response of the cone model to an excitation of frequency $\omega = 0$, whereas the dynamic stiffness coefficient is based on the one-dimensional propagation of a wave through the cone model. This reflects the doubly-asymptotic nature of the dynamic impedance function, in which convergence to the true values is attained at the limits $\omega = 0$ and $\omega = \infty$.

3.4.2 Special Considerations

Inspection of results from rigorous solutions of the dynamic-impedance coefficients (stiffness and damping) of a disk on a homogeneous half-space reveals that special treatment is required for the vertical and rocking oscillations of foundations (where dilatational waves are produced) in nearly incompressible soils, $1/3 \leq \nu_s \leq 1/2$. This treatment appertains to two aspects: the first relates to the value of the dilatational wave velocity and the second to the consideration of a "trapped" mass oscillating in-phase with the foundation. Both of these factors will be presented in this section.

For the torsional and horizontal translational modes of vibration, only shear waves are generated. Therefore, the value of the shear wave velocity v_s is applied in the relevant equations to determine the cone dimensions and the values of the dynamic-impedance coefficients. The value of the shear wave velocity is equal to:

$$v_s = \sqrt{\frac{G_s}{\rho}} = \sqrt{\frac{E_c(1-2\nu_s)}{2\rho(1-\nu_s)}} \qquad (3.16)$$

and remains finite for all values of Poisson's ratio ν_s of the soil.

For the case of the rocking and vertical translational modes, the dilatational wave velocity v_p is incorporated in the relevant equations, where:

$$v_p = \sqrt{\frac{E_c}{\rho}} = \sqrt{\frac{2G_s(1-\nu_s)}{\rho(1-2\nu_s)}} \qquad (3.17)$$

It may be seen that the value of v_p approaches infinity for values of ν_s equal to *0.5*, which is the case for saturated soils. Substitution of a dilatational wave velocity $v_p = 2v_s$ into the equations of the dynamic-impedance coefficients for the case of nearly incompressible soils, where $1/3 \leq \nu_s \leq 1/2$ is deemed to be the most suitable selection for the following reasons:

- This value yields the correct asymptote for high-frequency damping for both values of $\nu_s = 1/3$ and $1/2$.
- It provides a best-fit for the low-frequency range of excitation.

Therefore, the values of the dilatational wave velocity for the relationships defining all aspects of the cone model (aspect ratio of apex height to equivalent foundation radius and dynamic-stiffness coefficients) and for the different Poisson's ratios are as follows:

$$v = v_p \quad \text{for} \quad \nu_s \leq 1/3 \tag{3.18a}$$

$$v = 2\,v_s \quad \text{for} \quad 1/3 < \nu_s \leq 1/2 \tag{3.18b}$$

The second feature, i.e. the "trapped" mass, may be explained as follows. Recalling Eq. 3.3b:

$$\frac{R_0}{u_o} = K_a(\omega) = \left(K - M\omega^2\right) + iC\omega \tag{3.3b}$$

it may be noticed that the dynamic spring (real) term of the dynamic impedance formula is augmented by a mass oscillating in-phase with the basemat. This trend is also observed as a downward-parabolic tendency in the rigorous expressions for the dynamic-stiffness for certain values of Poisson's ratio (ν_s) and dimensionless frequencies, $a_o = \omega r_o / v_s$ (Figs. 2.6, 2.7, 2.21 in Ref. [W8]). For all values of ν_s, except exactly ν_s = 1/2, the trapped mass gradually melts away with increasing values of a_o. In this case, the dynamic-stiffness curve displays an increase until all the mass is dissipated and only the spring remains. In the discrete-element representation of the cone model, this trapped mass is determined through the application of curve-fitting techniques to obtain the values shown in Table 3.1.

Mode of vibration	Horizontal	Vertical		Rocking		Torsional
Poisson's ratio	All ν_s	$\leq 1/3$	$1/3 < \nu_s < 1/2$	$\leq 1/3$	$1/3 < \nu_s \leq 1/2$	All ν_s
Wave velocity	v_s	v_p	$2v_s$	v_p	$2v_s$	v_s
Trapped mass ΔM, ΔM_θ	0	0	$2.4(\nu_s - 1/3)\rho A_o r_o$	0	$1.2(\nu_s - 1/3)\rho I_o r_o$	0

Table 3.1: Trapped masses and relevant wave velocities for various Poisson's ratios and modes of vibration.

3.4.3 Static Stiffness Coefficient of Cone Model

3.4.3.1 Translational Modes of Vibration

The geometric properties of the semi-infinite truncated cone are such that the cross-sectional area, representing the stress distribution under the basemat of a point load applied on the equivalent disk at the surface, increases linearly with depth as:

$$A = \left(\frac{z}{z_o} \right)^2 A_o \tag{3.19}$$

where A is the cross-sectional area of the cone at any depth z, and $A_o = \pi r_o^2$ is the area of the equivalent disk on the surface (see Fig. 3.2). This equivalent radius of the massless foundation is determined for the translational modes by equating the area of the rectangular foundation to that of an equivalent disk. Gazetas et al. [G4] have cast doubts on the validity of this approximation for embedded foundations with aspect ratios $L/B > 3$ where L and B are the foundation length and width, respectively. These doubts extend to the rotational degree-of-freedom as well. Roesset et al. [R5], however, have demonstrated the validity of this approach for square foundations.

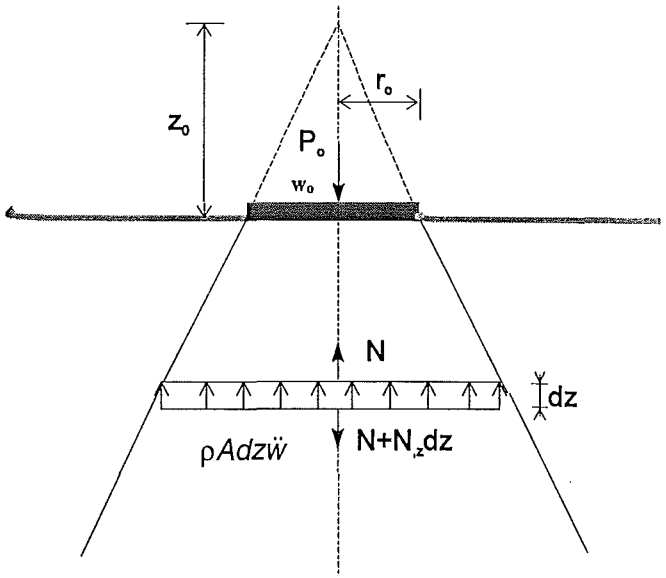

Fig.3.2: Cone model of soil beneath rigid foundation for translational degree-of-freedom (adapted from Wolf [W12]).

Consider an element of infinitesimal height dz and cross-sectional area z, subjected to an axial force N resulting from a vertical force P_o acting on the equivalent disk (representing the foundation). The axial displacement resulting from P_o is w_o at the disk and w at any depth z along the axis, measured from the cone apex. The condition of static equilibrium at the element is expressed as:

$$-N + N + \frac{\partial N}{\partial z} dz = 0 \tag{3.20}$$

By applying the force-displacement and constitutive relationships, the following relationship is obtained:

$$N = E_c A \frac{\partial w}{\partial z} \tag{3.21}$$

where E_c is the constrained modulus defined as $E_c = \rho v_p^2$ or, alternatively, as $E_c = (2G_s)(1-\nu_s)/(1-2\nu_s)$, where ρ is the mass density (kg/m^3), v_p is the dilatational wave velocity (m/s), G_s is the elastic shear modulus (N/mm^2) and ν_s is Poisson's ratio of the soil.

Substituting Eq. 3.21 into Eq. 3.20 leads to:

$$\frac{\partial^2 w}{\partial z^2} + \frac{2}{z}\frac{\partial w}{\partial z} = 0 \qquad (3.22a)$$

which may be expressed as:

$$\frac{\partial^2}{\partial z^2}(zw) = 0 \qquad (3.22b)$$

The solution of Eq. 3.22 is of the form $wz = c_1 + c_2 z$, where c_1 and c_2 are integration constants. Applying the boundary conditions:

$$w(z = z_o) = w_o$$
$$w(z = \infty) = 0 \qquad (3.23a,b)$$

leads to:

$$w = w_o(z_o/z) \qquad (3.24)$$

At the surface of the soil (i.e. at $z = z_o$), the axial force N is equal to the external vertical load P_o. Recalling Eq. 3.21, this leads to:

$$P_o = -E_c A_o \frac{\partial w_o}{\partial z} \qquad (3.25)$$

Substituting Eq. 3.24 into this equation yields:

$$P_o = \frac{E_c A_o}{z_o} w_o \qquad (3.26)$$

$$K = \frac{E_c A_o}{z_o} \qquad (3.27)$$

The latter equation defines the static stiffness K of the translational cone in vertical motion. In a similar manner, the case of the static stiffness coefficient of a translational cone in the horizontal direction may be derived, leading to an expression similar to Eq. 3.27 with the elastic shear modulus G_s in lieu of E_c. If these two values, G_s and E_c, are expressed in terms of the corresponding shear wave velocities, the general expression for the translational cone is obtained as:

$$K = \frac{\rho v^2 A_o}{z_o} \tag{3.28}$$

where v equals v_p (dilatational wave velocity) and v_s (shear wave velocity) for the vertical and horizontal motions, respectively.

3.4.3.2 Rotational Modes of Vibration

The radius of the equivalent disk is determined for the rotational modes of vibration (rocking and torsion) by equating the moment of inertia (second moment of area) of the basemat to the moment of inertia (rocking) or polar moment of inertia (torsion) of an equivalent disk (the same reservations apply here for the case of an embedded foundation as in the translational vibration modes [G4]). In this section, the derivation of the static-stiffness coefficient K_θ of the equivalent (massless) disk of radius r_o, subjected to a moment M resulting in a rotation θ, is presented (see Fig. 3.3). This disk, with moment of inertia (second moment of area) $I_o = (\pi/4) r_o^4$ for the rocking mode, is supported on the surface of a linearly elastic nonlayered homogeneous soil. The moment of inertia at any depth z may be expressed as $I = I_o (z/z_o)^4$. Substituting the moment-rotation relationship $M = E_c I \partial\theta/\partial z$ into the equation of static equilibrium of an infinitesimal element within the cone at depth z yields:

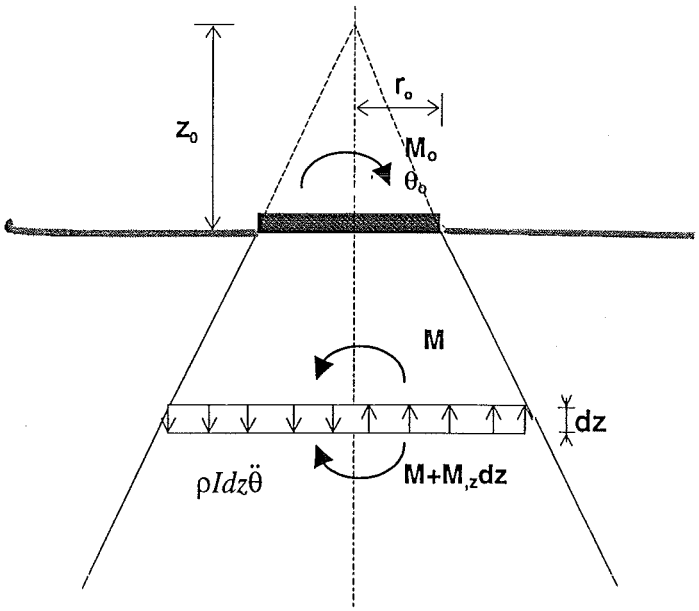

Fig.3.3: Cone model of soil beneath rigid foundation for rotational degree-of-freedom (adapted from Wolf [W12]).

$$-M + M + \frac{\partial M}{\partial z} dz = 0 \tag{3.29}$$

leads to:

$$\frac{\partial^2 \theta}{\partial z^2} + \frac{4}{z} \frac{\partial \theta}{\partial z} = 0 \tag{3.30}$$

The solution of Eq. 3.30 is of the form $\theta = z^\alpha$ which, when substituted into Eq. 3.30, leads to:

$$\alpha^2 + 3\alpha = 0 \Rightarrow \alpha_1 = 0 \ , \alpha_2 = -3 \tag{3.31}$$

The solution is thus:

$$\theta = c_1 + c_2 \frac{1}{z^3} \tag{3.32}$$

Enforcing the boundary conditions, $\theta(z = z_o) = \theta_o$ and $\theta(z = \infty) = 0$, allows the determination of the coefficients c_1 and c_2. Equation 3.32 is therefore:

$$\theta = \theta_o \left(\frac{z_o}{z} \right)^3 \tag{3.33}$$

Recalling the moment-rotation relationship:

$$M_o = -M(z = z_o) = -E_c I_o \frac{\partial \theta_o}{\partial z} \tag{3.34}$$

Substituting Eq. 3.33 into Eq. 3.34 results in:

$$M_o = \frac{3E_c I_o}{z_o} \theta_o \tag{3.35}$$

The static stiffness of the disk is therefore:

$$K_\theta = \frac{3E_c I_o}{z_o} \tag{3.36}$$

The torsional static stiffness may be derived in an analogous manner with the shear modulus G_s and polar moment of inertia $I_o = (\pi/2) r_o^4$ substituted in lieu of E_c and I_o respectively. Expressing the moduli in terms of the respective wave velocities yields:

$$K_\theta = \frac{3\rho v^2 I_o}{z_o} \tag{3.37}$$

where v equals v_p for the rocking mode and v_s for the torsional mode.

3.4.4 Aspect Ratios of Cone Models

From the static stiffness coefficients of the cone models derived above, it is now possible to derive their aspect ratios. This is achieved by equating the static stiffness of the cone model (derived above) to the rigorous solution of the disk with radius r_o on the surface of a half-space derived by other researchers (e.g. [G2, G6, P1] and reproduced in Table 3.2) for each degree-of-freedom. As an example, this will be presented below for the vertical vibration mode.

Equating Eq. 3.28 to the static-stiffness coefficient of a disk on a half-space:

$$\frac{\rho v^2 \pi r_o^2}{z_o} = \frac{4\rho v_s^2 r_o}{1-\nu_s} \tag{3.38}$$

leads to:

$$\frac{z_o}{r_o} = \frac{\pi}{4}(1-\nu_s)\left(\frac{v}{v_s}\right)^2 \tag{3.39}$$

It may be seen from Table 3.2 that the cone model approach differs from other methods in that the opening angle of the cone is a function of the Poisson's ratio of the soil and not a fixed value (e.g. 45° as assumed by Gazetas and Dobry [G3]).

Mode of vibration	Horizontal	Vertical	Rocking	Torsional
Static stiffness	$8G_s r_o/2-\nu_s$	$4G_s r_o/1-\nu_s$	$8G_s r_o^3/3(1-\nu_s)$	$16G_s r_o^3/3$
Aspect ratio z_o/r_o	$\frac{\pi}{8}(2-\nu_s)$	$\frac{\pi}{4}(1-\nu_s)\left(\frac{v}{v_s}\right)^2$	$\frac{9\pi}{32}(1-\nu_s)\left(\frac{v}{v_s}\right)^2$	$\frac{9\pi}{32}$

Table 3.3: Static stiffness coefficients of rigid disk on surface of half-space [G2] and aspect ratios of truncated semi-infinite cone models [W8].

3.4.5 Dynamic Stiffness Coefficients of Cone Model

3.4.5.1 Translational Mode of Vibration

The same infinitesimal element as shown in Fig. 3.2 is subjected to a harmonic force resulting in inertial forces in the element:

$$-N + N + \frac{\partial N}{\partial z}dz - \rho A \ddot{w} dz = 0 \tag{3.40}$$

The wave propagation equation results from substitution of Eq. 3.21 into Eq. 3.40:

$$\frac{\partial^2}{\partial z^2}(zw) - \frac{1}{v_p^2}\frac{\partial^2}{\partial t^2}(zw) = 0 \tag{3.41}$$

If only outwardly propagating waves are considered, the solution of Eq. 3.41 is:

$$zw = z_o f\left(t - \frac{z - z_o}{v_p}\right) \tag{3.42}$$

where f is an arbitrary function which is equal to $f(t) = w_o$ when $w(z = z_o) = w_o$, leading to:

$$w = \frac{z_o}{z} w_o \left(t - \frac{z - z_o}{v_p} \right) \tag{3.43}$$

The first derivative of Eq. 3.43 with respect to z (i.e. the strain along the wave path) is:

$$\frac{\partial w}{\partial z} = -\frac{z_o}{z^2} w_o \left(t - \frac{z - z_o}{v_p} \right) - \frac{z_o}{z v_p} w'_o \left(t - \frac{z - z_o}{v_p} \right) \tag{3.44}$$

where w'_o is the first derivative of w_o with respect to the argument $[t - (z - z_o / v_p)]$.

Applying Eq. 3.44 into Eq. 3.21 at $z = z_o$ leads to:

$$P_o = -N(z = z_o) = \frac{\rho v_p^2 A_o}{z_o} w_o + \rho v_p A_o \dot{w}_o \tag{3.45}$$

where $\dot{w}_o = w'_o (t - (z - z_o)/v_p)$ at $z = z_o$. The definition $E_c = \rho v_p^2$ was incorporated in the right-hand side of the equation. Equation 3.45 is the force-displacement relationship for vertical vibration that may be generalized to express both components of translational motion, i.e. vertical and horizontal, as follows:

$$P_o = \frac{\rho v^2 A_o}{z_o} w_o + \rho v A_o \dot{w}_o \tag{3.46}$$

or $$P_o = K w_o + C \dot{w}_o \tag{3.47a}$$

with $$K = \frac{\rho v^2 A_o}{z_o} \tag{3.47b}$$

and $$C = \rho v A_o \tag{3.47c}$$

defining the frequency independent stiffness and damping coefficients, respectively. The value of v is equal to v_p for vertical translations when $\nu \leq 1/3$ and is equal to v_s for horizontal modes of vibration. The formulation for the nearly incompressible state (i.e. when $1/3 < \nu \leq 1/2$) will be presented in a subsequent section (Section 3.4.6) as this case necessitates the consideration of certain aspects (Section 3.4.2).

3.4.5.2 Rotational Mode of Vibration

The dynamic equilibrium of an infinitesimal element within the cone model in rocking (Fig. 3.3) may be expressed as:

$$-M + M + \frac{\partial M}{\partial z} dz - \rho I \ddot{\theta} dz = 0 \tag{3.48}$$

where M is the moment applied on the element and θ is the ensuing rotation. Recalling the moment-rotation relationship $M = E_c I \partial\theta/\partial z$ and substituting in Eq. 3.48 leads to:

$$\frac{\partial^2\theta}{\partial z^2} + \frac{4}{z}\frac{\partial\theta}{\partial z} - \frac{1}{v_p^2}\frac{\partial^2\theta}{\partial t^2} = 0 \tag{3.49}$$

This is the wave-propagation equation for the rotational mode of vibration corresponding to the translational mode expression of Eq. 3.41. Assuming a harmonic excitation which elicits a response of the form $\theta(\omega) = \theta_o e^{i\omega t}$, where θ_o is the amplitude of the response, and substituting into Eq. 3.49 yields:

$$\frac{\partial^2\theta(\omega)}{\partial z^2} + \frac{4}{z}\frac{\partial\theta(\omega)}{\partial z} - \frac{\omega^2}{v_p^2}\theta(\omega) = 0 \tag{3.50}$$

The solution of this equation in the asymptotic limit of high-frequency excitation is of the form:

$$\theta(\omega) = \theta_o(\omega)\left(\frac{z_o}{z}\right)^m e^{-i\frac{\omega}{v_p}(z - z_o)} \tag{3.51}$$

in which the prescribed rotation $\theta(\omega)$ elicits waves propagating only in the positive x-direction with amplitude $\theta_o(\omega)$. The exponent m in Eq. 3.51 is determined by substituting Eq. 3.51 into Eq. 3.50:

$$m^2 - 3m + \frac{i\omega z}{v_p}(2m - 4) = 0 \tag{3.52}$$

For the solution at the asymptotic limit, $\omega \to \infty$, the imaginary term of Eq. 3.52 dominates and $m = 2$ is obtained. Equation 3.51 is thus:

$$\theta(\omega) = \theta_o(\omega)\left(\frac{z_o}{z}\right)^2 e^{-i\frac{\omega}{v_p}(z - z_o)} \tag{3.53}$$

Substituting the derivative of Eq. 3.53 at $z = z_o$ into the moment-rotation relationship $M_o(\omega) = E_c I_o \dfrac{\partial\theta_o(\omega)}{\partial z}$, yields:

$$M_o(\omega) = \left(\frac{2\rho v_p^2 I_o}{z_o} + i\omega\rho v_p I_o\right)\theta_o(\omega) \tag{3.54}$$

From this equation, the following coefficients in the high-frequency limit may be identified, expressed in terms of the general wave velocity v:

$$K_{\theta\infty} = \frac{2\rho v^2 I_o}{z_o} \tag{3.55a}$$

$$C_\theta = \rho v I_o \tag{3.55b}$$

Comparing the damping coefficients expression for the translational (Eq. 3.47c) and rotational (Eq. 3.55b) modes of vibration, the independence of these terms from the height of the cone z_o is noted.

The semi-infinite prismatic rod is represented by the cone model at $z_o = \infty$. This results in K from Eq. 3.47b being equal to zero and the damping C equal to ρv_p in the vertical direction and ρv_s in the two tangential directions (Eq. 3.47c). This verifies the aforementioned (Section 3.4.1) doubly-asymptotic nature of the dynamic stiffness coefficients derived by the cone model.

3.4.6 *Discrete-Element Representation of the Foundation-Soil System*

In the preceding sections, the dynamic impedance coefficients of the semi-infinite truncated cone were derived. In this section, the incorporation of these coefficients into an equivalent spring-mass-dashpot system, i.e. the formulation of the discrete-element model, will be presented. For the case of the translational degrees-of-freedom, this entails the incorporation of the dynamic-stiffness coefficients into a spring-mass-dashpot system attached to the underside of the basemat (Fig. 3.4). The properties of this system are defined by the force-displacement relationship of Eq. 3.47a:

$$P_o = K w_o + C \dot{w}_o \tag{3.47a}$$

with $$K = \frac{\rho v^2 A_o}{z_o} \tag{3.47b}$$

and $$C = \rho v A_o \tag{3.47c}$$

where, for $v \le 1/3$, $v = v_s$ for horizontal translation and $v = v_p$ for vertical translation. An added mass is incorporated for the vertical degree-of-freedom in a nearly incompressible soil mass ($1/3 < v_s \le 1/2$), as follows (see Section 3.4.2 and Table 3.1):

$$P_o = K w_o + C \dot{w}_o + \Delta M \ddot{w}_o(t) \tag{3.56}$$

where the trapped mass ΔM is determined from curve-fitting to be equal to:

$$\Delta M = \mu \rho r_o^3 \tag{3.57}$$

with $$\mu = 2.4\pi(\nu_s - 1/3) \tag{3.58}$$

and $v = 2v_s$ (3.59)

These equations, 3.47a and 3.56, are the rigorous discrete-element representations of the translational cone with frequency-independent coefficients.

The situation is slightly more complicated for the rotational degree-of-freedom as the moment-rotation relationship involves the recursive evaluation of a convolution integral (since the numerical quadrature is an inefficient and impractical solution technique). This convolution integral, defined by Wolf [W8] as the regular or lingering part, represents the "memory" of the moment-rotation formulation as it depends on all previous values of the rotational velocity.

The moment-rotation formulation is expressed as:

$$M_o(t) = K_\theta \theta_o(t) + C_\theta \dot{\theta}_o(t) - \int_0^t h_1(t-\tau) C_\theta \dot{\theta}_o(\tau) d\tau \qquad (3.60a)$$

where K_θ and C_θ are given in Eqs. 3.37 and 3.55b as follows:

$$K_\theta = \frac{3\rho v^2 I_o}{z_o} \qquad (3.37)$$

and $C_\theta = \rho v I_o$ (3.55b)

The first two terms of Eq. 3.60a are known as the singular part or the instantaneous contribution to the response as they are functions of the current values of the rotation and rotational velocity, θ_o and $\dot{\theta}_o$, respectively. The negative integral is the aforementioned convolution integral in which the first term is the unit-impulse response function:

$$h_1(t) = \frac{c}{z_o} e^{-\frac{v}{z_o}t} \quad \text{for } t \geq 0 \qquad (3.60b)$$

$$= 0 \quad \text{for } t < 0 \qquad (3.60c)$$

The singular part of Eq. 3.60a represents the cone model with the corresponding implication of exact results for the limits of high- and low-frequency excitation. The regular (convolution integral) term is pertinent only in the intermediate-frequency range. This term may be implicitly incorporated in the discrete-element model, shown in Fig. 3.4, as an additional internal degree-of-freedom θ_1 with a connected mass moment of inertia M_θ:

$$M_\theta = \rho z_o I_o \qquad (3.61)$$

Equation 3.60a applies for the torsional degree-of-freedom with $v = v_s$ and $I_o = \pi r_o^4/2$. For the rocking degree-of-freedom when $v_s \leq 1/3$, the definitions $v = v_p$ and $I_o = \pi r_o^4/4$ apply for the wave velocity and mass moment of inertia, respectively. However, for nearly incompressible soil ($1/3 < \nu_s \leq 1/2$), the incorporation of an additional mass to the singular part of Eq. 3.60a becomes necessary (Section 3.4.2 and Table 3.1):

$$M_o(t) = K_\theta \theta_o(t) + C_\theta \dot{\theta}_o(t) + \Delta M_\theta \ddot{\theta}_o(t) - \int_0^t h_1(t-\tau) C_\theta \dot{\theta}_o(\tau) d\tau \qquad (3.62)$$

where $\Delta M_\theta = \mu_\theta \rho r_o^5$ (3.63)

$$\mu_\theta = 0.3\pi(\nu_s - 1/3) \qquad (3.64)$$

and $v_p = 2v_s$, $I_o = \pi r_o^4/4$.

In order to demonstrate the equivalence of the assumed discrete-element models to the moment-rotation relationships (Eqs. 3.60a and 3.62), the case of Eq. 3.60a will be presented below.

The equations of dynamic equilibrium for the two degrees of freedom, θ_o and θ_1, are as follows:

$$M_o = K_\theta \theta_o + C_\theta(\dot{\theta}_o - \dot{\theta}_1) \qquad (3.65)$$

$$C_\theta(\dot{\theta}_1 - \dot{\theta}_o) + M_\theta \ddot{\theta}_1 = 0 \qquad (3.66)$$

Substituting C_θ from Eq. 3.55b and M_θ from Eq. 3.61 into Eq. 3.66 results in:

$$\frac{z_o}{v}\ddot{\theta}_1 + \dot{\theta}_1 = \dot{\theta}_o \qquad (3.67)$$

In order to solve this second-order ordinary differential equation (first-order with respect to $\dot{\theta}_1$), a correspondence is established with the solution of the equation for the translational degree-of-freedom case in the following manner. Equation 3.47a, shown again below:

$$P_o = K w_o + C \dot{w}_o \qquad (3.47a)$$

may be expressed as:

$$\frac{z_o}{v}\dot{h}_1 + h_1 = \frac{P_o}{K} = \delta(t) \qquad (3.68)$$

where $h_1 = w_o$ is the unit-impulse response function for the translational cone and $\delta(t)$ is the Dirac-delta impulse. The solution of this unit-impulse response function is similar to that of Eq. 3.60a and Eq. 3.62, (see Equations 3.60b and c).

The solution of Eq. 3.68 is obtained by determination of the Duhamel's integral, representing the total response of the contributions of the infinitesimal pulse $(1/K)P_o(\tau)d\tau$ to the unit-impulse response function $h_1\ (t-\tau)$ for the time-interval $(t-\tau)$:

$$u_o(t) = \int_0^t h_1(t-\tau)\frac{P_o(\tau)}{K}d\tau \qquad (3.69)$$

Noting that Eq. 3.67 is analogous to Eq. 3.68, therefore the solution of the former equation is analogous to Eq. 3.69 as follows:

$$\dot{\theta}_1(t) = \int_0^t h_1(t-\tau)\dot{\theta}_o(\tau)d\tau \qquad (3.70)$$

Substitution of this equation into Eq. 3.65 yields Eq. 3.60a, thereby establishing the coincidence of the discrete-element representation with the moment-rotation relationship of a disk on a homogeneous half-space, derived from the cone model.

3.4.6.1 Alternative Method of Derivation of Lumped-Parameter Model Coefficients

In parallel with the above derivations, a mathematical derivation of consistent lumped-parameter models has also been postulated by Wolf [W7].

Conventional lumped-parameter representations (e.g. [R2]) assume an initial spring-mass-dashpot configuration with unknown coefficients. A transfer function in the frequency domain is derived which is a non-linear function of these unknown coefficients. The coefficients are subsequently determined through the application of suitable curve-fitting techniques (over the frequency range of interest) between the transfer function and the exact value determined from a rigorous solution, such as the boundary element method. The drawbacks of this method may be enumerated as follows:

- Some of the coefficients derived in this manner may be complex numbers necessitating the application of special algorithms in the dynamic analysis. This restricts the applicability of conventional dynamic analysis software.
- The assumed configuration of the spring-mass-dashpot system, upon which the transfer function is based, will determine the likelihood of obtaining real coefficients. An inappropriate selection will lead to a system of non-linear equations from the curve-fitting process and complex coefficients. In addition, stability is not guaranteed. This means that the validity of the initial configuration can only be ascertained at the end of the analysis when the deviation of the derived coefficients from the real values is assessed.

These factors have compelled researchers to formulate a systematic procedure for the determination of the (real) coefficients of the assumed lumped-parameter model. The procedure postulated by Wolf [W7] overcomes the above deficiencies. This technique may be summarized as follows.

The dynamic stiffness coefficient in the frequency domain (Eq. 3.6 expressed in terms of the dimensionless frequency) is taken as the transfer function. This coefficient is decomposed into a singular part (which is equal to its asymptotic value at the limit $a_o \rightarrow \infty$) and the remaining regular part. This regular part is approximated as a ratio of two polynomials in ia_o with the degree of the numerator being one less than the denominator (i.e. *m-1* assuming the degree of the latter is *m*). This ratio is expressed as a partial-fraction expansion and the *2m-1* real coefficients are determined through a curve fitting technique based on the least-squares method. Each term of the resulting expansion (containing real coefficients) represents a discrete-element model with varying degrees of approximation. The coefficients of the singular part are:

$$S_s(a_o) = K(k + i a_o c) \tag{3.71}$$

where a_o is the dimensionless frequency ($\omega r_o / v_s$), K is the static stiffness, k and c are the non-dimensional coefficients of the spring and dashpot. For the translational degree-of-freedom in the horizontal direction c may be determined by equating the second term in Eq. 3.71 to Eq. 3.47c:

$$\frac{i\omega K r_o}{v_s} c = i\omega A_o \rho v_s \tag{3.72}$$

For the vertical and rotational degrees of freedom, v_s is replaced by v_p and the foundation area A_o is replaced by the second moment of area I_o. The non-dimensional spring coefficient (k) vanishes for a plane basemat-soil interface.

3.5 Soil Properties Incorporated in this Study

In order to highlight the effects of soil-structure interaction on the structural configurations implemented in this study, soft soil conditions (sand) were assumed. The relevant soil properties for the soil-structure interaction model are presented in the table below. These were chosen from representative values cited in the indicated reference.

	Mass density (kg/m^3)	Shear wave velocity (m/s)	Dilatational wave velocity (m/s)	Poisson's ratio
Sand	1750	81.2	152	0.3

Table 3.4 : Properties of sand incorporated in soil-structure interaction model [D4].

Since this study involves conventional multi-storey structures, it was not deemed necessary to complicate the analysis through the incorporation of a large number of soil parameters. Only those parameters that are necessary to elucidate the differences in the neglect of the soil mass on the dynamic response of the structure were incorporated. For this reason aspects such as the effects of soil porosity, water content, effective confining stresses, etc. were not investigated.

Reference [E5] presents the characteristics of the soil profile prevalent in Christchurch. The top layer (25 meters) of the coastal region (extending from South New Brighton to Avonside) is predominantly sand (Silty sand to sand), while the City (Cathedral Square) consists of a top layer (approximately 10 meters) of peat of highly organic fine grained soils underlain by a thick layer (>25 meters) of predominantly gravelly material. Thus, a seismic event in the Christchurch region will be highly susceptible to magnification due to these deep quaternary sediment deposits.

3.6 Summary

The consideration of soil-structure interaction has developed from foundations of machines [B1, G2] and nuclear energy facilities [L3, L18, L19] to more conventional civil engineering structures such as dams and multi-storey buildings [J3, W10]. Extensive analytical and numerical studies have been conducted to model this complex phenomenon and to facilitate the application of these findings into conventional design office practice. Comparisons of the actual response of structures to the predicted design response values has also been investigated [G1, Z1, Z2] in addition to experimental corroboration of the theoretical findings [C5, G5]. Many problems are inherent in the soil-structure interaction phenomenon; some of these relate to the determination of dynamic soil properties [A3, D3, H2-H6, L1, L8, P6, P7, Q4, R3, S4, S9 , T2], the modelling of the foundation with respect to embedment conditions, side-wall contact, and geometry of foundation [A6, B6, E6, F6, F7, G4, G6, H7, L14, M13, N8, S10, W6, W9, W11], while other factors include the site soil profile [L18-L20, W13].

The implementation of a simple mechanical model allows for the representation of the nonlinear behaviour of the soil and overcoming the approximations (pertaining to the boundary conditions) requisite in an analytical solution. The model implemented in this study is the basic lumped-parameter model presented by Wolf [W8]. The assumptions incorporated in this study in the application of this model are as follows:

- All foundations were designed as square surface foundations since the required embedment depth was considered to be negligible in comparison with the layer thickness. The presence of rigid tie beams ensured their stability in the lateral direction and enforced rigid behaviour of the foundation system (i.e. foundation flexibility was not considered).
- An unlayered homogeneous soil deposit (sand) supported the structures.
- Perfect bond existed between the supporting soil and foundations.
- Radiation damping only was assumed to exist in the soil mass due to the assumption of a Constant Damping model (5% for all modes) for the numerical model incorporated in RUAUMOKO [C1].

The main source of error in the numerical model lies in the 2-dimensional modelling of the 3-dimensional system. This gross simplification leads to an overestimation of the 2-dimensional radiation damping and an underestimation of the stiffness in comparison to the actual 3-dimensional case [M10].

A schematic representation of the soil-structure interaction model implemented in this study is shown in Fig. 3.4 incorporated under the foundations of the twelve-storey frame.

4. THROUGH-SOIL COUPLING

4.1 Introduction

When the proximity of structures is such that pounding is a realistic possibility, the transfer of dynamic response effects through the soil must also be taken into consideration. As in the case of soil-structure interaction (Chapter 3), the development of the dynamic response matrix of the soil mass to time-varying forces (impedance matrix) is an important step in the analysis process. The same precept applies for multiple foundation systems. However, in this case, the effect of the adjacent foundation is the introduction of certain modes of response that would not have been apparent in the single foundation case. In addition, some of the degrees-of-freedom will be coupled.

Although the study of soil-structure interaction has developed at a notable pace, the same cannot be said of the through-soil coupling problem. The development of comprehensive mathematical models, and the analytical or numerical solution thereof, are daunting tasks in light of the many parameters involved.

4.2 Solution Methods

Various analytical and finite element techniques have been utilized in the development of the dynamic stiffness matrix for multi-foundation systems. Warburton et al. [W2] implemented an averaging method in what is considered to be the first study of through-soil coupling effects. However, since this solution method is applicable only to relatively large separation distances and for limited frequency ratios, Lee et al. [L3] effected modifications to allow for small separation distances.

The boundary element method is widely used in modern numerical solution methods [e.g. L20, W13]. In this method, an equation is formulated which describes the three-dimensional wave propagation due to a surface excitation. The ensuing surface displacements are expressed as Green's functions, which are a set of boundary integral equations, the solutions of which are attained through the assumption of certain conditions with respect to displacement and/or stress conditions. These boundary integral equations are analogous to the assumed form functions of the finite element method.

Discretization of the foundation-soil interface (half-space Green's function) or of the entire surface of interest (full-space Green's function) is then effected. Other forms of Green's function that necessitate the discretization of interior points of the domain [L20] have been developed. Prescribed displacement field and/or stress distribution are the conditions which are enforced to arrive at a solution of the boundary integral equations. These equations are then solved numerically after their reduction to a set of linear algebraic equations. The next step is the enforcement of (displacement) compatibility at the foundation-soil interface, leading to the compliance matrix of the foundation-soil system.

The accuracy of the solution depends on the type of elements incorporated in the discretization process and the assumed boundary conditions. As regards the latter factor, the prescribed stress distribution (or variation of displacement field) under the footings is of particular importance. It has been found that the coefficients of the dynamic impedance matrix are highly dependent on the discretization scheme for small separation distances [W13]. One of the main drawbacks of this method is its inability to model nonlinear behaviour [N7].

The boundary element method is advantageous in the following respects:

- Only a surface discretization is necessary in the boundary element method, compared to the necessity of discretization of the full domain of interest in the finite element method. In this manner, only the soil surface (at the foundation-soil interface and also the area between the foundations) needs to be discretized.
- The boundary element method is capable of modelling an infinite domain whereas the finite element method is limited to the representation of limited domains.
- The radiation condition at infinity is satisfied automatically in the boundary element method without recourse to the implementation of complicated non-reflecting boundaries as is necessary in the finite element method.

Researchers have also implemented other solution methods such as the hybrid method [L9], the substructure deletion method [B4] and the combined method [Q1, Q2]. Modern solution methods utilize a combined boundary element-finite element approach [e.g. I2, K7, M17, and S1].

In addition to theoretical studies, experimental validation of the analytical and numerical results has also been conducted by a number of researchers [K8, S7].

4.3 Simplifying Assumptions Implemented in Through-Soil Foundation Interaction Studies

In light of the many analytical, semi-analytical and numerical methods incorporated in the development of the through-soil interaction model, various simplifying assumptions are required in order to achieve the solution of the pertinent system equations. These assumptions pertain to the structuring of the underlying soil (layered or half-space), foundation characteristics (shape, mass, rigidity, etc.), excitation characteristics (harmonic force or wave, form of wave, angle of incidence, etc.) and the presence of a supported structure.

Two forms of harmonic excitation are assumed in the various studies: a force applied externally on the structure or foundation and a plane (either vertically or obliquely incident) seismic wave. As such, the effects of through-soil interaction on the dynamic response of the foundation, or supported structure, are assessed through the comparison of either the impedance function (for the former loading situation) or the foundation input motion matrix (for the seismic wave excitation).

Most studies consider material (hysteretic) damping in the form of a damping factor [e.g. L3, L9, L15, L16, and R5] in addition to radiation damping. However, it has been observed that the only effect of increased damping is on the amplitudes of the response [L3, W2].

4.4 Findings of Through-Soil Foundation Interaction Studies

4.4.1 Analytical Study by Warburton et al. [W2]

The two-dimensional analytical study by Warburton et al. [W2] considered surface cylindrical foundations (with various height to diameter ratios), bonded to the surface of an elastic half-space. The influence of an adjacent (passive) foundation of similar geometry on the dynamic response of the excited foundation was investigated in addition to the response of the passive foundation itself.

The effect of the adjacent foundation was primarily the introduction of modes of vibration not observed in the single foundation case. Therefore, for the harmonic vertical excitations implemented in this study, small amplitude horizontal and rocking modes of vibration were identified (with the former smaller than the latter component of motion). The maximum response of both foundations was related to the resonant frequencies of a single mass system. Under harmonic vertical excitation, the vertical vibration was dominant and only slightly affected by the presence of the second mass.

As in the response of the excited mass, the maximum response of the passive foundation was related to the resonant frequencies of a single mass system. The vertical oscillation was independent of the cylinder height, with maxima occurring at the resonant frequency of the vertical translational mode associated with the mass of the passive foundation. For the case of zero cylinder height, the same observation with respect to the occurrence of maxima applied to the horizontal translational (in the direction of the axis connecting the foundation centers) and the rocking modes. For foundation heights greater than zero, coupling of the horizontal and rocking modes of vibration occurred, with the maxima of each of these modes coincident with the resonant frequencies of the coupled vibration mode for a single mass system.

Increasing the separation distance decreased the amplitudes of response of the passive foundation. However, under resonant conditions a noticeable rocking response at the periphery of the second mass was observed even at large separation distances, with an amplitude which exceeded the translational vibration of the excited mass.

4.4.2 *Effect of Through-Soil Interaction on Flexible Structures, Lee and Wesley [L3]*

The three-dimensional analytical study by Lee and Wesley [L3] investigated the three-dimensional through-soil coupled response of a group of flexible structures, representative of a nuclear installation. Two structural configurations were considered: the first was a three-structure system comprising two identical single degree-of-freedom (SDOF) oscillators and a third dissimilar SDOF model. The second case represented a two-structure system in which the superstructures were represented by two identical three-mode models. The containment structure was idealized as a single-mass oscillator and the prestressed concrete reactor vessel as a two-mass system. The foundations of these superstructures were modelled as circular, rigid disks bonded to the surface of an elastic half-space.

For the case of two adjacent SDOF structures, the following parameters were identified as influencing the effects of coupling on the dynamic response:

- Shear wave velocity of the soil (V_s).
- Inertia of the structures.
- Natural frequency of structures.
- Separation distance between structures.

As in the study by Warburton et al. [W2], the lateral response attained a maximum at resonance. The adverse effects of through-soil interaction increased for relatively stiffer structures. With the decrease of soil stiffness, the adverse effects of coupling were initiated at lower natural frequencies. For stiff soils, through-soil coupling had a beneficial effect throughout the range of oscillator natural frequencies investigated. These beneficial effects diminished with increasing stiffness of the supporting soil.

The foregoing conclusions were observed at a constant separation distance. Variation of this distance leads to a different trend. Increase of structural mass increased the beneficial effects of coupling throughout the natural frequencies and separation gaps investigated.

The analyses were then conducted in the presence of the third oscillator, which was assumed to be of lighter mass compared to the other two. All structures were assumed to possess the same natural frequency and the excitation was applied in two directions. The configuration of the three structures was such that the imaginary lines connecting the centers of their bases formed an isosceles triangle. The earthquake excitation was applied in two directions: lateral (Case A) and orthogonal (Case B) to the identical structures.

Small amplitude displacements perpendicular (lateral and vertical) to the direction of excitation were detected in the two identical structures. Rotations of the base slabs about the three principle axes were also noted. Comparison of the response in the direction of the applied excitation revealed significant reductions in the response of the identical structures. The third structure also experienced reductions of response, with the larger amplitudes in the case of the excitation orthogonal to the identical structures. These reductions were due to the modes of vibration of the two structures and the ensuing effects on the third structure; subtractive in Case A and additive in Case B. The peak response values of the identical structures were noted to be dependent on the resonant frequency of the third structure. In addition, it was noted that the presence of the third mass was analogous to the effect of a tuned-mass damper with respect to its influence on the magnitude and number of peaks in the response of the two identical structures.

For the case of the multi-mode systems, the structural masses were varied while maintaining constant natural frequencies. A reduction in the response for various separation ratios was witnessed. The same effect of structural mass as in the previous case was observed (i.e. increasing the structural mass increased the beneficial effects of coupling).

4.4.3 Finite-Element Approach of Roesset et al. [R5]

A finite-element formulation, incorporating a consistent boundary, was used to determine the interaction between two surface masses or two simple structures represented by SDOF systems. Two loading cases were considered; that of a harmonic force applied at one of the masses and a base motion. A three-dimensional solution was applied with sub-structure method. The underlying soil mass was a horizontally stratified layer on bedrock, with a depth equal to four times the length of the foundation side and a material (hysteretic) damping ratio of 5%.

The following response characteristics were observed:

- Under the effect of a horizontal harmonic excitation applied to one of the foundations, the presence of the second mass causes an amplification of the response at certain frequencies and a deamplification at others. Compared to the single foundation case, a shift in the natural frequencies at which these peaks occur was also observed. The through-soil interaction increases with increase in both masses (and of the passive foundation, especially). The horizontal translations induced in the passive mass increase with increasing mass. No vertical translations were detected below the cutoff (fundamental) frequency of the soil layer, but they become significant at frequencies close to the resonant frequencies of vertical excitation of each mass. Rocking was observed when both masses were equal to a mass ratio of 2 and was small in other cases.

- The dependence of the through-soil response on the frequency of excitation was apparent in the case of an excitation in the form of horizontal accelerations simulating ground motion. As in the previous case, in which a horizontal force was applied, the main effect of the adjacent mass is a shift in the frequency of the peak response. Peaks were apparent at the resonant frequencies of rotation and are dependent on the mass ratio of the two foundations.

The effect of through-soil coupling on the response of adjacent structures, idealized as single-degree-of-freedom structures, was also investigated. Various combinations of nondimensionalized stiffness and mass ratios were incorporated with the same excitations as applied in the case of foundation masses only. The difference in the case of the horizontal force was that it was applied at the top of one of the structures. Interaction effects were most prominent when both structures were of the same (compliant foundation) natural frequency and when the masses were large. The main

contribution of the increase in top storey horizontal displacement was from the base rotation.

In the case of seismic ground motion, interaction effects are highest when the two structures are of similar mass and stiffness. These effects are manifested in the form of double peaks in the response accompanied by a decrease in amplitude. As mentioned in the previous section, this is analogous to the effect of a tuned-mass damper.

The main findings of the study were:

- The appearance of modes of vibration which would not appear in the case of a single foundation. When the excitation is in the form of an external force applied to one of the structures or foundations, the ensuing response in the active foundation is due to a feedback from the adjacent passive structure. These "feedback responses" decay very rapidly with distance. The through-soil coupled response is much higher when the excitation is in the form of a ground motion (resulting in the excitation of both masses), with a slower rate of decay with respect to distance.
- A change is effected in the natural frequencies of the combined soil-structure system.
- The effect of the adjacent mass on the response of the active foundation, when the latter is excited by a horizontal force, is more pronounced on the rotational degrees-of-freedom than on the translational ones. The response of the passive foundation mass is comparable to that of the active foundation.
- When the foundation masses are excited by a base motion, the amplitudes of the translational vibration modes increase, with a reduction in the amplitudes of the rotational response. These effects are more pronounced with increasing masses and when their natural frequencies on an elastic foundation are similar.
- The same conditions as above, vis-a-vis natural frequencies and masses, exaggerate the increase in translational amplitudes in the case of adjacent structures when one mass is excited by a horizontal force applied at the top (i.e. at the level of the mass). This increase is caused by the base rotations.
- Through-soil interaction reduces the peak response of two adjacent structures excited by a base motion. This decrease is also attributed to the base rotations and is of the same order as the increase witnessed in the previous case (i.e. that of the horizontal force).

4.4.4 *Coupled Response of a Series of Shear Walls, Murakami et al. [M17]*

The through-soil interaction of a series of infinitely long (two-dimensional) equally spaced shear walls on an elastic homogeneous and isotropic half-space was investigated. The foundations were assumed to be rigid and semi-cylindrical. The applied ground motions were in the form of harmonic SH-waves (i.e. particle motion parallel to the long direction of the walls) with non-vertical incidence.

The analytic solution revealed the sensitivity of the input motion and the soil impedance function (force-displacement interaction matrix) to the presence of an adjacent foundation. The largest deviations from the case of a single foundation occurred at frequencies corresponding to the "Rayleigh frequencies":

$$\frac{\omega^* a}{v_s} = 2m\pi\frac{a}{b}(1 \pm \cos\Theta)^{-1} \; ; \qquad n = 0, 1, 2, 3, \ldots \tag{4.1}$$

at which constructive interference was effected between the incident waves and the scattered fields from the foundations. The values represented in this equation are as follows:

Θ = angle of incidence of the SH wave.

ω^* = frequency corresponding to the Rayleigh wavelength.

v_s = shear wave velocity in soil.

a = radius of semicircular foundation.

b = distance between centres of the foundations. (It is to be noted that the wave number in soil is the value $k = \omega / v_s$).

The base response at low excitation frequencies may be amplified due to through-soil interaction effects. For small separation distances, it was noted that for long wavelengths (i.e. low frequency excitations) coupling with more distant structures must be considered. For high frequency excitations, only the adjacent structures affect the base response of the building under consideration. It was also postulated that the coupling effects may account for the complex nature of the Fourier spectra of recorded earthquake strong motion.

It must be borne in mind that the results presented in this study do not account for coupled effects apparent in a three-dimensional analysis.

4.4.5 *Hybrid Method of Near- and Free-Field Discretization, Lin et al. [L9]*

In this study, the interaction effects between two square foundations embedded in a soil stratum whose depth is equal to the foundation width were investigated. A material damping factor (ζ = 0.05) was incorporated in the soil, to account for hysteretic damping. Only harmonic excitations were applied to the system. Both foundations were embedded to the same level with sides that were parallel to each other. Two cases were considered; embedded and surface foundations. For each of these two embedment conditions, different separations and configurations were investigated. One configuration is when the two foundations are aligned along the x-axis (passing through the centre of the foundations, i.e. the x-axis is an axis of symmetry) while the other is an alignment along the diagonals. In addition, various mass ratios of the two structures were analyzed.

It was found that the motions induced in the adjacent foundation are comparable to those of the active foundation, albeit of lower amplitude. Through-soil interaction was also found to effect coupling between various degrees-of-freedom. Coupling effects were also apparent in the case of adjacent foundations aligned along one of their diagonals. These effects, however, were less noticeable than when the foundations were aligned along the axes passing through their centres. For embedded foundations, the rocking induced by a horizontal excitation was affected significantly by the adjacent (embedded) foundation. When foundation inertia was considered, a reduction in the characteristic frequencies of the adjacent foundation was witnessed. This reduction was enhanced with foundation embedment.

4.4.6 *Rigid Structures with Arbitrary-Shaped Foundations, Kawakami et al. [K7]*

In this study, the response of arbitrarily shaped foundations supporting rigid structures to three types of vertically incident waves (SV-, SH-, and P-waves, i.e. in-plane, antiplane and vertical) was investigated. The supporting soil medium was assumed to be an elastic half-space. The effects of the excitation frequency and the magnitude of the separation distance were evaluated. The heights of the structures above the foundations were considered to be zero in order to cancel the effect of (single foundation) coupling between the horizontal and rocking response. The radii of the two foundations were assumed to be equal. Thus the influence of the individual foundation mass on the coupled response was also investigated in addition to the separation effects. A boundary element solution was effected in this study.

Varying the mass of the second foundation had a more perceptible influence on coupled response than the variation of the mass under consideration. The effect of coupling, i.e. increase or decrease, was contingent upon the separation distance and the frequency of excitation. The peak response shifted to a lower frequency with an increase in separation distance.

4.4.7 Multi-Structure System Embedded in Layered Soil, Imamura et al. [I2]

The seismic response of a nuclear reactor building embedded in two layered elastic half-space was studied. Rigid foundations, perfectly bonded to the underlying soil, were assumed and the effects of through-soil interactions were investigated.

The building under investigation was a reactor building that formed part of a three building nuclear reactor complex. The turbine and control buildings were, respectively, heavier and lighter than the reactor building. All superstructures were modelled as lumped-mass systems. The reactor building was embedded to a depth of 26 metres in the 18 metre deep surface layer. The embedment of the other two buildings was equal to this surface layer depth. The total depth of the supporting soil medium was 167 metres, with a shear wave velocity of 250m/s and 500m/s for the surface and underlying half-space layers, respectively. An artificially generated ground motion was incorporated as the excitation, with a maximum acceleration of 0.3g at a depth of 167 metres from the surface.

It was found that as the number of adjacent buildings increases, the response of the reactor building above ground level is amplified. On the other hand, the shear forces in the embedded portion decrease. It was also noted that the presence of a building of large inertia, compared to the building under investigation, affects the response of the latter building regardless of the direction (plane) of excitation. In other words, the presence of a heavy building (lying in the E-W direction of the building under investigation), transverse to the plane of the N-S excitation, will affect the response of the building under investigation through coupling effects. However, when the excitation is in the direction of alignment of the heavy structure (E-W excitation), the presence of the lighter control building in the transverse direction is minimal.

The effect of the soil between the structures on coupled response was also investigated. Three cases were considered: fully-filled case, in which soil was present between all the buildings, a partially-filled case, where only the region between the reactor building and control building (i.e. in the direction of excitation) was filled with soil, and the separated model. The embedded portion of the structures was

considered to be flexible and friction was neglected at all surfaces. The response of each of the structures (transfer functions with respect to the input motion) at ground level was compared.

It was observed that the maximum accelerations of the upper structures were affected by the presence of this soil while the foundations (i.e. embedded portions) were not. The maximum shear forces developed under the ground level were lowest in the fully-filled case. The shear forces developed in the embedded portions of all the structures were functions of the areas of contact of the structures with the surrounding soil.

4.4.8 *Dynamic Stiffness Matrix of Circular Surface Foundations, Liou [L15]*

Firstly, the foundation stiffness matrix for two independent circular foundations on the surface of an elastic half-space by the substructure technique was derived in this study. A numerical example was solved in which excitations were applied to the three-dimensional foundation system from all directions. A hysteretic damping ratio of ζ = 0.05 was incorporated in the complex shear modulus ($G_\zeta = G_s(1+2\zeta i)$). The effects of various clear separation distances on the dynamic stiffness matrices were determined.

The following general conclusions were drawn from this investigation.

- Low frequency excitations emphasize the through-soil interaction of adjacent foundations more than high frequency excitations.
- The influence on the imaginary parts of the dynamic stiffness functions due to the existence of another foundation is less significant than the influence on the real part.
- The effects of an adjacent foundation must be taken into account if the two foundations are in sufficient proximity ($d / r_0 \leq 4$ where d is the clear separation distance between the foundations and r_0 is the radius of the footing).

4.4.9 *Comparison of Analytically Determined Through-Soil Coupling Effects with the Provisions of ATC-3, Qian et al. [Q1]*

A boundary element solution of a three-dimensional system of massless rigid foundations was implemented in this study. These foundations were assumed to be perfectly bonded to the surface of an elastic half-space. Harmonic time-varying external forces were applied and the interaction between two and four foundations as a function of distance and excitation frequency was assessed. A set of four rigid, massless foundations, bonded to the surface of an elastic half-space, and with one

foundation subjected to a harmonic excitation, was studied. Through implementation of the boundary element solution developed in this study (allowing the use of higher-order elements), it was found that increasing the number of foundations increased the through-soil coupling effects for small foundation separation and low frequencies of excitation for vertical and *x*-direction translations. For pitching about the *y*-axis and torsion, through-soil coupling is apparent only for small separation distances and high vibration frequencies. The differences between the two and four foundation cases were small for the latter modes of vibration.

The ATC-3 [A4] gives approximate values for the horizontal translation and rocking soil dynamic stiffnesses, allowing for the reduction ΔV of the base shear V based on these soil-structure interaction effects. It states that consideration of through-soil coupling will reduce the dynamic stiffness of the soil, thereby increasing the factor ΔV. Neglect of through-soil interaction will, therefore, lead to conservative results.

The present study investigated this aspect and found that this assertion, i.e. that consideration of cross-interaction always reduces the dynamic stiffnesses of the soil when the foundations are closely spaced, is not always valid. In fact, the horizontal translational stiffness increases for a broad band of frequencies, while the rocking stiffness seems to be insensitive to through-soil coupling effects. In addition, increasing the number of footings does not always result in a greater cross-interaction effect.

4.4.10 Through-Soil Interaction of Flexible Footings by Combined Boundary Element and Finite Element Methods, Qian et al. [Q2]

A numerical method, based on the finite element and boundary element methods, was developed to determine the cross-interaction effects between adjacent flexible footings of arbitrary shape on the surface of an elastic half-space. The dynamic response of adjacent foundations, with various relative rigidities and separation distances, to harmonic and transient point load and distributed forces was examined.

The study suggests that, in practice, footings are to be treated as rigid when:

$$E = \frac{1}{12}\frac{E_f}{E_s}\left(\frac{h}{a}\right)^3 > 1.0 \qquad (4.2)$$

where E_f and E_s are Young's modulus of the footing and soil, respectively. The thickness of the foundation is h and its width is $2a$.

For the case of a single flexible foundation, it was found that the response depends on the distribution of the applied force if the footing is fairly flexible, which is also the case for the response of the active foundation in a two-foundation system. The response of the passive foundation appeared to be insensitive to the load distribution in the low-frequency range. However, the influence of the load distribution increased at higher frequencies of excitation. The passive footing did not influence the response of the active foundation. However, the passive foundation was affected by the presence of the active foundation and its response was a function of the separation distance and distribution of the applied load. In particular, for the flexible system under a point load, displacements induced in the passive footing may be significant over a wide range of frequencies while they decay rapidly for a stiff footing.

For a uniformly distributed load, the coupling effects between the footings decay rapidly at high frequency irrespective of the stiffness of the footings. In the case of the two foundation system under the action of a load suddenly applied to one of the footings, the response of the active footing may be significant during the loading period. The response of the passive footing, though quite small in magnitude, may continue for a longer time interval than that of the active footing.

4.4.11 Adjacent Foundations Subjected to Obliquely Incident Harmonic Waves, Qian et al. [Q3]

An analytical model was developed in this study to represent the through-soil coupling between two adjacent rigid, massless, or massive, 3-dimensional foundations of arbitrary shape. These foundations were assumed to be bonded to the surface of an elastic half-space.

The excitation implemented in this study was in the form of R- (Rayleigh, i.e. in which the vertical angle of incidence θ_V = 0), SV-, SH- (in-plane and antiplane shear, respectively) and P- (dilatational) harmonic waves defined by horizontal and vertical angles of incidence. The effects of through-soil coupling on the response of both foundations for a number of separation distances, types of seismic wave and angles of incidence were investigated.

In the case of the massless foundations, cross-interaction effects were manifested in the appearance of displacement components and fluctuations in the response not apparent in the single foundation case. A phase difference, due to wave transmission between the adjacent foundations, was also witnessed. The rotational components of motion were more affected by through-soil interaction effects than the translational degrees-of-freedom.

When the masses of the foundations were considered, it was noted that the resonant frequencies of the foundations were not affected by the presence of the adjacent foundation with small mass. The noticeable oscillations in the "upstream" foundation, due to coupling effects, decreased with increasing separation gap and increased with the increase of either mass. The "upstream" foundation response consisted of several peaks, due to the presence of the adjacent foundation, when both foundations were closely spaced and of sizable masses. Thus, the responses became more pronounced within a broader frequency range.

A marked phase difference was apparent in the response of the two foundations, indicating the likelihood of large rotational motions being developed in the case of structures subjected to seismic excitations.

4.4.12 Determination of Through-Soil Interaction by the Substructure Deletion Method, Betti [B4]

A boundary element formulation was developed to determine the interaction of adjacent three-dimensional, arbitrary shaped, embedded foundations. The supporting medium was modelled as an homogeneous viscoelastic half-space and the foundations were subjected to incoming SH-, P- and SV-waves with arbitrary angles of incidence in the horizontal and vertical directions. This study developed upon Reference [Q3] in that the effects of foundation embedment were investigated.

Comparisons were made between the extent of interaction between the two foundations for various types of motion. The interaction between the translational, rocking and torsional components of motion were quite conspicuous in the low-frequency range of excitations and tended to disappear with increasing frequency of incoming waves and distance between the foundations. The translational and rocking components of motion of the two foundations were either in-phase or 180^0 out-of-phase with respect to each other. The phase of the response of the foundations with respect to the free-field was a function of excitation frequency. These trends became more complicated for seismic waves impinging with various angles of incidence.

4.4.13 Experimental Studies

In addition to the analytical and semi-analytical studies mentioned above, experimental research has also been conducted to evaluate practically the effects of through-soil coupling and to validate the findings of theoretical studies.

The experimental results of Kobori et al. [K8] compared well with the response values obtained by the analytical solution of the equations of motion, despite the difficulty of

modelling the soil nonlinearity and layering effects. The properties of the surface layer were found to influence the through-soil coupling phenomenon to a large extent. A strong correlation was established between coupling effects and the direction of excitation.

The shake-table test of Shohara et al. [S7] modelled a typical nuclear reactor used in Japan. The excitations were in the form of sinusoidal shake table motions and impulse hammering in two orthogonal directions with respect to the foundation configuration. Larger through-soil coupling effects were observed in the case of the shake-table excitation mainly due to the influence of the adjacent foundation on the foundation input motion. While the effects of adjacent foundations on the displacement and acceleration response were limited, this was not the case for the stresses at the foundation-soil interface. The reduction of stresses at the edge closest to the adjacent foundation was noted, especially when the excitation was applied in the direction of foundation alignment. This was prompted by the small separation gap between the foundations, which induced the two foundations to act as a single unit.

For the determination of the impedance matrix, the hammering test was carried out with the load applied at two locations, at foundation level and at a certain distance above the foundation. An increase was noted in the sway (horizontal) and rocking elements of the impedance matrix for foundation 1 due to through-soil coupling, especially in the case of excitation in the direction of alignment. The only effect of the adjacent foundation on the effective input motion is a phase shift to a lower frequency.

Analytical tests were conducted by the finite element and boundary element methods and the results were compared with those obtained from the tests. Three-dimensional effects were accounted for in the two-dimensional analysis through the incorporation of dashpots. The impedance functions derived from the finite element analysis compared poorly with the test results. However, the transfer functions of the foundation acceleration versus the acceleration at the surface of the experimental setup compared well. The results from the 3-dimensional BEM compared well with the test results for all cases.

4.5 Mechanical Representation of Through-Soil Interaction

In the continuum method of soil-structure analysis, the soil medium is represented as an elastic half-space and the solution of the wave propagation equations is effected by various analytical, semi-analytical or numerical methods. This technique is, however, not amenable to straightforward implementation in standard design office software.

Various mechanical models have been proposed, ranging in complexity from the simple Winkler model to more sophisticated models based on boundary element solutions which are capable of simulating structure-soil-structure interaction. The through-soil interaction model developed by Mulliken [M16] is cited as an example of the latter models. In this study, the coupling functions were determined through the time-domain responses of the loaded and unloaded foundations to impulsive loads. Arbitrary coupling terms were assumed and the time-history response was compared with existing rigorous solutions. The time-domain boundary element solution of Huang [H8] was utilized as a paradigm. The coupling functions were modified iteratively until convergence with the rigorous boundary element solution was effected. The time-lag effects between the two foundations were also considered in the formulation.

In the present study, a through-soil interaction model is developed based on a beam element resting on a two-parameter foundation. This model is to be implemented in RUAUMOKO [C1] to simulate the normal and shear deformation characteristics of the soil between the foundations of the adjacent buildings. (The discrete-element soil-structure interaction model presented in Chapter 3 is representative of the force-deformation response of the supporting soil mass underlying the foundation footings whose inertial properties are included in the discrete-element model). Details of this beam element and the derivation of the pertinent two-parameter coefficients are presented in the following sections.

4.5.1 Development of a Basic Through-Soil Interaction Model

The simplest mechanical model implemented in the representation of soil behaviour is the Winkler spring. In this model, a spring with an experimentally derived coefficient (k_w) simulates the force-displacement properties of the soil mass. The soil pressure developed beneath the applied force is a function of the spring displacement ($p = k_w.w$).

The main shortcoming of the Winkler spring is inherent in its inability to simulate the continuous nature of the soil medium as its representation is restricted to the soil beneath the loaded region. In addition, the definition of the Winkler constant is problematic and is based, generally, on semi-empirical formulations (although a number of analytical definitions have been proposed, e.g. [V4]). The former deficiency (representation of continuity) has been obviated through the incorporation of interaction elements between the Winkler springs. These elements are in the form of elastic layers capable of pure shear deformations, elastic beams or elastic membranes. A second approach in the refinement of the basic Winkler model has

been the introduction of simplifying assumptions to the distribution of stresses and displacements in the analytical (elastic continuum) model. These modifications to the Winkler spring have led to the development of what is known as the two-parameter elastic model. This appellation is indicative of the two elastic constants necessary to define the model, compared to the single parameter (k_w) required in the basic Winkler model.

Either of the two approaches presented above (i.e. introduction of interaction elements to the Winkler spring or the incorporation of simplifying assumptions to the continuum equations) results in the following general form of the force-displacement relationship:

$$q(x) = kw(x) - k_1 \frac{d^2 w(x)}{dx^2} \tag{4.3}$$

The first term on the right-hand side of the above equation represents the simple Winkler model (with coefficient k) while the second term models the shear interaction between the adjacent Winkler springs. The applied loading is defined by $q(x)$ with the deflections (and the derivatives thereof) designated by w.

Although the derivations presented below are of a modified Winkler spring (which allows for the simulation of shear interaction, as expounded previously), the soil-structure interaction in this study is represented by the basic lumped-parameter model of Wolf et al. [W7,W8]. The through-soil interaction phenomenon is simulated by an element with properties derived from the shear interaction term (k_1) of the two-parameter element to be presented in the following sections.

4.5.2 *Elastic Beam on Two-Parameter Soil : Formulation of System Equation*

The problem may be represented by a beam element with four degrees-of-freedom (at either end a vertical translation w and rotation θ about the out-of-plane axis, see Fig. 4.1) resting on a two-parameter soil (Eq. 4.3). In matrix formulation, the displacements and loads are respectively expressed as $\{d\} = \{w_i, \theta_i, w_j, \theta_j\}$ and $\{r\} = \{Q_i, M_i, Q_j, M_j\}$(see Fig. 4.1).

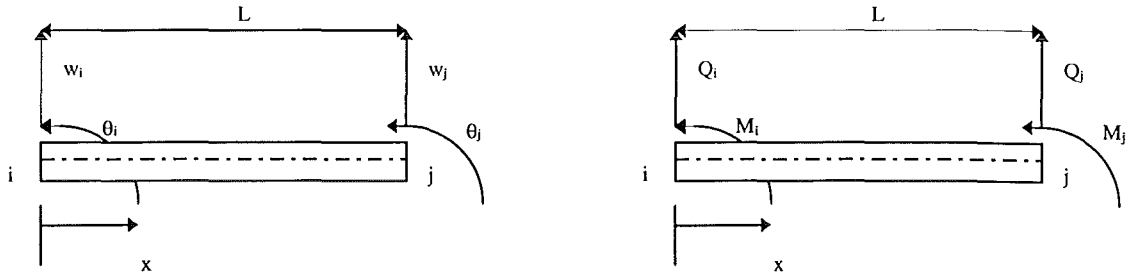

Fig. 4.1: Nodal degrees-of-freedom and corresponding nodal forces on beam element (adapted from Zhaohua et al. [Z3]).

It is to be noted that in the force matrix $\{r\}$, the shear force $Q(x)$ is the combined action of the beam shear and the foundation soil (represented by the second parameter k_1 of Eq. 4.3) as follows:

$$Q(x) = V(x) + V_1(x) \tag{4.4}$$

where $$V(x) = EI\frac{d^3 w(x)}{dx^3} \tag{4.5}$$

is the beam shear, and $$V_1(x) = -k_1\frac{dw(x)}{dx} \tag{4.6}$$

represents the shear contribution from the two-parameter foundation.

The governing system equation may be developed from the equilibrium of a differential beam element (neglecting transverse shear) and from elementary beam theory as follows (see Fig. 4.2):

$$\frac{dV(x)}{dx} = q(x) - p(x) \tag{4.7}$$

$$\frac{dM(x)}{dx} = V(x) \tag{4.8}$$

$$EI\frac{d^2 w(x)}{dx^2} = M(x) \tag{4.9}$$

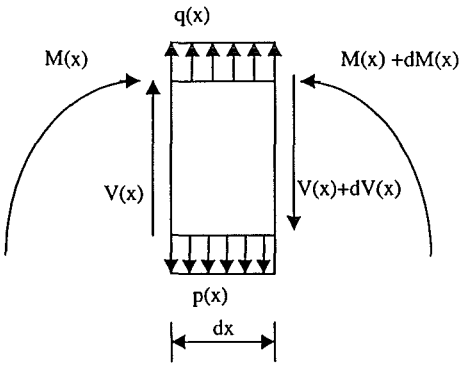

Fig. 4.2: Infinitesimal beam element on elastic foundation (adapted from Zhaohua et al. [Z3]).

From Eqs. 4.3 and 4.7 to 4.9, the governing differential equation of the bending of a beam on an elastic two-parameter foundation may be expressed as:

$$EI\frac{d^4 w(x)}{dx^4} - k_1\frac{d^2 w(x)}{dx^2} + kw(x) = q(x) \tag{4.10}$$

4.5.3 *Definition of Two-Parameter Model Coefficients*

Recourse is made to the method utilized by Vlazov and Leontiev [V5] in defining suitable expressions for the two coefficients k and k_1 appearing in Eq. 4.10 above. The derivation of these expressions is detailed below.

As mentioned in a preceding section, the improvements on the Winkler spring model, vis-a-vis its ability to simulate a continuous medium, followed two distinct approaches: the first was the incorporation of a physical shear interaction mechanism (shear beam or plate, membrane in tension, incompressible shear layer, etc.). The second method entailed the imposition of constraints with respect to the state of stress and/or displacement distribution in the equations defining the elastic continuum.

The model proposed by Vlazov and Leontiev [V5] was derived based on the application of Galerkin's variational principle to the analytical model of a linear elastic isotropic continuum. The state of strain was assumed to be of the form:

$$u(x,z) = 0 \qquad \text{and} \qquad w(x,z) = w(x).h(z) \qquad (4.11a,b)$$

where $u(x,z)$ and $w(x,z)$ are the x- and z-direction displacements, respectively. The distribution of the latter was assumed to vary with depth as $h(z)$. Linear and hyperbolic variations were two of the many forms of $h(z)$ assumed by Vlazov and Leontiev, as shown respectively in Eqs. 4.12 below:

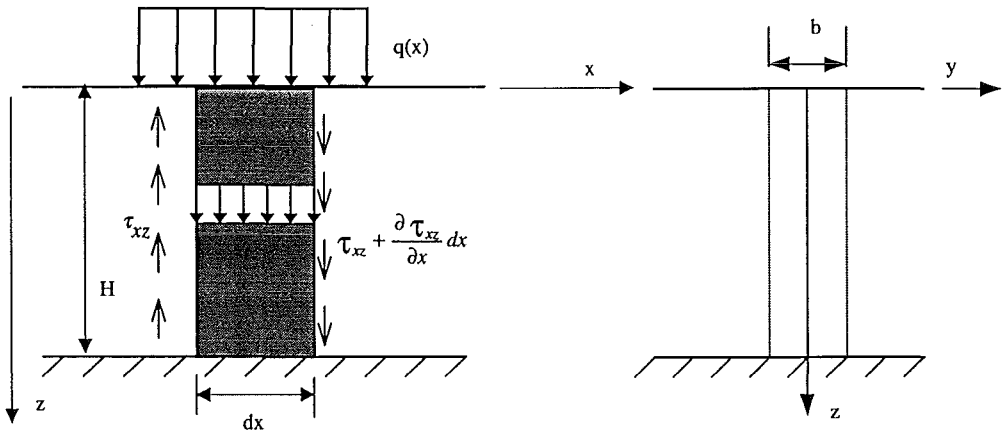

Fig. 4.3: Derivation of the Vlazov-Leontiev model (adapted from Selvadurai [S6]).

$$h(z) = \left(1 - \frac{z}{H}\right) \qquad \text{and} \qquad h(z) = \frac{sinh[\gamma(H-z)/L]}{sinh[\gamma H/L]} \qquad (4.12a,b)$$

The values of constants γ and L will be presented subsequently.

Under the assumption of plane strain conditions and applying Lagrange's Principle of Virtual Work to obtain the equation of equilibrium in the *z*-direction, the response function of the soil to an arbitrary load *q(x)* (see Fig. 4.3) is obtained:

$$q(x) = kw(x) - 2t\frac{d^2w}{dx^2} \tag{4.13}$$

which is similar in form to Eq. 4.3. The coefficients in Eq. 4.13 are defined as:

$$k = \frac{E_0}{(1-\nu_0^2)}\int_0^H \left(\frac{dh}{dz}\right)^2 dz \qquad t = \frac{E_0}{4(1+\nu_0)}\int_0^H (h)^2\, dz \tag{4.14a,b}$$

These expressions have the same physical definition as the coefficients k and k_1 of Eq. 4.3. Assuming a linear variation of displacement with depth z (Eq. 4.12a) leads to the following definitions of the two-parameter coefficients:

$$k = \frac{E_0}{H(1-\nu_0^2)} \qquad t = \frac{E_0 H}{12(1+\nu_0)} \tag{4.15a,b}$$

For the case of a relatively deep soil deposit, the hyperbolic variation of displacement (Eq.4.12b) was assumed. This leads to the following definitions of the two-parameter coefficients:

$$k = \frac{E_0 \gamma B}{2L(1-\nu_0^2)} \frac{sinh(\gamma.H/L)cosh(\gamma.H/L)+(\gamma.H/L)}{sinh^2(\gamma.H/L)} \tag{4.16}$$

$$t = \frac{E_0 LB}{8\gamma(1+\nu_0)} \frac{sinh(\gamma.H/L)cosh(\gamma.H/L)-(\gamma.H/L)}{sinh^2(\gamma.H/L)} \tag{4.17}$$

In the above expressions:

$$E_0 = \frac{E_s}{(1-\nu_s^2)} \qquad \text{and} \qquad \nu_0 = \frac{\nu_s}{(1-\nu_s)} \tag{4.18a,b}$$

where E_s and ν_s are, respectively, the elastic modulus and Poisson's ratio of the soil in terms of plane strain. The coefficient γ is a measure of the non-linear variation of normal strain with depth. The characteristic length L is defined from a parameter incorporated in the homogenous solution of Eq. 4.10, with k_1 and q both equal to zero:

$$EI\frac{d^4w}{dx^4} + kw = 0 \tag{4.19}$$

the solution of which is assumed to be of the following form:

$$w = (C_1 cos\lambda x + C_2 sin\lambda x)e^{\lambda x} + (C_3 cos\lambda x + C_4 sin\lambda x)e^{-\lambda x} \tag{4.20}$$

Our interest is focused on the parameter λ (of dimensions L^{-1}), which is equal to:

$$\lambda = \sqrt[4]{\frac{k}{4EI}} \tag{4.21}$$

Equation 21 is an indication of the relative soil to beam stiffness. The reciprocal of λ is the characteristic length. It describes the extent of lateral spread of vertical deformations on the soil surface resulting from the application of a load to a beam supported by the soil mass. This spread is due to the disparity in stiffnesses between the beam and supporting soil. For example, when the beam is very stiff with respect to the supporting soil, the characteristic length ($1/\lambda$) is large. This implies that a load applied to the beam will cause deflections of the beam and the soil to a considerable distance from the point of load application.

The definition of the elastic characteristic length L according to Vlazov and Leontiev [V5] is:

$$L = \sqrt[3]{\frac{2EJ(1-\nu_0^2)}{E_0 B}} \tag{4.22}$$

where $J=Bh^3/12(1-\nu_b^2)$ is the equivalent moment of inertia of the beam (or strip of slab) of width B and Poisson's ratio ν_b.

In analytical studies conducted on loaded flexible plates, Jones et al. [J6] implemented the exponential variation of Eq. 4.12b. They showed that the parameter (γ / L) is a function of the shape and flexibility of the plate in addition to the form of loading.

Chambers [C3] proposed a model representative of soil flexibility that was incorporated in RUAUMOKO [C1] as the GROUND element. This element allows the implementation of a number of analytical models to represent soil-structure interaction and through-soil coupling, one of which is the two-parameter model detailed above. However, many ambiguities prevail in the definition of the various parameters in the numerical model based on the hyperbolic variation of displacements with depth (Eq. 4.12b), as detailed in the preceding paragraphs. Therefore, an alternative definition of the two parameters of Eq. 4.13 is proposed in the following section. This model was subsequently incorporated as an option of the GROUND element in RUAUMOKO.

4.5.4 Alternative Definitions of Two-Parameter Model Coefficients

The definitions of the two-parameter coefficients k and k_1, presented in Eqs. 4.16 and 4.17, necessitate the assumption of pertinent values of γ and L. The ambivalence pertaining to the designation of appropriate values (let alone the definitions) of the

latter quantities may be obviated by applying alternative definitions for k and k_1 to those presented above [S6].

The coefficient of subgrade modulus k, expressed in terms of plane strain conditions, was defined rationally by Vlazov and Leontiev [V5] as:

$$k = \frac{E_s(1-\nu_s)B}{(1+\nu_s)(1-2\nu_s)} \int_0^\infty \left(\frac{dh(z)}{dz} \right)^2 dz \qquad (4.23)$$

where $h(z)$ is the assumed function describing the variation of vertical displacement with depth in the soil layer (see Eqs. 4.11, 4.12 and 4.14) and B is the beam width. The Young's modulus and Poisson's ratio of the soil in plane strain are designated by E_s and ν_s. These values are supplanted by E_o and ν_o, respectively, for plane stress conditions (see Eqs. 4.18). The function $h(z)$ is assumed in this case to vary exponentially, which is an acceptable approximation for an infinitely deep layer:

$$h(z) = e^{-\mu z} \qquad (4.24)$$

In Eq. 4.24, z is the depth and μ is a constant (of dimension L^{-1}) defining the rate of decay (with depth z) of the vertical displacement. It is also sometimes employed as a correlation constant to establish a best-fit with exact (continuum) solutions.

Substitution of Eq. 4.24 into Eq. 4.23 leads to the following definition of the coefficient of subgrade modulus:

$$k = \frac{E_s(1-\nu_s)}{(1+\nu_s)(1-2\nu_s)} \frac{\mu B}{2} \qquad (4.25)$$

The analytical solution for the maximum bending moments beneath an infinite beam loaded by a concentrated load and supported by a linearly elastic half-space was derived by Biot [B5]. The extension of this solution and the expression of the results in terms of displacements (in addition to other parameters) was achieved by Vesic [V4]. Based on these results, an expression correlating the Winkler coefficient with the results of the half-space solution was derived. Comparison of Eq. 4.25 with that proposed by Vesic leads to the following approximation of the product μB appearing in the former equation:

$$1 < \mu B < 2 \qquad (4.26)$$

In a soil with $\nu_s = 0.3$ and for infinitely long beams, $k = 0.65$ and Eq. 4.25 becomes:

$$\frac{E_s(1-\nu_s)}{(1+\nu_s)(1-2\nu_s)} \frac{\mu B}{2} = 0.65 \qquad (4.27)$$

resulting in a value of $\mu B = 1.06$. It has also been shown by Vlazov and Leontiev [V5] that the incorporation of a value of $\mu = 1.0$ for the case of a point load on an elastic half-space results in surface displacements slightly smaller than those obtained from the solution of the Boussinesq problem.

With regard to the second parameter (denoted as k_1 in Eq. 4.10 and $2t$ in Eq. 4.13), Vlazov and Leontiev [V5] proposed the following definition:

$$k_1 = \frac{E_0 B}{2(1+\nu_0)} \int_0^\infty h^2(z) dz \tag{4.28}$$

Assuming the same distribution of vertical displacements as given by Eq. 4.24 results in the following definition of k_1:

$$k_1 = \frac{E_0}{4(1+\nu_0)} \frac{B}{\mu} \tag{4.29}$$

or, for plane strain conditions:

$$k_1 = \frac{E_s}{4(1+\nu_s)} \frac{B}{\mu} \tag{4.30}$$

Fletcher and Herrmann [F4] developed graphical representations of the coefficients k and k_1 which provide the best-fit to the exact (continuum) solutions. The case that they considered was of an infinitely long beam subjected to a point load. The average modulus of the supporting soil was considered to be less than $2\text{x}10^2$-$3\text{x}10^2$ MN/m^2 (medium dense to dense sand). This restriction ensues from the assumption that the ratio of subgrade modulus to beam modulus (E_s / E) was less than 0.01 in the cases examined. This is why the ordinates of their graph are independent of the beam properties. Their results compare accurately with the continuum solution of an infinite beam on a half-space.

Upon comparison of the results of Fletcher and Herrmann [F4] with those obtained by Vlazov and Leontiev [V5], a discrepancy in the derivation of the values of the two-parameter coefficients is evident [S3]. For the case of an infinite beam, and assuming the Poisson's ratio of soil $\nu_s = 0.3$, Fletcher and Herrmann obtained $k / E_s = 0.49$. Substituting this value into Eq. 4.25 resulted in $\mu B = 0.728$. When this value of μB was substituted into Eq. 4.30, the resulting value obtained in Eq. 4.31:

$$\frac{4S}{E_s B^2} = 1.057 \tag{4.31}$$

$$\frac{4S}{E_s B^2} = 1.057 \qquad (4.31)$$

did not bear any semblance to the value of 7.6 obtained by Fletcher and Herrmann for a best-fit of deflection in the two problems. Therefore, Scott [S3] recommends the definition of S (also denoted as k_1, G or $2t$) as an independent curve-fitting parameter rather than relating it to k through the depth function $h(z)$ (Eq. 4.24).

A comparison is conducted in the present study between the results obtained from the numerical model presented in the preceding sections (Vlazov-Leontiev definition of the two-parameter model) and an analytical expression [S3] defining the maximum (static) displacement of a point-loaded beam (Appendix G). The maximum displacements under the point load obtained by the two methods compared well. In addition, the (numerically derived) variation of the deflections along the length of the elastic beam appeared to behave in a consistent manner. This validated the performance of the numerical model derived herein.

4.6 Summary

The choice of suitable physical models representative of through-soil interaction is not as extensive as those available for soil-structure interaction. This is due to the extensive number of variables involved in the former, hindering the development of mathematical formulations and solutions thereof. The analytical [L3, L15, M19, Q3, W2] and numerical [B4, I2, K7, L9, L16, Q1, Q2, R5, S1] studies conducted to date have revealed the significant influence of through-soil coupling on structural response. The effect of foundation mass, embedment and separation distance in addition to the influence of the excitation properties on the extent and characteristics of the coupling have been identified in the studies presented above.

The inconsistencies inherent in the through-soil interaction model developed by Chambers [C3] have been remedied in this study through the definition of the Vlazov two-parameter model [V5] in terms of an exponential variation of displacement with depth (Eq. 4.24). Parameter studies were conducted to investigate the influence of the coefficient μ on the response values (Appendix A). It was found that the variation of μ within the allowed range (Eq. 4.26) did not perceptibly influence the results. The verification of the validity of this model is presented in Appendix G in which the displacements of a beam resting on an elastic soil are compared with those obtained from an analytical expression (point load). This model was then incorporated in the present study to simulate the normal and shear deformation characteristics of the soil between the adjacent foundations. The applicability of this model to a dynamic

analysis in which soil-structure interaction is accounted for is contingent upon the incorporation of inertial effects. In the present study, these were accounted for in the discrete-element (cone model) simulating the soil mass directly beneath the foundation footings (see Chapter 3).

5. PRESENTATION OF RESULTS

5.1 Introduction

To the best of the author's knowledge, the only study that considers specifically the effects of soil-structure interaction on pounding structures is that by Schmid and Chouw [S2]. As outlined in Chapter 2, this study investigated an elastic system with impacts assumed to occur at the top storey of the shorter building only. The soil-structure system was discretised by a finite-element mesh while the superstructures were modelled by beam elements with continuously distributed mass. The authors concluded that soil-structure interaction was an important factor that must be considered in structural pounding studies due to its influence on the dynamic characteristics of the system.

The study by Anagnostopoulos et al. [A2] modelled viscoelastic foundation behaviour through a spring-dashpot system. The effects of pounding were investigated in elastic and inelastic multi-degree-of-freedom structures in which impact elements were incorporated along the heights of the structures. For the case of storey-to-storey pounding of two adjacent buildings of equal number of stories, it was shown that foundation compliance had a beneficial effect on the response. These benefits were manifested as reductions in storey shears (elastic analysis) and displacement ductilities (for an inelastic response), expressed as ratios of pounding to no pounding response values. Increasing the soil flexibility increased these beneficial effects.

Kasai et al. [K5], in their survey of structural pounding damage which occurred during the 1989 Loma Prieta earthquake, noted the correlation between the incidence of pounding and the soil conditions prevalent at these sites. They postulated that the increased intensity of shaking due to soft soil conditions and/or the possible occurrence of structural settlement and rocking at these sites may have been contributing factors to pounding.

Valles and Reinhorn [V1] suggested a mathematical expression to determine the critical separation gap required to preclude pounding. In this equation, an expression accounting for foundation rotation due to soil-structure interaction effects was included.

The aim of the present study is the assessment of the effects of incorporating the influence of soil flexibility, i.e. soil-structure interaction and/or through-soil foundation coupling, on the dynamic response of impacting buildings colliding at storey levels only.

Two structural configurations are investigated: the first comprises two adjacent twelve-storey frames while the second case pertains to the pounding of a twelve-storey frame and an adjacent six-storey frame. Comparisons are made between the response values obtained from the following assumptions of foundation fixity conditions for each configuration:

- The conventional fixed-base assumption.
- The compliant foundation case (i.e. soil-structure interaction only is considered).
- The case allowing for through-soil interaction between the foundations of the adjacent structures.

The no pounding storey displacement response for two conditions of foundation fixity (fixed and compliant) are first compared. The force-displacement response of the supporting soil mass directly beneath each of the individual foundation footings is expressed through the discrete-element model presented in Chapter 3. The pounding case is subsequently examined and the effects of various separation gaps on the dynamic response of the impacting systems are compared. This allows the assessment of the degree of approximation of conventional pounding analyses, which ignore the effects of soil-structure interaction. A further refinement is implemented in which through-soil interaction effects are incorporated and the results compared with the previous cases. The two-parameter model (Chapter 4) represents the soil between the exterior foundations of the adjacent buildings, the distance of which is assumed to be constant at 5.00 meters.

5.2 Definitions

In order to maintain brevity and clarity in this chapter a number of terms are used throughout the following sections, the definitions of which are as follows:

- Configuration 1 designates the case of the two adjacent twelve-storey (Rahman and Tabuchi) frames. The second case is defined as Configuration 2 and involves the pounding of a twelve-storey (Rahman) frame and a six-storey (Jury) frame (see Fig. 5.1).
- A positive earthquake describes a seismic excitation applied from the direction of the Rahman frame for either of the two configurations. It is to be noted that the Rahman frame in both cases is located to the left of the adjacent twelve- or six-storey frame, depending on the configuration.

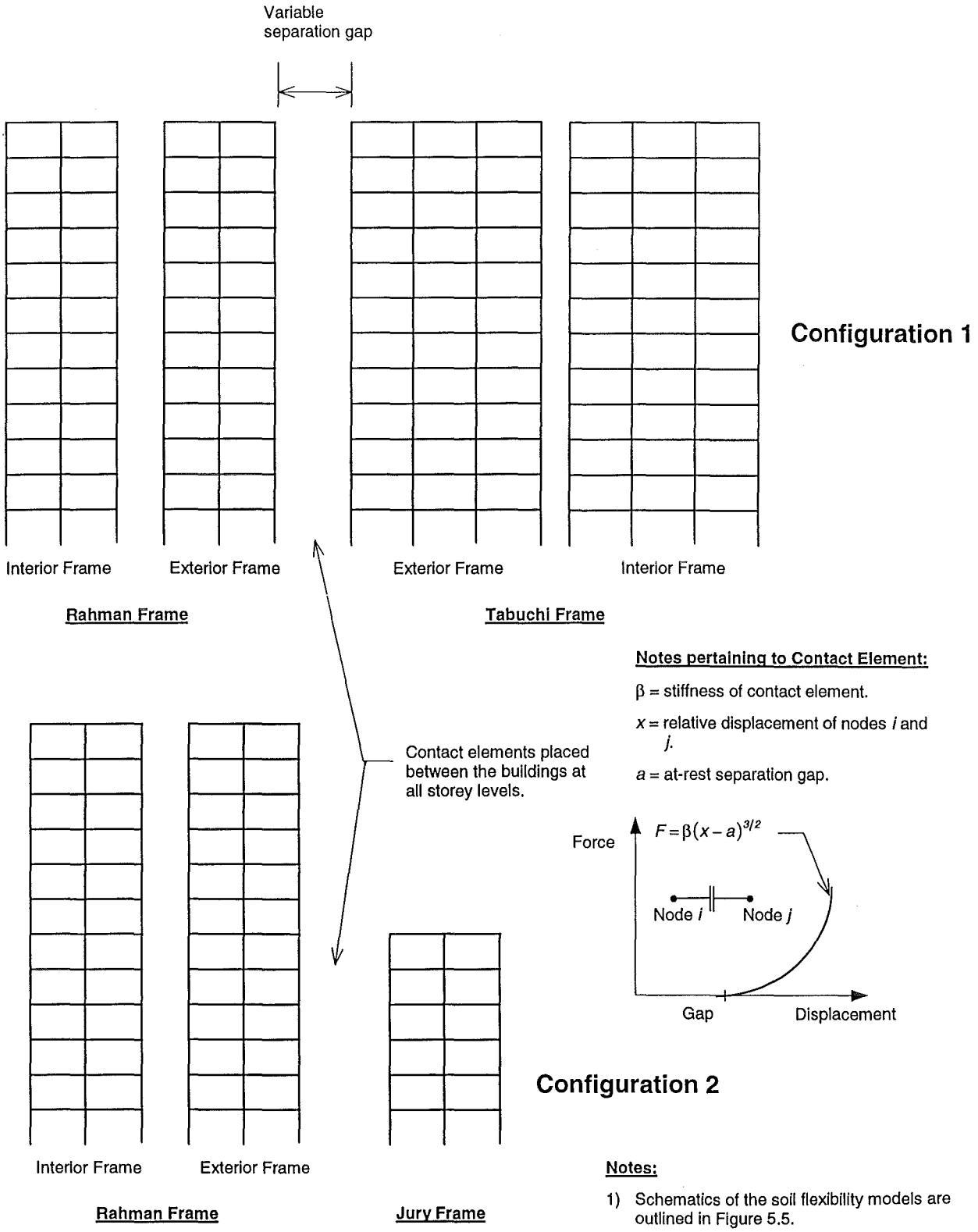

Fig. 5.1: Conceptual representation of the two configurations assumed in the numerical analyses.

- The sign convention in the software RUAUMOKO assumes positive shears as those that result in a counterclockwise couple (or, correspondingly, the transverse forces that are in the negative and positive y-directions at ends 1 and 2 of the member, respectively).
- Soil (or foundation) flexibility refers to the effects of soil-structure interaction (soil compliance) and/or through-soil foundation interaction on the structural systems.
- In this study, assessment of the effects of pounding is accomplished by means of two response values: storey displacements and impact-side column shears. Column moments will not be examined since the seismically induced moments are directly related to shear.
- In order to limit the copious volume of output produced by the analyses, only the time-histories relevant to the top stories are presented, when required. Additional response characteristics are presented in the relevant Appendices.
- The response amplification ratios represent the aforementioned response values normalized with respect to the fixed base no pounding cases.

5.3 Structural Models

Two structural systems are investigated in this study: a two twelve-storey configuration (Configuration 1) and a twelve- and six-storey configuration (Configuration 2). All structures are reinforced concrete moment-resistant frames of equal storey heights (3.65m) designed according to the principles of the capacity-design method [P4]. The twelve-storey two-bay Rahman frame (Fig. 5.2) is designed in accordance with the relevant New Zealand design codes [N5,N6]. The twelve-storey three-bay Tabuchi frame [C2] and the six-storey two-bay Jury frame [J7] (Figs. 5.3 and 5.4, respectively) were designed in compliance with earlier versions of the same codes. Details of the numerical models incorporated in RUAUMOKO are presented in Appendix F.

The mass ratio of the two twelve-storey buildings is approximately 1:2.5 (with the Tabuchi frame heavier than the Rahman frame) while the ratio of their fixed-base natural periods is 1:1.14. In the case of the twelve- and six-storey configuration, the mass ratio is 1:2.29 (the Jury frame is of lower mass than the Rahman frame) while the ratio of fixed-base periods is 1:2.32. In both configurations, the Rahman frame (more flexible in both cases) is located to the left of the Tabuchi and Jury frames (see Fig. 5.1).

5.3.1 Modelling Assumptions

For the numerical models implemented in RUAUMOKO [C1], a bilinear moment-curvature (post-yield stiffness, r = 10%) is assumed for all inelastic elements (beams and ground floor columns) of the Rahman frame. In the Tabuchi frame, all inelastic beams and columns are assumed to behave elastoplastically, while those of the Jury frame are modelled by the modified Takeda degrading stiffness hysteresis rule [O1]. These differences in the numerical models reflect the uncertainties pertaining to all aspects of the adjacent structure(s), which are often owned by different parties. The pounding response (1mm separation gap) of the compliant foundation Configuration 1 case was investigated for a post-yield stiffness of 2% in the Rahman frame (Figs. A.2). As can be seen, a significant difference is apparent, even in the Tabuchi frame response. The latter is attributable to the differences in impact forces for the two cases of post-yield stiffness, due to the difference in hysteretic damping in the two cases. The lower value of post-yield stiffness contributes to larger system damping thereby reducing the system pounding response. The lower hysteretic damping provided by the higher value of post-yield stiffness was considered to be sufficient in light of the additional (5%) continuous damping assumed for all modes.

The Constant Damping model [C1] (constant 5% damping for all modes) incorporated in this study obviated the need to specify different damping ratio for each of the sub-systems (i.e. the superstructures and the soil mass). Ideally, the soil material damping could have been represented by an appropriate hysteresis rule (such as the Ramberg-Osgood rule) or a suitable element (e.g. friction element [M13]). Leger et al. [L4] noted that for long-period structures (i.e. T > 1.5 seconds) the choice of a Rayleigh damping model (initial elastic stiffness or instantaneous tangential stiffness) does not affect the seismic response.

Analytical (SDOF models) and experimental (scale models) research has been conducted to determine the most suitable choice of damping model for different cases. Otani [O2] attempted to reproduce analytically the results of an experimental study of the inelastic response of a scale-model of a 3-storey reinforced concrete frame. The damping matrices used were mass-proportional and tangent (instantaneous) stiffness-proportional in which the proportionality coefficients were derived from the initial elastic properties. Otani found that for large-displacement oscillations either model was suitable. However, for low-amplitude displacements, the stiffness-proportional damping provided a better representation of the experimentally-derived results.

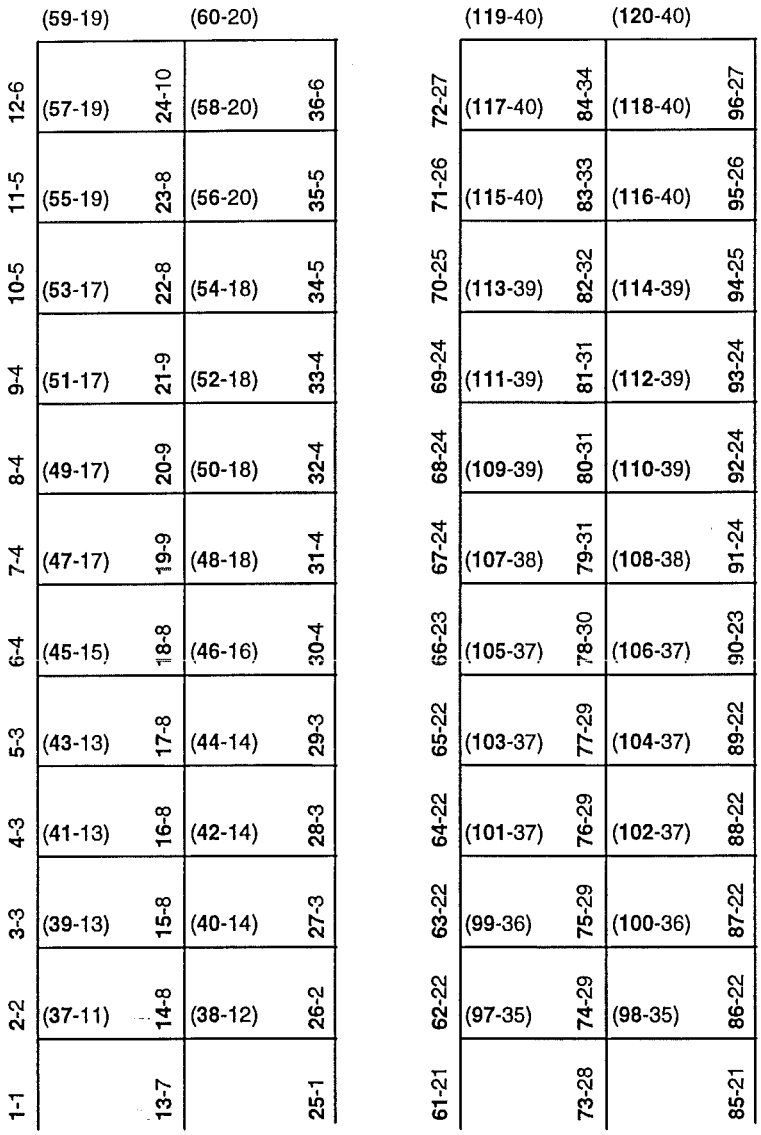

Interior Frame

Exterior Frame

Key: e.g. (97 - 35) = (**Member No.** - Member Type)

Rahman Frame

Interior Frame		
Mem. Type	**Level**	**Dim.**
Columns		
1-3	1-5	0.65x0.75 exterior
4	6-9	0.6x0.7 exterior
5-6	10-12	0.5x0.7 exterior
7-10	1-12	0.4x0.4 interior
Beams		
11-20	1-12	0.4x0.4

Exterior Frame		
Mem. Type	**Level**	**Dim.**
Columns		
21-22	1-5	0.65x0.75 exterior
23-24	6-9	0.6x0.7 exterior
25-27	10-12	0.5x0.7 exterior
28-29	1-5	0.65x0.75 interior
30-31	6-9	0.6x0.7 interior
32-34	10-12	0.5x0.7 interior
Beams		
35-37	1-5	0.45x0.7
38-39	6-9	0.45x0.6
40	10-12	0.45x0.45

Notes:

(1) Square bays 6.00 x 6.00 m., 6 bays (2 external and 4 internal).

(2) Storey height = 3.65m.

(3) kN.m.sec units.

(4) Modulus of elasticity of concrete E = 30 x 10^6 kN/m^2.

(5) Shear modulus of concrete G = 12.5 x 10^6 kN/m^2.

(6) Slab length of 0.35m added to each side of beams in calculation of geometric properties.

Figs. 5.2 and 5.3: Schematic representation of geometric properties of Rahman and Tabuchi frames (next page) [C2] incorporated in numerical models.

Key: e.g. (208 - 80) = (**Member No.** - Member Type)

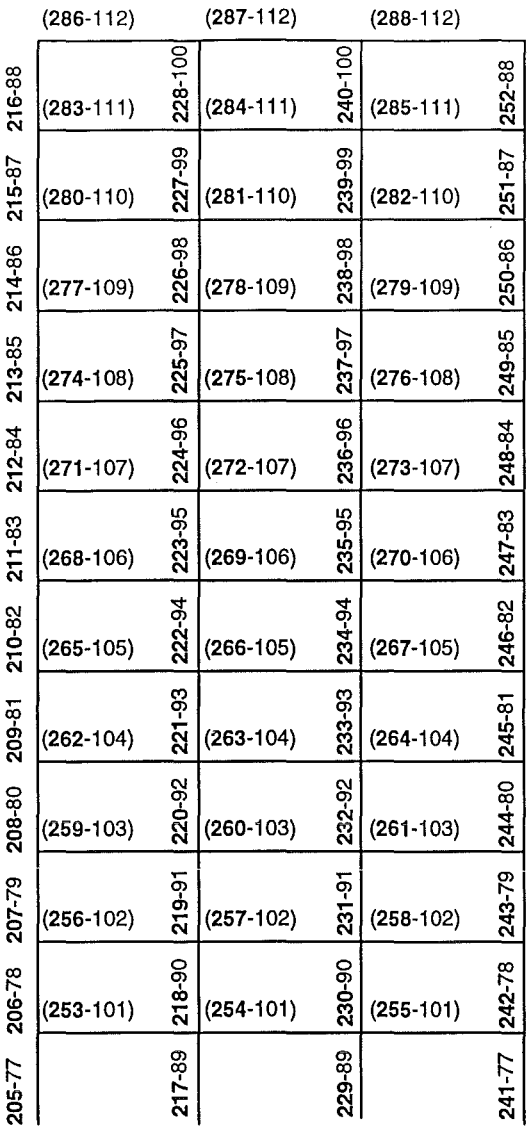

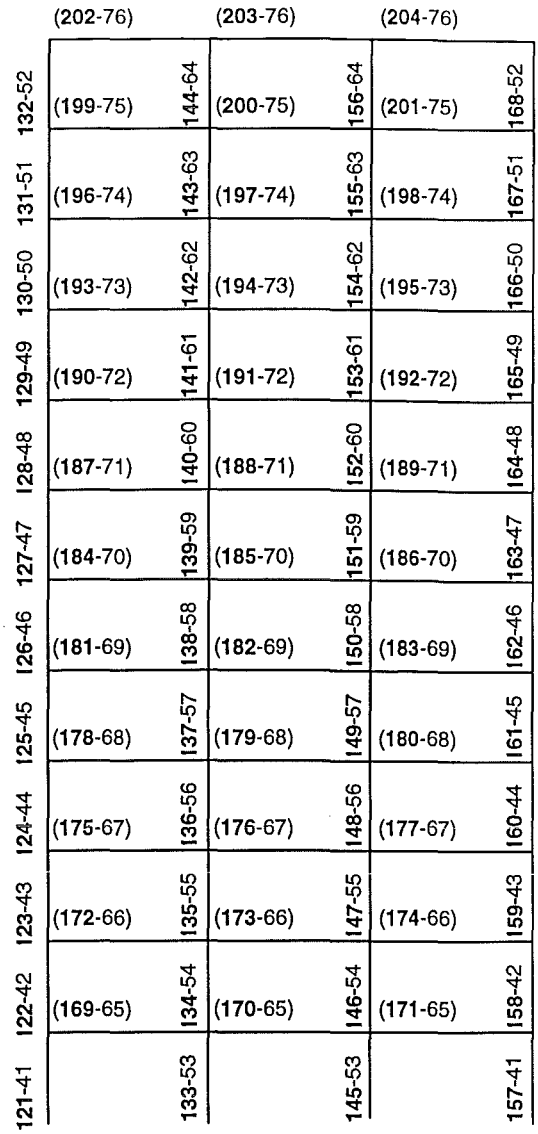

Tabuchi Interior Frame

Interior Frame

Member Type	Level	Total Area (m^2)	Shear Area (m^2)	Moment of Inertia (m^4)
Columns				
77-80	1-4	2.45	1.225	6.01E-2
81-84	5-8	2.113	1.056	4.46E-2
85-88	9-12	1.8	0.9	3.24E-2
89-92	1-4	2.45	0.225	8.01E-2
93-96	5-8	2.113	1.056	5.95E-2
97-100	9-12	1.8	0.9	4.32E-2
Beams				
101-104	1-4	1.4	0.7	4.0E-2
105-108	5-8	1.313	0.656	3.32E-2
109-112	9-12	1.225	0.613	2.7E-2

Tabuchi Exterior Frame

Exterior Frame

Member Type	Level	Total Area (m^2)	Shear Area (m^2)	Moment of Inertia (m^4)
Columns				
41-44	1-4	0.98	0.49	2.4E-2
45-48	5-8	0.845	0.423	1.78E-2
49-52	9-12	0.72	0.36	1.30E-2
53-56	1-4	0.98	0.49	3.2E-2
57-60	5	0.845	0.423	2.38E-2
61-64	9-12	0.72	0.36	1.73E-2
Beams				
65-68	1-4	0.56	0.28	1.36E-2
69-72	5-8	0.525	0.263	1.13E-2
73-76	9-12	0.49	0.245	9.24E-3

Notes:

(1) Modulus of elasticity = 25 x 10^6 kN/m^2.

(2) Shear modulus = 10.4 x 10^6 kN/m^2.

(3) Modified Takeda hysteresis rule (unloading and reloading stiffnesses equal to zero with reloading stiffness power factor equal to zero and unloading as in DRAIN-2D).

(4) Damage indices computed (positive and negative ductilities equal to 30.0).

(5) All bays 8.00 x 8.00 m.

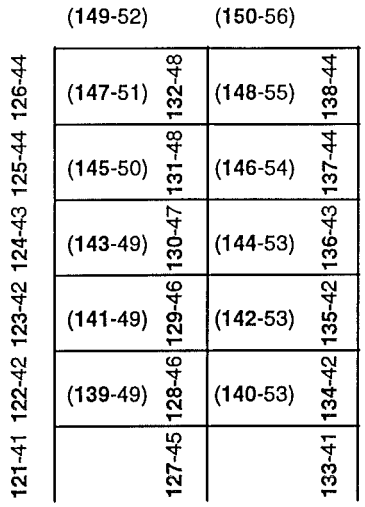

Key: e.g., (121 – 41) = (Member No. - Member Type)

Element	Member Type	Area (m^2)	Shear Area (m^2)	Moment of Inertia (m^4)	Plastic Hinge Length (m)
Beams	49 and 53	0.1050	0.1050	0.00315	0.3
	50-56	0.0963	0.0963	0.00243	0.28
External Columns	41-42	0.1688	0.1688	0.003516	0.25
	43-44	0.1519	0.1519	0.002563	0.23
Internal Columns	45-46	0.2269	0.2269	0.005719	0.28
	47-48	0.1875	0.1875	0.003906	0.25

Notes:
(a) The Jury frame consists of six identical frames. The properties above are representative of single elements.
(b) Member and member type numbering are as implemented in numerical analyses.
(c) Modulus of elasticity E = 25×10^6 kN/m^2.
(d) Shear modulus G = 10.4×10^6 kN/m^2.
(e) Bay width = 5.5m.
(f) Column hysteresis is bi-linear elastic (bi-linear factor r = 0.2%).

Jury Frame

Fig. 5.4: Schematic representation of geometric properties of Jury frame [J7] incorporated in numerical model.

The influence of the impact spring damping is negligible on the peak response envelopes [A5,M6].

The assumptions applied in the development of a numerical model for the Rahman frame for implementation in RUAUMOKO are as follows:

In order to account for cracking of concrete elements, effective areas ($A_{eff.}$) for all elements are taken as $A_{eff.}=0.5A_g$, where A_g is the gross area of the prismatic element.

- Similarly, the shear area ($A_{veff.}$) is considered to be half of the gross shear area (A_v), where $A_v=5/6\ A_g$ [M4].
- Effective moments of inertia are as recommended in NZS 3101: 1995 [N6]. These values were amended to account for actual axial force levels in columns.
- Rigid end-blocks are assumed for the inelastic beams and columns as this was considered to represent more accurately the actual condition with respect to the stiffness of the beam-column assemblage. The lengths of these blocks are equal to one-half the depth of the adjoining element at that joint [J7].
- A plastic-hinge zone equal to one-half the section depth is assumed for all inelastic structural elements [P4].

- Some software packages [M3,M5] assume in-plane rigidity of the floor diaphragms. This implies the simultaneous contact of the total floor masses of the adjacent buildings. In fact, only the local masses of the impacting nodes are involved at the first instant of contact. Travelling wave effects in the floor diaphragm, in addition to its relative flexibility, lead to the gradual contribution of the other nodal masses at the same level at subsequent time stations. This results in significant differences in the response of the exterior columns as reported by Sinclair [S3]. The present study incorporates the recommendations of Sinclair [S3] regarding the independence of the lateral degrees of freedom of the nodes of each frame (i.e. the horizontal degrees of freedom for each level are unslaved).
- A Newmark Constant Average Acceleration integration scheme ($\beta = 0.25$) is implemented in the dynamic time-history analyses.
- A lumped-mass matrix is utilized in the idealization of the mass distribution of the structures. The results obtained by this idealization are sufficiently accurate and do not differ significantly from those of a distributed mass representation [P3].
- The time-step used in all analyses is 0.001 seconds, which is comparable to the recommendations of other studies [S8, A2]. Such a small temporal increment is necessary to detect the short-duration impact events. Comparison of various response values (envelopes and time-histories) which were calculated assuming different time-steps ($5x10^{-4}$, $1x10^{-3}$ and $5x10^{-3}$ seconds) has shown that, while a discrepancy in impact force characteristics may be detected, the effect of this discrepancy on the other response values (at both global and local levels) is negligible (see Figs. A.1).

Figure 5.4 facilitates the visual perception of the numerical model developed to represent the dynamic response of the underlying soil mass. The discrete-element models utilized in the representation of the soil-structure interaction (between the isolated building and the supporting soil mass directly beneath its footings) and the normal and shear force-deformation characteristics of the soil between the adjacent buildings are clearly indicated in the figure. Details of the soil-structure interaction model and the assumptions pertaining to the properties of the supporting soil are presented in Chapter 3 while Chapter 4 presents the through-soil coupling model. The impact element is presented in Chapter 2. Figure 5.5 shows a schematic representation of the soil flexibility numerical models.

5.4 Earthquake Records

The first fifteen seconds of two (unfactored) excitations are applied separately from both directions (i.e. left-right and right-left). A five second period of free-vibration is allowed at the end of each analysis. These two excitations are the N-S component of the 1940 El Centro earthquake (peak ground acceleration (PGA) = 0.348g) and the S-14^0-W component of the 1971 Pacoima Dam earthquake (PGA = 1.23g). The former is representative of a benchmark excitation, commonly used in structural dynamics studies and aseismic design codes (e.g. [N5]). The Pacoima Dam excitation is a high-intensity earthquake with most of the strong motion activity occurring within the first 10 seconds of the event. Distinctive characteristics of the spectral accelerations of each of these records are presented in the discussion below. The excitations are initially applied from the direction of the more flexible (Rahman) frame and, subsequently, from the opposite direction. The direction of seismic attack is an important aspect which is worthy of consideration in pounding studies [K6,S8]. This is due to its influence on the time at which the first impact occurs, the dynamic response of the individual systems and the hysteretic behaviour assumed in the numerical models.

5.5 Separation Gaps

Various separation gaps, based on different levels of code-specified static loadings, are considered in compliance with the requirements of the New Zealand Loadings Code (NZS: 4203) [N5]. Accordingly, five initial separation gaps are implemented:

- A 1mm gap, simulating complete contact, i.e. no separation gap case.
- An arbitrary intermediate value of 10mm.
- 24mm, which is the minimum code requirement (Section 2.5.4.2 [N5]).
- 150mm, representing the code-specified requirement in which both twelve-storey buildings are separated by a distance equal to the sum of their elastic displacements (determined from equivalent static lateral load analyses [N5]).
- A separation gap of 380mm equal to the sum of the absolute maximum displacement of the top storey of each twelve-storey building determined from an inelastic analysis (El Centro record).

For each of the excitations used in this study, the code-specified gap of 150mm is sufficient to preclude pounding of the twelve-storey frame configuration for all cases of foundation fixity. Therefore, only four cases are investigated: the 1mm, 10mm and 24mm cases, in addition to the no-pounding case which is used as a bench-mark. A

separation gap of 75mm, equal to the elastic displacement of the Rahman frame (determined from an equivalent lateral static force analysis), was also considered. However, it was not further investigated due to the limited number of impacts and their restriction to the upper levels.

It is to be noted that the separation gaps referred to herein relate to the clear distance between the buildings. The distance between the center-lines of the footings is constant (5.0 meters). The soil underlying this region is modelled by the GROUND element in the present study.

5.6 Presentation of Results

5.6.1 No-Pounding Case

Firstly, the effects of soil flexibility on the overall dynamic response of the frames in each of the two configurations are presented. The effects of through-soil coupling are not apparent on storey displacements but are obvious on the impact-side column shears, even for the large separation gaps assumed for the no pounding case (5 meters).

5.6.2 Natural Period of Vibration

As discussed in a preceding chapter (Chapter 3), the introduction of additional modes of vibration (horizontal and rotational in addition to a coupled mode) is one of the most important features of soil-structure interaction. These new modes of vibration increase the natural periods of the structures from the fixed base case. For the Rahman frame, the fixed base natural period increased 21%, from 2.27 seconds to 2.76 seconds (see Fig. 5.6). The corresponding values for the Tabuchi frame were 1.99 seconds to 2.31 seconds (representing a 16% increase), while the Jury frame increased approximately 28% from 0.98 seconds to 1.25 seconds. Since the differences between the results of the two flexible soil cases are almost negligible, only the compliant foundation case results are compared with those of the fixed base condition.

The following sections elucidate the modifications to the dynamic response of the three frames effected by the increases in their natural periods.

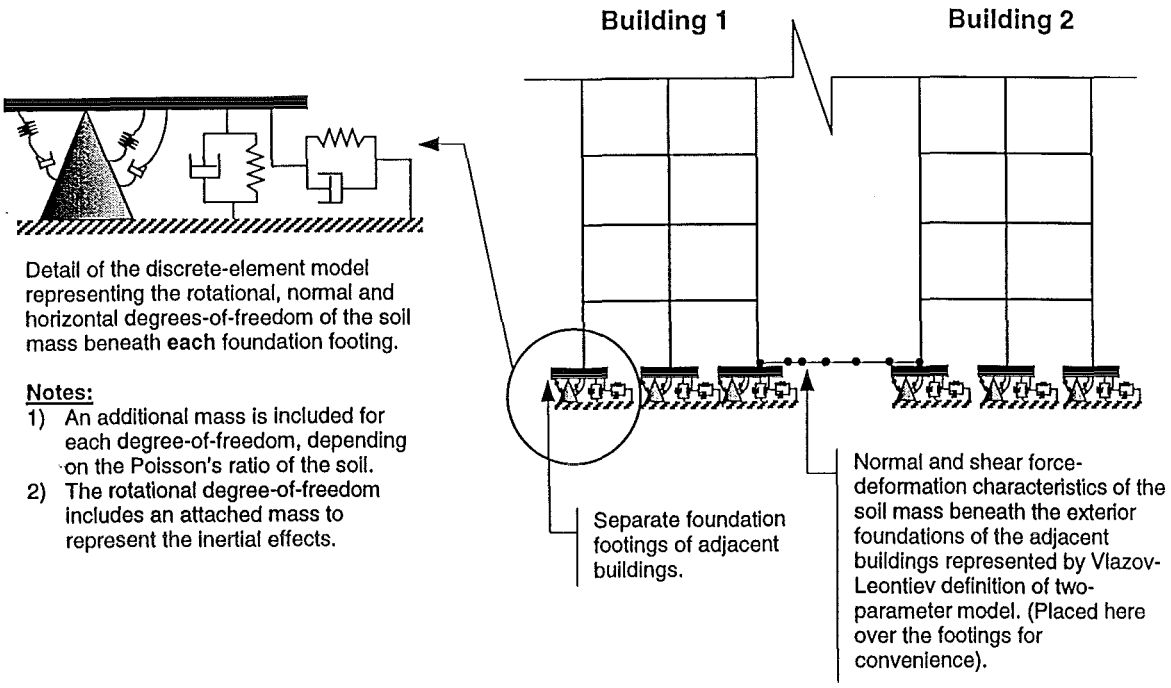

Fig. 5.5: Conceptual representation of the soil-flexibility models implemented in the numerical analyses.

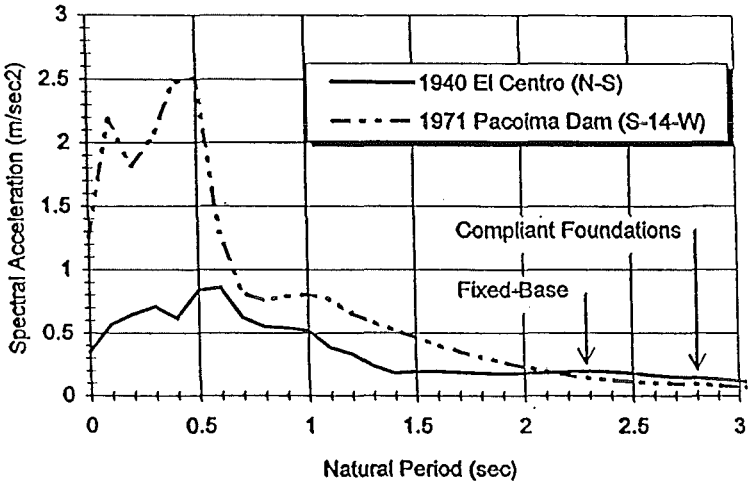

Fig. 5.6: Response spectra of excitations implemented in this study and effect of foundation compliance on natural period of Rahman frame.

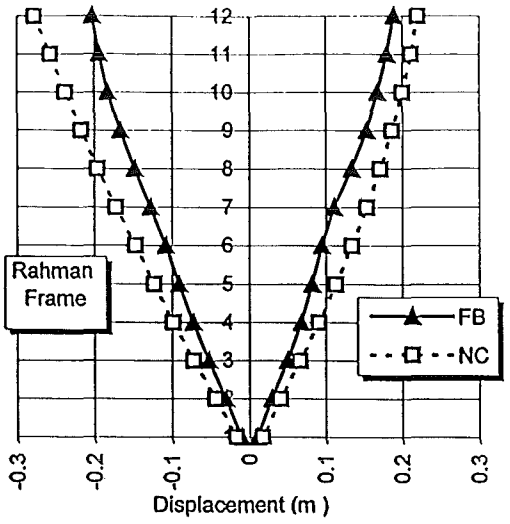

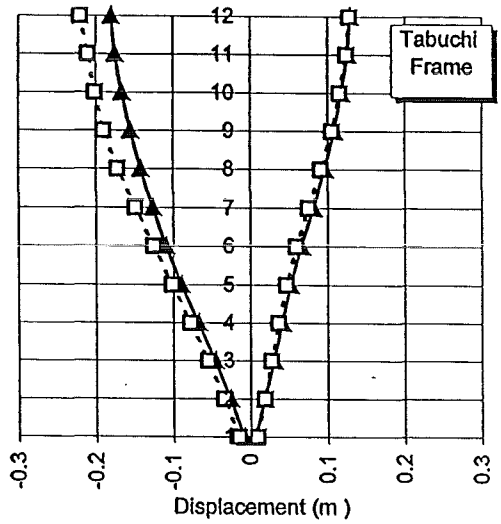

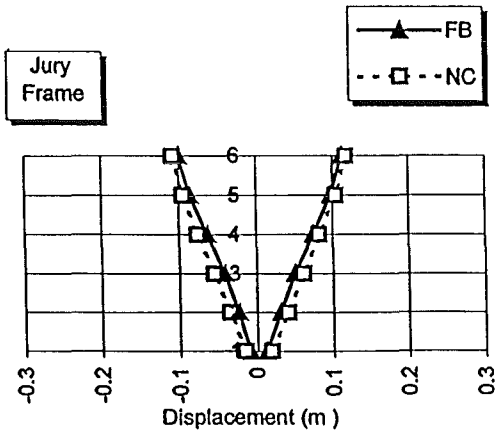

Fig. 5.7: Displacement envelopes for no pounding case. 1940 El Centro applied left-right.

FB = Fixed Base
NC = Non-Coupled (i.e. through-soil coupling not considered)

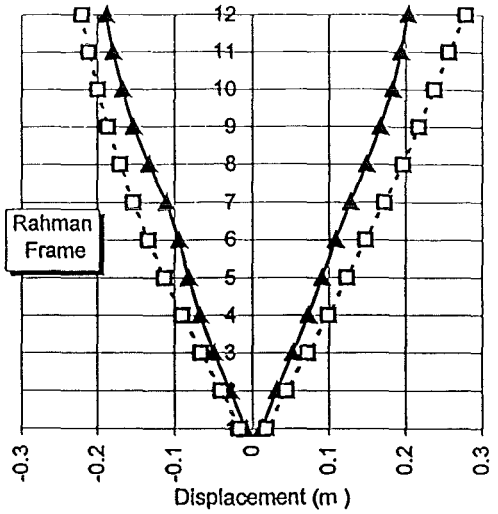

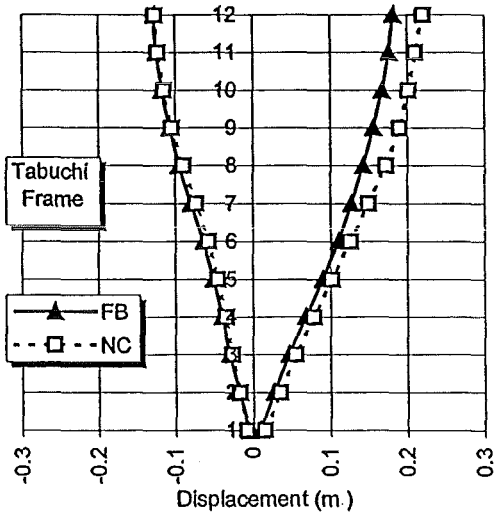

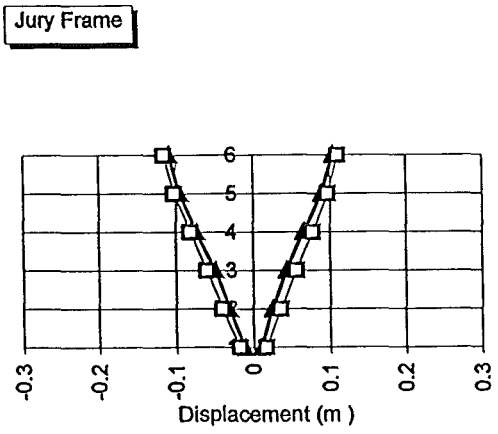

Fig. 5.8: Displacement envelopes for no pounding case. 1940 El Centro applied right-left.

FB = Fixed Base
NC = Non-Coupled (i.e. through-soil coupling not considered)

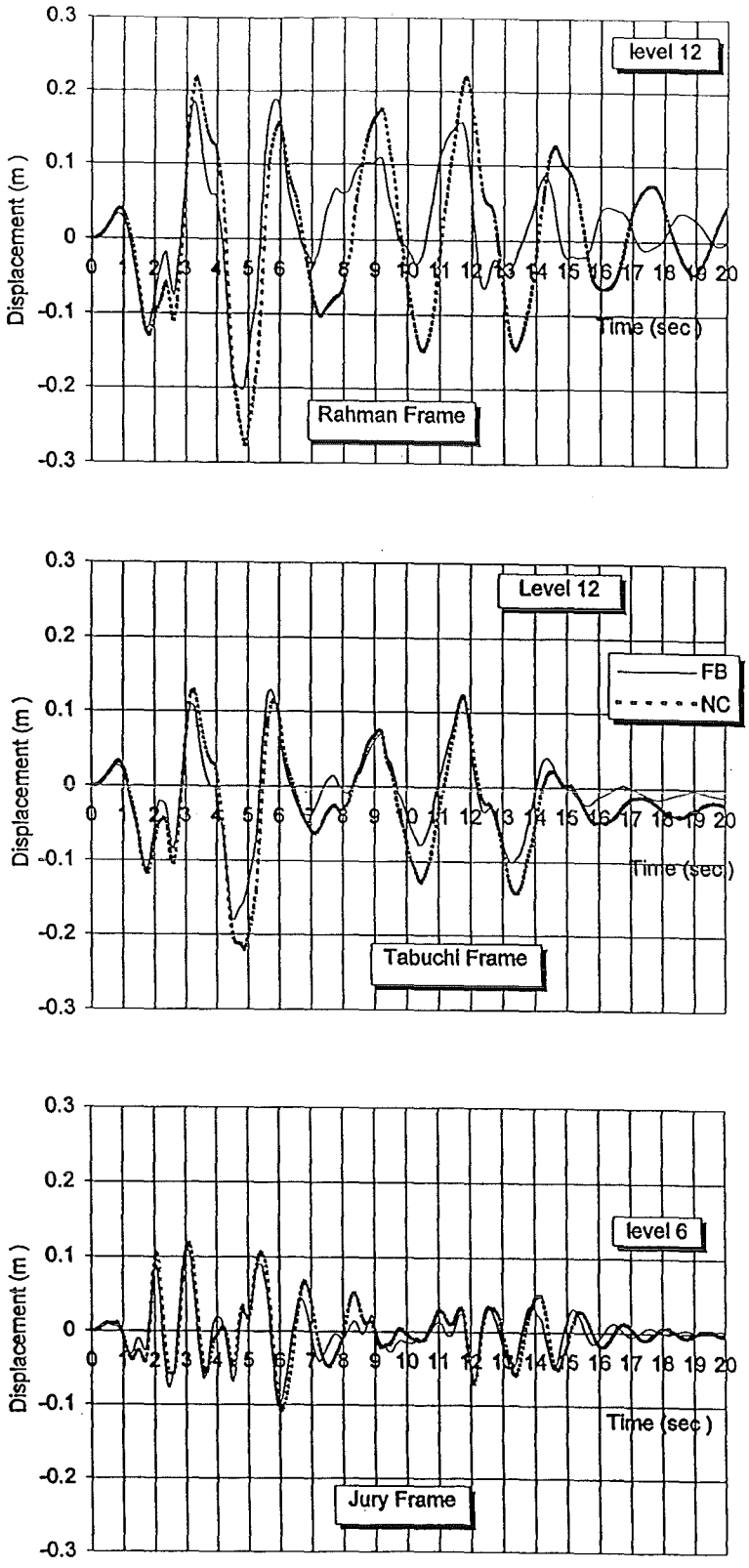

Fig. 5.9: Effect of foundation compliance on top-storey displacement time-history for no pounding case. 1940 El Centro earthquake applied left-right.

FB = Fixed Base
NC = Non-Coupled (i.e. through-soil coupling not considered)

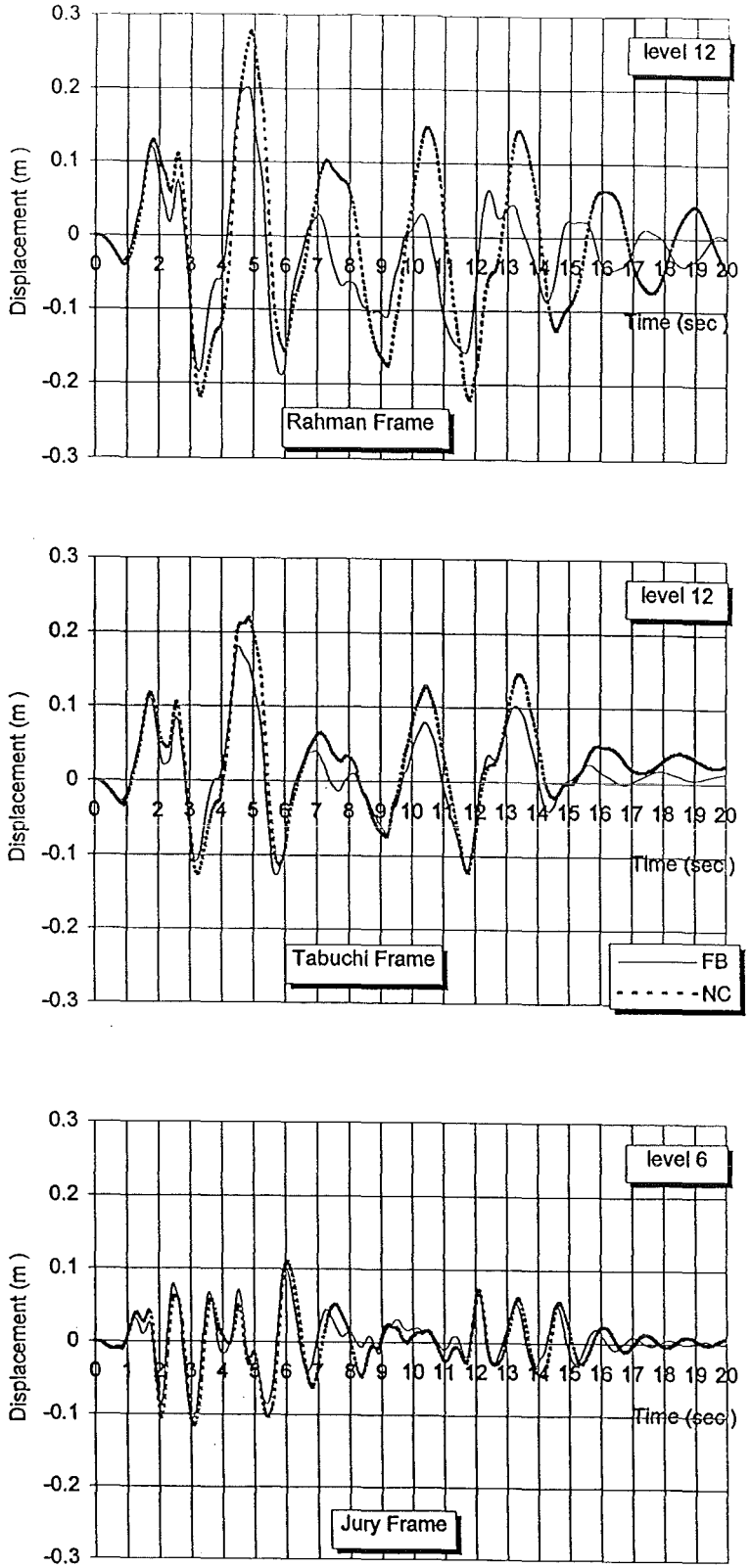

Fig. 5.10: Effect of foundation compliance on top-storey displacement time-history for no pounding case. 1940 El Centro earthquake applied right-left.

FB = Fixed Base
NC = Non-Coupled (i.e. through-soil coupling not considered)

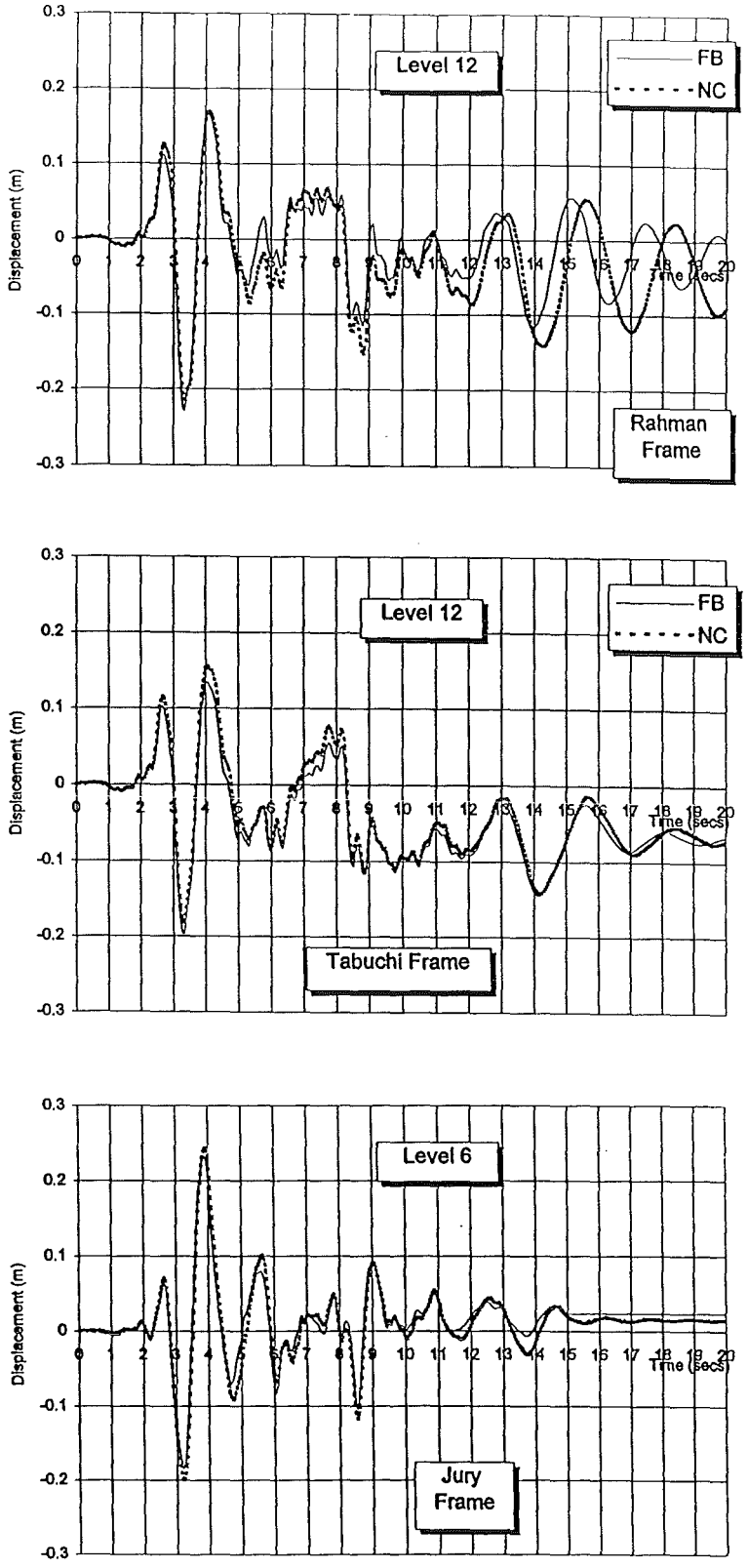

Fig. 5.11: Effect of foundation compliance on top-storey displacement time-history for no pounding case. 1971 Pacoima Dam earthquake applied left-right.

FB = Fixed Base
NC = Non-Coupled (i.e. through-soil coupling not considered)

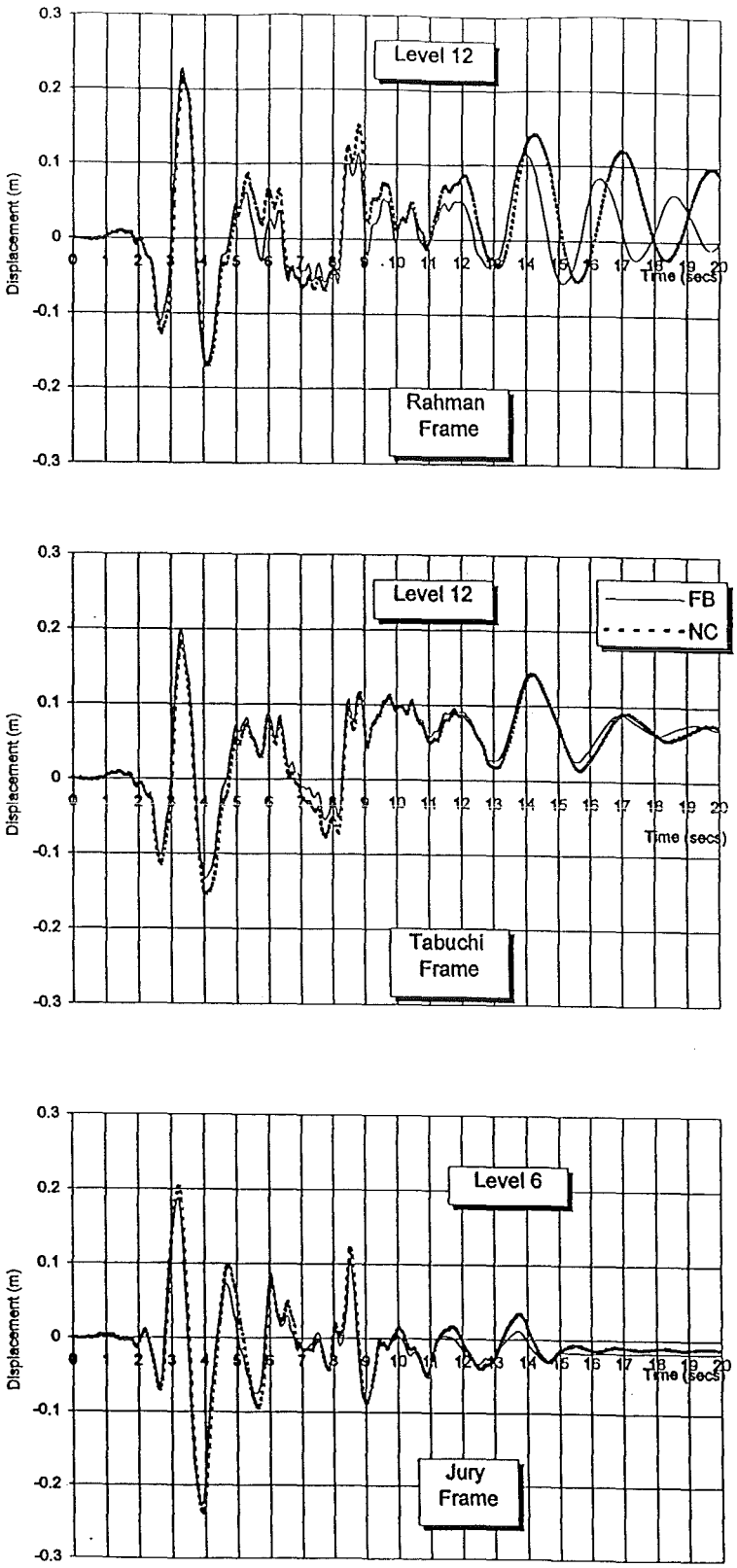

Fig. 5.12: Effect of foundation compliance on top-storey displacement time-history for no pounding case. 1971 Pacoima Dam earthquake applied right-left.

FB = Fixed Base
NC = Non-Coupled (i.e. through-soil coupling not considered)

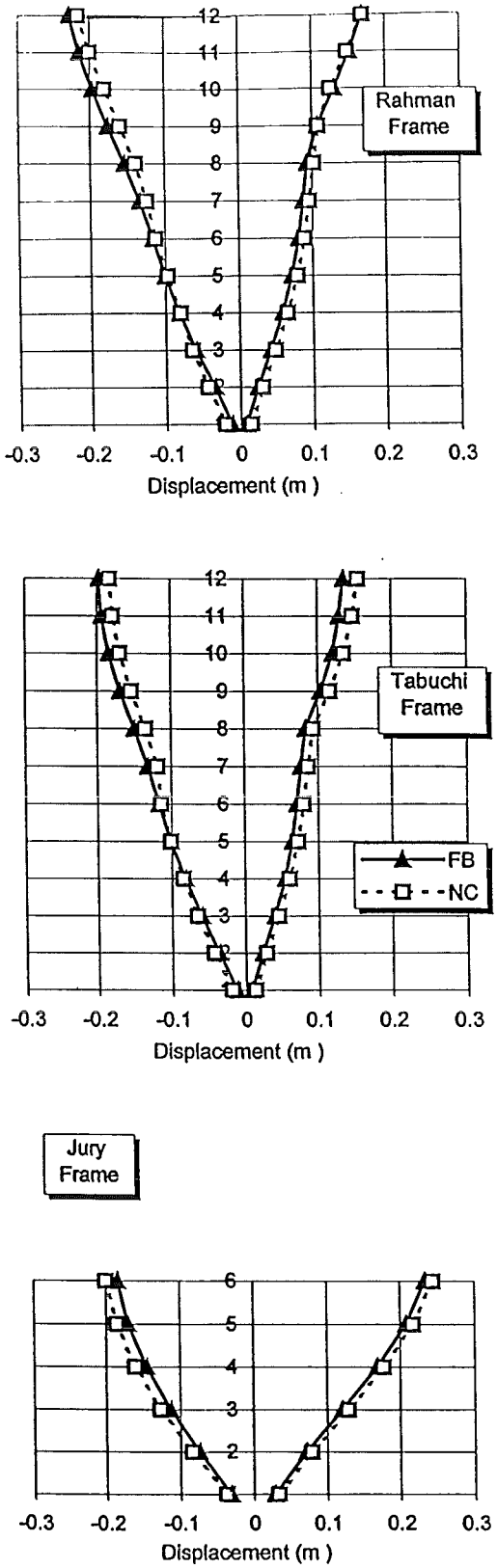

Fig. 5.13: Displacement envelopes for no pounding case. 1971 Pacoima Dam applied left-right.

FB = Fixed Base
NC = Non-Coupled (i.e. through-soil coupling not considered)

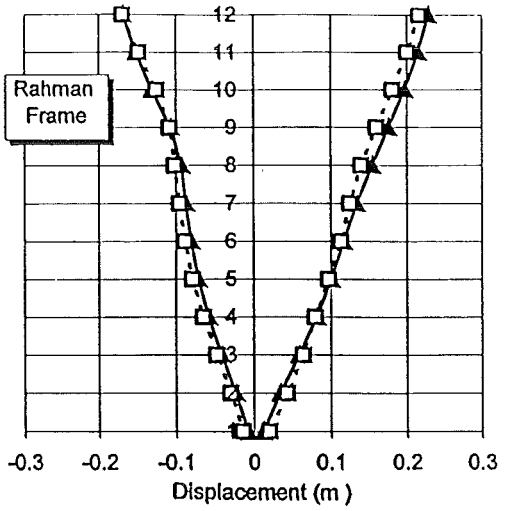

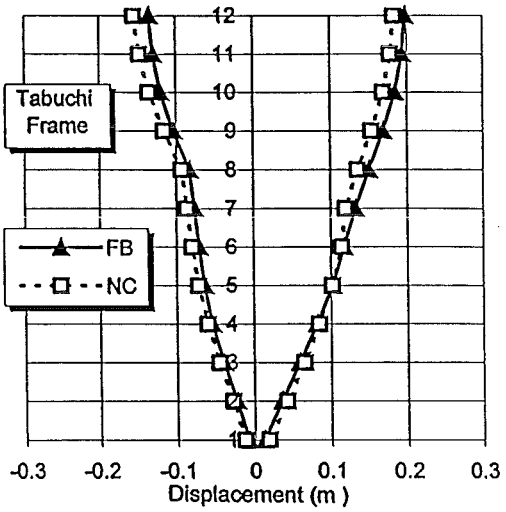

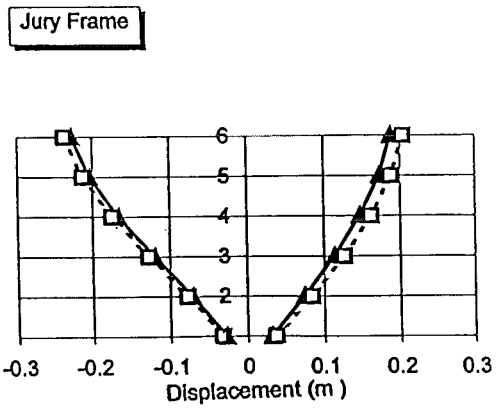

Fig. 5.14: Displacement envelopes for no pounding case. 1971 Pacoima Dam applied right-left.

FB = Fixed Base
NC = Non-Coupled (i.e. through-soil coupling not considered)

5.6.3 Storey Displacements

a) 1940 El Centro Earthquake

An overall increase in storey displacements and variations in their time-histories are observed. For each of the three frames, the variations in maximum storey displacements, for both directions of excitation, are shown in Figs. 5.7 and 5.8. The increases sustained by the Rahman frame are the highest of the three frames and are biased towards the direction of seismic attack, especially at the upper levels.The manifestation of the increase in natural periods as an increase in displacement amplitudes, in addition to a shift in response phase, is demonstrated in the time-history plots of Figs. 5.9 and 5.10. During the free-vibration stage, the fixed base and compliant foundation cases are out-of-phase. This feature is evident at an earlier stage in the more flexible structure (Rahman frame). In addition, when foundation compliance is considered, a shift in residual displacement at the end of the analysis is observed in the Tabuchi and Rahman frames. This shift is in the direction of seismic attack in the Rahman frame while the Tabuchi frame shifts in the opposite direction.

b) 1971 Pacoima Dam Earthquake

In this excitation case, all three frames display a residual displacement at the end of the analysis (Figs. 5.11 and 5.12), with significantly different characteristics from those observed above. While the shift in the Jury frame displacement is directed towards the direction of seismic excitation, the Tabuchi and Rahman frames are in the opposite direction. These residual displacements are higher than those observed in the El Centro earthquake case. While the effects of soil compliance on the Rahman frame displacement time-history exhibits the same features as those witnessed under the El Centro excitation (especially with regard to free-vibration displacement time-history), these effects are not as evident on the response of the other frames.

Another notable feature in this case is the reduction in maximum displacements in the direction of the source of the earthquake in both the Rahman and Tabuchi frames (Figs. 5.13 and 5.14). No increase in maximum storey displacements towards the direction of seismic attack is noted in the top levels of the Rahman frame while displacements increased slightly along the height of the Tabuchi frame. Soil-structure interaction increased the maximum storey displacements at all levels in the Jury frame and for both directions of excitation.

5.6.4 Impact-Side Column Shears

a) 1940 El Centro Earthquake

The sensitivity of the coupled foundation response of the Rahman frame to the presence of adjacent structures, even for the large separation gaps implemented in this study in the no pounding case (5 meters), is shown in Figs. 5.16 to 5.18. However, closer inspection of the compliant foundation case also reveals a discrepancy in the results of the Rahman frame in the two configurations, where no differences should be tangible. The reasons for this discrepancy are twofold. Firstly, although similar time-steps were implemented in the dynamic analyses of the two configurations (0.001 seconds), the time-stations at which the results were output to the postprocessor differed. Therefore, results were recorded at 0.01 second intervals in Configuration 2 and every 0.004 seconds in the Configuration 1 analyses. This was initially thought to have been the reason for the small differences (the magnitudes of which may be estimated by comparison of the compliant foundation case results of the Rahman frame in the two configurations).

This oversight was rectified in the Pacoima Dam excitation cases, with all results of both configurations output at 0.01 seconds. Differences in the results of the compliant foundation cases persisted, however, and were not constant over the height of the Rahman frame. It was, therefore, concluded that these differences are due to numerical round-off errors resulting from the marked difference in memory requirements between the two configurations. A significant increase in band-width of the relevant matrices is effected, due not only to the increased number of stories from six to twelve but also in the number of bays (from two in the Jury frame to three in the Tabuchi frame). In addition, the incorporation of pounding elements along the heights of the frames and the discrete-element soil compliance models are all contributing factors to the considerably increased size of the analyses.

In spite of the above sources of error, comparison of response amplification ratios of the Rahman frame columns in the two configurations (at levels that did not display discrepancies between the compliant foundation cases) revealed marked through-soil interaction effects (Figs.5.15 to 5.18), especially at ground floor level. Under a positive direction earthquake, the presence of the Jury frame results in a reduction in positive impact-side column shear at ground level (Fig. 5.16).

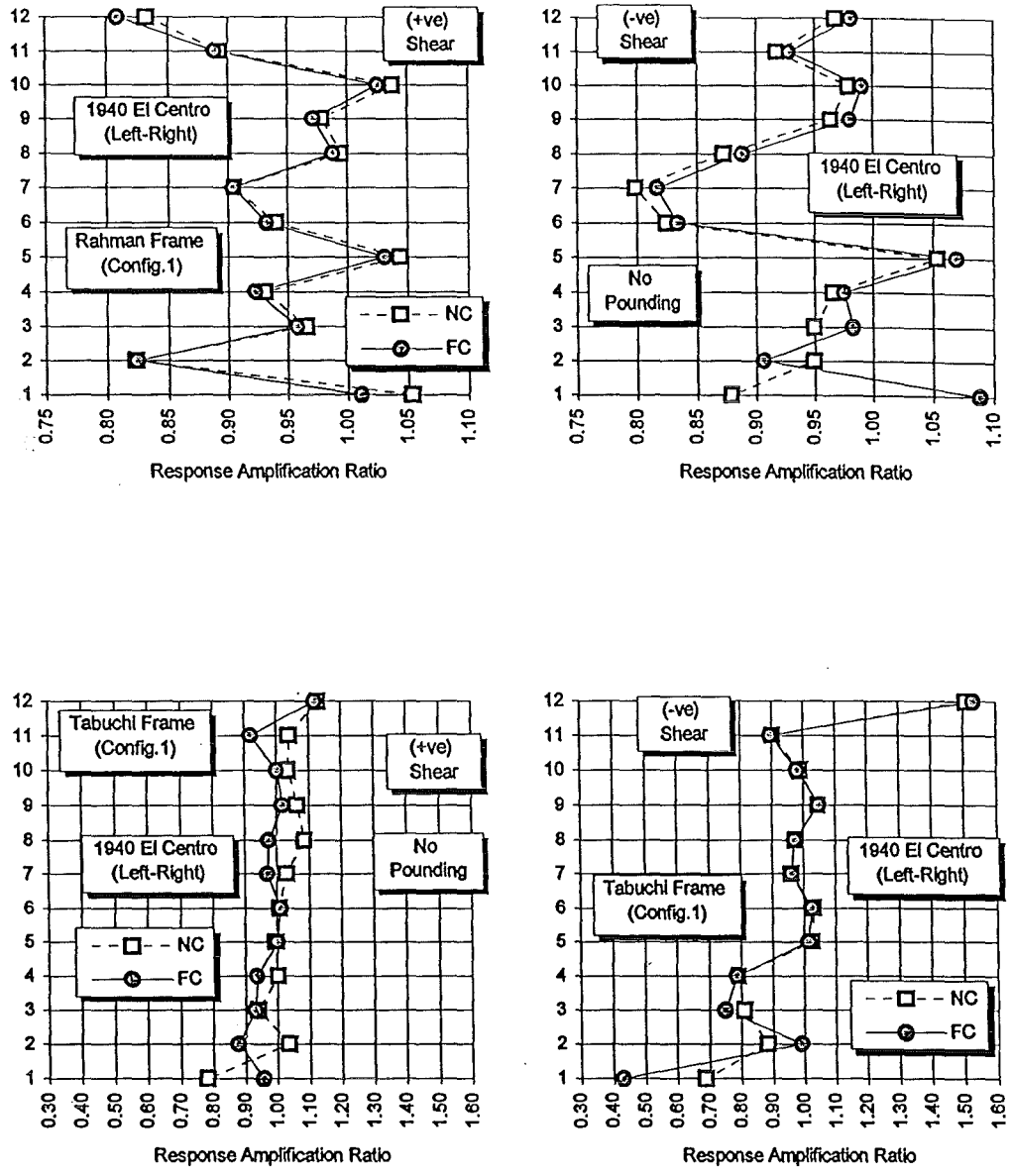

Fig. 5.15: Response amplification ratio (from fixed base no pounding case) of impact-side columns in Configuration 1 (Rahman and Tabuchi) Frames for various conditions of foundation fixity (no pounding case).
1940 El Centro earthquake applied left-right.

NC = Non-Coupled (i.e. only soil-structure interaction considered)
FC = Foundations Coupled

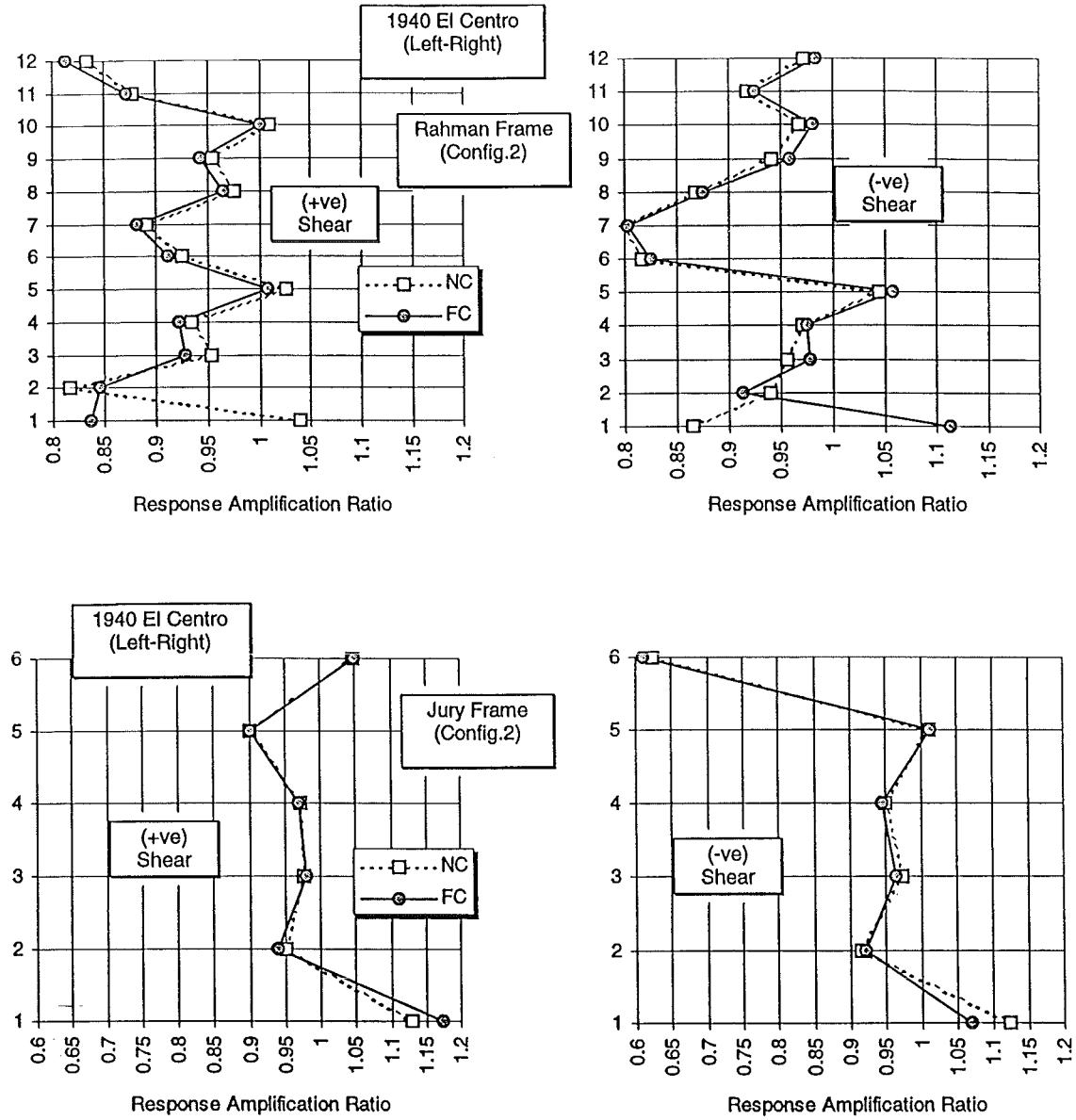

Fig. 5.16: Response amplification ratio (from fixed base no pounding case) of impact-side columns in Configuration 2 (Rahman and Jury) Frames for various conditions of foundation fixity (no pounding case).
1940 El Centro earthquake applied left-right.

NC = Non-Coupled (i.e. only soil-structure interaction considered)
FC = Foundations Coupled

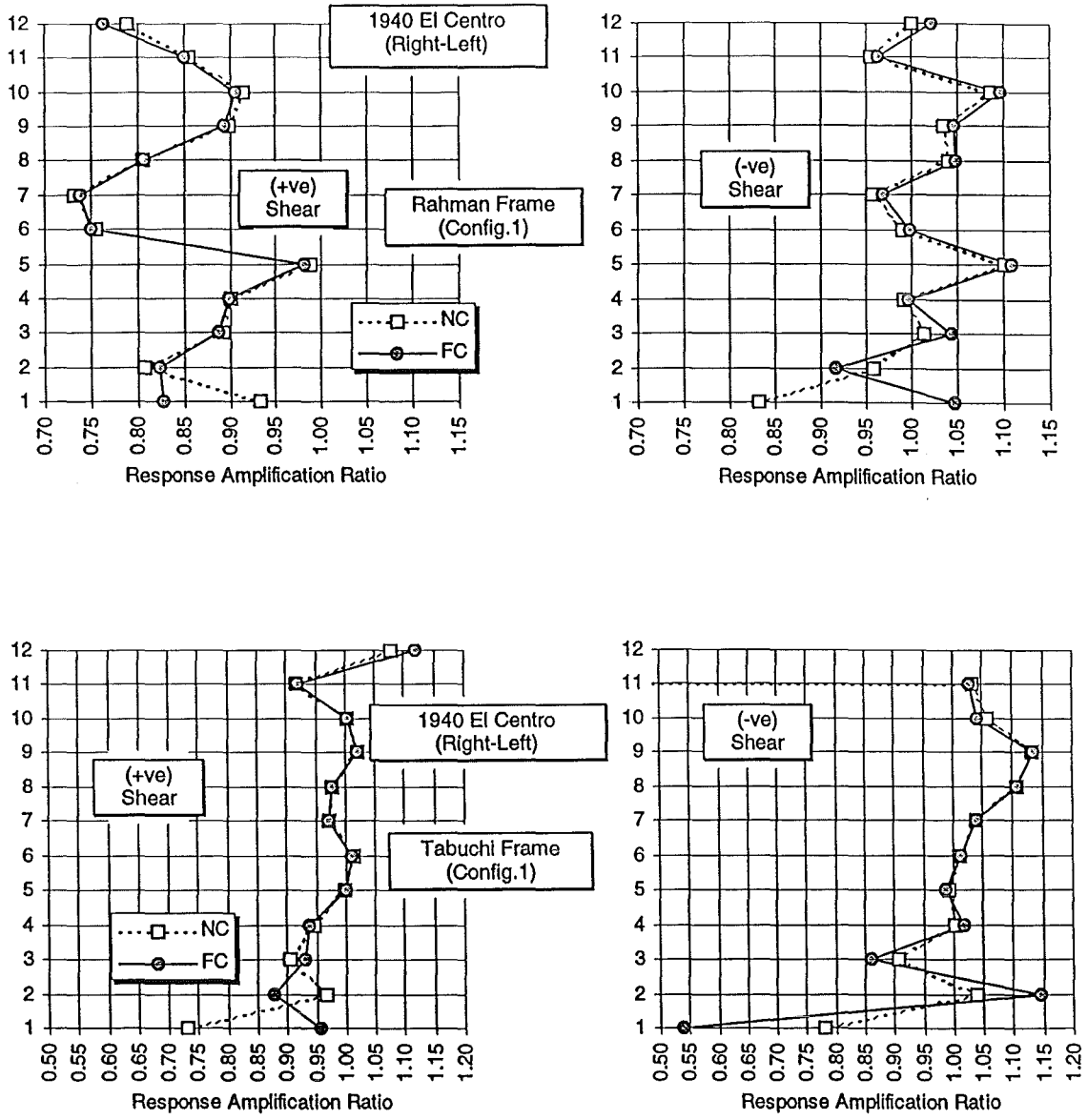

Fig. 5.17: Response amplification ratio (from fixed base no pounding case) of impact-side columns in Configuration 1 (Rahman and Tabuchi) Frames for various conditions of foundation fixity (no pounding case).
1940 El Centro earthquake applied right-left.

NC = Non-Coupled (i.e. only soil-structure interaction considered)
FC = Foundations Coupled

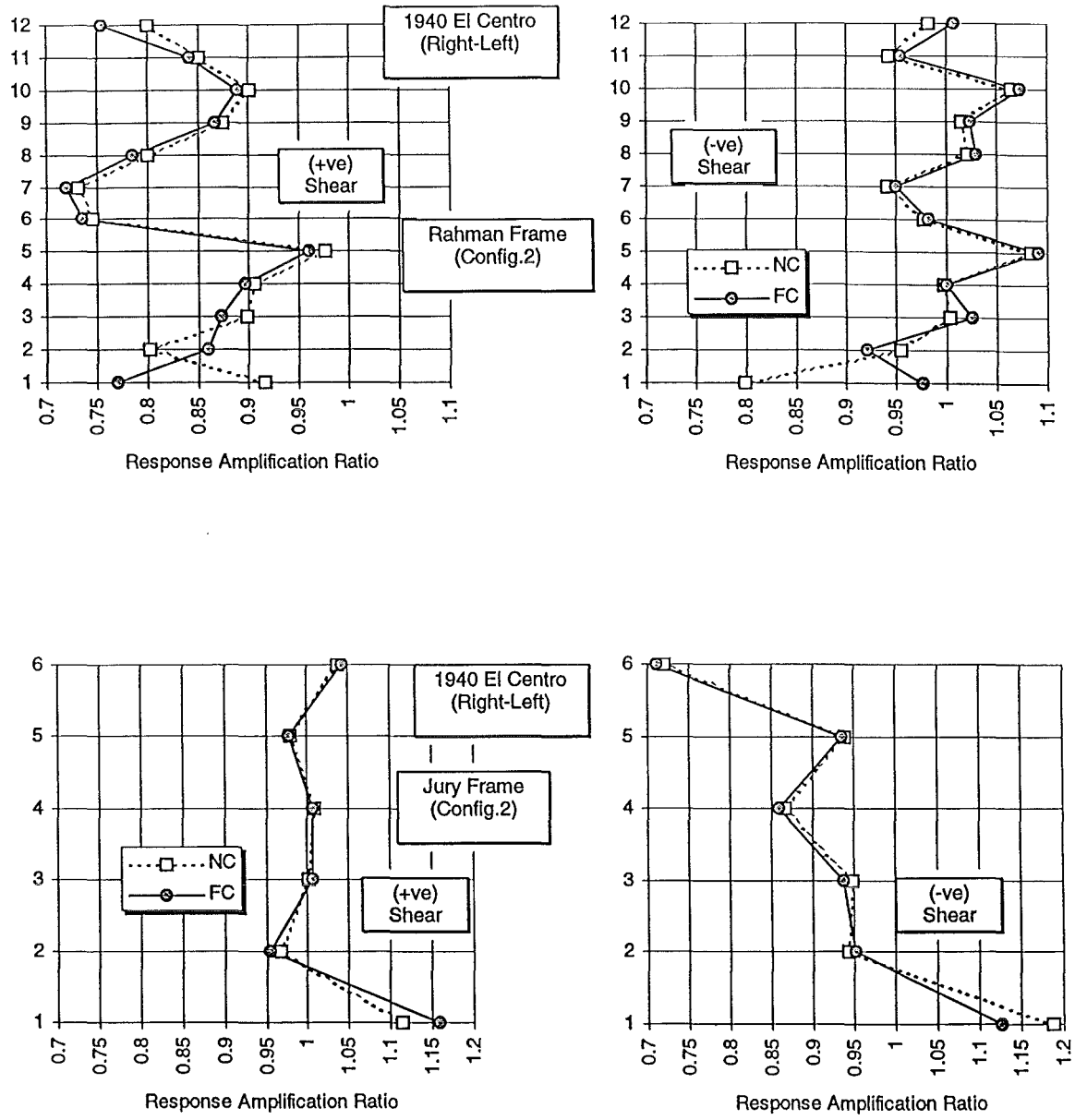

Fig. 5.18: Response amplification ratio (from fixed base no pounding case) of impact-side columns in Configuration 2 (Rahman and Jury) Frames for various conditions of foundation fixity (no pounding case).
1940 El Centro earthquake applied right-left.

NC = Non-Coupled (i.e. only soil-structure interaction considered)
FC = Foundations Coupled

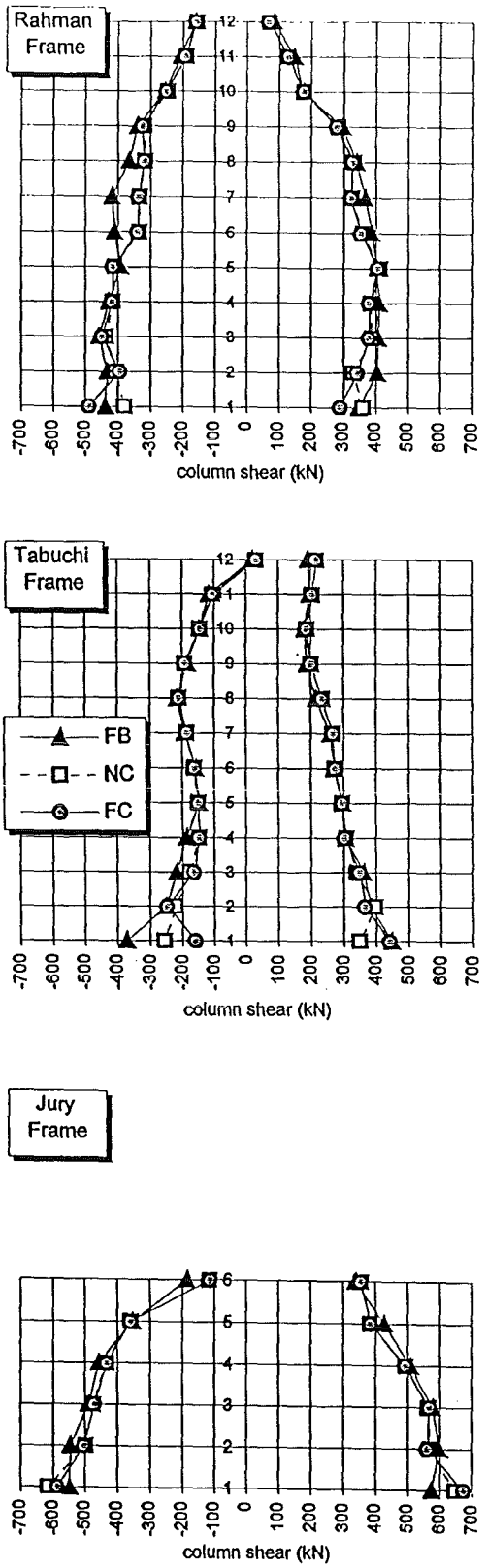

Fig. 5.19: Effect of foundation fixity assumptions on impact-side column shear envelope for no pounding case.
1940 El Centro earthquake applied left-right.

FB = Fixed Base
NC = Non-Coupled (i.e. through-soil coupling not considered)
FC = Foundations Coupled

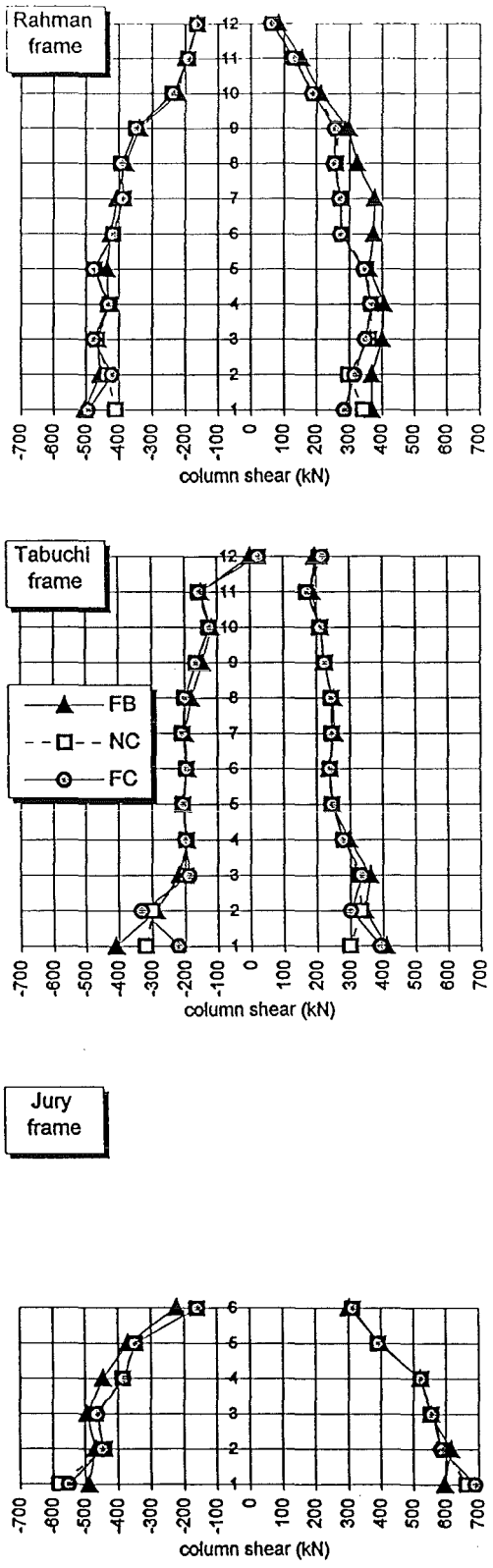

Fig. 5.20: Effect of foundation fixity assumptions on impact-side column shear envelope for no pounding case.
1940 El Centro earthquake applied right-left.

FB = Fixed Base
NC = Non-Coupled (i.e. through-soil coupling not considered)
FC = Foundations Coupled

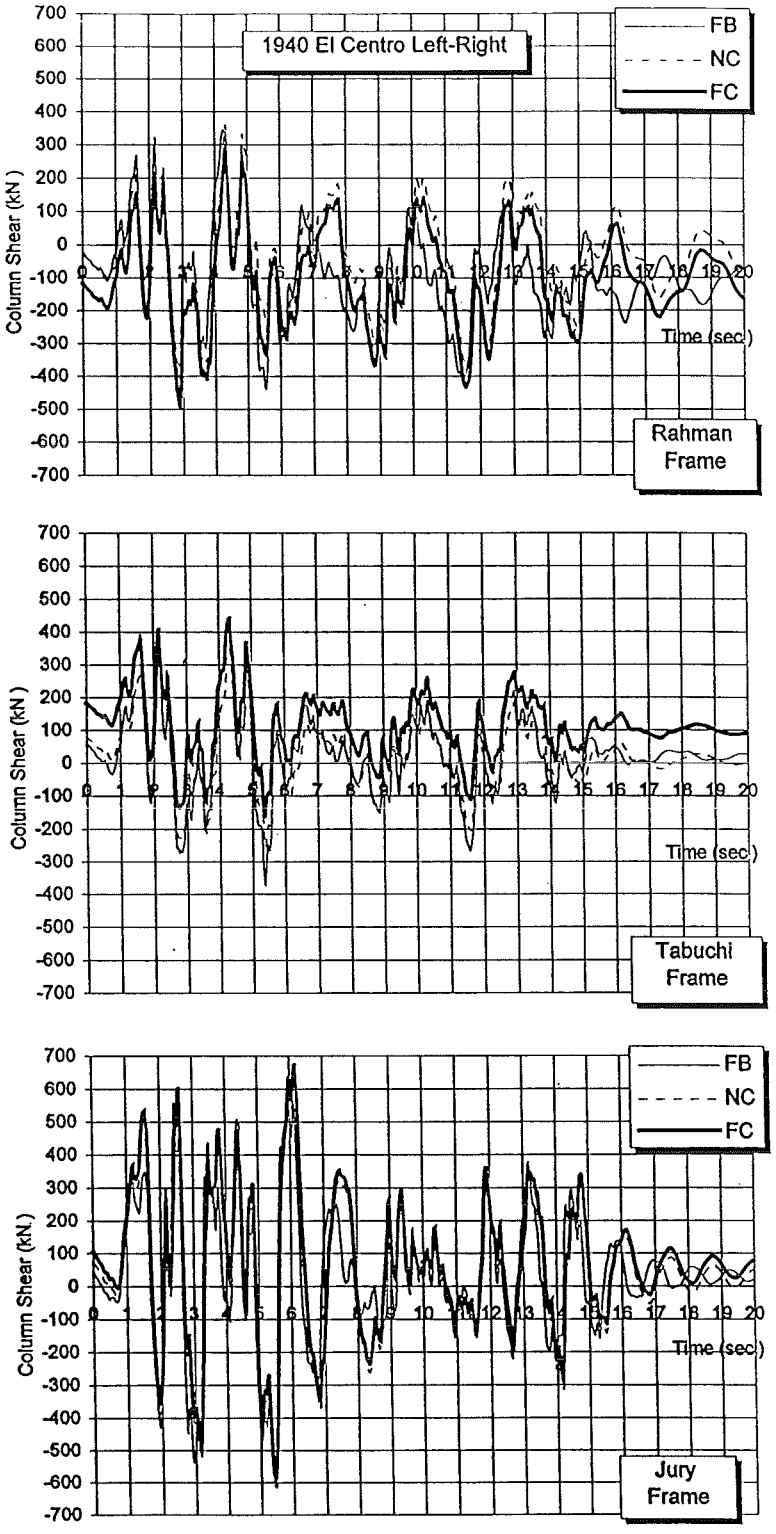

Fig. 5.21: Effect of foundation fixity conditions on time history of impact-side column shear for no pounding case.
1940 El Centro earthquake applied left-right.

FB = Fixed Base
NC = Non-Coupled (i.e. through-soil coupling not considered)
FC = Foundations Coupled

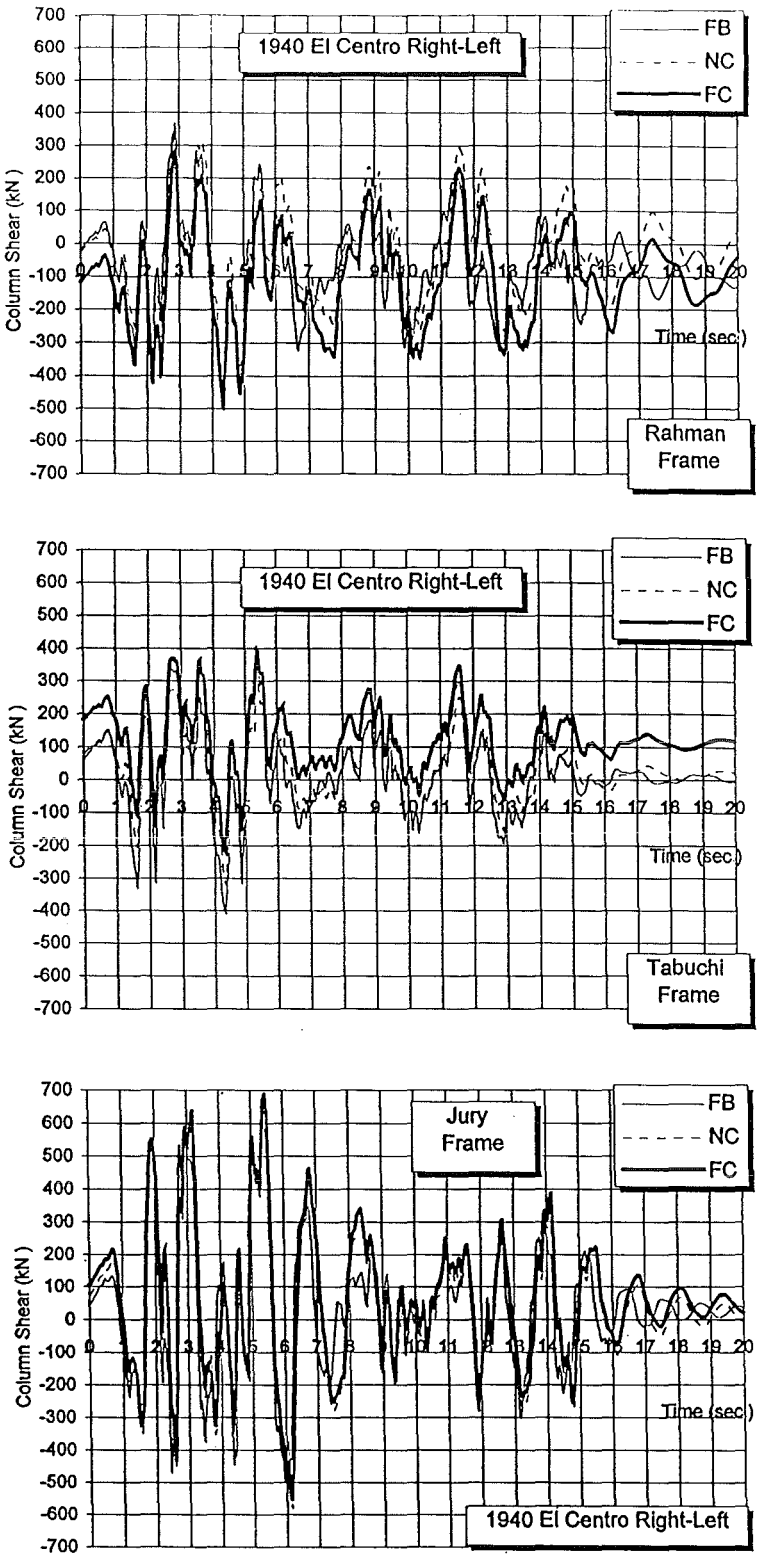

Fig. 5.22: Effect of foundation fixity conditions on time history of impact-side column shear for no pounding case.
1940 El Centro earthquake applied right-left.

FB = Fixed Base
NC = Non-Coupled (i.e. through-soil coupling not considered)
FC = Foundations Coupled

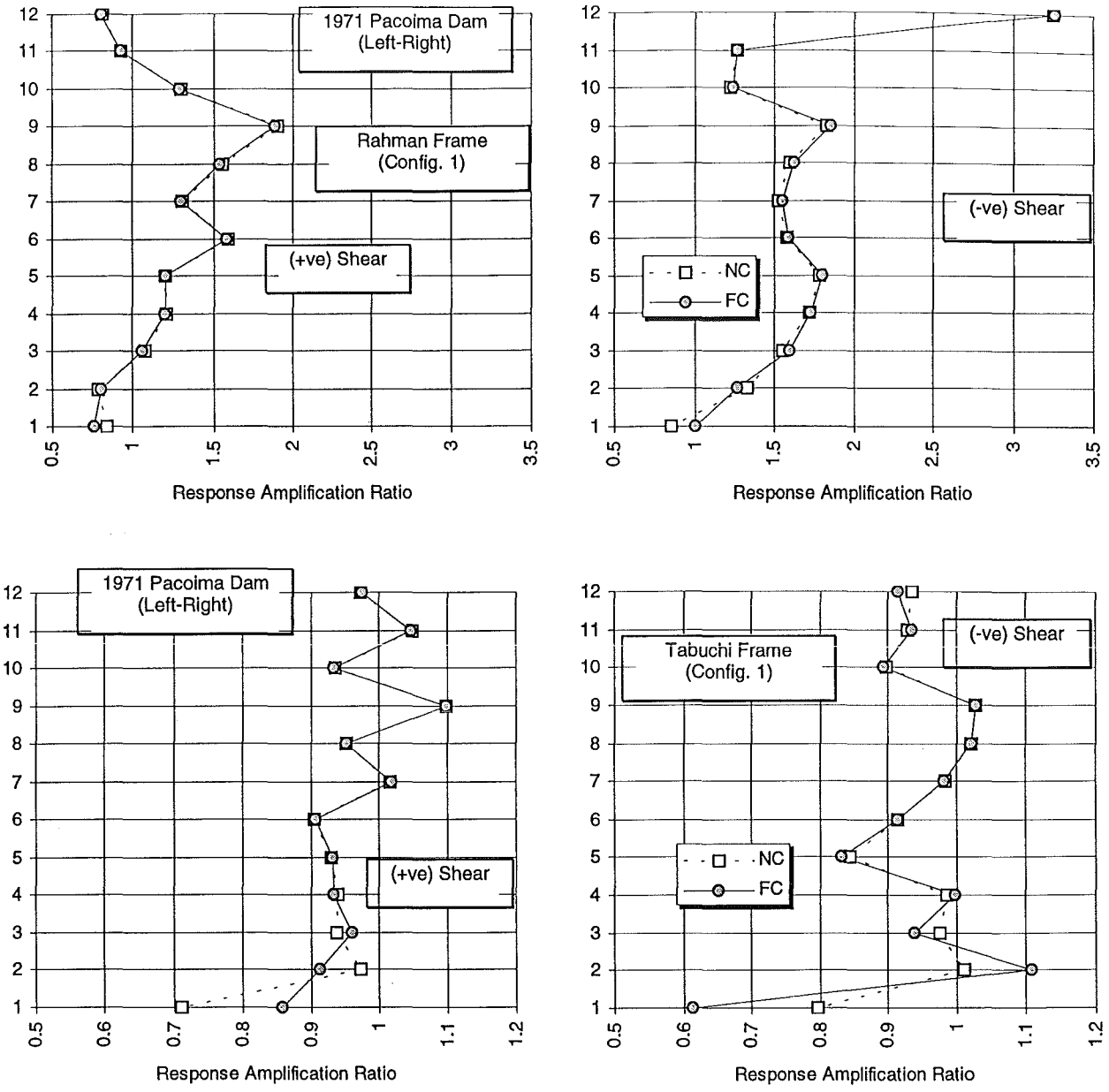

Fig. 5.23: Response amplification ratio (from fixed base no pounding case) of impact-side columns in Configuration 1 (Rahman and Tabuchi) Frames for various conditions of foundation fixity (no pounding case).
1971 Pacoima Dam earthquake applied left-right.

NC = Non-Coupled (i.e. only soil-structure interaction considered)
FC = Foundations Coupled

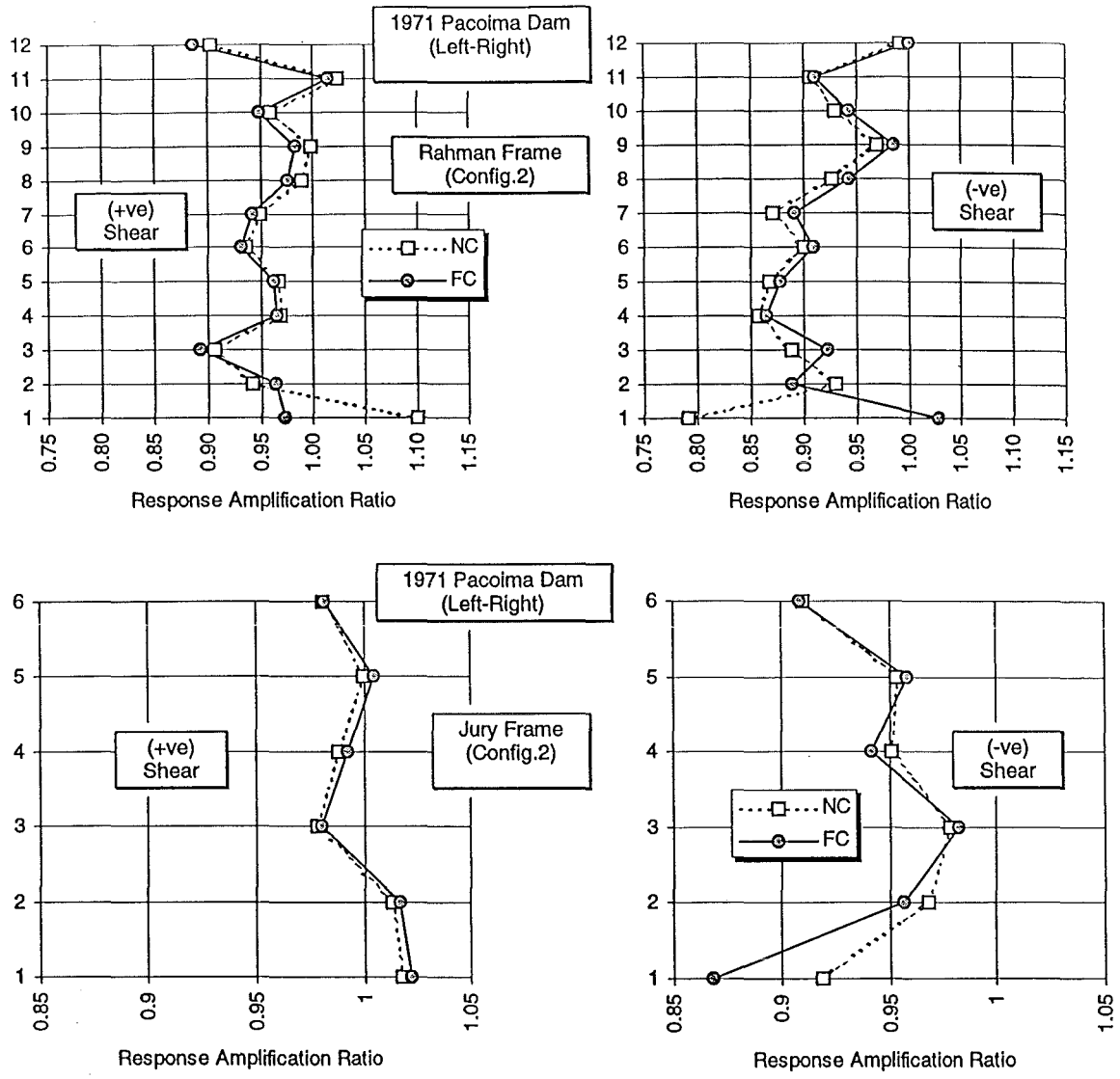

Fig. 5.24: Response amplification ratio (from fixed base no pounding case) of impact-side columns in Configuration 2 (Rahman and Jury) Frames for various conditions of foundation fixity (no pounding case).
1971 Pacoima Dam earthquake applied left-right.

NC = Non-Coupled (i.e. only soil-structure interaction considered)
FC = Foundations Coupled

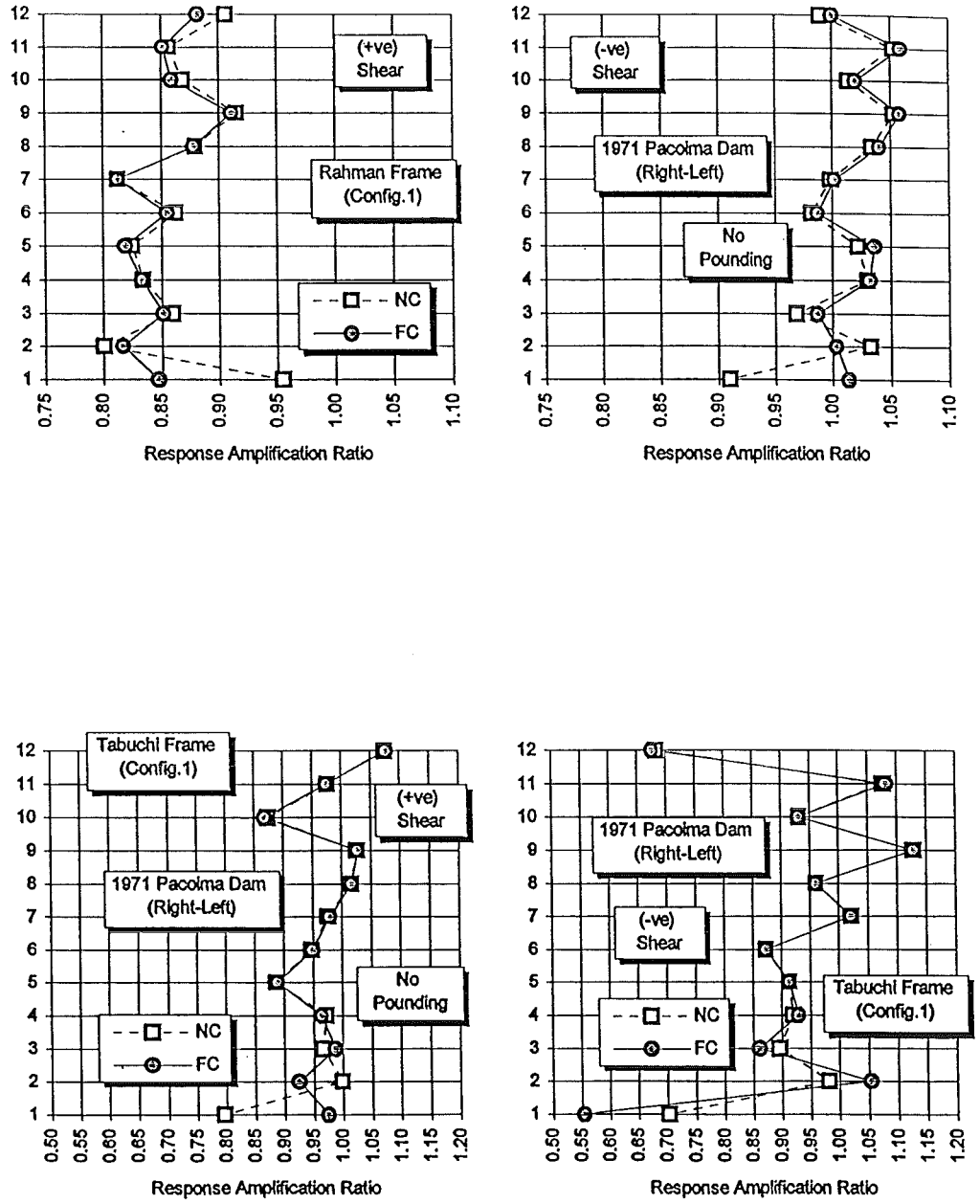

Fig. 5.25: Response amplification ratio (from fixed base no pounding case) of impact-side columns in Configuration 1 (Rahman and Tabuchi) Frames for various conditions of foundation fixity (no pounding case).
1971 Pacoima Dam earthquake applied right-left.

NC = Non-Coupled (i.e. only soil-structure interaction considered)
FC = Foundations Coupled

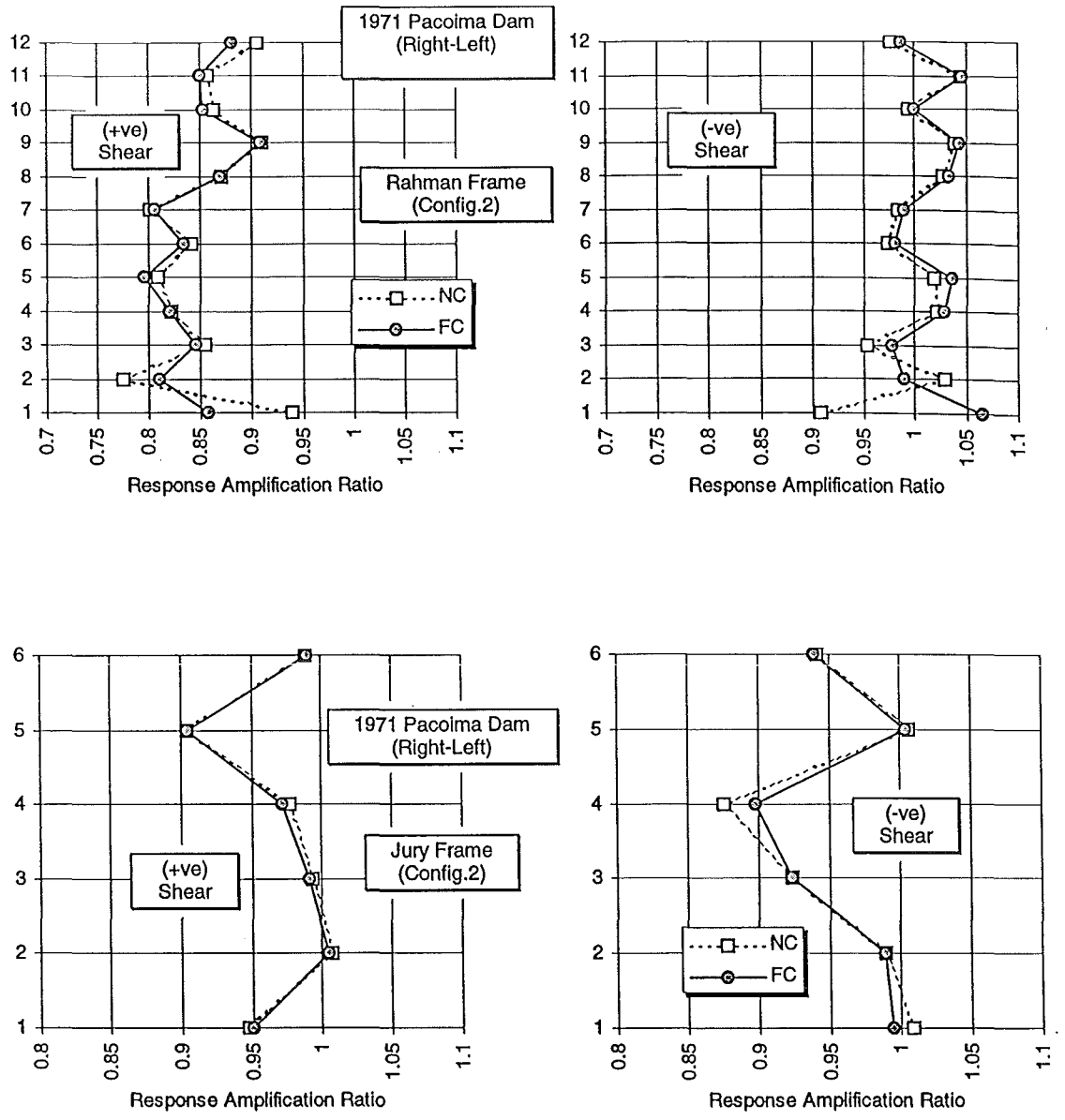

Fig. 5.26: Response amplification ratio (from fixed base no pounding case) of impact-side columns in Configuration 2 (Rahman and Jury) Frames for various conditions of foundation fixity (no pounding case).
1971 Pacoima Dam earthquake applied right-left.

NC = Non-Coupled (i.e. only soil-structure interaction considered)
FC = Foundations Coupled

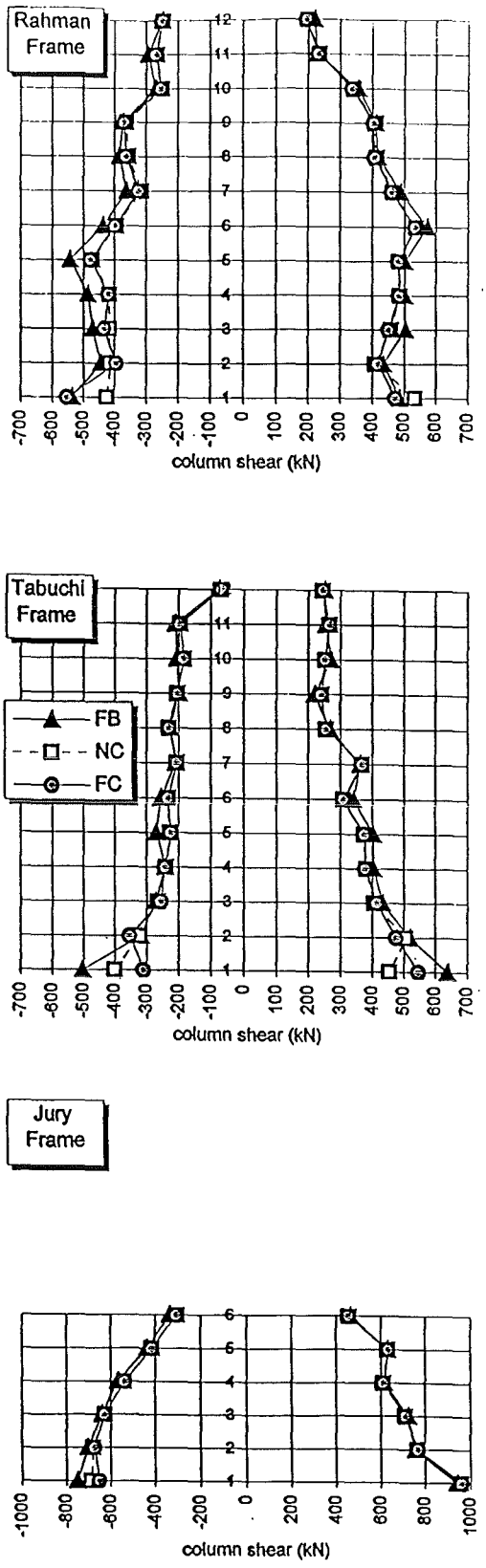

Fig. 5.27: Effect of foundation fixity assumptions on impact-side column shear envelope for no pounding case.
1971 Pacoima Dam earthquake applied left-right.

FB = Fixed Base
NC = Non-Coupled (i.e. through-soil coupling not considered)
FC = Foundations Coupled

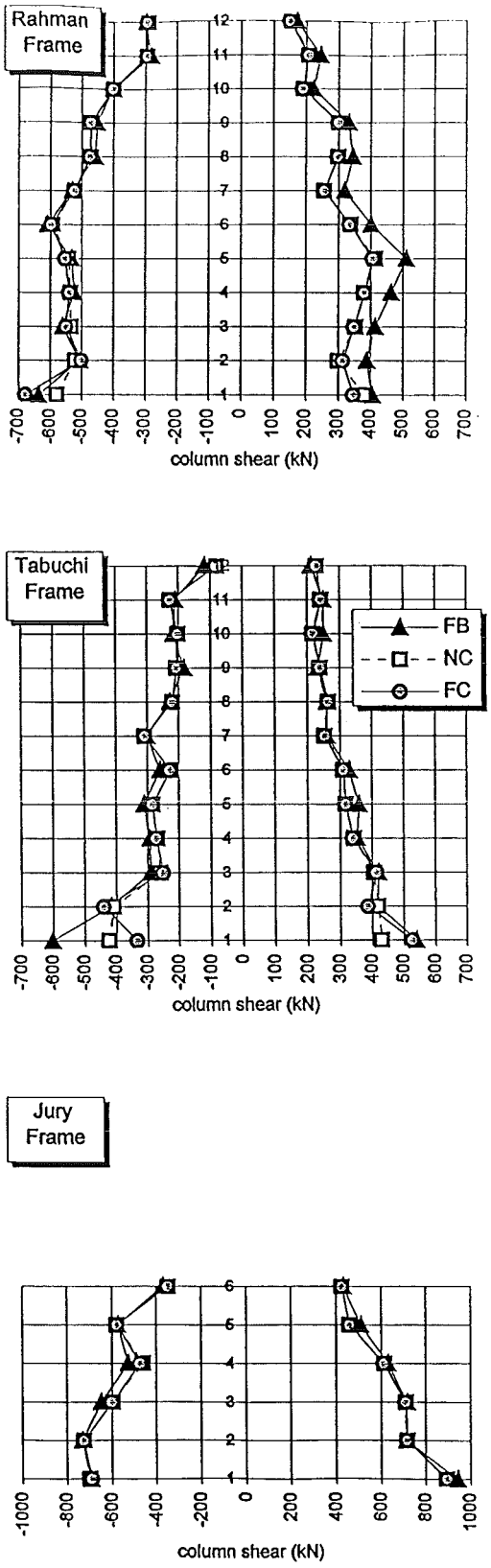

Fig. 5.28: Effect of foundation fixity assumptions on impact-side column shear envelope for no pounding case.
1971 Pacoima Dam earthquake applied right-left.

FB = Fixed Base
NC = Non-Coupled (i.e. through-soil coupling not considered)
FC = Foundations Coupled

This beneficial influence of the Jury frame is even more conspicuous when the excitation is applied from the opposite direction (i.e. negative direction earthquake, Fig. 5.18). This aspect merits further investigation to assess the effects of adjacent buildings on structural design and performance under seismic loading.

While large reductions (30-40%) may be observed in the shear amplification ratios of the level 6 columns of the Jury frame due to soil-structure interaction (Figs. 5.16 and 5.18), the overall effects of through-soil foundation coupling are not as conspicuous as in the Rahman frame. In addition, the negative shear amplification ratios are more sensitive to the direction of seismic attack.

The beneficial effects of through-soil foundation interaction are highly apparent in the Tabuchi frame (Figs.5.15 and 5.17), especially for the negative shear amplification ratios at ground floor level (between 50-60%). The unusually large increase in negative shear at the top storey column of the Tabuchi frame (Fig. 5.17) is due to a large increase in small values. The effects of foundation flexibility on the values of maximum impact-side column shears for the three frames may be identified quantitatively in Figs. 5.19 and 5.20.

The effects of foundation fixity assumptions on response characteristics are highlighted in the free-vibration phase of the time-histories in Figs. 5.21 and 5.22 (shown here for ground floor level columns). The Jury and Rahman frames display similar trends in this respect with a significant change in the frequency content of the response (out-of-phase) compared to the fixed base case. Residual shear forces, which are present in all frames, do not exhibit a change in sign with direction of excitation.

b) 1971 Pacoima Dam Earthquake

The Tabuchi frame experiences the highest reductions due to through-soil coupling, as is evidenced in the shear amplification plots (Figs. 5.23 to 5.26). The effects of the adjacent structures on the response of the Rahman frame are also manifested for this excitation case, especially in the positive direction (Figs. 5.23 and 5.24).

Inspection of impact-side column shear envelopes for this case (Figs. 5.27 and 5.28) reveals trends similar to those observed for the case of the 1940 El Centro excitation, namely:

- A larger variation in ground column shears is discernible for the different foundation conditions of the Tabuchi frame.

- The benefits of foundation compliance in the Rahman frame are not as obvious as in the previous excitation although the differences between the results in which soil-structure interaction is incorporated and those considering through-soil foundation coupling are just as conspicuous. Through-soil interaction effects in the Jury frame are not as apparent as in the previous excitation cases. A notable exception to this is the positive excitation case where the reductions in ground floor negative shear amplification ratios in the Jury frame exceed 20%.

The same observations are noted regarding the shear time-histories as in the El Centro excitation case (see Figs. A.4 and A.5).

5.6.5 Pounding Case

The response trends of impact force variation for the various cases are presented in Appendix B. The sections below review the most prominent trends exhibited in the various cases investigated.

5.6.5.1 Configuration 1

a) 1940 El Centro Excitation

The effect of foundation compliance on the maximum impact forces is evident in this case (Figs. 5.29 and 5.30). Moreover, the characteristics of the impact forces (envelopes and time-histories) are highly dependent on the direction of excitation for all conditions of foundation fixity (e.g. for top storey pounding shown in Figs. 5.31 and 5.32). The effects of through-soil coupling on maximum impact forces are very similar to those of soil-structure interaction, except for the 1mm separation gap case (Figs. 5.29 and 5.30) where a slight reduction of maximum impact forces at mid-height is apparent.

The influence of through-soil coupling on pounding time-history is clearly discernible, typified in Figs. 5.31 (1mm gap) and 5.32 (24mm gap) for level 12. A slight reduction in impact force amplitudes is observed in addition to damping of the low amplitude multiple impacts.

When fixed base structures are assumed, a negative direction earthquake effects lower impact forces and fewer levels which sustain pounding compared to the opposite direction of excitation. This is especially evident for the larger separation gaps at lower levels. However, with the consideration of soil-structure interaction, the following observations may be noted:

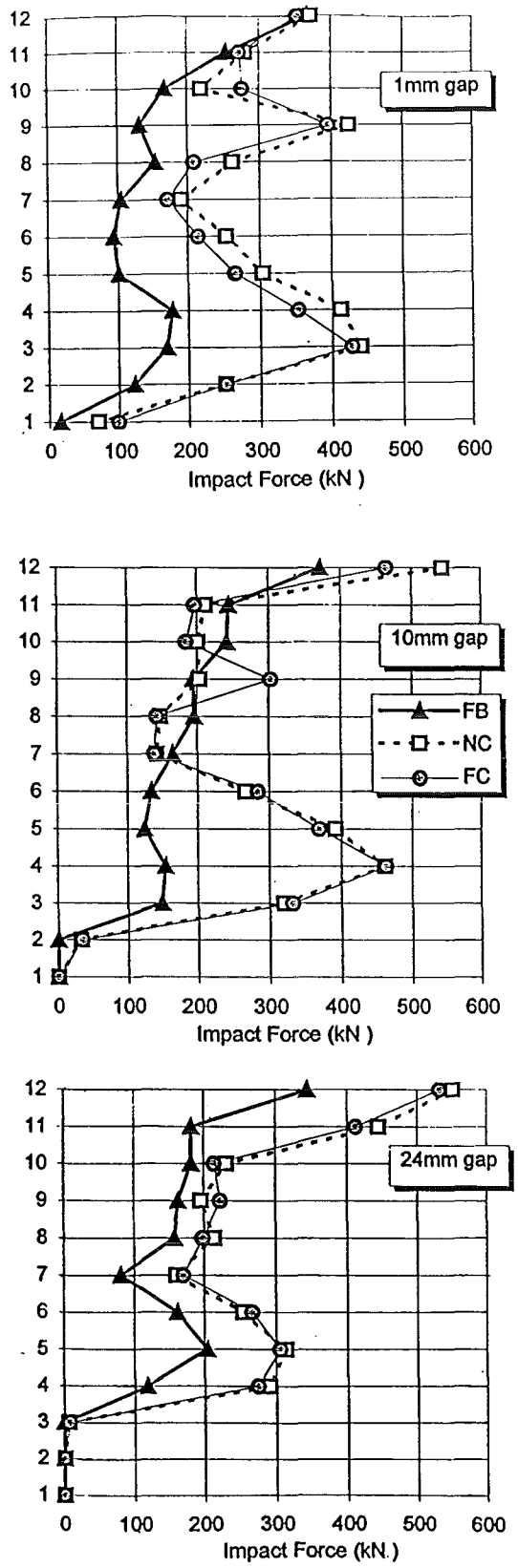

Fig. 5.29: Impact force envelopes for various separation gaps and foundation conditions.
1940 El Centro earthquake applied left-right.

FB = Fixed Base
NC = Non-Coupled (i.e. compliant foundations without through-soil interaction modelling)
FC = Foundations Coupled

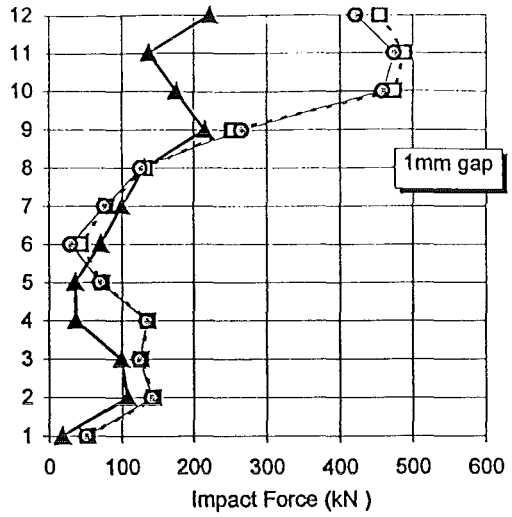

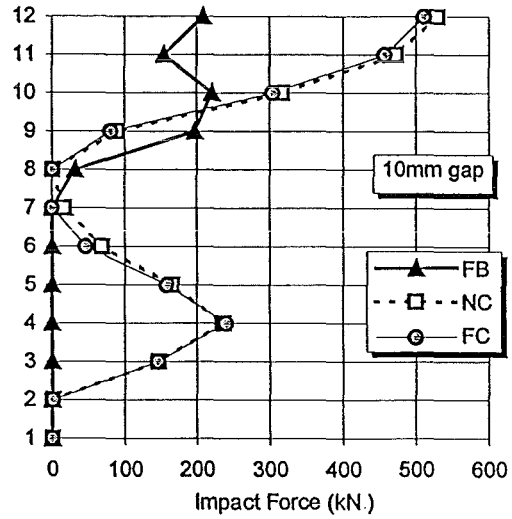

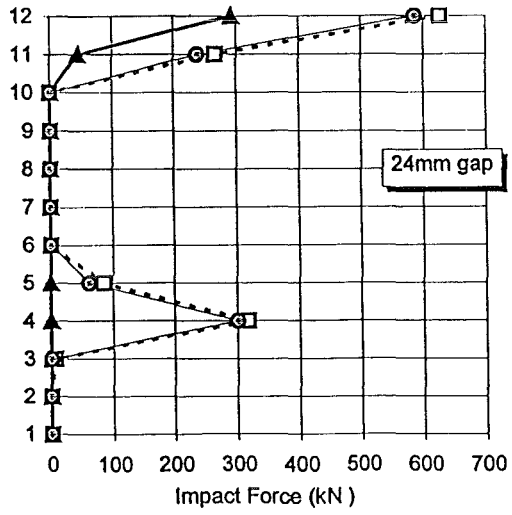

Fig. 5.30: Impact force envelopes for various separation gaps and foundation conditions.
1940 El Centro earthquake applied right-left.

FB = Fixed Base
NC = Non-Coupled (i.e. compliant foundations without through-soil interaction modelling)
FC = Foundations Coupled

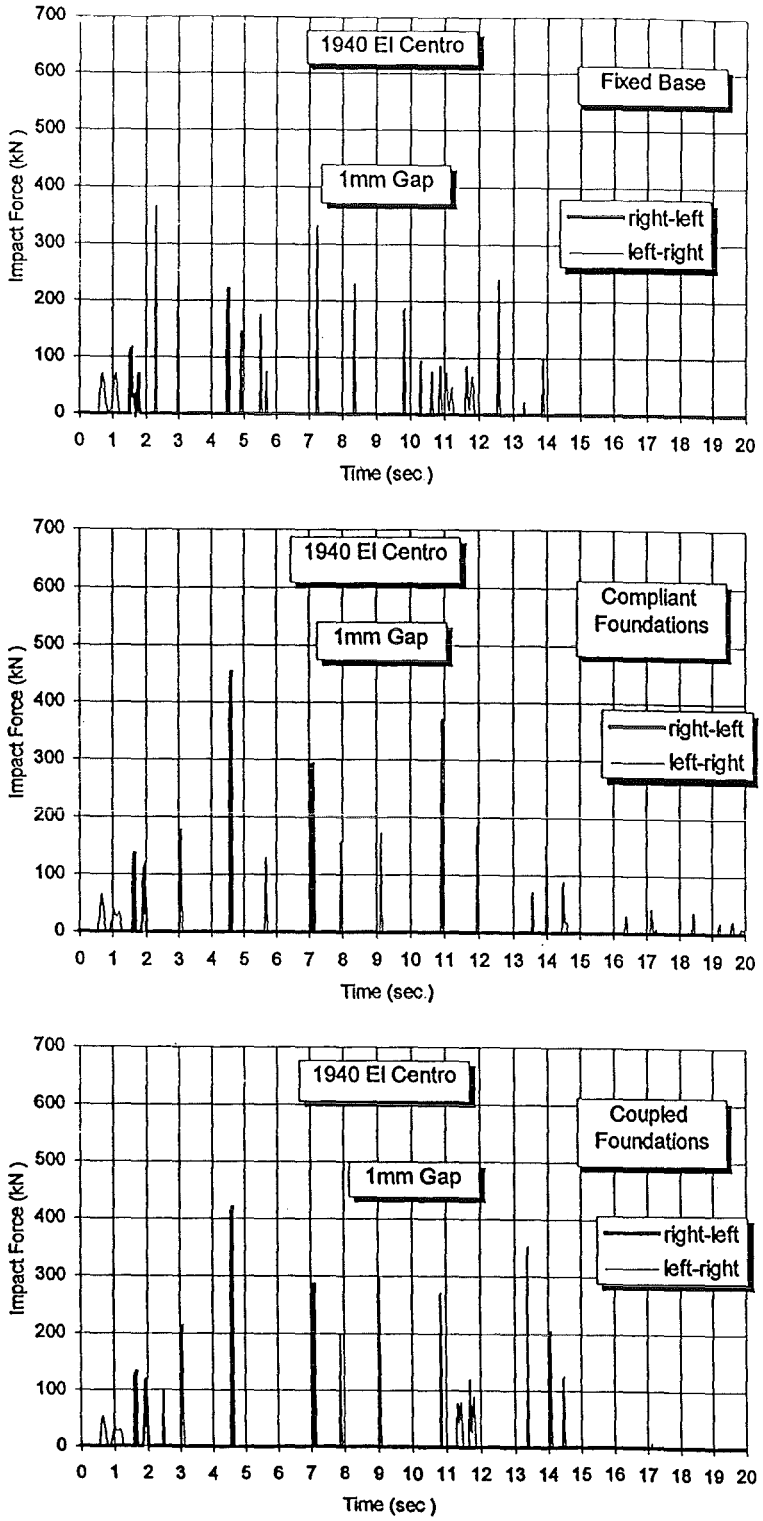

Fig. 5.31: Effect of earthquake direction on level 12 impact force time-history for various foundation conditions and 1mm separation gap. Rahman and Tabuchi Frames. 1940 El Centro earthquake.

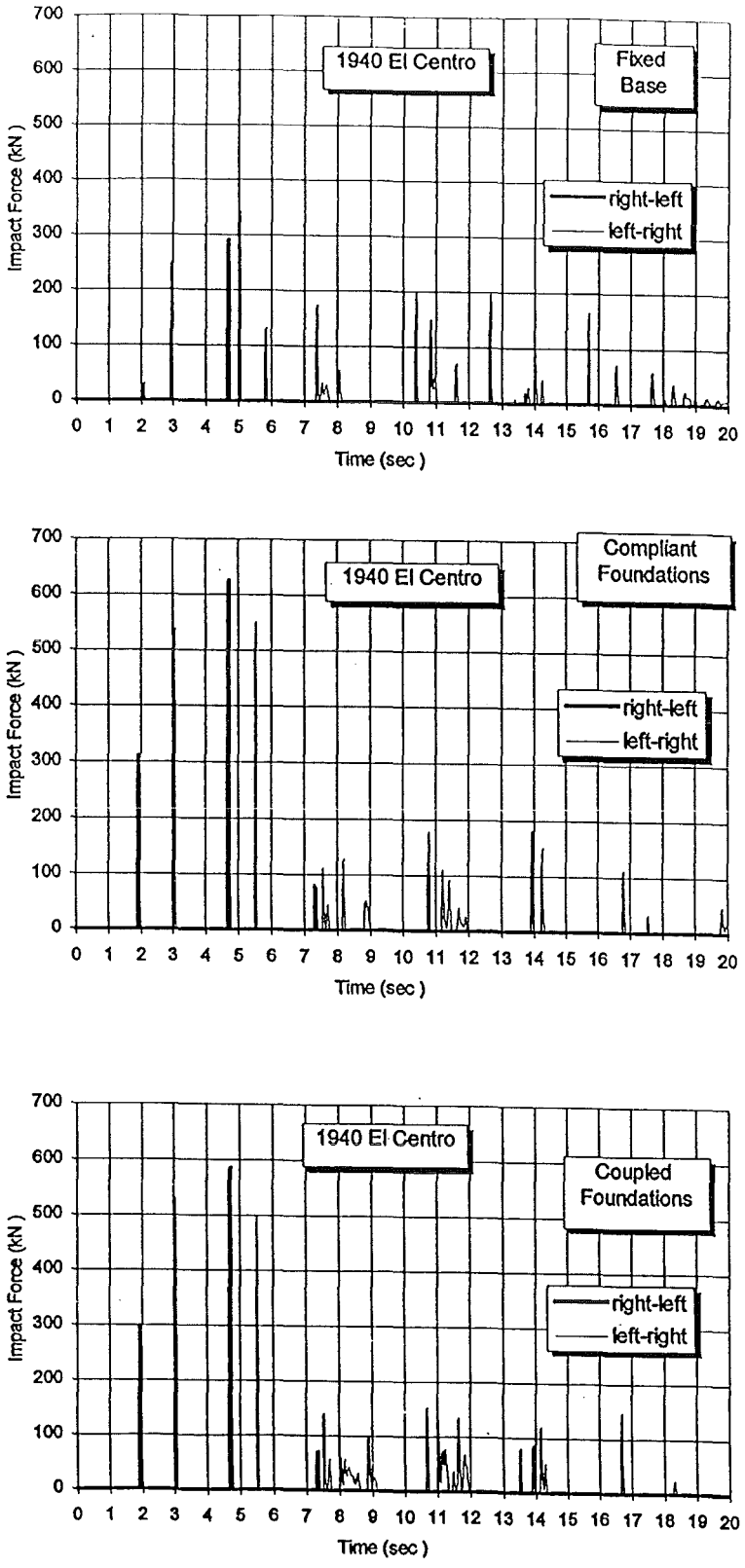

Fig. 5.32: Effect of earthquake direction on level 12 impact force time-history for various foundation conditions and 24mm separation gap. Rahman and Tabuchi Frames. 1940 El Centro earthquake.

- Under positive earthquake excitations, the impact forces at levels 11 and 12 for the 1mm separation gap are almost equal to those of the fixed base case (Fig. 5.29). The increases due to soil-structure interaction are restricted to levels 1 to 10 for this case of initial separation gap.
- For the same direction of excitation as above, the increases (due to compliance) at the lower levels in impact force magnitudes for all separation gaps are more conspicuous than those observed at the upper levels.
- Under the influence of a negative direction excitation, the fixed base impacts are of smaller magnitudes at all levels and for all separation gaps considered in comparison with the positive excitation cases (Fig. 5.30). In addition, the number of levels which sustain pounding decrease markedly with increasing initial separation gap. However, when compliance is accounted for, the impact forces attained at the top level are comparable to those attained under a positive earthquake. The number of stories which experience pounding in the systems with the larger separation gaps is still fewer than the number of stories in the corresponding cases for the opposite direction of excitation (i.e. from the direction of the Rahman frame).
- For the larger separation gaps, compliance results in the manifestation of pounding at locations where no impacts are witnessed in the fixed base case. This is especially evident in the systems subjected to a negative direction earthquake and with larger separation gaps (Fig. 5.30).

Figs. 5.29 and 5.30 demonstrate the validity of recommendations pertaining to the location of the contact element at the upper level of numerical and analytical models in pounding studies [e.g. J1, K4, K6, M3, and M5]. Exceptions are noted, however, for the smaller separation gaps (1mm and 10mm) when soil-structure interaction is taken into account. The lower levels may experience impact forces comparable to (or exceeding) those developed at the top storey.

The importance of the direction of excitation on pounding time-history is demonstrated in Figs. 5.31 (1mm gap) and 5.32 (24mm gap) for top storey pounding, as an example. When soil flexibility is taken into account, larger impact forces are developed when the excitation is applied from the direction of the smaller period Tabuchi frame (negative earthquake). However, the number of impacts is significantly higher for the opposite direction of seismic excitation.

Another significant effect of foundation fixity conditions is the temporal shift at which maximum impacts occur. These shifts are discernible only in the case of positive direction excitation.

b) 1971 Pacoima Dam Earthquake

The pounding response appears to be more sensitive in this excitation case to the direction of seismic excitation than the El Centro earthquake case (Figs. 5.33 and 5.34). In addition, the effects of through-soil foundation coupling are more conspicuous. Soil flexibility is beneficial in reducing the maximum impact forces for the systems subjected to a positive direction earthquake (Fig. 5.33). Under an opposite direction excitation a slight increase in maximum impact forces, compared to the fixed base case, is perceived especially at the upper levels. For this (negative) direction of excitation, the difference between fixed base and coupled foundation impacts (i.e. considering through-soil interaction) increases with increasing separation gap. A different trend is noted for the case of the 1mm separation gap where the intermediate levels experience a reduction due to soil flexibility effects.

The effect of soil flexibility on the manifestation of pounding is opposite to that noted for the El Centro case (Figs. 5.29 and 5.30): the impacts detected at certain levels assuming fixed base conditions do not occur under flexible soil conditions.

A number of similarities to the case of the El Centro earthquake excitation may be identified. These are as follows:

- Maximum impact forces comparable to top level impacts are developed at the lower levels in the (flexible soil) 1mm separation gap case. As in the El Centro case, this is only evident under positive direction excitation.
- The impact forces at the upper levels are significantly higher for flexible soil conditions under negative direction excitation.

The influence of foundation flexibility and direction of earthquake on level 12 impact time-history for the 1mm and 24mm separation gaps is presented in Figs. 5.35 and 5.36, respectively. The main features are:

- A significant reduction in the number of top-level impacts is observed when the excitation is applied from the negative direction.
- For a positive direction earthquake the magnitudes of the impact forces are lower at top level for both separation gaps when foundation flexibility is accounted for.

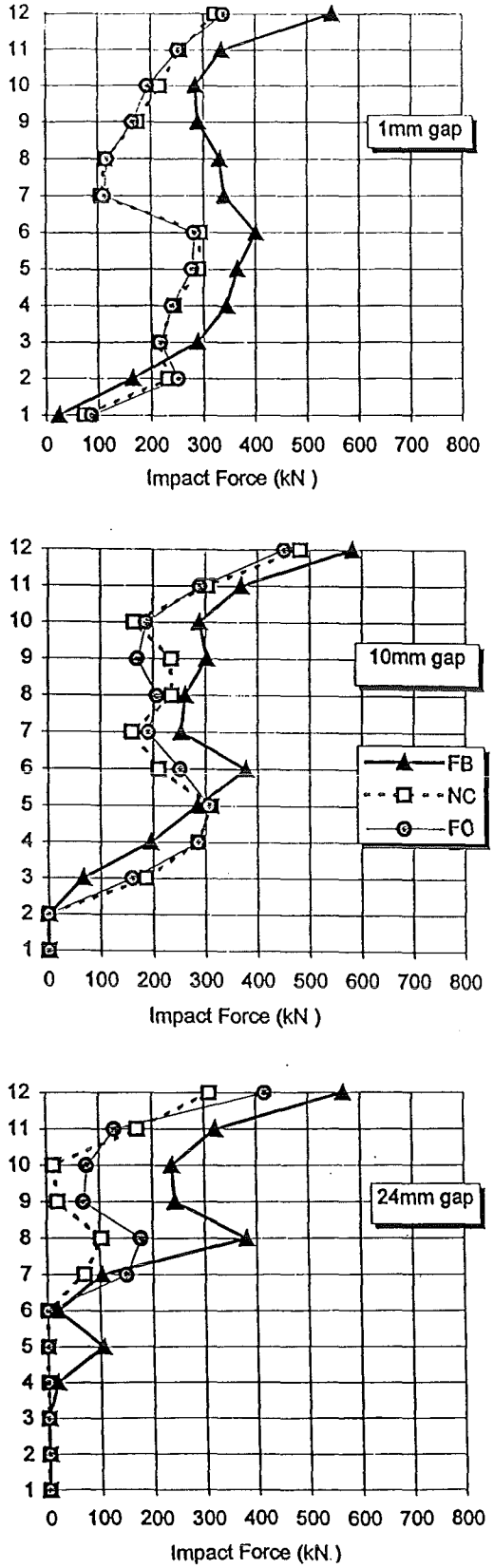

Fig. 5.33: Impact force envelopes for various separation gaps and foundation conditions.
1971 Pacoima Dam earthquake applied left-right.

FB = Fixed Base
NC = Non-Coupled (i.e. compliant foundations without through-soil interaction modelling)
FC = Foundations Coupled

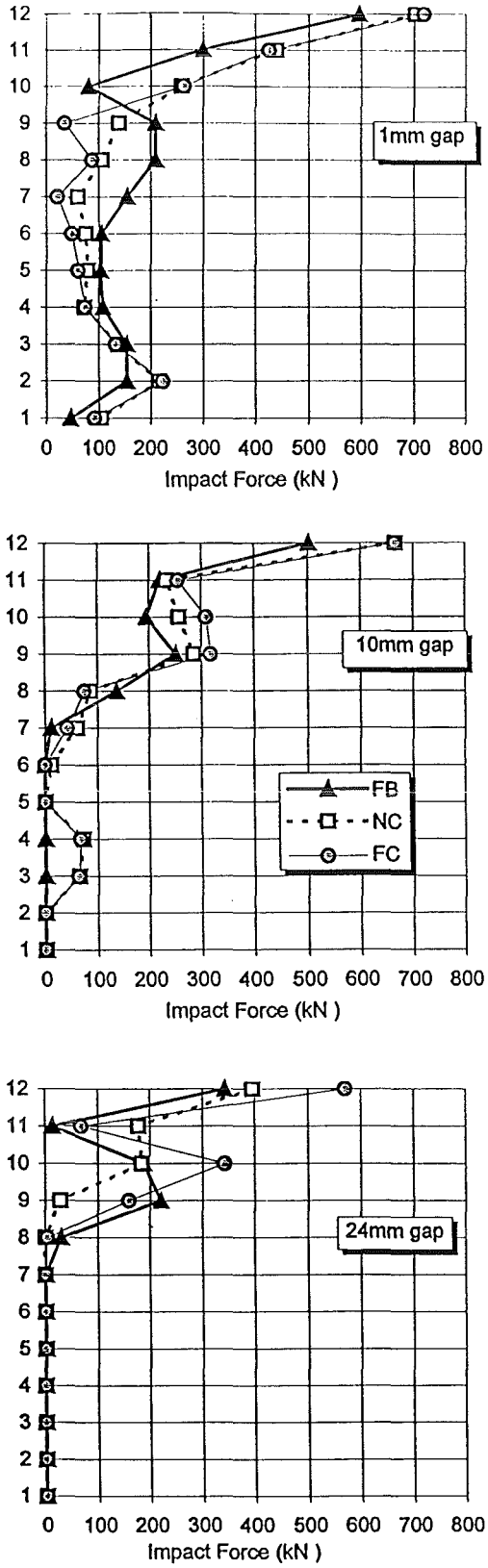

Fig. 5.34: Impact force envelopes for various separation gaps and foundation conditions.
1971 Pacoima Dam earthquake applied right-left.

FB = Fixed Base
NC = Non-Coupled (i.e. compliant foundations without through-soil interaction modelling)
FC = Foundations Coupled

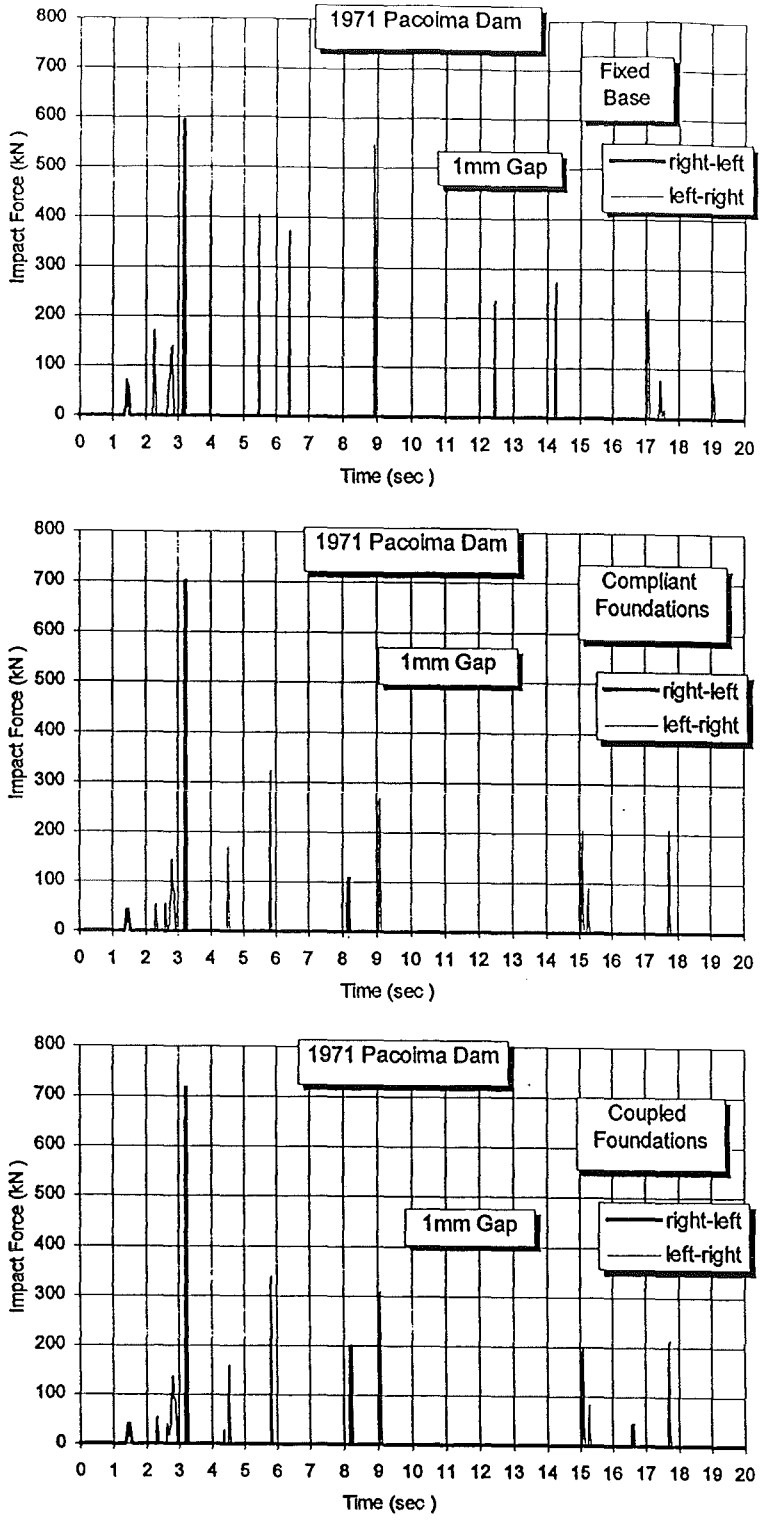

Fig. 5.35: Effect of earthquake direction on level 12 impact force time-history for various foundation conditions and 1mm separation gap. Rahman and Tabuchi Frames. 1971 Pacoima Dam earthquake.

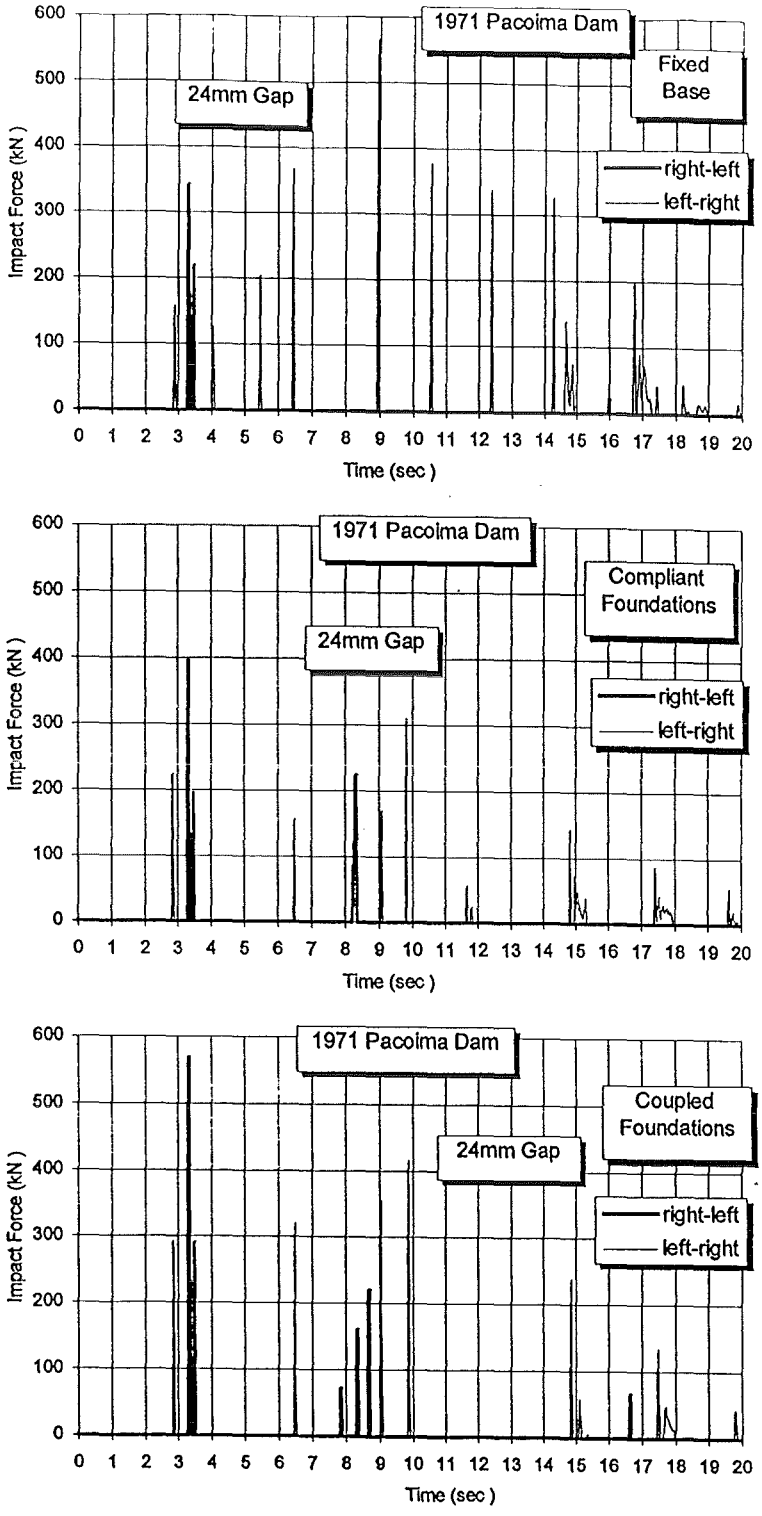

Fig. 5.36: Effect of earthquake direction on level 12 impact force time-history for various foundation conditions and 24mm separation gap. Rahman and Tabuchi Frames. 1971 Pacoima Dam earthquake.

- The effects of through-soil interaction are highly dependent on the initial separation gap and the direction of excitation. For top storey pounding of the configuration under investigation, the larger separation gap appears to be more sensitive to the effects of excitation direction. For this separation gap, through-soil coupling results in an increase in the magnitudes of impact forces, especially when the excitation is applied from the positive direction. An increase in the number of small amplitude impacts may is observed for the negative direction excitation case. Temporal shifts of impact forces under positive direction excitation are also discernible in this earthquake.

5.6.5.2 Configuration 2

a) 1940 El Centro Earthquake

A more coherent trend is discernible in the variation of maximum impact forces for all cases of separation gaps in this configuration than those observed in the Configuration 1 cases. For all separation gaps, base fixity conditions and directions of excitation, the impact forces developed at the six levels in this configuration are much higher than the corresponding values of the two twelve-storey frame configuration.

The most notable characteristics observed for this configuration under the El Centro earthquake are:

- An increase in maximum impact forces at all levels and for both directions of excitation due to soil-structure interaction (Figs. 5.37 and 5.38).
- Level 6 impacts are significantly higher than those developed at the other levels for both directions of seismic excitation.
- For fixed base buildings, the maximum impact forces in each case of separation gap size are independent of the direction of excitation. This is not the case when foundation flexibility is accounted for. A negative direction earthquake produces larger impact forces for all initial separation gaps when soil flexibility is considered.
- The effect of through-soil coupling is evident only in the case of the 1mm separation gap for positive direction excitation (Fig. 5.37).

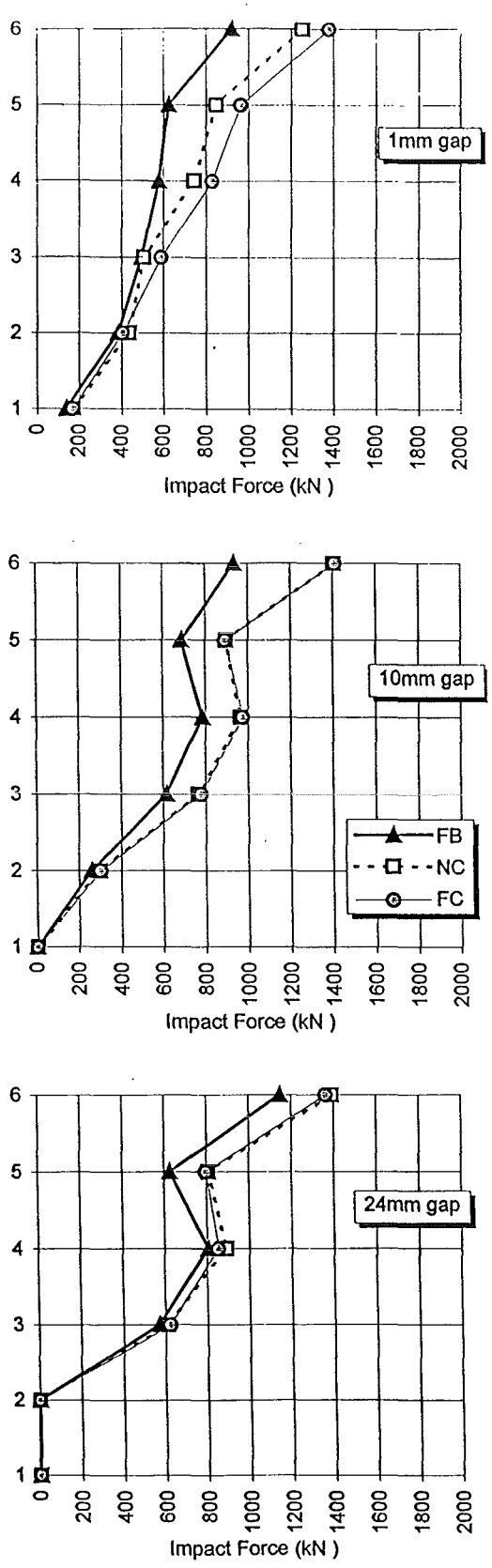

Fig. 5.37: Impact force envelopes for various separation gaps and foundation conditions. Rahman and Jury Frames. 1940 El Centro earthquake applied left-right.

FB = Fixed Base
NC = Non-Coupled (i.e. compliant foundations without through-soil interaction modelling)
FC = Foundations Coupled

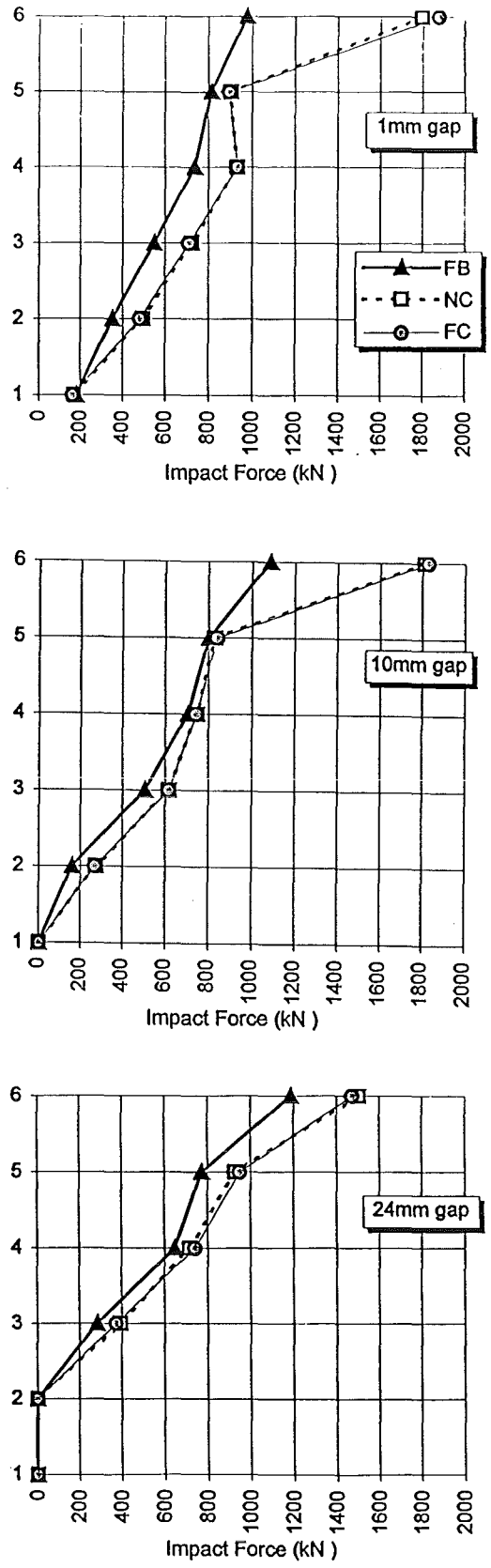

Fig. 5.38: Impact force envelopes for various separation gaps and foundation conditions (Rahman and Jury Frames). 1940 El Centro earthquake applied right-left.

FB = Fixed Base
NC = Non-Coupled (i.e. compliant foundations without through-soil interaction modelling)
FC = Foundations Coupled

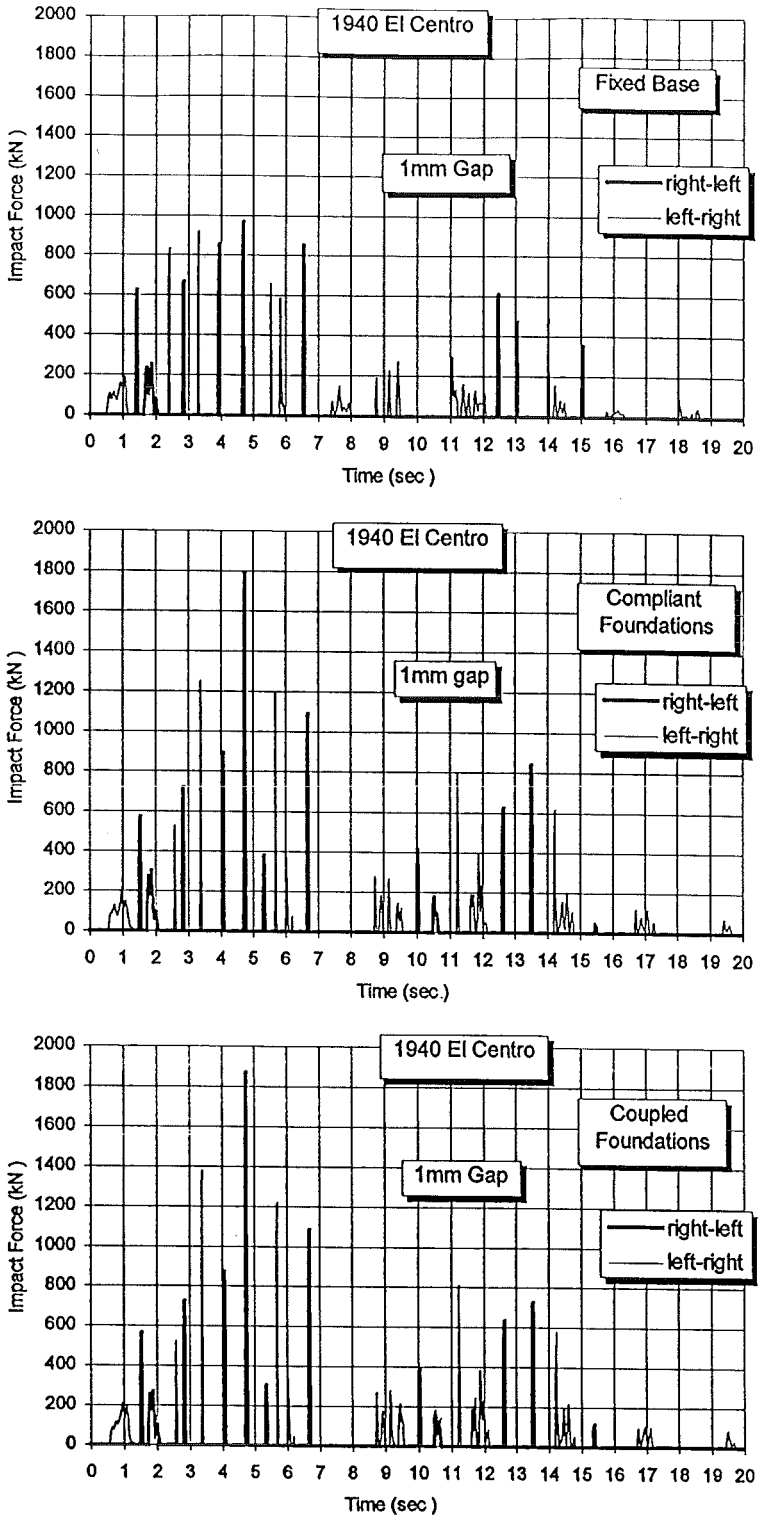

Fig. 5.39: Effect of earthquake direction on level 6 impact force time-history for various foundation conditions and 1mm separation gap. Rahman and Jury Frames. 1940 El Centro earthquake.

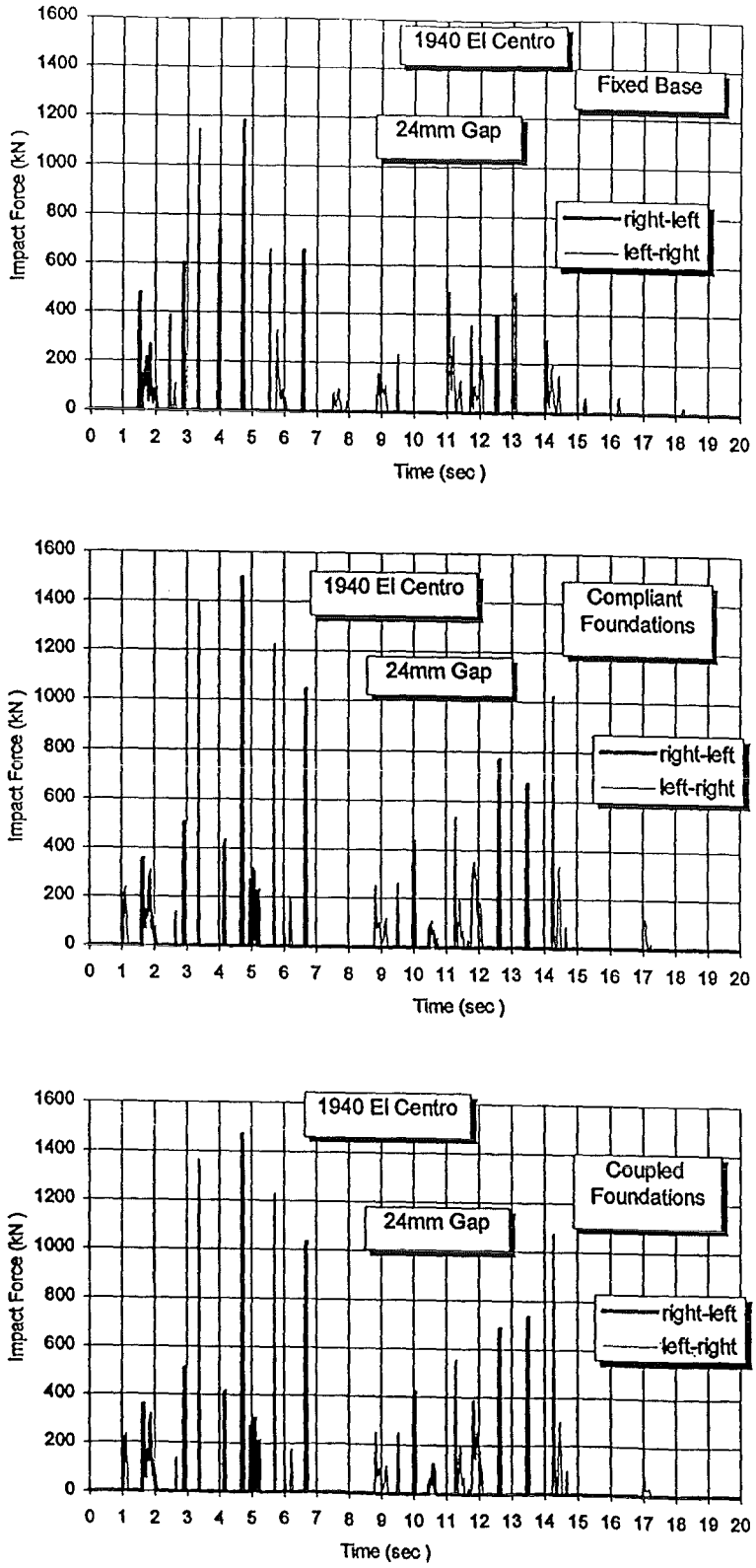

Fig. 5.40: Effect of earthquake direction on level 6 impact force time-history for various foundation conditions and 24mm separation gap. Rahman and Jury Frames. 1940 El Centro earthquake.

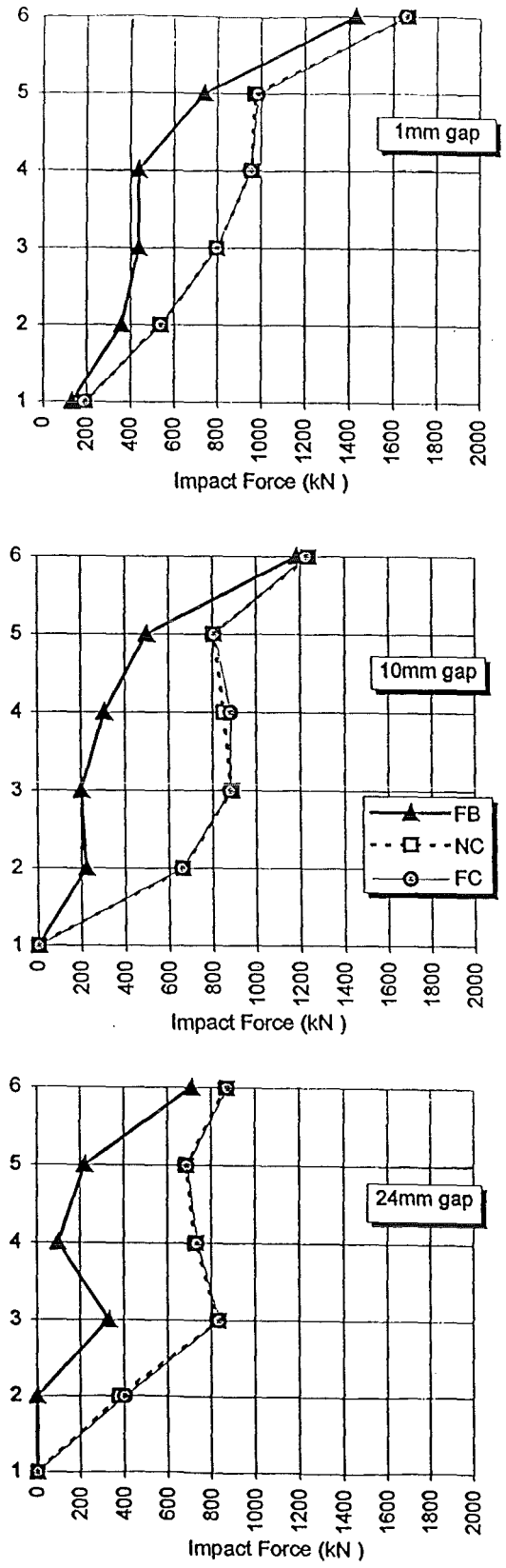

Fig. 5.41: Impact force envelopes for various separation gaps and foundation conditions (Rahman and Jury Frames). 1971 Pacoima Dam earthquake applied left-right.

FB = Fixed Base
NC = Non-Coupled (i.e. compliant foundations without through-soil interaction modelling)
FC = Foundations Coupled

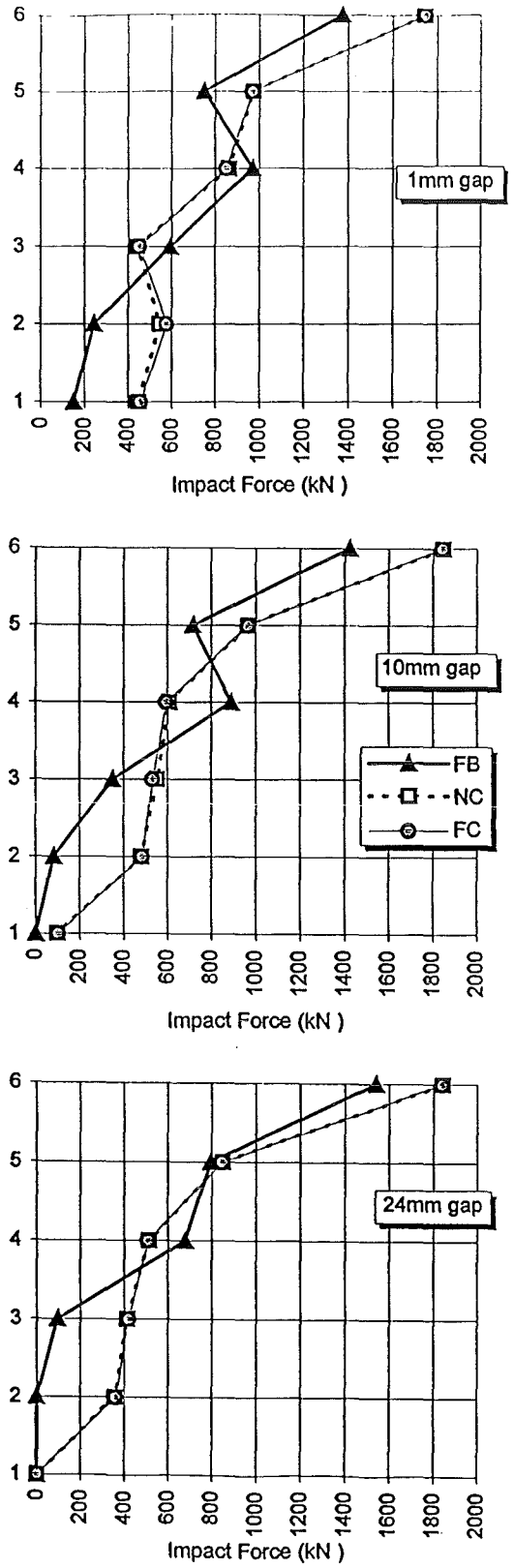

Fig. 5.42: Impact force envelopes for various separation gaps and foundation conditions (Rahman and Jury Frames). 1971 Pacoima Dam earthquake applied right-left.

FB = Fixed Base
NC = Non-Coupled (i.e. compliant foundations without through-soil interaction modelling)
FC = Foundations Coupled

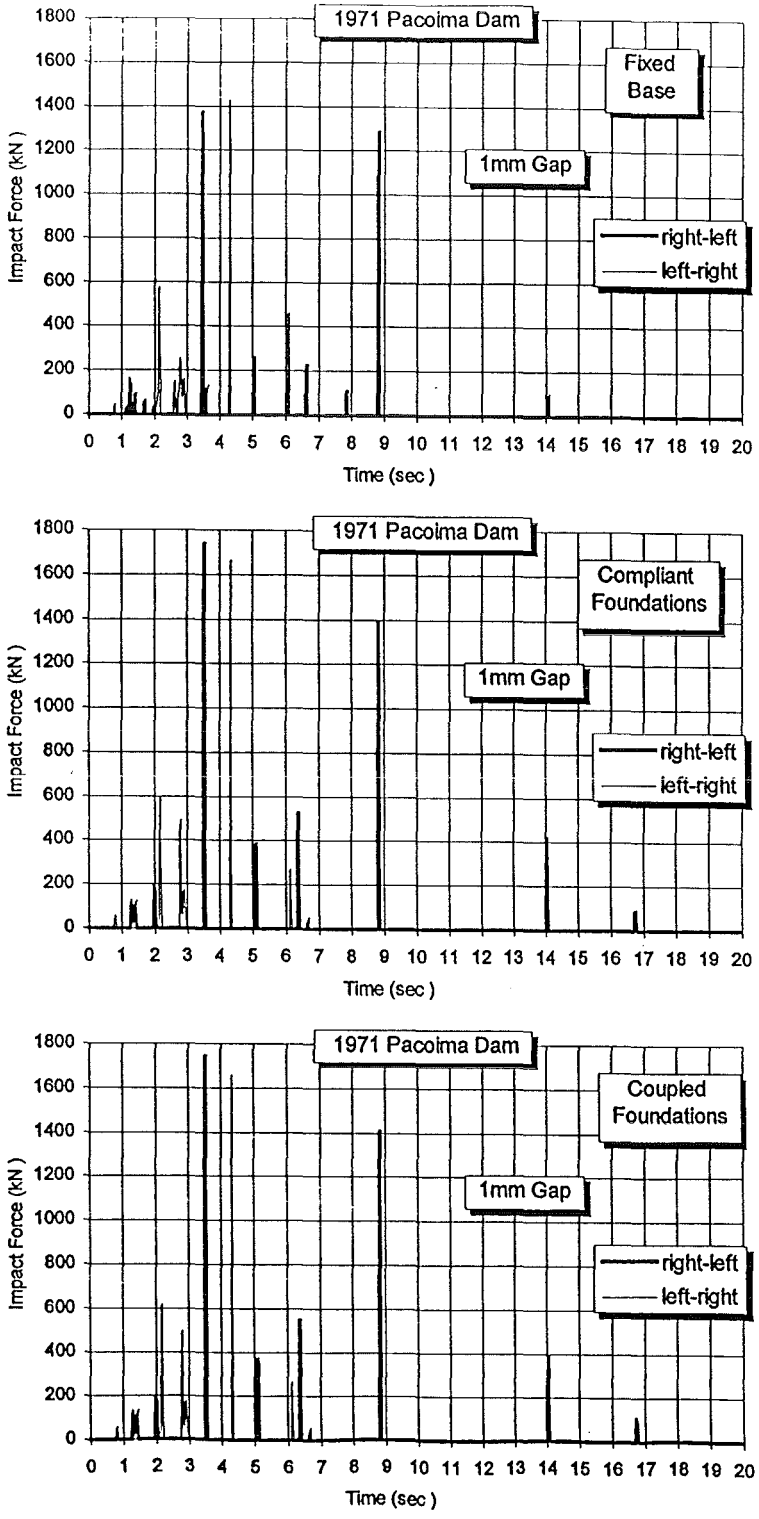

Fig. 5.43: Effect of earthquake direction on level 6 impact force time-history for various foundation conditions and 1mm separation gap. Rahman and Jury Frames. 1971 Pacoima Dam earthquake.

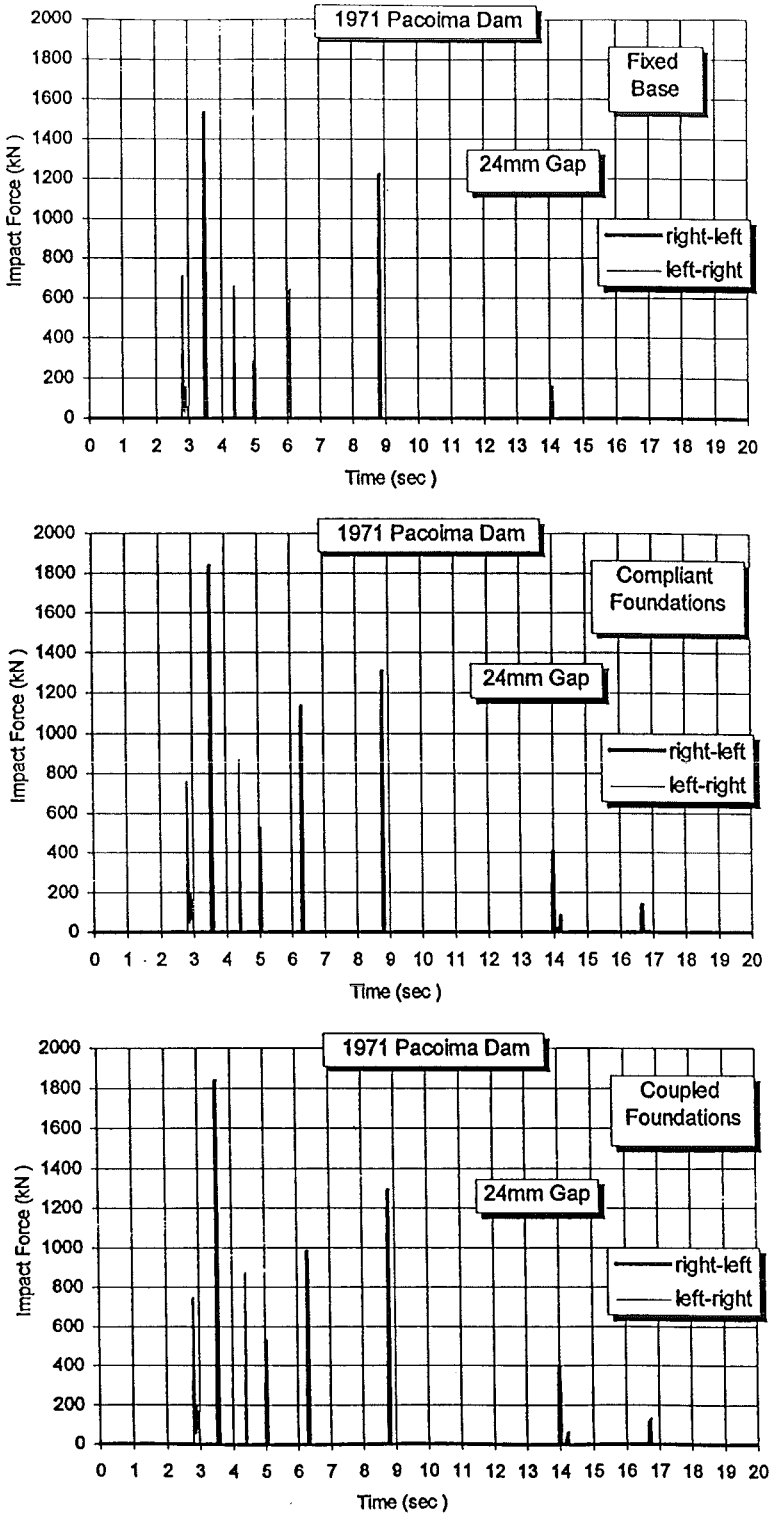

Fig. 5.44: Effect of earthquake direction on level 6 impact force time-history for various foundation conditions and 24mm separation gap. Rahman and Jury Frames. 1971 Pacoima Dam earthquake.

The influence of excitation direction and foundation conditions on the time-history of level 6 impact force are presented in Figs. 5.39 (1mm separation gap) and 5.40 (24mm gap). As in the previous configuration (two twelve-storey frames), consideration of soil-structure interaction results in an increase in the number and magnitude of impact forces. The direction of the seismic excitation clearly influences the times at which the impacts occur in addition to the frequency content and magnitudes of impacts. However, the temporal effects of foundation compliance on the occurrence of maximum impact are not as conspicuous as in the previous configuration. In addition, the influence of through-soil coupling is minimal.

b) 1971 Pacoima Dam Earthquake

As in the case of the El Centro excitation, the various cases of separation gaps display similar trends depending on the direction of excitation (Figs. 5.41 and 5.42). However, the nature of these trends differs markedly from those observed for the El Centro excitation. These trends may be enumerated as follows:

- The effect of foundation flexibility conditions on the maximum impact forces, with respect to the assumption of a fixed base, is dependent on the direction of excitation. For positive excitation, compliance increases the impact forces at mid-height of the Jury (six-storey) frame and has either no (10mm gap) or limited effect (1mm and 24mm gaps) on the top level impact forces (Fig. 5.41).
- The influence of excitation direction is especially notable with respect to the effect of separation gap on the maximum impact force developed at level 6. The smaller separation gaps results in progressively larger impact forces for positive excitation. A negative direction earthquake results in larger impact forces that are independent of the initial separation gap magnitude.
- The effects of through-soil foundation interaction are negligible for all cases of excitation and separation gaps.

The influence of earthquake direction, in addition to separation gap and foundation fixity conditions, on level 6 impact time-history is presented in Figs. 5.43 and 5.44 (for 1mm and 24mm separation gaps, respectively). The effects of foundation flexibility are not as conspicuous as in the twelve-storey cases (Configuration 1). The increased number and magnitude of impacts for the case of excitation from the direction of the frame with lower natural period (i.e. Jury frame) is apparent.

5.6.6 Shear in Impact-Side Columns

In this section, the results of variation of initial separation gap on the column shears for the coupled foundations case only will be presented. Quantitative comparisons presented in Appendices C-E highlight the effect of pounding on column shears (in addition to other response characteristics) in the three frames for the different foundation conditions and (positive direction) excitations implemented in this study.

5.6.6.1 Configuration 1

a) 1940 El Centro Earthquake

As an example of the effects of foundation fixity conditions, Fig. 5.45 presents the response amplification ratios of column shear in the Tabuchi frame for various initial separation gaps. While the fixed base response of the Tabuchi frame appears to be relatively insensitive to the magnitude of the initial separation gap, consideration of soil flexibility reveals that this is not the case. Reductions of up to 60% are witnessed in the negative shears at ground floor level columns for the coupled foundation case. The conventional fixed base assumption gives the erroneous impression that variations from the no pounding case are almost negligible at this level. These trends are displayed quantitatively in Fig. 5.46. Similar observations may be made for the other frames regarding the influence of foundation fixity conditions in all the cases considered.

In certain cases (e.g. the upper levels of the Tabuchi frame in Fig. 5.49), the response amplification ratios exhibit unusually large variations. This is due to the small magnitude of the response values at these locations. Since the ground floor column shears are of relatively higher magnitudes than at other levels, the response amplification ratios at this level are more indicative of the actual effects of the various factors investigated.

The effects of earthquake direction and magnitude of separation gap are presented in Figs. 5.48 and 5.49 as shear amplification ratios for the coupled Rahman and Tabuchi frames. The Rahman frame displays a higher sensitivity to variations in separation gap size, especially for negative shears. Under the influence of positive excitation, where impacts developed at mid-levels are comparable to those at level twelve (Figs. 5.47), large variations are noted at these levels in the Rahman frame. These effects extend to the ground floor columns, which is even evident in the less sensitive Tabuchi frame (Fig. 5.48).

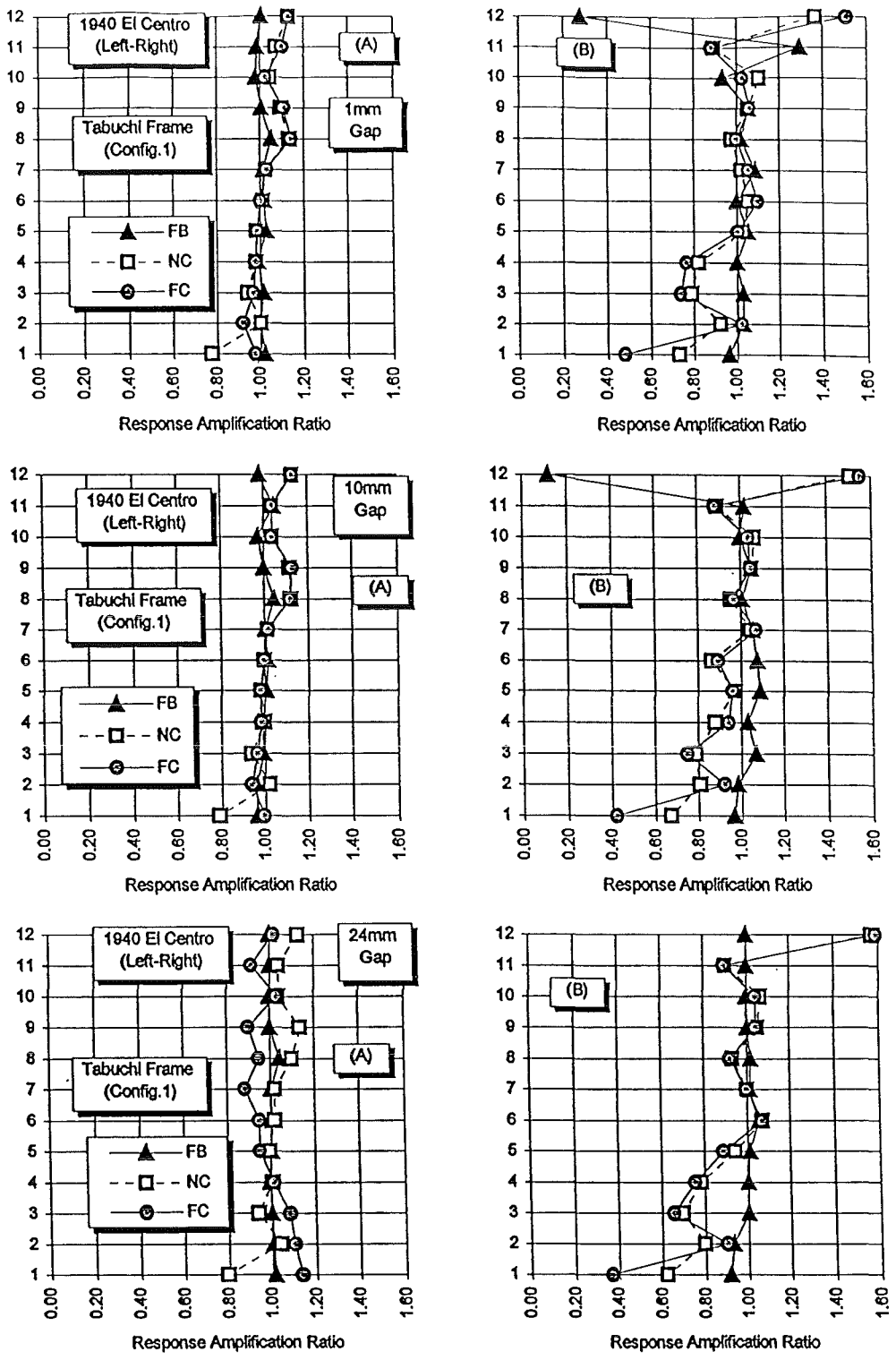

Fig. 5.45: Response amplification ratio (from fixed base no pounding case) of impact-side column shear in Tabuchi Frame (Configuration 1) due to pounding for separation gaps and foundation conditions. 1940 El Centro earthquake applied left-right.

A = Positive Shear B = Negative Shear
FB = Fixed Base
NC = Non-Coupled (i.e. only soil-structure interaction considered)
FC = Foundations Coupled

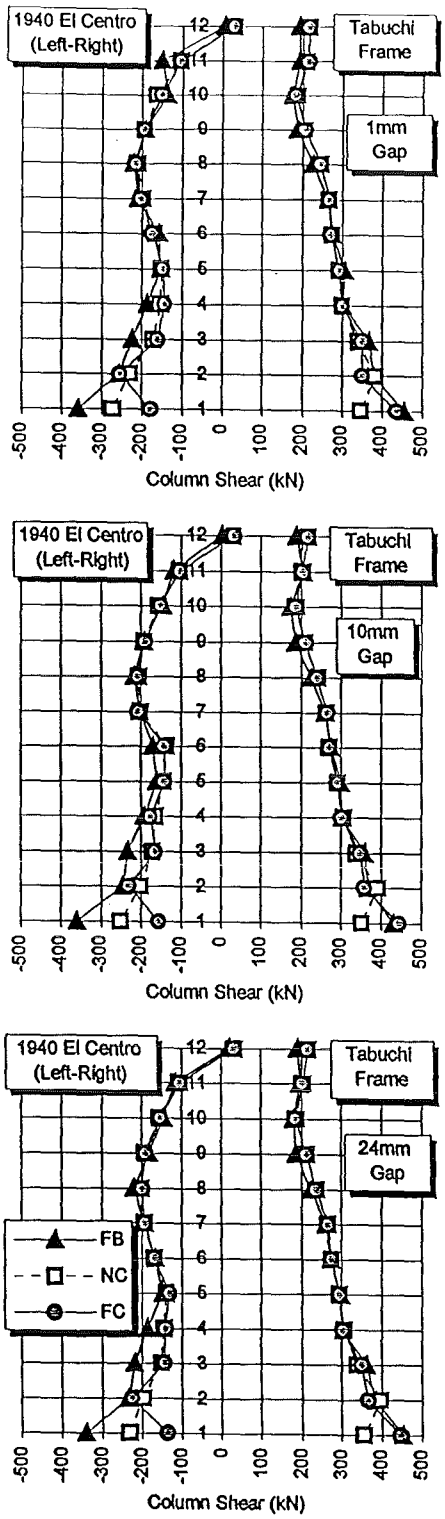

Fig. 5.46: Effect of foundation fixity conditions on impact-side column shears of twelve-storey Tabuchi Frame for various initial separation gaps. 1940 El Centro earthquake applied left-right.

FB = Fixed Base
NC = Non-Coupled (i.e. only soil-structure interaction considered)
FC = Foundations Coupled

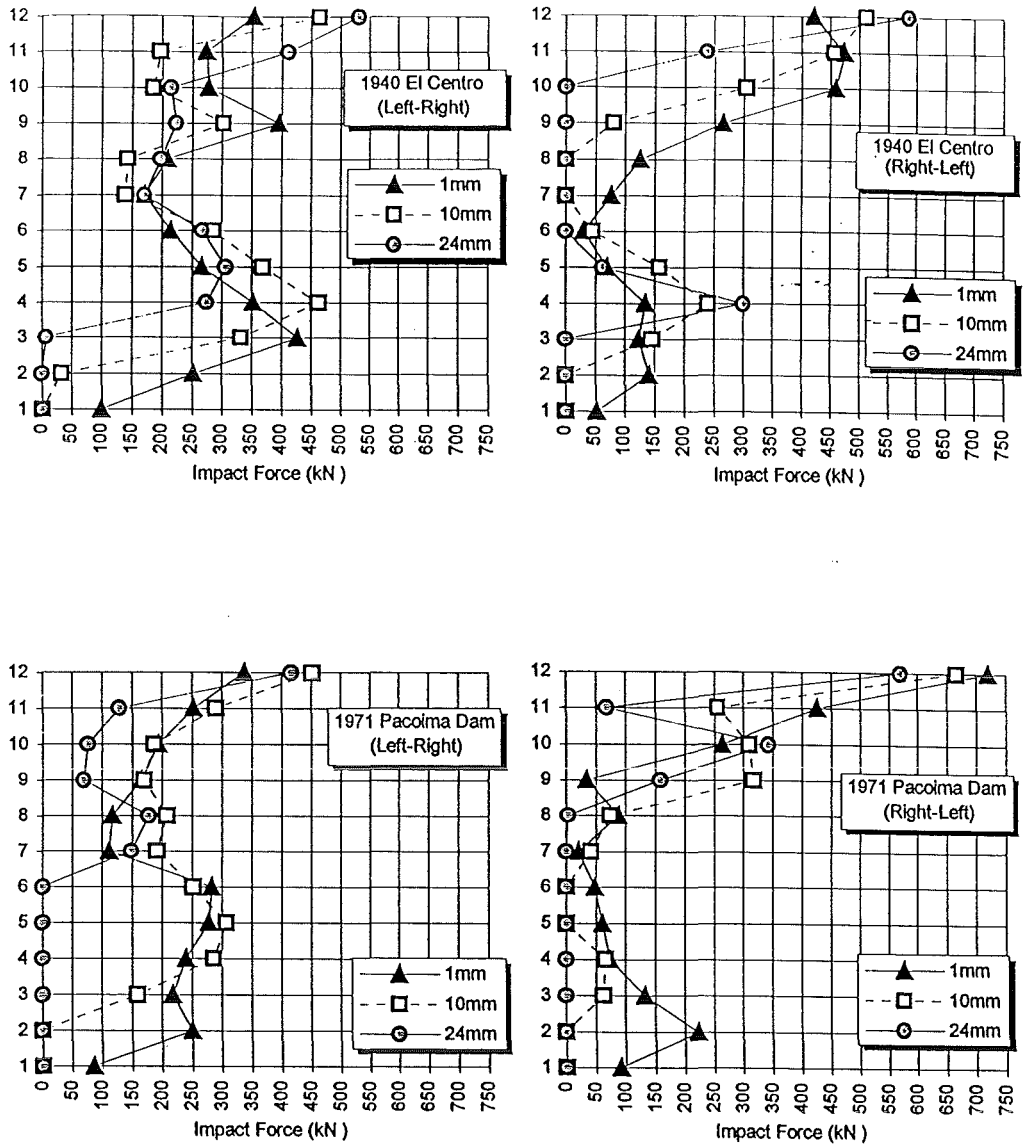

Fig. 5.47: Impact forces developed in Configuration 1 for the various earthquakes and separation gaps. Through-soil interaction case.

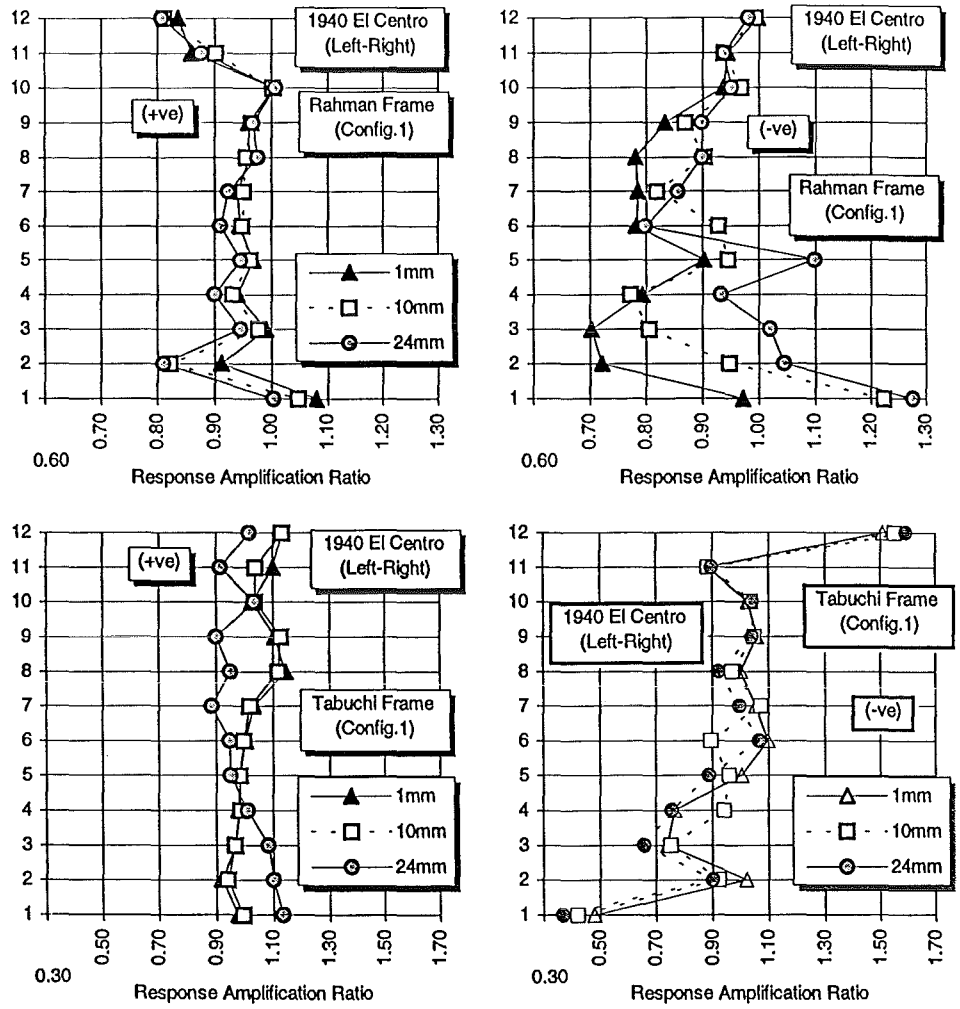

Fig. 5.48: Effect of separation gap on response amplification ratio (from fixed base no pounding case) of impact-side column shear of Configuration 1 frames for coupled foundations case.
1940 El Centro earthquake applied left-right.

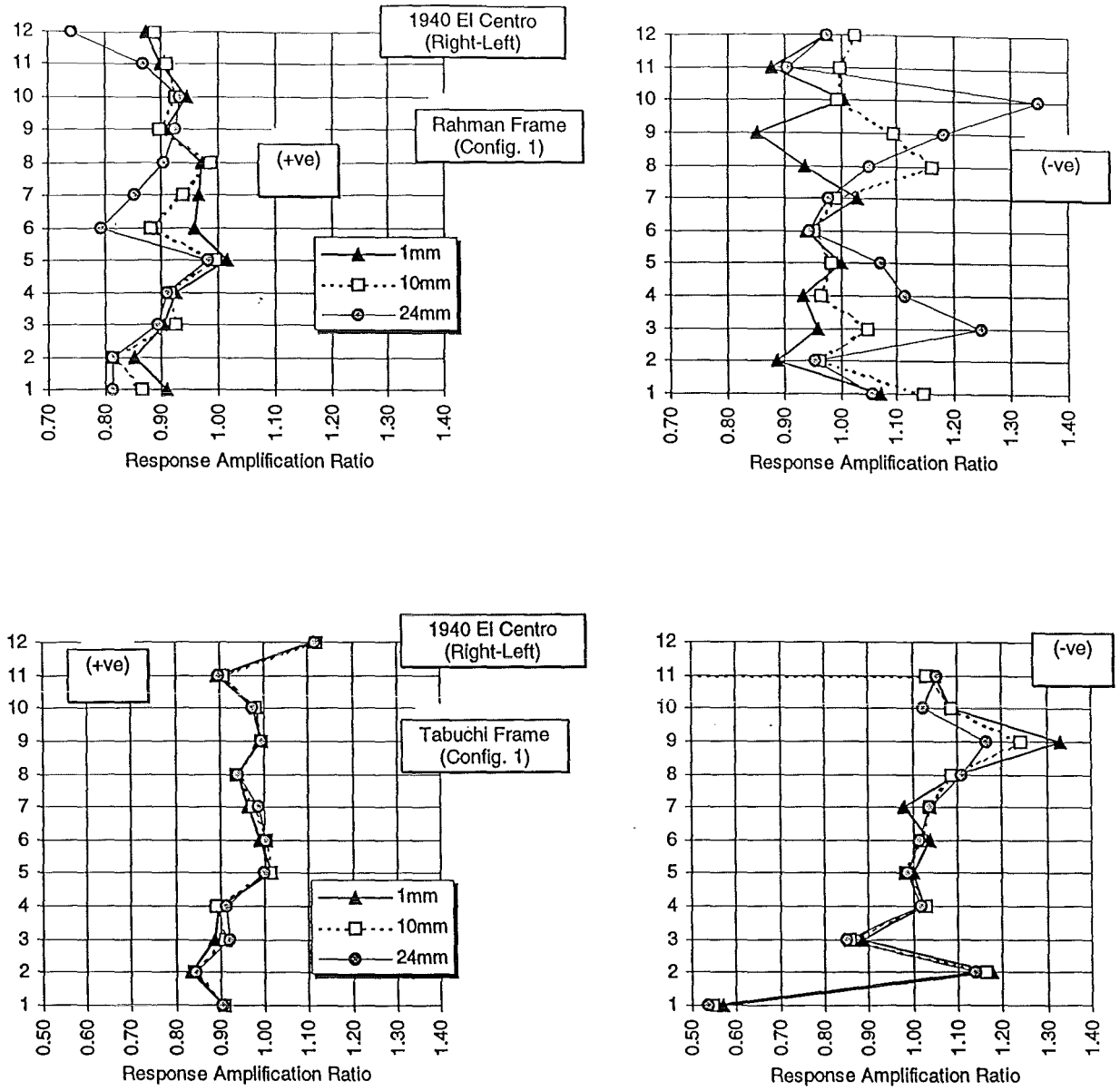

Fig. 5.49: Effect of separation gap on response amplification ratio (from fixed base no pounding case) of impact-side column shear of Configuration 1 frames for coupled foundations case.
1940 El Centro earthquake applied right-left.

The following observations may be noted with respect to positive earthquake excitation:

- The increasing magnitudes of the top storey impacts with increasing separation gap are manifested as corresponding increases in the negative response amplification ratios at the lower levels of the Rahman frame.
- The time-stations at which impacts occur at adjacent levels significantly influence the nature of the response amplification at the level considered. For example, although only four levels sustain pounding in the 24mm case, the effect on the negative shears of the Rahman frame is quite marked for this case. This may be attributed to the close succession of impacts at these levels (within approximately 0.2 seconds of each other), resulting in an augmentation of the resulting impact forces.
- Generally, pounding has a beneficial effect on the response of the Rahman frame for small separation gaps and on the Tabuchi frame regardless of gap size.

Application of the excitation in the opposite direction reveals similar trends (Fig. 5.49). Impact forces induced by a separation gap of 24mm result in reductions exceeding 20% in the positive response ratios of the Rahman frame. At the same time, an increase of about 35% at level 10 negative shear is observed. The Tabuchi frame maintains the insensitivity to separation gap size exhibited in the case of excitation in the opposite direction.

b) 1971 Pacoima Dam Earthquake

The sensitivity of the response to the direction and characteristics of the excitation is highlighted in the plots of the response amplification ratios (Figs. 5.50 and 5.51). The impact forces developed in this earthquake are presented in Figs. 5.47. Reductions in response due to pounding are apparent in both frames, with those in the Tabuchi frame of larger magnitude than the response ratios of the Rahman frame, especially at ground floor level.

The Rahman frame displays relative insensitivity to variations in the initial separation gap size under a positive excitation (Fig. 5.50). This is not the case for the negative direction excitation, which produces larger impact forces for all gap sizes than the previous case (Figs. 5.47).

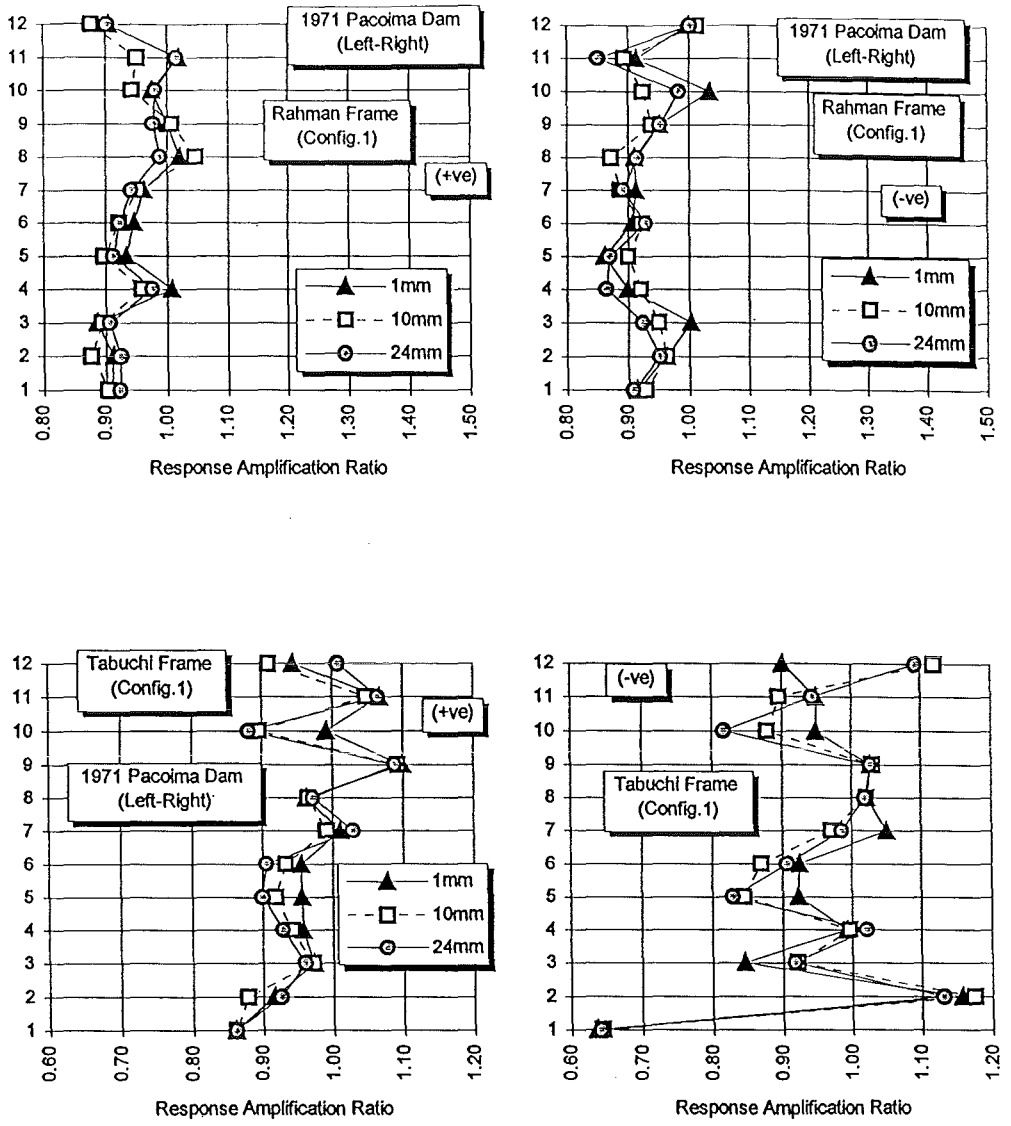

Fig. 5.50: Effect of separation gap on response amplification ratio (from fixed base no pounding case) of impact-side column shear of Configuration 1 frames for coupled foundations case.
1971 Pacoima Dam earthquake applied left-right.

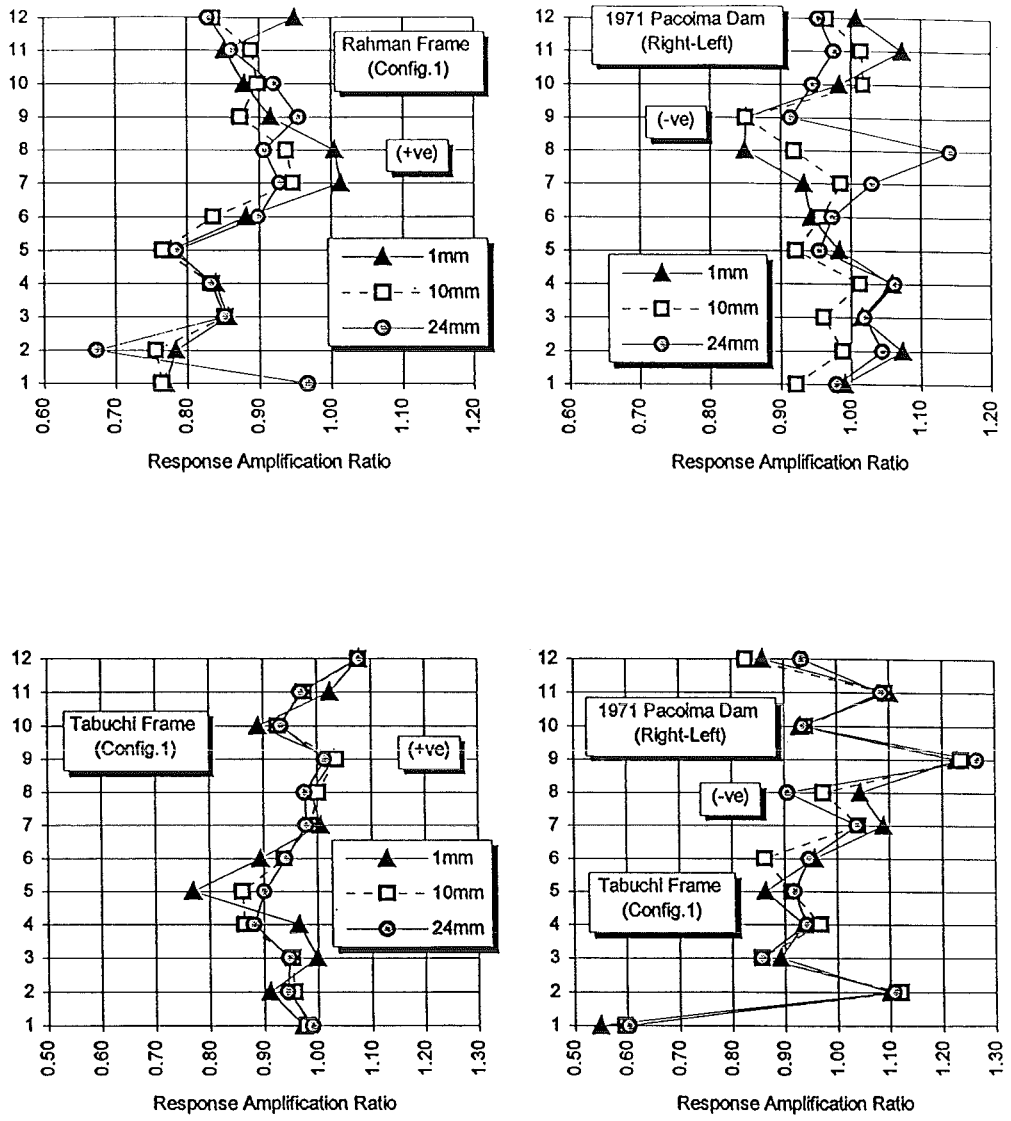

Fig. 5.51: Effect of separation gap on response amplification ratio (from fixed base no pounding case) of impact-side column shear of Configuration 1 frames for coupled foundations case. 1971 Pacoima Dam earthquake applied right-left.

As in the negative El Centro earthquake, impacts at the upper levels in the 24mm separation case occur within a short time interval. This leads to deviations of the response from the trends exhibited by the other cases of separation gaps. It may be noted that for this case of separation gap, pounding occurred only in the upper half of the structures.

The response of the Tabuchi frame displays a higher sensitivity to the effects of pounding, with larger reductions in the negative response ratios than those witnessed in the Rahman frame. The relative insensitivity of the Tabuchi frame to direction of excitation and gap size is also apparent in the figures.

5.6.6.2 Configuration 2

a) 1940 El Centro Earthquake

The larger impact forces developed in this configuration (Figs. 5.52) resulted in more marked variations in response than those observed in Configuration 1. The following observations may be made regarding this case from inspection of Figs. 5.53 and 5.54:

- Significant increases in the Rahman frame response are noticeable, especially at levels exceeding those of the Jury frame. At these levels, increases comparable to (and in some instances exceeding) those sustained at the lower levels may be observed. In addition, the variations due to separation gap sizes are more obvious at these levels than those at levels 1 to 6.
- The larger separation gaps produce larger increases in shear amplification ratios at the top level of the Jury frame whereas, in the Rahman frame, the maximum amplification ratios in level twelve are produced by the smaller separation gaps.
- A significant difference in the magnitudes of the increases in negative response ratios at the ground floor of the Rahman frame are evident for the two directions of seismic attack. This is despite the similarity of the maximum impact forces developed at the lower levels. While both cases of seismic excitation display simultaneous impacts at levels 2 to 6, the magnitudes of the secondary impacts at the various levels differ in the two excitation cases. The larger amplitude secondary impacts result in the larger increases in ground floor level response values.

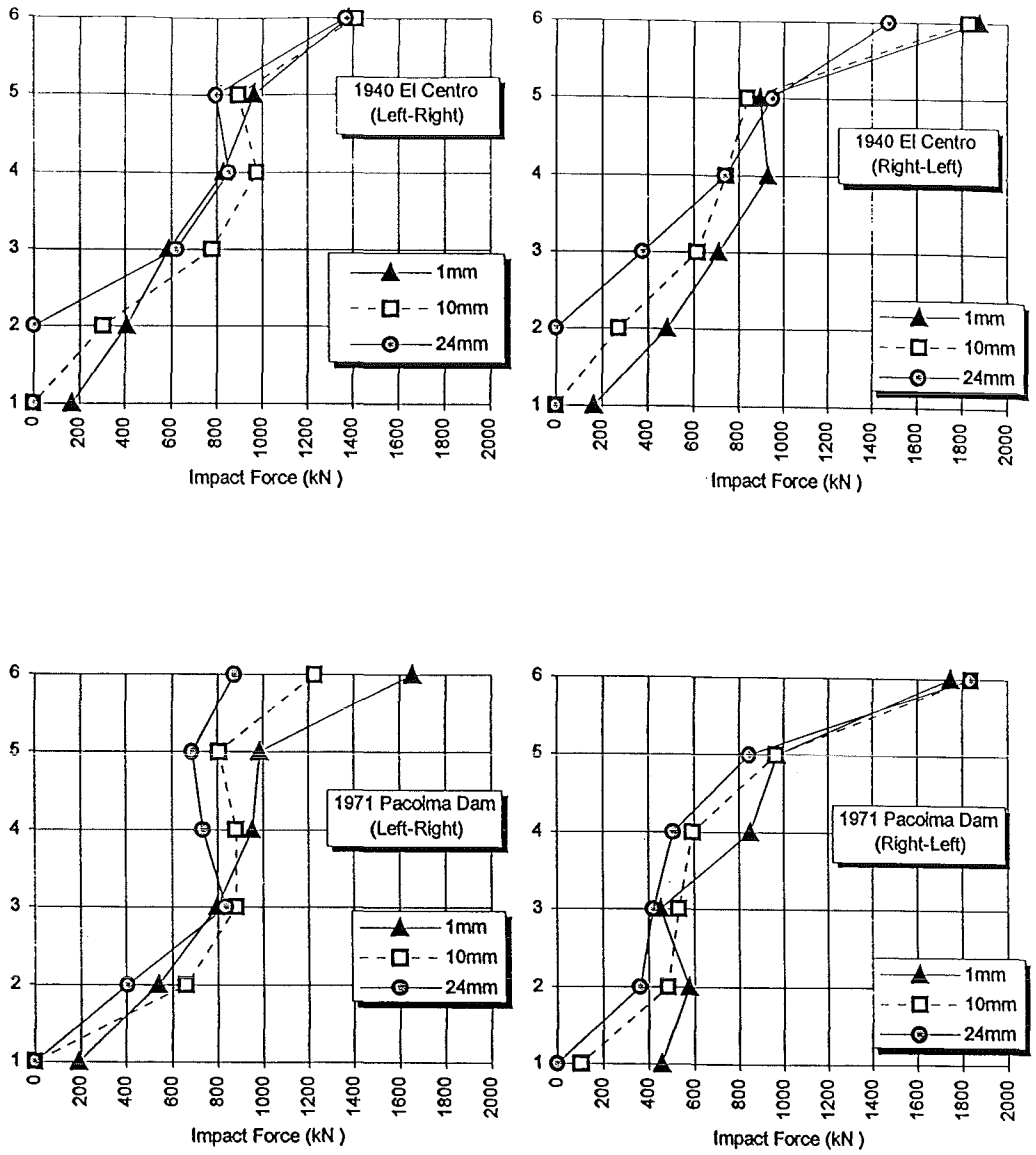

Fig. 5.52: Impact forces developed in Configuration 2 for the various earthquakes and separation gaps. Through-soil interaction case.

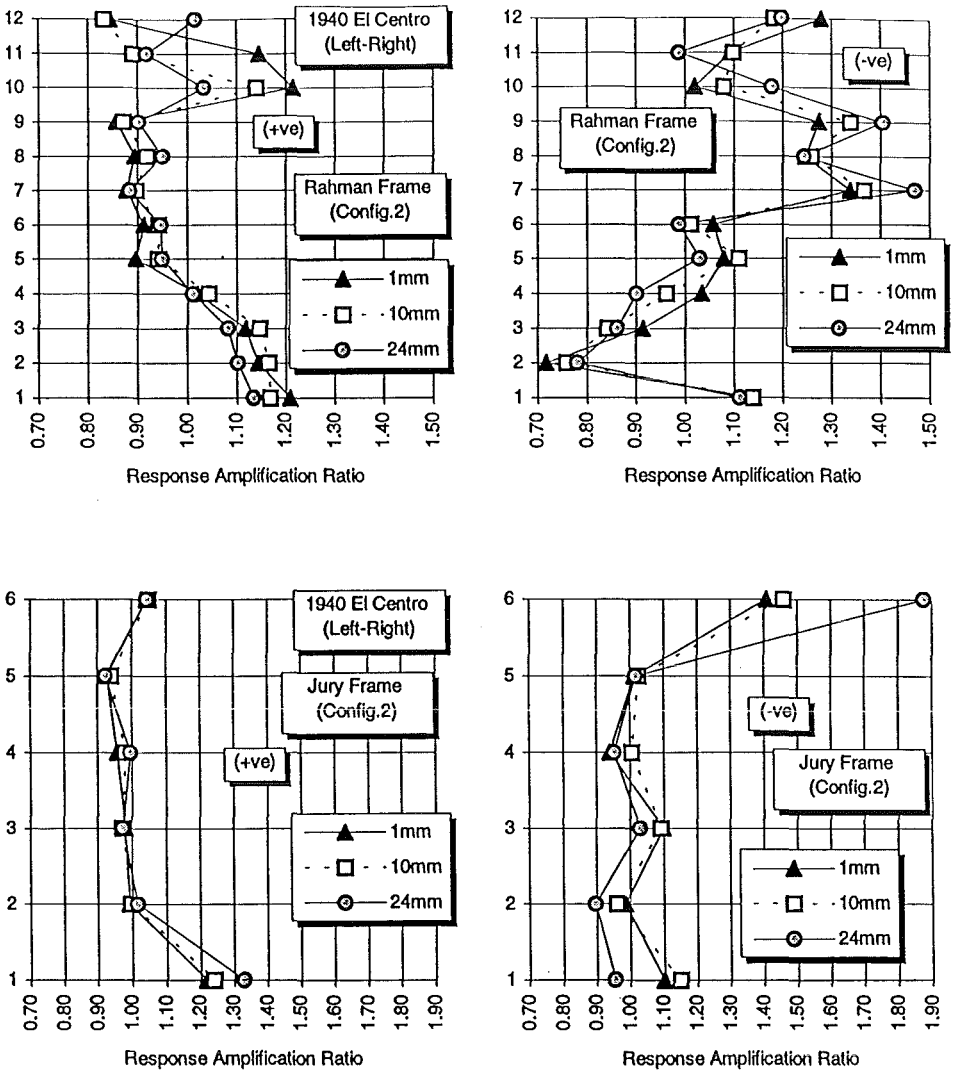

Fig. 5.53: Effect of separation gap on response amplification ratio (from fixed base no pounding case) of impact-side column shear of Configuration 2 frames for coupled foundations case.
1940 El Centro earthquake applied left-right.

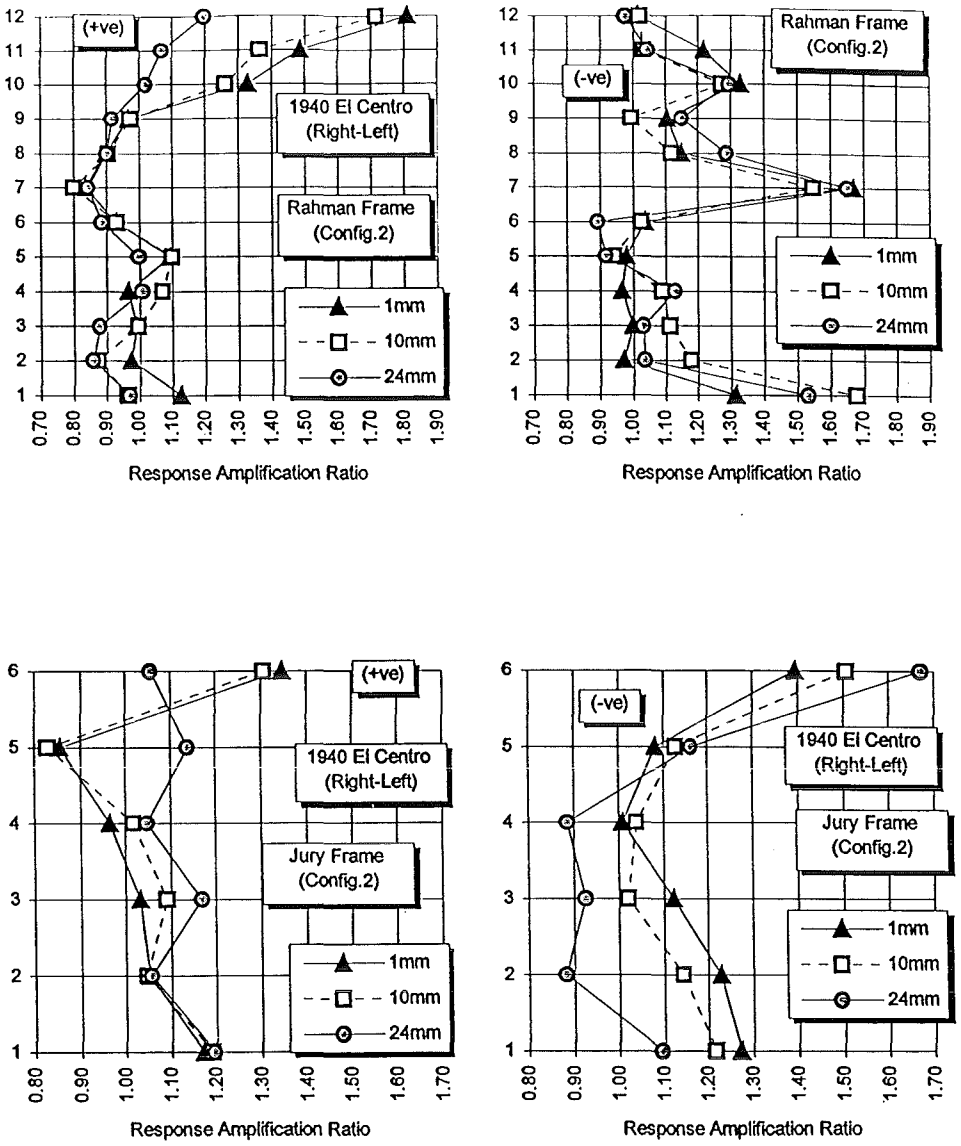

Fig. 5.54: Effect of separation gap on response amplification ratio (from fixed base no pounding case) of impact-side column shear of Configuration 2 frames for coupled foundations case.
1940 El Centro earthquake applied right-left.

- The influence of the separation gap on the Jury frame response amplification differs markedly for the two directions of seismic excitation. Under the effects of a negative earthquake, a reduction in level 5 positive response in the Jury frame is observed for the 1mm and 10mm separation gaps. However, the increases in column negative shear response at the ground floor level in both cases exceed those of the 24mm separation gap case. For the opposite direction of excitation, the ground floor columns all witness an equal increase in positive shear amplification ratios for all separation gaps (20% to 30%). In addition, the increases in the response amplification ratios of the Jury frame at all levels are relatively insensitive to initial separation gap magnitudes.

b) 1971 Pacoima Dam Earthquake

Despite the significant differences in level 6 impacts under positive direction excitation for the various separation gaps (Fig. 5.52), similar shear amplification ratios in the Jury frame columns are manifested regardless of the magnitude of these gaps (Fig. 5.55). Reductions to the order of 10% are attained along the height of the building. In comparison, significant increases in negative shears are observed in the Rahman frame at ground floor level and level 7. The only perceptible influence of separation gap magnitude is at level 7. At this location, the difference between the response ratios produced by the 10mm gap on the one hand, and the 1mm and 24mm gaps on the other, is of the order of 15%.

Conversely, under negative direction excitation (where the level 6 impacts are equal for the various separation gaps) the top level response ratios of the Jury frame are dependent on separation gap magnitude (Fig. 5.56). A 20% increase in the negative shear of the top level column is observed for the 1mm gap case, which decreases with increasing separation gap. At lower levels, reductions of the same order of magnitude are observed in the positive shear amplification ratios of the ground floor columns for the 1mm and 10mm gaps, in addition to levels 3 and 4 (for the former gap size). These reductions may be attributable to the impacts at level 1 which are evident in the 10mm separation gap case as well.

Although reductions are also observed in the shear amplification ratios of the Rahman frame columns at level 11 for the same (negative) direction of excitation, the increases in the stories above level 6 are exceptionally high. An increase of approximately 50% in negative response ratios may be observed at level 7 and gradually decreases to zero at level 10. At levels below level 6 no variation is discernible in negative response ratios of the Rahman frame columns.

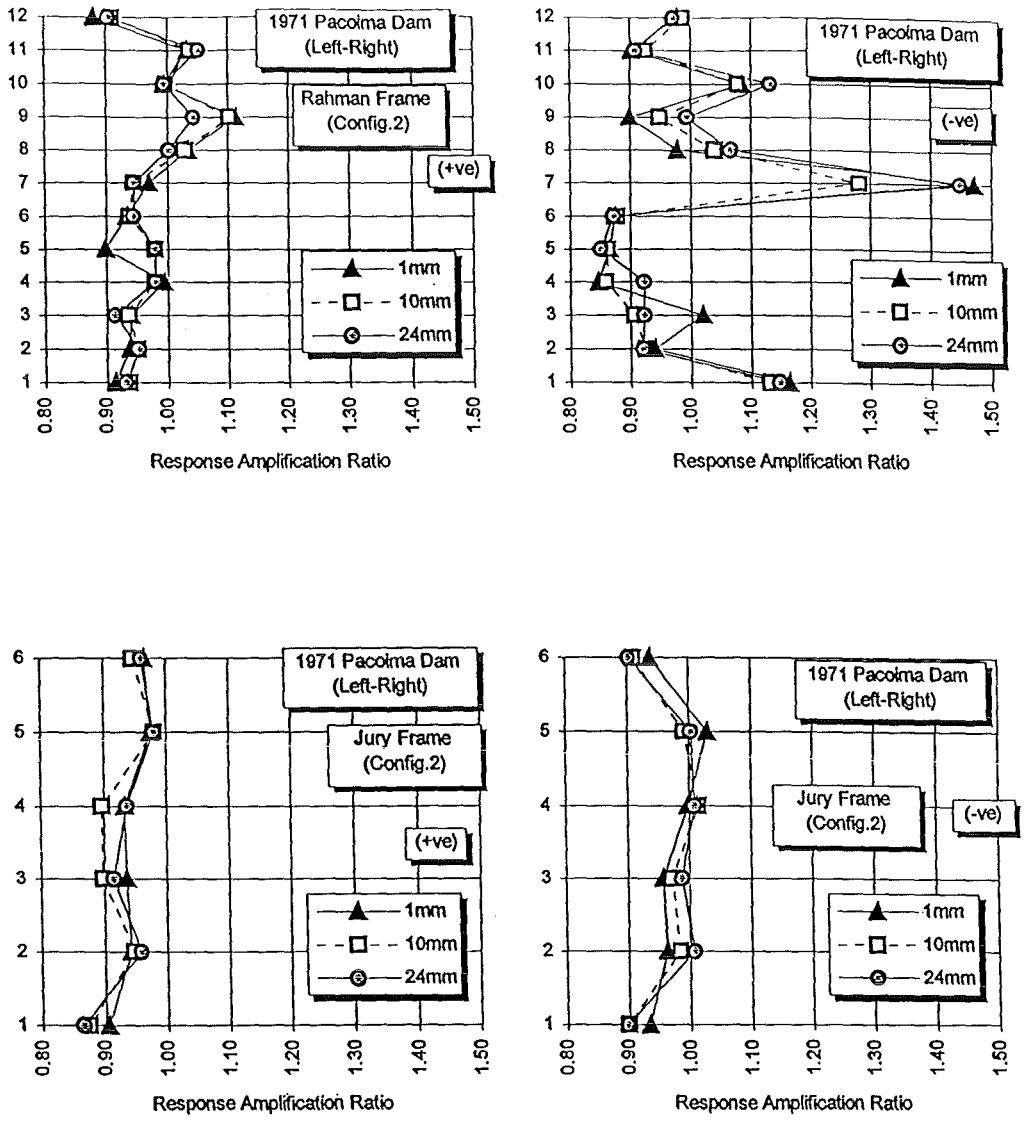

Fig. 5.55: Effect of separation gap on response amplification ratio (from fixed base no pounding case) of impact-side column shear of Configuration 2 frames for coupled foundations case.
1971 Pacoima Dam earthquake applied left-right.

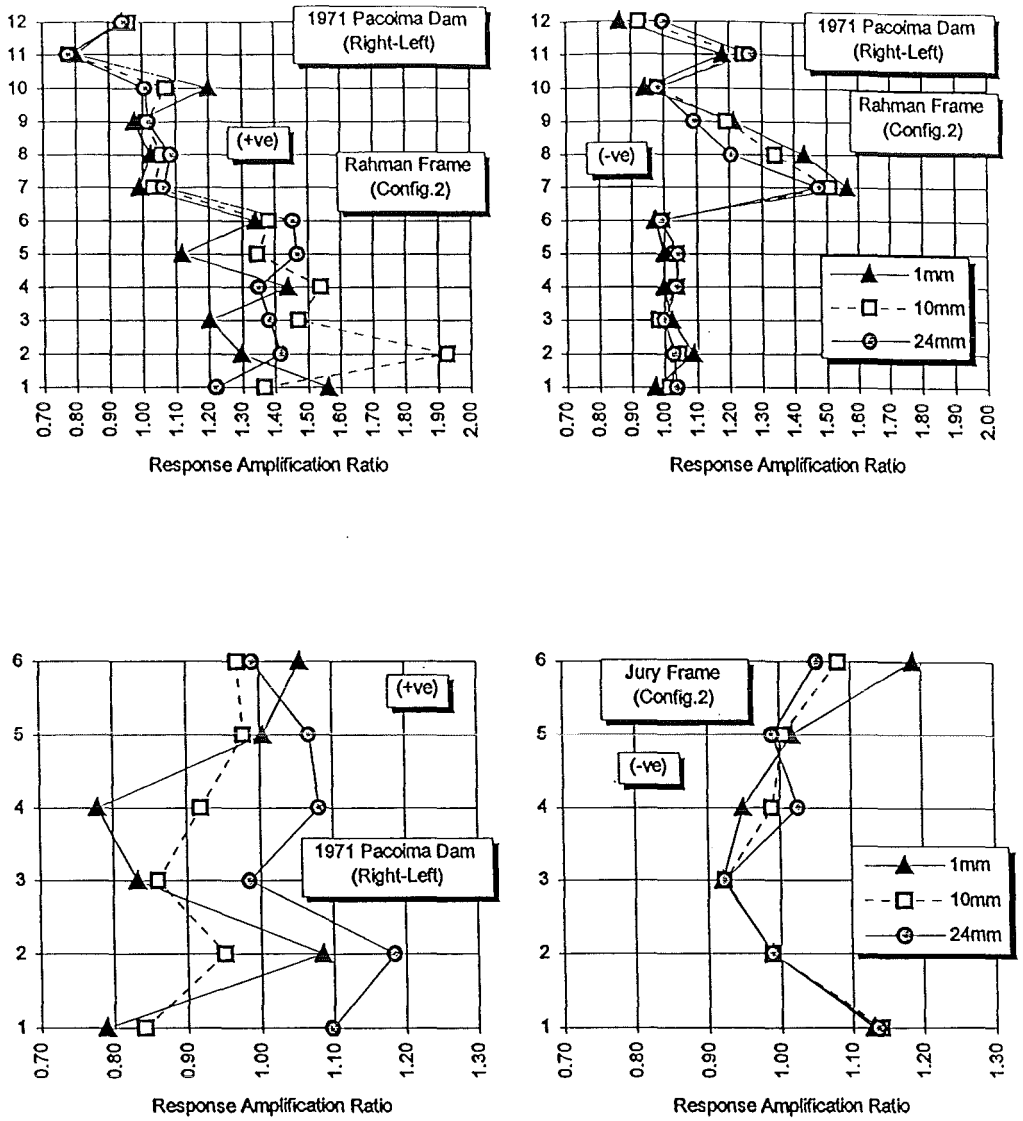

Fig. 5.56: Effect of separation gap on response amplification ratio (from fixed base no pounding case) of impact-side column shear of Configuration 2 frames for coupled foundations case.
1971 Pacoima Dam earthquake applied right-left.

The opposite trend is noted, however, for the positive shear amplification ratios of the same frame. Levels 1 to 6 all experience increases of various magnitudes while no variations are observed in the levels above the Jury frame. A conspicuous increase (90%) in the positive response ratio of the Rahman frame is observed in the case of the 10mm separation gap. This is due to the nearly simultaneous impact of several floors (2 to 6), thereby effecting an augmentation of impact forces (constructive interference).

5.6.7 Relative Storey Accelerations

The effects of foundation fixity conditions, initial separation gap and earthquake excitation type and direction on relative storey accelerations are presented below for Configuration 2.

The most obvious feature is that the acceleration amplification ratios (normalized with respect to the corresponding storey accelerations for the fixed-base no pounding case) appear to be independent of the earthquake magnitude. Figures 5.57 and 5.58 show that the storey accelerations developed in either direction of the El Centro earthquake are higher than the corresponding values of the Pacoima Dam earthquake (Figs. 5.59 and 5.60). Also, the results of the latter earthquake are more sensitive to the foundation conditions, as is evident from the differences for each separation gap. For the Rahman frame, these differences are localized around level 6 for the larger separation gaps. However, for the 1mm separation gap case all the levels below level 6 are sensitive to the assumed foundation fixity condition.

Figure 5.59 shows the influence of initial separation gap on the acceleration amplification ratio for both directions of the 1940 El Centro earthquake with through-soil interaction effects taken into consideration. The lower levels of the Jury frame appear to be more sensitive to a negative direction earthquake (i.e. applied from right-left). The 24mm separation gap produced the highest increase in accelerations in the lower levels of the Rahman frame under a positive direction earthquake.

Under the Pacoima Dam excitation, the increases in both frames and for all separation gaps were not as significant as in the El Centro excitation case (Figs. 5.60-5.62). The Jury frame sustained the highest increases especially at the upper levels under a negative direction earthquake (Fig. 5.61). Figure 5.62 shows that only level 1 of the Rahman frame and level 6 of the Jury frame were sensitive to the magnitude of the initial separation gap.

These results indicate the sensitivity of the storey accelerations to the characteristics, and not the magnitude, of the earthquake excitation. Therefore, the impact force

envelope (such as that shown in Fig. 5.52 for Configuration 2) is not a suitable indication of the expected storey accelerations. This is highlighted in Fig. 5.63, which shows the time-history of the level 4 relative acceleration (of both the Rahman and Jury frames) under the positive El Centro excitation. The large acceleration amplification ratio at level 4 shown in Fig.5.57 for the 24mm separation gap case occurs between 3 and 4 seconds. This corresponds to the time-station at which large impacts occur at levels 6 to 3 in addition to a positive direction pulse in the earthquake excitation (see Fig. 5.64).

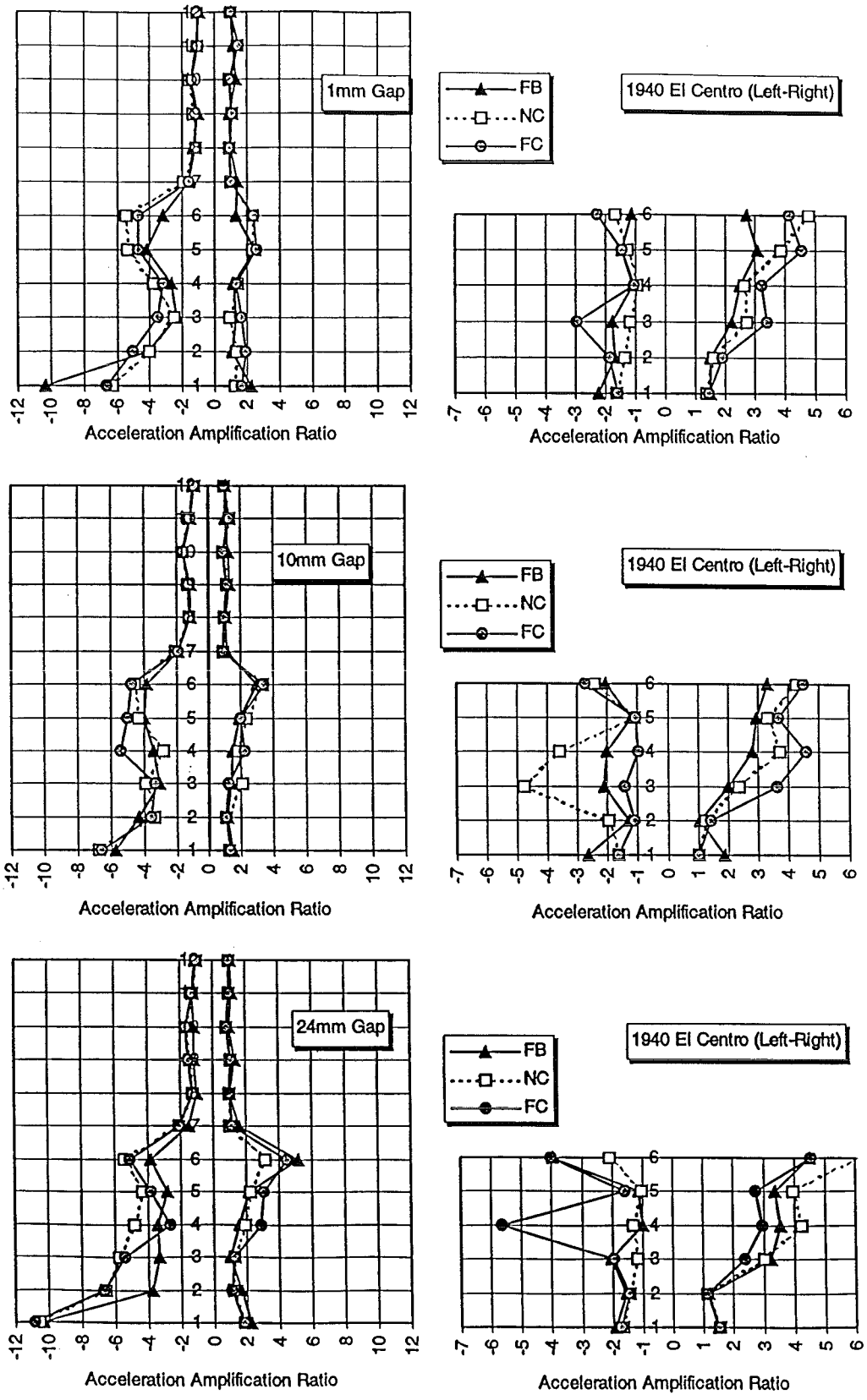

Fig. 5.57: Effect of foundation fixity assumption on acceleration amplification ratio (normalised with respect to no pounding fixed base case) for various separation gaps. 1940 El Centro earthquake applied left-right.

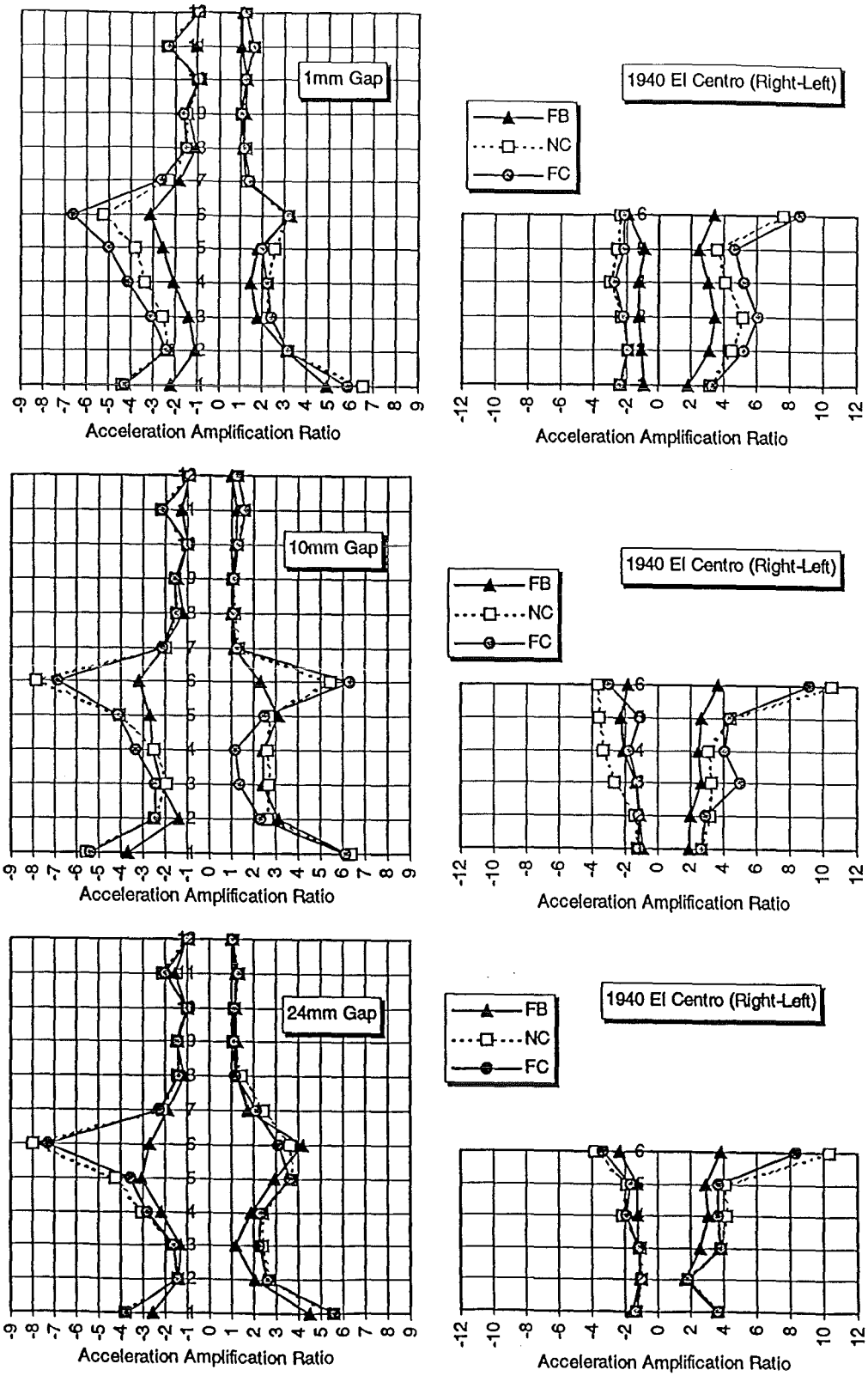

Fig. 5.58: Effect of foundation fixity assumption on acceleration amplification ratio (normalised with respect to no pounding fixed base case) for various separation gaps. 1940 El Centro earthquake applied right-left.

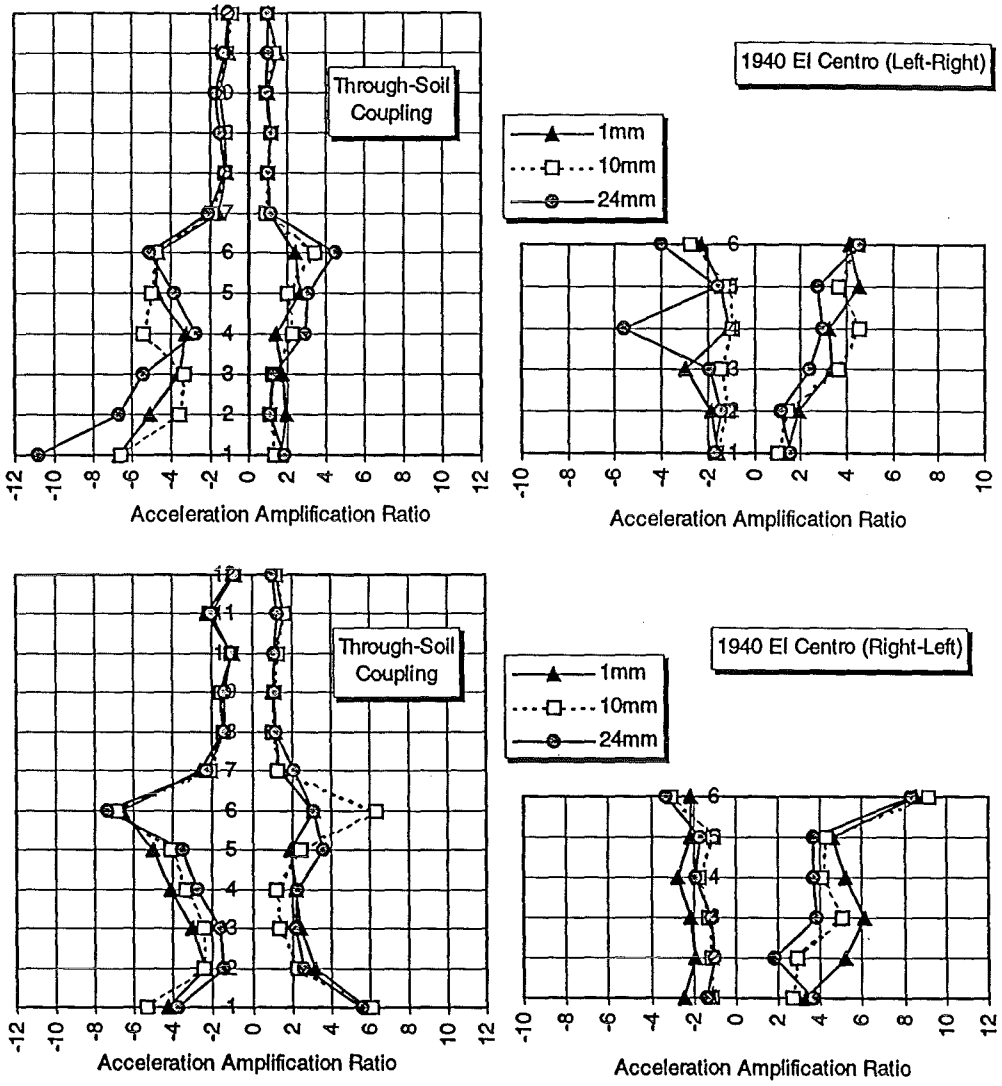

Fig. 5.59: Effect of initial separation gap on (relative) acceleration amplification ratio (normalised with respect to no pounding fixed base case) for through-soil interaction case. 1940 El Centro earthquake.

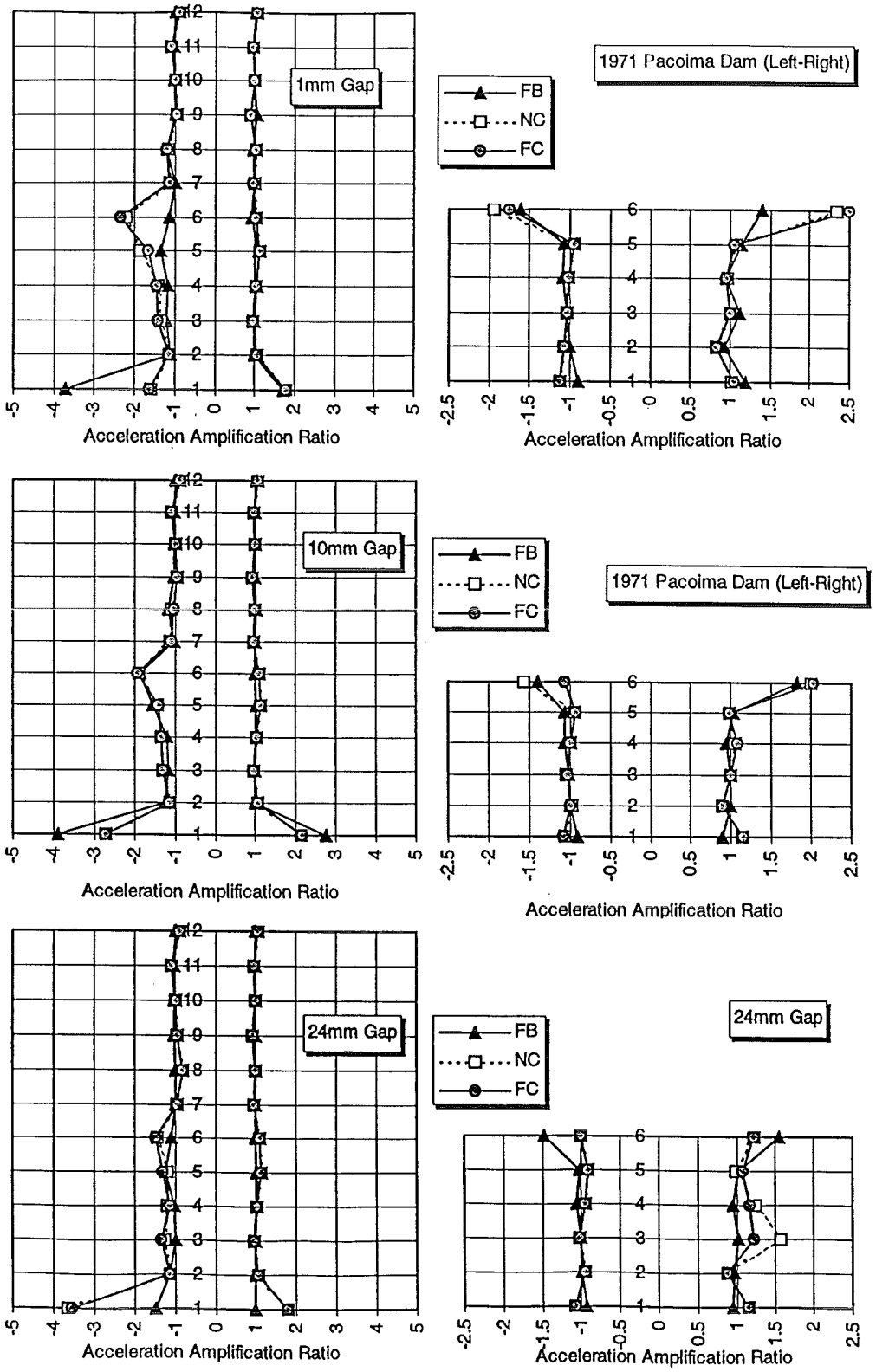

Fig. 5.60: Effect of foundation fixity assumption on acceleration amplification ratio (normalised with respect to no pounding fixed base case) for various separation gaps. 1971 Pacoima Dam earthquake applied left-right.

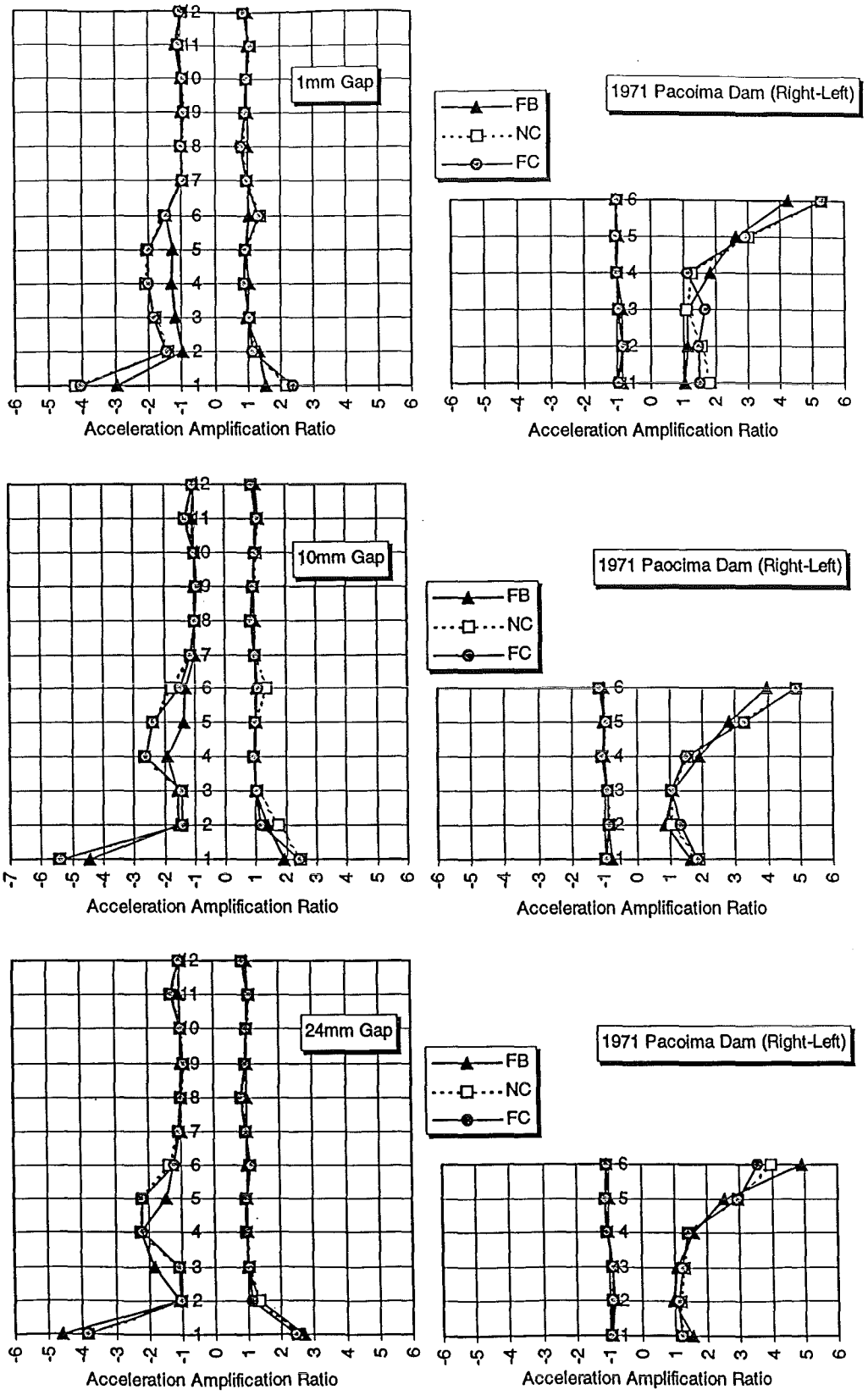

Fig. 5.61: Effect of foundation fixity assumption on acceleration amplification ratio (normalised with respect to no pounding fixed base case) for various separation gaps. 1971 Pacoima Dam earthquake applied right-left.

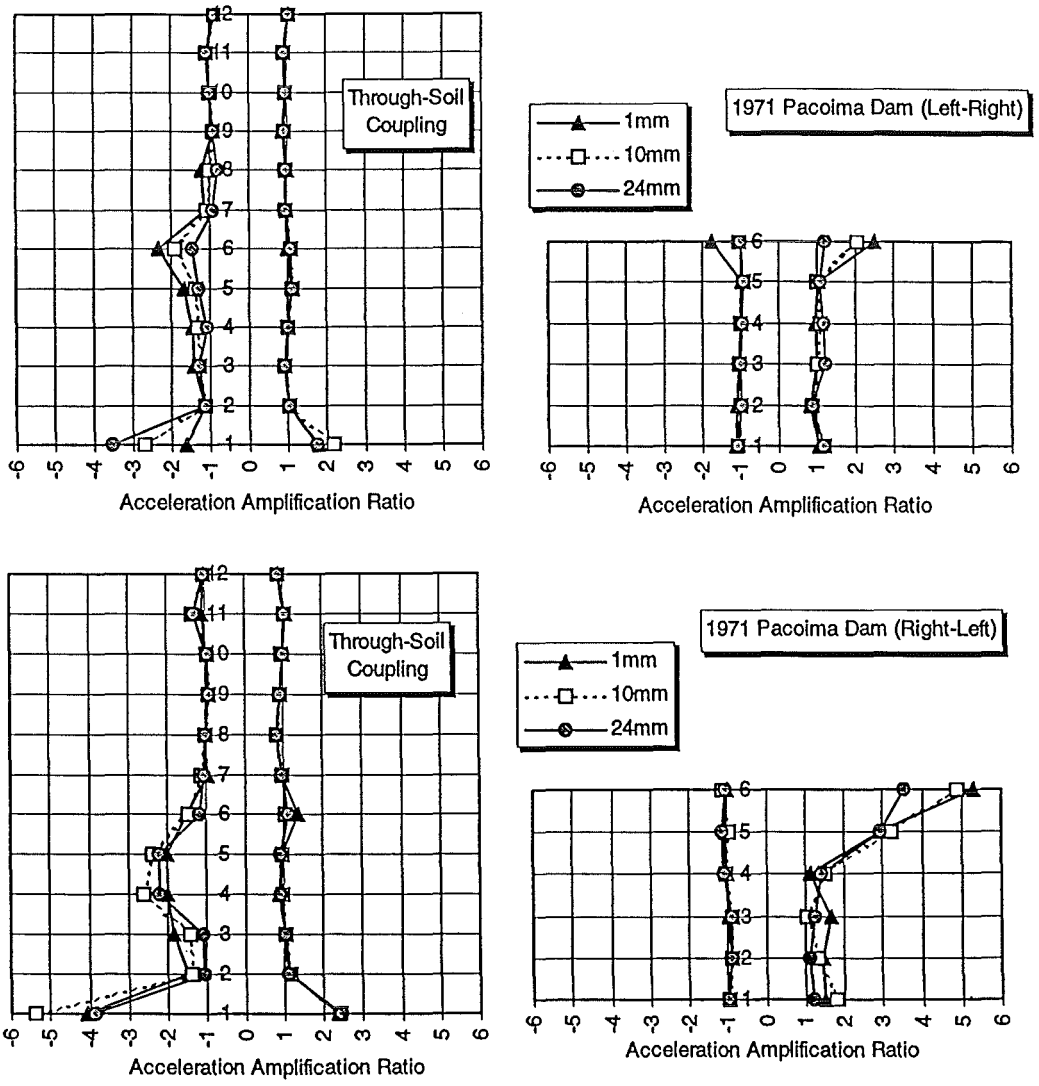

Fig. 5.62: Effect of initial separation gap on (relative) acceleration amplification ratio (normalised with respect to no pounding fixed base case) for through-soil interaction case. 1971 Pacoima Dam earthquake.

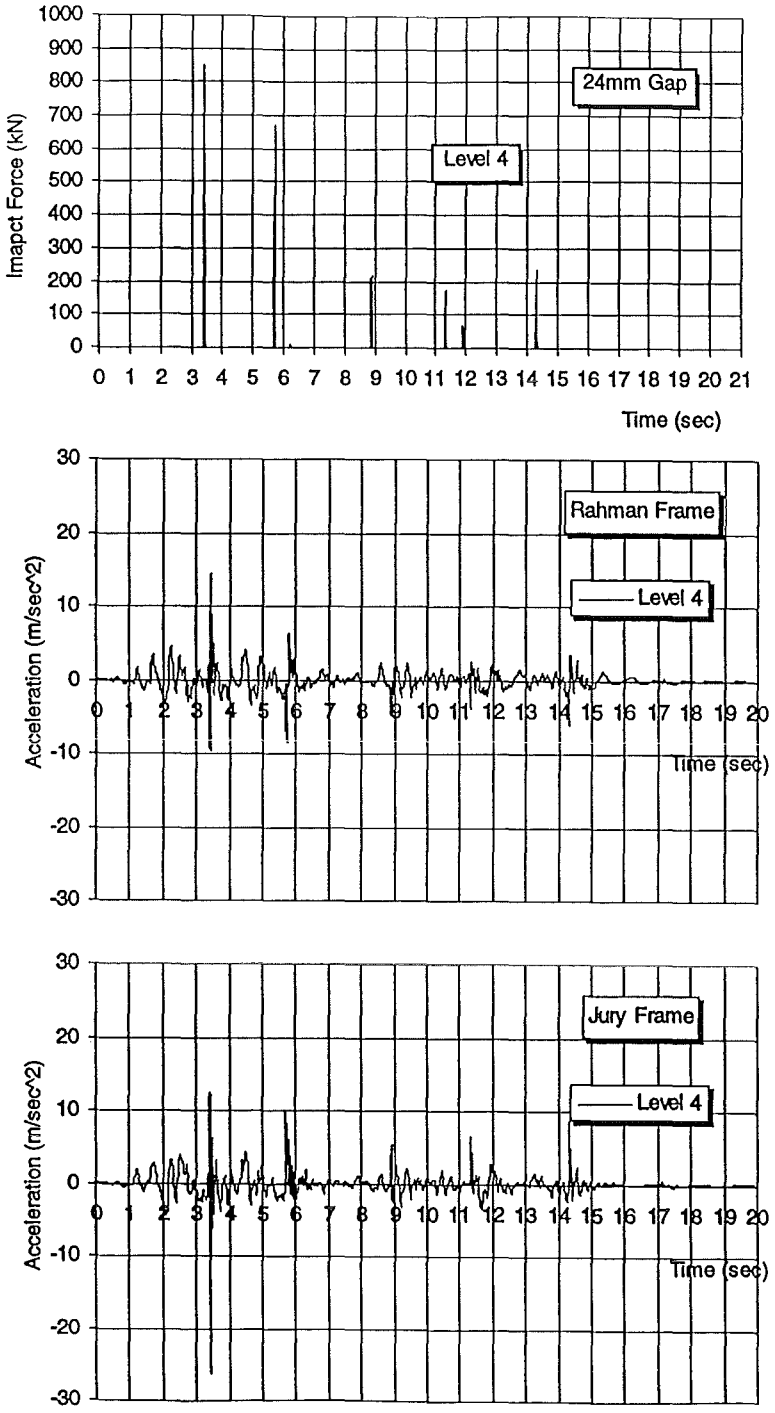

Fig. 5.63: Impact forces and relative storey accelerations at level 4 for 24mm separation gap case. 1940 El Centro earthquake applied left-right with through-soil interaction considered.

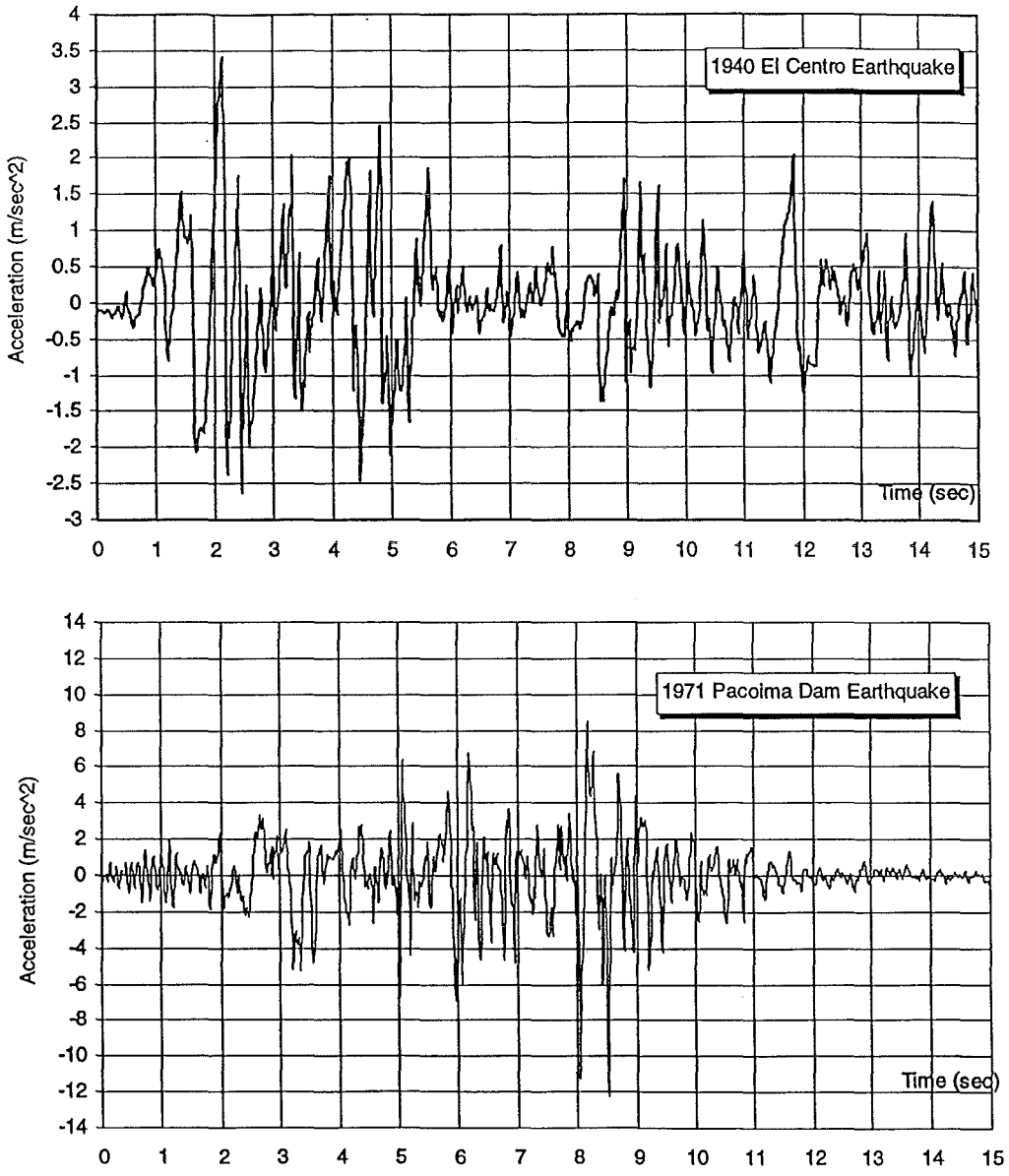

Fig. 5.64: Earthquake excitation time-histories (left-right) implemented in study.

6. DISCUSSION AND RECOMMENDATIONS FOR FUTURE RESEARCH

6.1 No Pounding Response

Inspection of the acceleration response spectra of the two excitations (Fig. 5.6) reveals the reason for the reduced maximum displacements in the Pacoima Dam case. For natural periods longer than 2 seconds, the spectral accelerations for damped (5%) and undamped systems are almost identical in the case of the Pacoima Dam event. In addition, the reduction in spectral accelerations is slightly larger than that witnessed in the El Centro earthquake.

One of the main effects of soil-structure interaction, besides the increase of the flexibility of the dynamic system, is the increase of damping [M13]. In the case of the Pacoima Dam excitation, this latter effect does not significantly influence the displacement response. In addition, the change in system flexibility, hence in natural period, has an almost negligible effect on the maximum displacements for the reasons cited above (smaller spectral accelerations with increased natural period). The increased system flexibility induced by soil-structure interaction is more obvious in the pounding response.

6.2 Pounding Response

1. Studies have shown that adjacent structures modelled as bi-linear systems and/or which develop large ductility may exhibit a biased response [N1]. Yamanouchi and Yomo [Y1] found that the initial phase angle of the causative seismic waves affects this residual displacement or bias of the bi-linearly modelled vibrating system. (The initial phase angle is defined as the phase angle at zero circular frequency of the Fourier phase spectra). In their study, they found that the magnitude of the bias in single degree-of-freedom systems with elastoplastic hysteresis is independent of the peak intensity of the impinging wave. These residual displacements have also been witnessed in damage reconnaissance surveys [B2, M1]. Therefore, the difference in the positive and negative direction displacement responses of each frame may be ascribed to the sensitivity of the assumed hysteresis rules to the direction of applied earthquake loading [K6,S8], and the characteristics of the excitation itself [A5,Y1]. In addition, the parameters defining these hysteresis relationships, such as post-yield stiffness, unloading stiffness

degradation parameter, etc. [O3], influence the nature of the displacement response.

2. The direction of excitation was shown to be significant in the determination of the pounding response characteristics. Davis [D1] has shown that the velocity of a SDOF damped oscillator at first impact against a barrier is dependent on the direction of initial excitation of the oscillator with respect to the barrier. Leibovich et al. [L7] indicated the significance of earthquake direction on the pounding response of inelastic systems. Kasai et al. [K6] noted the significance of direction of seismic attack, due to its effects on the residual displacement at the termination of the ground motion excitation. The necessity of investigating the response with application of the earthquake excitation from the opposite direction was also suggested by Sinclair [S8].

3. The influence of soil flexibility on the free-vibration response of the impacting frames is typified in Figs. 6.1 and 6.2 for a 1mm separation gap pounding case. These figures also show the residual displacements sustained by the frames in each of the two configurations affected by pounding and the variation from the fixed base pounding condition. Significant deviations from the fixed base condition are apparent in both magnitude and response phase depending on the configuration, the characteristics of the seismic excitation and its direction of impingement. The displacement response time-history does not appear to be sensitive, however, to initial gap size.

   The above characteristic (i.e. with respect to the manifestation of soil flexibility effects in the free-vibration response) may be explained by separating the response of the structure into two parts; a forced-vibration part and a free-vibration phase [J1]. The forced-vibration segment of the response is when the structure is subjected to an initially weak excitation followed by a high amplitude shaking. The structural response is influenced by the characteristics of the excitation and the adjacent structures will vibrate in-phase. As the intensity of the excitation weakens, the structures, which were initially experiencing a high-amplitude oscillation, will respond in a free-vibration state in their differing natural periods (free-vibration response). Thus, it is during the transitional (i.e. initial and final) phases of near-field excitations that adjacent structures may be most susceptible to pounding, i.e. in the free-vibration response stages.

4. The influence of adjacent storey impacts on the response amplification of the storey under investigation is clearly demonstrated in this study. For example,

considering the pounding response of Configuration 2, where the impacts at the lower levels are much smaller than those sustained by the top storey, significant variations in the shear amplification response are identified for the different separation gaps. These variations are noted even in the fixed base case and are especially conspicuous in the Pacoima Dam earthquake cases. Analogous pounding studies (i.e. involving buildings of differing total heights such as [K4, M3, M6]) prescribe pounding at the top level of the shorter building only, mainly due to software limitations. These studies, therefore, do not take into account the modifications to the pounding-induced energy waves resulting from simultaneous pounding events at the adjacent levels.

5. The overall dynamic response of the impacting systems is relatively insensitive to the modelling of the contact elements, as has been indicated and verified in previous studies [A1, M3, M6, S8].

6. A large disparity exists between the pounding response of the structures in which a conventional fixed base is assumed and the results obtained from a soil-structure interaction analysis (see figures in Appendix). This difference is due to the increase in significance of the higher modes as a result of the consideration of soil-structure interaction. The effect of this higher mode contribution is to change the mode shapes and, therefore, the time-stations at which impacts occur. The effects related to the variations in the dynamic properties of the oscillating systems with respect to the characteristics of the earthquake have already been alluded to.

7. The main effects of foundation compliance are an increase in both the natural periods of vibration of the adjacent structures and in system damping. Therefore, the repercussions of the consideration of soil-structure interaction effects on the dynamic response of the system will depend on the spectral response characteristics of the predicted earthquake. In addition, the time-stations at which impacts occur will affect the subsequent impact events [S8]. Since these impacts impart an impulsive force to the adjacent structures and result in a sudden change in displacement direction, the time at which they occur, with respect to the earthquake time-history, is of vital importance for the total response time-history.

   The expected effect of foundation compliance would be to promote in-phase oscillation of the adjacent structure, due to the increased contribution to damping from the soil. However, this aspect must be considered in conjunction with the variations in the dynamic characteristics of the structures and the ensuing repercussions vis-a-vis the spectral characteristics of the excitation.

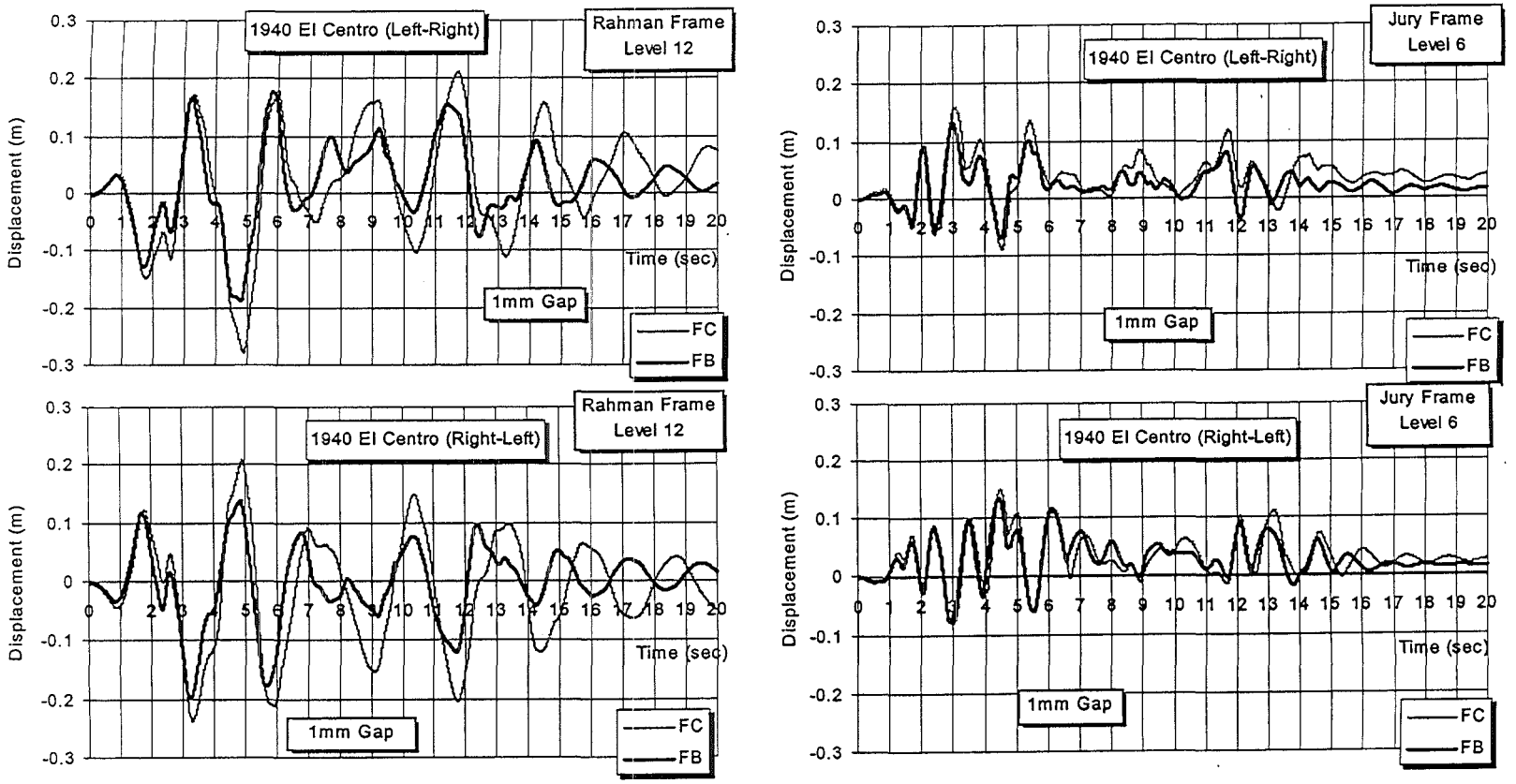

Fig. 6.1: Effect of foundation fixity assumption on storey displacement for 1mm separation gap (Configuration 2) pounding case. 1940 El Centro earthquake applied left-right (top) and right-left (bottom).

FB = Fixed Base FC = Foundations Coupled

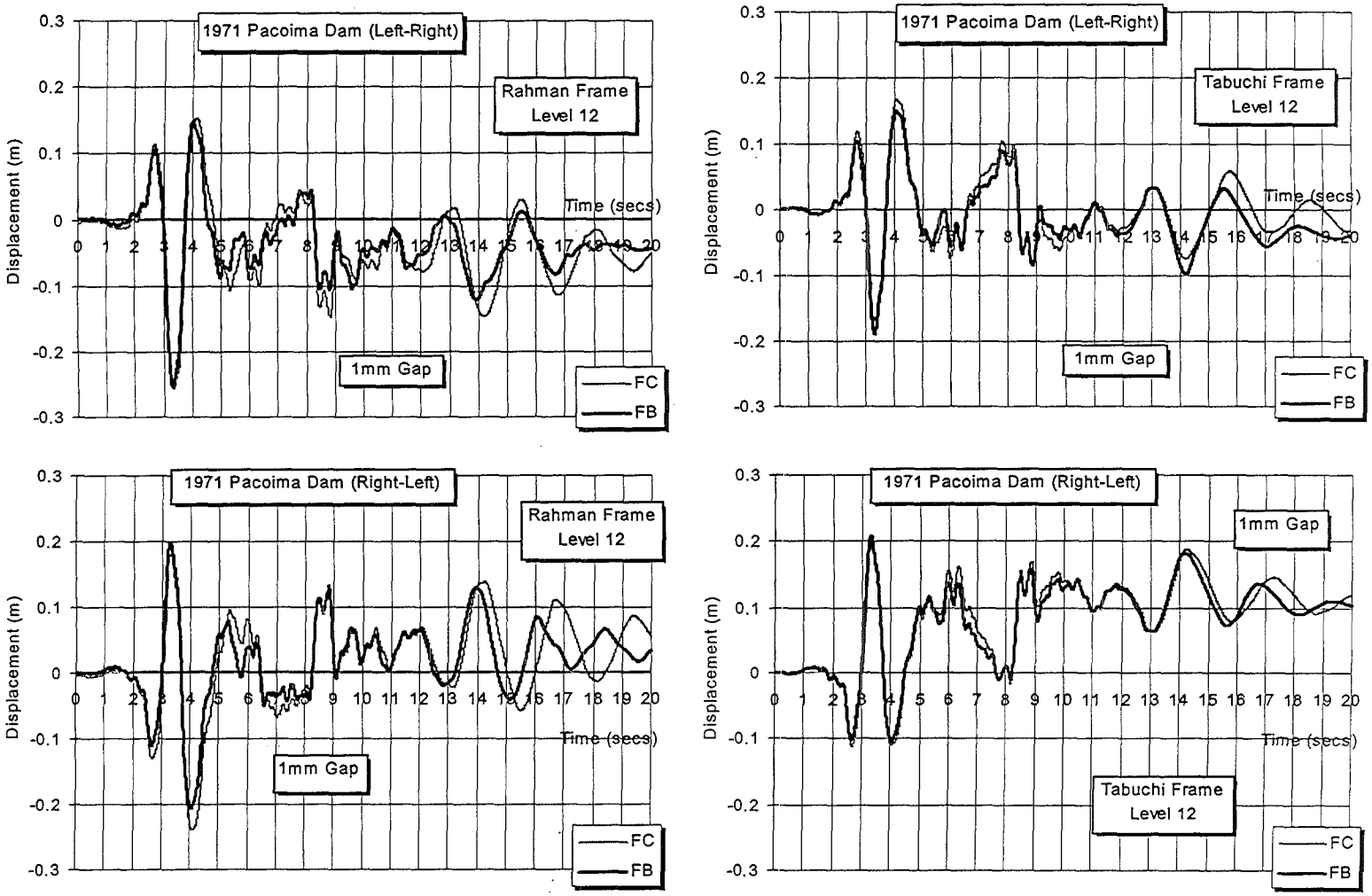

Fig. 6.2: Effect of foundation fixity assumption on storey displacement for 1mm separation gap (Configuration 1) pounding case. 1971 Pacoima Dam earthquake applied left-right (top) and right-left (bottom).

FB = Fixed Base FC = Foundations Coupled

8. The peak ground acceleration of the seismic event is not a sufficient indicator of the expected magnitude of the maximum impact forces. In Configuration 1, the Pacoima Dam event (PGA=1.23g) produced lower impact forces than the El Centro earthquake (PGA=0.348g) for most levels, separation gaps and for both directions of seismic attack. This is especially important in the development of floor response spectra since the maximum floor accelerations are highly dependent on both the impact and excitation time-histories, as was shown for the Configuration 2 case. Other factors pertaining to the earthquake characteristics, such as frequency content, duration of ground motion, and duration and sequence of high amplitude pulses, should also be considered and not only the peak ground accelerations.

9. The impact force envelope by itself is not a sufficient indicator of the accelerations developed along the height of the structure. The development of floor response spectra requires the consideration of the characteristics of the excitation in conjunction with the pounding time-history. For example, the oscillatory nature of the 1940 El Centro earthquake resulted in higher floor accelerations compared to the high-amplitude impulsive 1971 Pacoima Dam excitation.

10. The adjacent structure defines the response characteristics of the building under investigation due to through-soil foundation interaction [M19]. Anagnostopoulos et al. [A2] showed that, for fixed base multiple-sided pounding of adjacent equal storey-height structures (as in the case of a row of buildings), the ratio of periods of the impacting structures influences the response. The significance of this aspect increases with consideration of through-soil interaction effects. For example, it has been shown that the increase of mass of the adjacent structure increased the maximum response of the modes of vibration induced by interaction effects [I2, K7, L9].

9. Consideration of soil flexibility influences the reflections noted by some authors (e.g. Maison et al. [M3]) of the impact force energy waves from the fixed base of the structures. It has been postulated that these reflected waves alter (either augment or attenuate depending on the mode shape of the structures at which impacts occur [S8]) the distribution of shear forces and moments in the elements along the heights of the structures. Soil-structure interaction will alter the nature of the waves reflected into the structure. Through-soil interaction results in a transmission of these energy waves as shear forces to the adjacent building. In addition, the properties of the supporting soil will be affected.

The mechanism of shear amplifications in columns due to pounding has been presented by Sinclair [S8]. Briefly, Sinclair postulated that the amplification trends are dependent on the mode shapes of the impacting structures at the time at which pounding occurs.

10. The effect of soil flexibility on pounding response is particularly discernible in the free-vibration phase of the impact force time-history compared to the fixed base analyses. These effects were manifested as a marked variation in the frequency content and an increase or reduction of impacts during this phase. These variations in pounding characteristics are highly dependent on the stories investigated, the nature of the excitation and the dynamic properties of the structures. The implications of this aspect are important with respect to the investigations of local pounding effects.

11. For the Configuration 1 cases, a general trend may be identified in the variation of the response of the ground floor column shears due to pounding. The lighter frame is more sensitive to the variations in separation gap size while the heavier frame sustains larger reductions than the lighter frame of the same total height. The only exception noted for the latter trend is in the case of the negative El Centro earthquake. In this case the reductions in the (positive) response ratios of the (lighter) Rahman frame exceed those of the Tabuchi frame and increase with gap size.

12. Increasing the width of the gap separating adjacent buildings does not necessarily imply a corresponding reduction in amplification response ratios or impact forces (as was noted in previous studies [M6]). This was starkly exhibited at mid-height of the lighter frame of Configuration 1 (El Centro earthquake) and the top storey of the shorter Jury frame in Configuration 2. An exception is noted in the positive response ratios of the Rahman frame (Configuration 2) under positive El Centro earthquake. The amplification ratios are markedly lower in the upper levels than the corresponding values for the smaller separation gap sizes (which witnessed an increase of 80% for the 1mm gap case).

    As regards the impact forces, top level impacts increased in Configuration 1 with increasing separation gap for both directions of the El Centro excitation considering through-soil interaction effects. The larger separation gaps, however, had a marked effect on the number of stories that sustained pounding. Increasing the initial separation gap mitigated pounding at the lower levels for both earthquakes considered in this study. For the Configuration 2 pounding response,

increasing the separation gap size did not significantly alter level 6 pounding. The major exception was the positive direction Pacoima Dam earthquake. Increased separation gap significantly reduced the maximum impact forces developed at the upper levels. Impacts at the lower levels of this configuration decreased with increasing gap size.

13. Although a two-foundation system has been shown to be more sensitive to foundation flexibility effects than a single foundation system [L16], rigid foundations were assumed in this study. This is a valid assumption as the behaviour of most foundations may be considered to be rigid within a wide range of excitation frequencies. In addition, the effects of through-soil interaction are appreciably more conspicuous in rigid than flexible foundations [L16].

14. The findings of this study corroborate the findings of earlier analytical and numerical investigations [L3,L9,Q3,R7] with respect to the effects of mass, frequency content of excitation, shift in frequency of maximum response, the out-of-phase response due to soil flexibility

6.3 Recommendations for Further Research

1. It has been shown that adjacent structures significantly influence the dynamic response characteristics of the building under consideration due to soil flexibility effects, even when the separation gap is of large magnitude. Further research would be conducive in determining the repercussions of this aspect, not only those related to potential pounding risk, which must be accounted for in the design of buildings in built-up metropolitan areas. The fixed base pounding response of buildings in series has been investigated by a number of researchers [A1, A5].

2. The effects of soil flexibility on the eccentric pounding response of adjacent structures require further study. The orientation of structures with respect to the impinging seismic waves and the accumulation of debris between buildings are just some of the factors which render the likelihood of symmetric pounding response extremely small. In addition, through-soil interaction between adjacent structures induces torsional response in both structures under seismic excitation [L3, R7, L9, Q3]. Torsional pounding response of single-storey systems has been investigated by Leibovich et al. [L6, L7].

3. The available formulae defining the effective separation gaps to preclude pounding [J1, K6, L10, J2, P9] neglect the effects of soil flexibility. Most of these formulae are based on the statistical combination of the displacement response of the

adjacent structures, with some additional factors (such as damping) taken into account. The incorporation of soil flexibility, with the resulting variations to the system natural frequencies and modes of vibration (such as increasing the significance of higher modes in addition to reducing the difference between the natural frequencies in the various modes of each structure), may affect the accuracy, and hence the applicability, of some of these formulae.

4. The various assumptions incorporated in the numerical modelling of the structures play a significant role in the determination of the system response. The effects of implementing assumptions such as rigid-block length, the presence of plastic hinges in ground floor columns, the hysteretic models assumed for the various elements, etc. should be evaluated.

5. The influence of other aspects of through-soil interaction (such as the angle of incidence of the excitation and foundation embedment [Q3]) on pounding response require further investigation.

6. Base isolation has been suggested as a means of pounding mitigation [J2, K4]. The increased damping of the adjacent structures will promote in-phase oscillation of the adjacent structures, thereby reducing the pounding risk. Further investigation into this aspect is recommended as the efficiency of this technique is believed to be dependent on the characteristics of the seismic excitation.

7. The effects of inelastic soil behaviour on the pounding response, in addition to through-soil coupling effects, require further consideration. The main influence of hysteretic soil damping would be to promote in-phase vibration of the adjacent systems due to increased system damping. However, consideration of through-soil interaction with inelastic soil behaviour may induce higher pounding forces in addition to significant variations in impact time-history thereby increasing the sensitivity of the response to excitation characteristics.

8. The influence of the distance between exterior foundations of the adjacent buildings in addition to the separation gaps between the buildings themselves on pounding response. In this study, the separation gaps were effected only between the buildings, i.e. the distance between the exterior foundations of the adjacent structures was kept constant (5.0 meters). It is expected that the manifestation of through-soil interaction would be much more obvious if the foundations were in closer proximity.

9. The implementation of a force-limiting element in the contact model. The higher levels of pounding forces expected when the exterior foundations of adjacent buildings (in addition to the buildings themselves) are in close proximity requires the implementation of a more realistic element representing the actual condition of the impacting surfaces. The nonlinearly elastic Hertz contact rule, while adequately representing the increased area of contact due to degradation, does not allow for the specification of a maximum impact force beyond which no contact is manifested between the impacting surfaces. As an example, a level of pounding forces may be developed at a certain level which may lead to spalling of concrete. A "force-limiting" element at this level will ensure that no impacts will be detected at this storey when such a level of forces due to pounding has been attained.

7. REFERENCES

[A1] Anagnostopoulos, S.A., "Pounding Of Buildings In Series During Earthquakes", Earthquake Engineering and Structural Dynamics, Vol.16, pp.443-456, 1988.

[A2] Anagnostopoulos, S.A., and K.V. Spiliopoulos, "An Investigation Of Earthquake Induced Pounding Between Adjacent Buildings", Earthquake Engineering and Structural Dynamics, Vol.21, pp.289-302, 1992.

[A3] Anderson, D.G., and R.D. Woods, "Comparison of Field and Laboratory Shear Moduli", Proc. Conf. on In-Situ Measurement of Soil Properties, Geotechnical Div. Specialty Conf. ASCE, Vol.1, North Carolina State University, Raleigh, pp.69-92, 1975.

[A4] ATC-3, Applied Technology Council, Tentative Provisions for the Development of Seismic Regulations for Buildings, National Science Foundation and National Bureau of Standards, Washington, DC, 1st Edition 1978, 2nd Edition 1984.

[A5] Athanassiadou, C.J., G.G. Penelis, and A.J. Kappos, "Seismic Response of Adjacent Buildings with Similar or Different Dynamic Characteristics", Earthquake Spectra, Vol.10, No.2, pp.293-317, 1994.

[A6] Awojobi, A.O., and P.H. Tabiowo, "Vertical Vibration Of Rigid Bodies With Rectangular Bases On Elastic Media", Earthquake Engineering and Structural Dynamics, Vol.4, p.439,1976.

[B1] Barkan, D.D., "Dynamics of Bases and Foundations", McGraw-Hill Book Co., Inc., New York, 1962.

[B2] Bertero, V.V., and R.G. Collins, "Investigation of the Failures of the Olive View Stairtowers During the San Fernando Earthquake and Implications on Seismic Design", Report No. EERC 73-26, Earthquake Engineering Research Center, University of California, Berkeley, CA, 1973.

[B3] Bertero, V.V., "Observations On Structural Pounding", The Mexico Earthquakes- 1985, Factors Involved and Lessons Learned, M.A. Cassaro and E.M. Romero (eds.), ASCE, pp. 264-278, 1987.

[B4] Betti, R., "Effects of the Dynamic Cross-Interaction in the Seismic Analysis of Multiple Embedded Foundations", Earthquake Engineering and Structural Dynamics, Vol.26, pp.1005-1019, 1997.

[B5] Biot, M.A., "Bending of an Infinite Beam on an Elastic Foundation", Trans. ASME, Jour.Appl.Mech., 59, A1-A7, 1937.

[B6] Bycroft, G.N., "Forced Vibration Of Rigid Circular Plate On A Semi-Infinite Elastic Space And An Elastic Stratum", Philosophical Transaction Royal Society of London, Series A, Vol.248, No.948, pp.327-368, 1956.

[C1] Carr, A.J., "RUAUMOKO", Computer Program Library, Dept. of Civil Engineering, University of Canterbury, 1998.

[C2] Carr, A.J. and M. Tabuchi, "The Structural Ductility and the Damage Index for Reinforced Concrete Structure Under Seismic Excitations", Structural Dynamics-EURODYN '93, Moan et al. (eds.), pp.169-176, 1993.

[C3] Chambers, J.D., "A Distributed Spring Soil Model for Dynamic Soil-Structure Interaction Analysis", M.E. Thesis, Dept. of Civil Engineering, University of Canterbury, Christchurch, New Zealand, 1998.

[C4] Conoscente, J.P., R.O. Hamburger, and J.J. Johnson, "Dynamic analysis of Impacting Structural Systems", Proc. Xth World Conf. on Earthquake Engineering, Vol.7, pp.3899-3903, 1992.

[C5] Crouse, C.B., B. Hushmand, J.E. Luco, and H.L. Wong, "Foundation Impedance Functions: Theory Versus Experiment", Journal Geotechnical Eng., Vol.116, No.3, pp.432-449, Mar., 1990.

[C6] Carr, A.J., P.J. Moss, and A. Filiatrault, "Pounding of Adjacent Structures During Earthquakes: A Review of the Current State of Knowledge", 7th Canadian Conference on Earthquake Engineering, 5-7 Juney, 1995, Montreal, Canada, pp. 221-228..

[D1] Davis, R.O., "Pounding Of Buildings Modelled By An Impact Oscillator", Earthquake Engineering and Structural Dynamics, Vol.21, pp.253-274, 1992.

[D2] Der Kiureghian, A., "A Response Spectrum Method for Random Vibrations", EERC Report, UCB/EERC-80, Earthquake Engineering Research Center, University of California, Berkeley, CA 94720.

[D3] Dobry, R., "Damping in Soils: Its Hysteretic Nature and the Linear Approximation", Research Report R70-14, Massachusetts Institute of Technology, Dept. of Civil Engineering, Cambridge, Mass., 1970.

[D4] Dowrick, D.J., "Earthquake Resistant Design: A Manual for Engineers and Architects", John Wiley and Sons, 1977.

[E1] "Mindanao, Philippines Earthquake, August 17, 1976", Report EP-25 Earthquake Engineering Research Institute, 1977.

[E2] "Miyagi-ken-Oki, Japan Earthquake: June 12, 1978", P.I. Yanev (ed.), Earthquake Engineering Research Institute, Reconnaissance Report, Dec 1978.

[E3] "The Central Greece earthquakes of February-March, 1981", Earthquake Engineering Research Institute Reconnaissance and Engineering Report, 1982.

[E4] Ehlers, G., "The Effect of Soil Flexibility on Vibrating Systems", (in German) Beton und Eisen 41, pp.197-203, 1942.

[E5] Elder, D.G., I.F. McCahon, and M.D. Yetton, "The Earthquake Hazard in Christchurch: A Detailed Evaluation", Research Report to the EQC, Soils and Foundations, Ltd., Christchurch, 1991.

[E6] Erden, S.M., "Influence of Shape and Embeddment on Dynamic Foundation Response", thesis presented to the University of Massachusetts, at Amherst, Mass. in partial fulfillment of the requirements for the degree of Doctor of Philosophy, 1974.

[E7] Eurocode No.8: Structures In Seismic Regions- Design, Part 1, General and Building", Report EUR 12266 EN, Commission of the European Communities, Brussels, 1989.

[F1] Filiatrault, A., and B. Folz, "Nonlinear Earthquake Response of Structurally Interconnected Buildings", Canadian Journal of Civil Engineering, Vol.19, pp.560-572, 1992.

[F2] Filiatrault, A., M. Cervantes, B. Folz, and H. Prion, "Pounding Of Buildings During Earthquakes: A Canadian Perspective", Canadian Journal of Civil Engineering, Vol.21, pp. 251-265, 1994.

[F3] Filiatrault, A., P. Wagner, and S. Cherry, "Analytical Prediction Of Experimental Building Pounding", Earthquake Engineering and Structural Dynamics, Vol.24, pp.1131-1154, 1995.

[F4] Fletcher, D.Q., and L.R. Herrmann, "Elastic Foundation Representation of Continuum", Proc. ASCE, 97, EM1, pp.95-107,1971.

[F5] Ford, C.R., "Earthquakes and Building Construction", Whitcombe and Tombs, Auckland, 1926.

[F6] Fotopoulou, M., P. Kotsanopoulos, G. Gazetas, and J.L. Tassoulas, "Rocking Damping Of Arbitrarily Shaped Embedded Foundations", Journal of Geomechanical Engineering, ASCE, Vol.115, No.4, pp.473-490, 1989.

[F7] Fujimori, T., and T. Tsunoda, "Partial Embedment Effects on Soil-Structure Interaction", Xth World Conference on Earthquake Engineering, Spain, Vol.3, pp.1713-1718, July, 1992.

[G1] Ganev, T., F. Yamazaki, and T. Katayama, "Observation and Numerical Analysis of Soil-Structure Interaction of a Reinforced Concrete Tower", Earthquake Engineering and Structural Dynamics, Vol.24, pp.491-503, 1995.

[G2] Gazetas, G., "Analysis Of Machine Foundation Vibrations: State-Of-The-Art", Soil Dynamics and Earthquake Engineering, Vol.2, No.1, 1983.

[G3] Gazetas, G. and R. Dobry, "Simple Radiation Damping Model for Piles and Footings", J.Eng. Mechs., ASCE, Vol.110, No.6, pp.937-956, Jun.,1984.

[G4] Gazetas, G., R. Dobry, J.L. Tassoulas, "Vertical Response of Arbitrarily Shaped Embedded Foundations", Jour. of Geotechnical Engineering, ASCE, Vol.111, No.6, pp.750-771, June, 1985.

[G5] Gazetas, G., and K.H. Stokoe II, "Free Vibration Of Embedded Foundations: Theory Versus Experiment", Journal of Geomechanical Engineering, ASCE, Vol.117, No.9, pp.1382-1401, 1991.

[G6] Gazetas, G., "Formulas And Charts For Impedances Of Surface And Embedded Foundations", Journal of Geotechnical Engineering, Vol.117, No.9, pp.1363-1381, Sept.1991.

[G7] Glauser, E.C., "The May 6, 1976 Friuli Earthquake- Assessment and Interpretation of Building Damage", Proc. 6th World Conference on Earthquake Engineering, New Delhi, Vol I, pp. 279-288, 1977.

[G8] Goldsmith, W., "Impact: The Theory and Physical Behaviour of Colliding Solids", Edward Arnold Ltd., London, 1960.

[H1] Hanson, R.D., and H.J. Degenkolb, "The Venezuela Earthquake: July 29, 1967", American Iron and Steel Institute, NY, 1969.

[H2] Hardin, B.O., and F.E. Richart, Jr., "Elastic Wave Velocities in Granular Soils" , Journal of the Soil Mechanics and Foundations Division, ASCE,Vol.89, No.SM1, pp.33-65, 1963.

[H3] Hardin, B.O., and W.L. Black, "Vibration Modulus of Normally Consolidated Clay", Journal of the Soil Mechanics and Foundations Division, ACSE, Vol. 94, No.SM2, Proc. Paper 5833, pp.353-369, 1968.

[H4] Hardin, B.O., and W.L. Black, closure to "Vibration Modulus of Normally Consolidated Clay", Journal of the Soil Mechanics and Foundations Division, ACSE, Vol. 95, No.SM6, Proc. Paper 6894, pp.1531-1537, 1969.

[H5] Hardin, B.O., and V.P. Drnevich, "Shear Modulus and Damping in Soils: Measurement and Parameter Effects", Journal of the Soil Mechanics and Foundations Division, ACSE, Vol. 98, No.SM6, pp.603-624, 1972.

[H6] Hatakana, M., Y. Suzuki, T. Kawasaki, and M. Endo, "Dynamic Properties of Undisturbed Tokyo Gravel", Proc. Discussion Session on Influence of Local Soil Conditions on Seismic Response, XIIth ICSMFE, Rio de Janeiro, pp. 107-112, 1989.

[H7] Hatzikonstantinou, E., J.L. Tassoulas, G. Gazetas, P. Kotsanopoulos, and M. Fotopoulou, "Rocking Stiffness Of Arbitrarily Shaped Embedded Foundations", Journal of Geomechanical Engineering, ASCE, Vol.115, No.4, pp.457-472, 1989.

[H8] Huang, C.D., "Dynamic Soil-Foundation and Foundation-Soil-Foundation Interaction in 3-D", PhD Thesis, Dept. of Civil Engineering, College of Engineering, University of South Carolina, 1993.

[I1] Iguchi, M., and J.E. Luco, "Dynamic Response Of Flexible Rectangular Foundations On An Elastic Half-Space", Earthquake Engineering and Structural Dynamics, Vol.9, pp.239-249, 1981.

[I2] Imamura, A., M. Ishizaki, T. Watanabe, and M. Motossaka, "Seismic Response Characteristics of Embedded Structures Considering Cross Interaction", Xth World Conference on Earthquake Engineering, Spain, Vol.III, pp.1719-1724, 1992.

[I3] Ishihara, K., "Soil Behaviour in Earthquake Geotechnics", Clarendon Press, Oxford, 1996.

[J1] Jeng, V., K. Kasai, and B.F. Maison, "A Spectral Difference Method To Estimate Building Separations To Avoid Pounding", Earthquake Spectra, Vol.8, No.2, 1992.

[J2] Jeng, V., and K. Kasai, "Spectral Relative Motion of Two Structures Due to Seismic Travel Waves", Journal of Structural Engineering, Vol.122, No.10, pp.1128-1135, Oct. 1996.

[J3] Jennings, P.C., and J. Bielak, "Dynamics Of Building-Soil Interaction", Bulletin of the Seismological Society of America, Vol.63, No.1, pp.9-48, 1973.

[J4] Jing, H.-S., and M. Young, "Random Response of a Single-Degree-of-Freedom Vibro-Impact System With Clearance", Earthquake Engineering and Structural Dynamics, Vol.19, pp.789-798, 1990.

[J5] Jing, H.-S., and K.-C. Sheu, "Exact Stationary Solutions of the Random Response of a Single-Degree-of-Freedom Vibration Impact System", Journal of Sound and Vibration, 141(3), pp.363-373, 1990.

[J6] Jones, R., and J. Xenophontos, "The Vlazov Foundation Model", Int. Jour. of Mech. Sci., 19, 317-323, 1977.

[J7] Jury, R.D., "Seismic Load Demands on Columns of Multi-Storey Frames", M.E. Report 78-12, Dept. of Civil Engineering, University of Canterbury, 1978.

[K1] Karasudhi, P., L.M. Keer, and S.L. Lee, "Vibratory Motion Of A Body On An Elastic Half-Plane", Journal of Applied Mechanics, ASME, 35E, pp.697-705, 1968.

[K2] Kasai, K., V. Jeng, and B.F. Maison, "The Significant Effects of Pounding-Induced Accelerations on Building Appurtenances", Applied Technology Council, ATC-29, Proceedings Seminar and Workshop on Seismic Design and Performance of Equipment and Nonstructural Elements in Buildings and Industrial Structures, 1990.

[K3] Kasai, K., and B.F. Maison, "Observation Of Structural Pounding Damage From The 1989 Loma Prieta Earthquake", Proceedings of the Sixth Canadian Conference on Earthquake Engineering, Toronto, Ontario, pp. 735-742, 1991.

[K4] Kasai, K., B.F. Maison, V. Jeng, D.J. Patel, and P. Patel, "A Study on Earthquake Pounding Between Adjacent Buildings", Proc. 6th Canadian Conf. on Earthquake Engineering, Toronto, Canada, 1991.

[K5] Kasai, K., V. Jeng, P.C. Patel and J.A. Munshi, "Seismic Pounding Effects - Survey and Analysis", Proceedings of the Xth World Conference on Earthquake Engineering, Spain, Vol.7, Balkema, 1992.

[K6] Kasai, K., A.R. Jagiasi, and V. Jeng, "Inelastic Vibration Phase Theory for Seismic Pounding Mitigation", Journal of Structural Engineering, pp.1136-1146, Vol.122, No.10, 1996.

[K7] Kawakami, H., and S. Tasaki, "Soil-Structure Interaction Of Rigid Structures Considering Through-Soil Coupling Between Adjacent Structures", Proceedings of the 9th World Conference on Earthquake Engineering, Tokyo-Kyoto, Vol.III, pp.385-390, 1988.

[K8] Kobori, T., R. Minai, and K. Kusakabe, "Dynamical Cross-Interaction Between Two Foundations", Proceedings of the 6th World Conference on Earthquake Engineering, New Delhi, Vol.2, pp.1484-1489, 1977.

[K9] Komamura, F., R.J. Huang, "New Rheological Model for Soil Behaviour", Journal of the Geotechnical Engineering, ASCE, Vol.100, GT7, pp.807-823, July, 1974.

[L1] Ladd, R.S., and P. Dutko, "Small-Strain Measurements Using Triaxial Apparatus", Advances in the Art of Testing Soils Under Cyclic Conditions, V.Koshla, ed., ASCE, pp.148-166, 1985.

[L2] Lawson, A.C., "Report of the California Earthquake Commission", Report of the Carnegie Institution of Washington, pp.49-56, 1908.

[L3] Lee, T.H., and D.A. Wesley, "Soil-Structure Interaction Of Nuclear Reactor Structures Considering Through-Soil Coupling Between Adjacent Structures", Nuclear Engineering and Design, Vol.24, pp.374-387, 1973.

[L4] Leger, P., and S. Dussault, "Seismic-Energy Dissipation in MDOF Structures", Jour. of Structural Engineering, Vol.118, No.5, pp.1251-1269, 1992.

[L5] Leibovich, E., A. Rutenberg, and D.Z. Yankelevsky, "Seismic Response of Adjacent Buildings and Effects of Asymmetry", Stage II Report (in Hebrew), National Building Research Institute, Technion, Haifa, Feb. 1995.

[L6] Leibovich, E., A. Rutenberg, and D.Z. Yankelevsky, "On Eccentric Seismic Pounding of Symmetric Buildings", Earthquake Engineering and Structural Dynamics, Vol. 25, pp.219-233, 1996.

[L7] Leibovich, E., and A. Rutenberg, "Symmetric and Eccentric Seismic Pounding of Yielding Building Structures", European Workshop on Seismic Response of Asymmetric and Setback Structures, Anacapri, October 1996.

[L8] Liam Finn, W.D., M. Yogendrakumar, N. Yoshida, and H. Yoshida, "Analysis of Porewater Pressures in Seismic Centrifuge Tests", Soil Dynamics and Liquefaction, A.S. Cakmak (ed.), Elsevier Computational Mechanics Publications, NY, pp. 71-83, 1987.

[L9] Lin, H.-T., J.M. Roesset, and J.L. Tassoulas, "Dynamic Interaction Between Adjacent Foundations", Earthquake Engineering and Structural Dynamics, Vol.15, pp.323-343, 1987.

[L10] Lin, J-H., "Separation Distance to Avoid Seismic Pounding of Adjacent Buildings", Earthquake Engineering and Structural Dynamics, Vol. 26, pp. 395-403, 1997.

[L11] Lin, Y.J., "Dynamic Response Of Circular Plates On Visco-Elastic Half-Space", Journal of Applied Mechanics, ASME, Vol.45, Series E, No.2, pp.379-384, 1978.

[L12] Liolios, A.A., E.G. Galoussis, "Seismic Interaction Between Adjacent Buildings Under Second-Order Geometric Effects", Proc. Tenth WCEE, Spain, Vol.7. pp.3905-3909, 1992.

[L13] Liolios, A.A., "A Numerical Estimation for the Influence of Modifications to Seismic Interaction Between Adjacent Structures", Proc. Int. Conf. Earthquake Resistant Construction and Design, pp.461-467, 1989.

[L14] Liou, G.-S., "Vibration Of Surface Foundations Of Arbitrary Shapes", Earthquake Engineering and Structural Dynamics, Vol.20, pp.1115-1125, 1991.

[L15] Liou, G.-S., "Dynamic Stiffness Matrices For Two Circular Foundations", Earthquake Engineering and Structural Dynamics, Vol.23, pp.193-210, 1994.

[L16] Liou, G-S. "Effect of Slab Flexibility on Interaction Between Two Circular Foundations", Earthquake Engineering and Structural Dynamics, Vol.25, pp.561-583, 1996.

[L17] Luco, J.E., and R.A. Westmann, "Dynamic Response Of Circular Footings", Journal of Engineering Mechanics Division, ASCE, Vol.97, No.EM5, pp.1381-1395, 1971.

[L18] Luco, J.E., "Impedance Functions For A Rigid Foundation On A Layered Medium", Nuclear Engineering and Design, Vol. 31, pp.204-217, 1974.

[L19] Luco, J.E., "Vibrations Of A Rigid Disk On A Layered Visco-Elastic Medium", Nuclear Engineering and Design, Vol.36, p.325, 1976.

[L20] Luco, J.E., and R.J. Apsel, "On the Green's Functions for a Layered Half-Space, Part I", Bulletin of the Seismological Society of America, Vol.73, pp.909-929, 1983.

[M1] Mahin, S.A., V.V. Bertero, A.K. Chopra, and R.G. Collins, "Response Of The Olive View Hospital Main Building During The San Fernando Earthquake", Report No. EERC 76-22, Earthquake Engineering Research Center, University of California, Berkeley, CA, 1976.

[M2] Maison, B.F., and K. Kasai, "SLAM: A Computer Program For The Analysis Of Structural Pounding", National Information Service for Earthquake Engineering, University of California, Berkeley, Calif., 1988.

[M3] Maison, B.F., and K. Kasai, "Analysis For Type Of Structural Pounding", Journal of Structural Engineering, ASCE, Vol.116 (4), pp.957-977, 1990.

[M4] Maison, B.F., and C.F. Neuss, "SUPER-ETABS: An Enhanced Version Of ETABS Program", Technical Report to the National Science Foundation, J.G.Bouwkamp Inc., Darmstadt, Germany.

[M5] Maison, B.F., and K. Kasai, "SLAM-2: A Computer Program For The Analysis Of Structural Pounding", National Information Service for Earthquake Engineering, University of California, Berkeley, CA, 1990.

[M6] Maison, B.F., and K. Kasai, "Dynamics Of Pounding When Two Buildings Collide", Earthquake Engineering and Structural Dynamics, Vol.21, pp.771-786, 1992.

[M7] Maison, B.F., "PC-ANSR: A Computer Program For Non-Linear Structural Analysis", National Service for Earthquake Engineering, University of California, Berkeley, CA, 1992.

[M8] Malhotra, P.K., M.J. Huang, and A.F. Shakal, "Seismic Interaction at Separation Joints of an Instrumented Concrete Bridge", Earthquake Engineering and Structural Dynamics, Vol. 24, pp.1055-1067, 1995.

[M9] Meek, J.W., and A.S. Veletsos, "Simple Models For Foundation In Lateral And Rocking Motion", Proceedings of the Fifth World Conference on Earthquake Engineering, Rome 1974.

[M10] Meek, J.W., J.P. Wolf, "Insights on 2D vs. 3D-Modelling of Surface Foundations", Xth World Conference on Earthquake Engineering, Vol.III, Spain,1992.

[M11] Meek, J.W., J.P. Wolf, "Why Cone Models Can Represent the Elastic Half-Space", Earthquake Engineering and Structural Dynamics, Vol.22, pp.759-771, 1993.

[M12] Meek, J.W., and J.P. Wolf, "Material Damping For Lumped-Parameter Models Of Foundations", Earthquake Engineering and Structural Dynamics, Vol.23, pp.349-362, 1994.

[M13] Mita, A., and J.E. Luco, "Impedance Functions And Input Motions For Embedded Square Foundations", Journal of Geomechanical Engineering, ASCE, Vol.115, No.4, pp.491-503, 1989.

[M14] Moehle, J.P., (ed.), "Preliminary Report on the Seismological and Engineering Aspects of the January 17, 1994, Northridge Earthquake", Report No. UCB/EERC-94/01, Earthquake Engineering Research Center, University of California, Berkeley, CA, 1994.

[M15] Mondakar, D.P., and G.H. Powell, "ANSR-1: General Purpose Program For Analysis Of Non-Linear Structural Response", Rep. No. EERC-75/37, Earthquake Research Center, University of California, Berkeley, CA, 1975.

[M16] Mulliken, J.S., "Discrete models for Foundation-Soil-Foundation interaction in Time Domain", MSc Thesis, College of Engineering, Dept. of Civil Engineering, University of South Carolina, 1994.

[M17] Murakami, H., and J.E. Luco, "Seismic Response Of Periodic Array Of Structures", Journal of the Engineering Mechanics Division, ASCE, Vol.103, No.EM5, pp.965-977, 1977.

[N1] Nassar, A., and H. Krawinkler, "Seismic Demands for SDOF and MDOF Systems", John A. Blume Earthquake Engineering Center Rep. No.95, Stanford Univ., Stanford, Calif, 1991.

[N2] The Great Alaskan Earthquake of 1964, Engineering, NAS, Pub.1606, National Academy of Science, Washington, DC, 1973.

[N3] NBCC. Commentary of the National Building Code of Canada. Associates Committee on the National Building Code, National Research Council of Canada, Ottawa, Ont., 1990.

[N4] The Hyogo-ken Nanbu Earthquake of 17 January 1995, Bulletin of the New Zealand Society for Earthquake Engineering, Vol.28, No.1, pp.1-98, 1995.

[N5] Standards New Zealand, NZS 4203: 1992, Code of Practice for General Structural Design Loadings for Buildings, Standards New Zealand, Wellington, New Zealand, 1992.

[N6] Standards New Zealand, NZS 3101: Parts 1 and 2: 1995, Concrete Structures Standard and Commentary, Standards New Zealand, Wellington, New Zealand, 1992.

[N7] Nogami, T., "Simplified Subgrade Model for Three-Dimensional Soil-Foundation Interaction Analysis", Soil Dynamics and Earthquake Engineering, Vol. 15, pp.419-429, 1996.

[N8] Novak, M., and K. Sachs, "Torsional and Coupled Vibrations of Embedded Footings", Earthquake Engineering and Structural Dynamics, Vol.2, pp.11-33, 1973.

[O1] Otani, S., "*SAKE*, a Computer Program for Inelastic Response of R/C Frames to Earthquakes", Report UILU-Eng-74-2029, Civil Engineering Studies, University of Illinois at Urbana-Champaign, Nov. 1974.

[O2] Otani, S., "Nonlinear Dynamic Analysis of Reinforced Concrete Building Structures", Canadian Jour. of Civil Engrg., Vol;7, No.2, pp.333-344, 1980.

[O3] Otani, S., "Hysteresis Models of Reinforced Concrete for Earthquake Response Analysis", Jour. Faculty of Engineering, University of Tokyo, Vol.36, No.2, pp.125-159, 1981.

[P1] Pais, A., and E. Kausel, "Approximate Formulas For Dynamic Stiffnesses Of Rigid Foundations", Soil Dynamics and Earthquake Engineering, Vol.7, No.4, pp.213-227, 1988.

[P2] Papadrakakis, M., H. Mouzakis, N. Plevris, and S. Bitzarakis, "A Lagrange Multiplier Solution Method for Pounding of Buildings During Earthquakes", Earthquake Engineering and Structural Dynamics, Vol. 20, pp.981-998, 1991.

[P3] Papadrakakis, M., and H.P. Mouzakis, "Earthquake Simulator Testing of Pounding Between Adjacent Buildings", Earthquake Engineering and Structural Dynamics, Vol. 24, pp.811-834, 1995.

[P4] Paulay, T., and M.J.N. Priestley, "Seismic Design of Reinforced Concrete and Masonry Buildings", John Wiley and Sons, Inc., NY, 1992.

[P5] Pender, M.J., "Earthquake Soil-Structure Interaction, Spring, and Dashpot Models and Real Soil Behaviour", Bulletin of the New Zealand Society for Earthquake Engineering, Vol.16, No.4, pp.320-330, 1983.

[P6] Pender, M.J., "Earthquake Resistant Design of Foundations", Pacific Conference Earthquake Engineering, PCEE 95, Melbourne, Australia, Nov.1995.

[P7] Pender, M.J., "Linear and Nonlinear Earthquake Site Response", Proc. of the Wroth Memorial Symposium, G.T. Houlsby and A.N. Schofield (eds.), Predictive Soil Mechanics, pp.529-543, 1992.

[P8] Penzien, J., "Evaluation of Building Separation Distance Required to Prevent Pounding During Strong Earthquakes", Earthquake Engineering and Structural Dynamics, Vol.26, pp.849-858, 1997.

[Q1] Qian, J., and D.E. Beskos, "Dynamic interaction between 3-D Rigid Surface Foundations and Comparison with the ATC-3 Provisions", Earthquake Engineering and Structural Dynamics, Vol.24, pp.419-437, 1995.

[Q2] Qian, J., L.G. Tham, and Y.K. Cheung, "Dynamic Cross-Interaction Between Flexible Surface Footings by Combined BEM and FEM", Earthquake Engineering and Structural Dynamics, Vol.25, pp.509-526, 1996.

[Q3] Qian, J. and D.E. Beskos, "Harmonic Wave Response of Two 3-D Rigid Surface Foundations", Soil Dynamics and Earthquake Engineering, Vol.15, pp.95-110, 1996.

[Q4] Quinlan, P.M., "The Elastic Theory of Soil Dynamics", Symposium on Dynamic Testing of Soils, ASTM STP No. 156, pp.3-34, 1953.

[R1] Reissner, E., "Stationaere, axialsymmetrische, durch eine schuettelnde Masse erregte Schwingungen eines homogenen elastischen Halbraumes", Ing. Arch., Vol.7, p.381, 1936.

[R2] Richart, F.E., J.R. Hall, and R.B. Woods, "Vibration of Soils and Foundations", Prentice Hall, New Jersey, 1970.

[R3] Richart Jr., R.E., and E.B. Wylie, "Influence of Dynamic Soil Properties on Response of Soil Masses", Structural and Geotechnical Mechanics, Ed. W.J. Hall, Prentice Hall, NJ, 1977.

[R4] Robinson, A.R., "The Transmitting Boundary-Again", Structural and Geotechnical Mechanics, E.J. Hall (ed.) , Prentice Hall, NJ, 1977.

[R5] Roesset, J.M., and J.J. Gonzalez, "Dynamic Interaction Between Adjacent Structures", Proceedings of DMSR, Vol.I, Karlsruhe, pp.127-166, 1977.

[R6] Roesset, J.M., and M.M. Ettouney, "Transmitting Boundaries: A Comparison", Int. Jour. for Numerical Methods in Geomechanics, Vol.1, pp.151-176, 1977.

[R7] Roesset, J.M., "Stiffness and Damping Coefficients of Foundations", Dynamic Response of Pile Found., O'Neil and Dobry (ed.), ASCE, pp.1-30, 1980.

[S1] Savidis, S.A., and T. Richter, "Dynamic Interaction Of Rigid Foundations", Proceedings of the 9th International Conference on Soil Mechanics and Foundation Engineering, Tokyo, 2, pp.369-374, 1977.

[S2] Schmid, G., and N. Chouw, "Soil-Structure Interaction Effects on Structural Pounding", Proc. Xth World Conf. on Earthquake Engineering, Spain, Vol.3, pp.1651-1656, 1992.

[S3] Scott, R.F., "Foundation Analysis", Prentice-Hall Civil Engineering and Engineering Mechanics Series, NJ, 1981.

[S4] Seed, H.B., and I.M. Idriss, "Soil Moduli and Damping Factors for Dynamic Response Analysis," Rep. No. EERC 70-10, Earthquake Engineering Research Center, College of Engineering, University of California, Berkley, Dec. 1970.

[S5] Seed, H.B., J. Lysmer, and R. Hwang, "Soil-Structure Interaction Analyses For Seismic Response", Journal of the Geomechanical Engineering Division, ASCE, Vol.101, No.GT5, 1975.

[S6] Selvadurai, A.P.S., "Elastic Analysis of Soil-Foundation Interaction", Developments in Geotechnical Engineering, Vol.17, Elsevier Scientific Pub. Co., 1979.

[S7] Shohara, R., I. Kurosawa, Y. Shinozaki, and D. Sakamoto, "Tests on Dynamic Interaction Between Foundations", Xth World Conference on Earthquake Engineering, Spain, Vol.III, pp.1879-1884, 1992.

[S8] Sinclair, K.M., "The Response of Multi-Storey Frames to Seismic Pounding", ME report, University of Canterbury, 1993.

[S9] Stokoe II, K.H., and R.D. Woods, "In-Situ Shear Wave Velocity by Cross-Hole Method", J. Soil Mech. Found. Div., ASCE, Vol.98, No.SM5, pp.443-460, 1972.

[S10] Stokoe II, K.H., and S.M. Erden, "Influence Of Base Shape On Dynamic Response Of Surface Foundations", Geomechanical Engineering Report GP85-1, University of Texas at Austin, Austin, Tex., 1985.

[T1] Tezcan, S.S., V. Yerlici, and H.T. Durugunoglu, "A Reconnaissance Report for the Romanian Earthquake of 4 March 1977", Earthquake Engineering and Structural Dynamics, Vol. 6, pp.397-421, 1978.

[T2] Thiers, G.R., and H.B. Seed, "Cyclic Stress-Strain Characteristics of Clay", Journal of the Soil Mechanics Foundation Division, ACSE, Vol. 94, No.SM2, March, pp.555-569, 1968.

[T3] Tsai, H.-C., "Dynamic Analysis of Base-Isolated Shear Beams Bumping Against Stops", Earthquake Engineering and Structural Dynamics, Vol.26, pp.515-528, 1997.

[U1] UBC, 1990. "Uniform Building Code", International Conference on Building Officials, Whittier, CA.[105]

[V1] Valles, R.E., and A.M. Reinhorn, "Evaluation, Prevention and Mitigation of Pounding Effects in Building Structures", National Center for Earthquake Engineering Research Technical Report NCEER-97-0001, Feb.1997.

[V2] Veletsos, A.S., and B. Verbic, "Vibration Of Viscoelastic Foundations", Earthquake Engineering and Structural Dynamics, Vol. 2,No.1, pp.87-102, 1973.

[V3] Veletsos, A.S., and V.V. Nair, "Seismic Interaction of Structures on Hysteretic Foundations", Report No.21, Dept. of Civil Engineering, Rice University, Houston, Texas, 1974.

[V4] Vesic, A.S., "Bending of Beams Resting on Isotropic Elastic Solid", Proc. ASCE, 87, EM2, 35-51, 1961.

[V5] Vlazov, V.Z., and N.N. Leontiev, "Beams, Plates, and Shells on Elastic Foundations", translated from Russian by Israel Program for Scientific Translations, NTIS No.N67-14238, 1966.

[W1] Wada, A., Y. Shinozaki, and N. Nakamura, "Collapse Of Building With Expansion Joints Through Collision Caused By Earthquake Motion", Eighth World Conference on Earthquake Engineering, pp.855-862, 1984.

[W2] Warburton, G.B., J.D. Richardson, and J.J. Webster, "Forced Vibrations Of Two Masses On An Elastic Half-Space", Journal of Applied Mechanics, ASME, pp.148-156, 1971.

[W3] Westermo, B.D., "The Dynamics of Interstructural Connection to Prevent Pounding", Earthquake Engineering and Structural Dynamics, Vol. 18, pp.687-699, 1989.

[W4] Whitman, R.V., "Are the Soil Conditions in Mexico City Unique?", The Mexico Earthquakes-1985, Factors Involved and Lessons Learned, (ed.) M.A. Cassaro, and E.M. Romero, ASCE, pp.7-18, 1987.

[W5] Wolf, J.P., and P.E. Skrikerud, "Mutual Pounding Of Adjacent Structures During Earthquakes", Nuclear Engineering Design, Vol.57, pp.253-275, 1980.

[W6] Wolf, J.P., and D.R. Somaini, "Approximate Dynamic Model Of Embedded Foundation In Time Domain", Earthquake Engineering and Structural Dynamics, Vol.14, pp.683-703, 1986.

[W7] Wolf, J.P., "Consistent Lumped-Parameter Model For Unbounded Soil: Physical Representation", Earthquake Engineering and Structural Dynamics, Vol.20, pp.11-32, 1991.

[W8] Wolf, J.P., "Foundation Vibration Analysis Using Simple Physical Models", Prentice Hall, Englewood Cliffs, NJ,1994.

[W9] Wolf, J.P., and J.W. Meek, "Dynamic Stiffnesses Of Foundations On Layered Soil Half-Space Using Cone Frustums", Earthquake Engineering and Structural Dynamics, Vol.23, pp.1079-1095, 1994.

[W10] Wong, H.L., and M.D. Trifunac, "Two-Dimensional, Anti-Plane, Building-Soil-Building Interaction For Two Or More Buildings And For Incident Plane SH-Waves", Bulletin of the Seismological Society of America, Vol.65, No.6, pp.1863-1885, 1975.

[W11] Wong, H.L., and J.E. Luco, "Dynamic Response Of Rigid Foundations Of Arbitrary Shape", Earthquake Engineering and Structural Dynamics, Vol.4, pp.579-587, 1976.

[W12] Wong, H.L., J.E. Luco, and M.D. Trifunac, "Contact Stresses And Ground Motion Generated By Soil-Structure Interaction", Earthquake Engineering and Structural Dynamics, Vol.5, pp.67-79, 1977.

[W13] Wong, H.L., and J.E. Luco, "Dynamic Interaction Between Rigid Foundations in a Layered Half-Space", Soil Dynamics and Earthquake Engineering, Vol. 5, No. 3, pp.149-158, 1986.

[Y1] Yamanouchi, H., and T. Yomo, "Significant Phase Characteristics of Earthquake Ground Motions Potential to Structural Damage", Proc. 4th U.S. Conf. on Earthquake Engineering, 1990.

[Y2] Yoshimi, Y., M. Hatanaka, and H. Oh-oka, "A Simple Method for Undisturbed Sampling by Freezing", Proc. Specialty Session on Undisturbed Sampling, VIIIth ICSMFE, Tokyo, pp.23-28, 1977.

[Z1] Zhao, J.X., "Vertical Soil-Structure Interaction of the Gisborne Post Office Building", Pacific Conference on Earthquake Engineering, pp. 227-236, Melbourne, 20-22 Nov, 1995.

[Z2] Zhao, J.X., P.N. Davenport, and W.J. Cousins, "Response of the Christchurch Police Station to the 1994 Arthur's Pass Earthquake", Proc. Conf. New Zealand National Soc. for Earthquake Engineering, New Plymouth, pp.203-210, Mar. 1996.

[Z3] Zhaohua, F., and R.D. Cook, "Beam Elements on Two-Parameter Elastic Foundations", Jour. Engrg. Mechs., ASCE, Vol.109, No.6, pp.1390-1402, 1983.

APPENDIX A

PARAMETER STUDIES

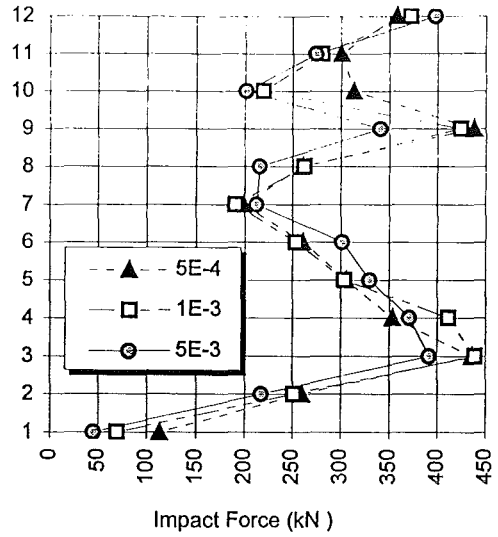

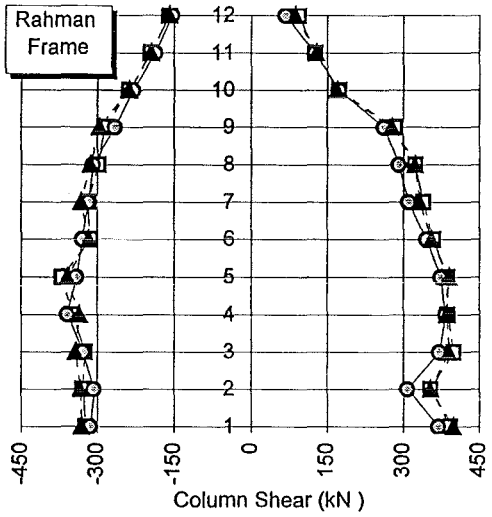

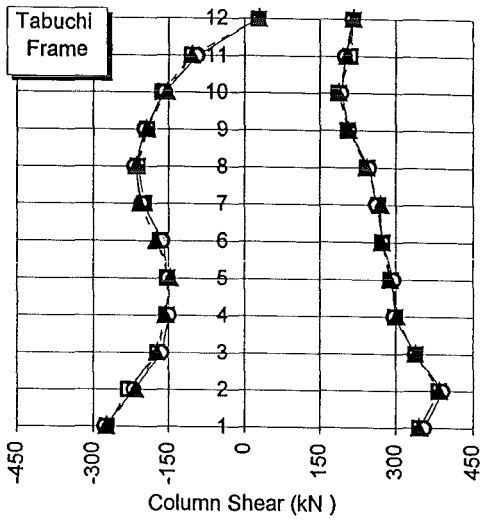

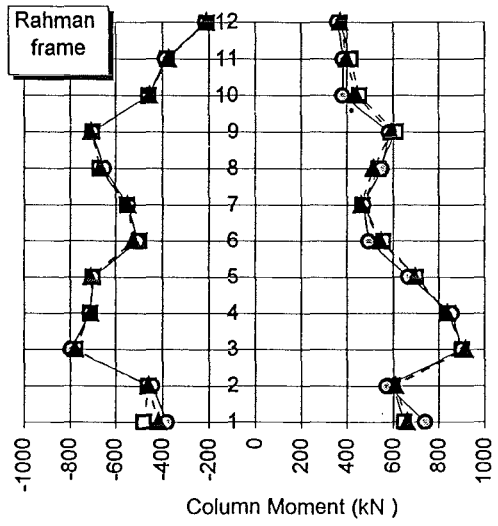

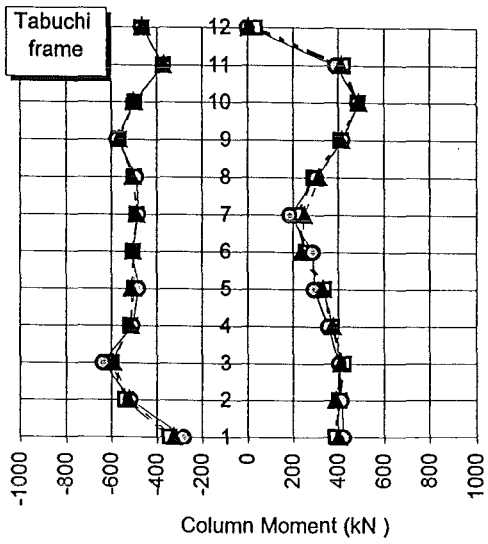

Fig. A.1: Effect of time-step implemented in time-history analysis on maxima of various pounding response values (1mm separation gap). Compliant foundations case. 1940 El Centro earthquake applied left-right.

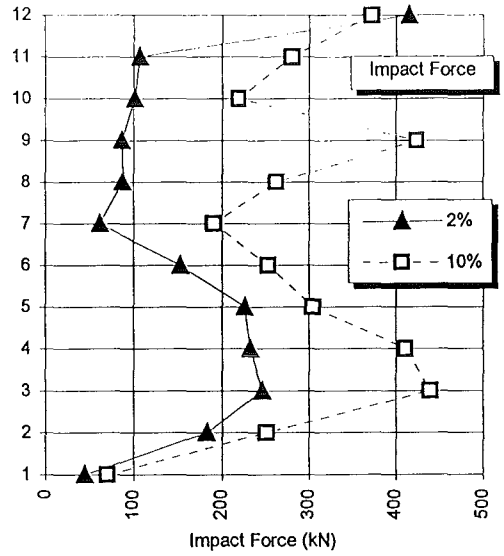

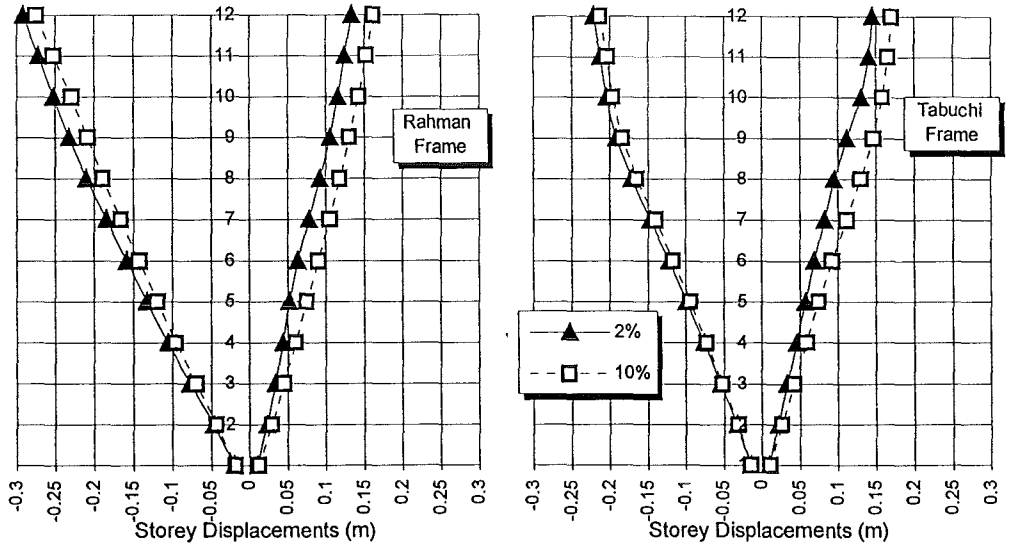

Fig. A.2a: Effect of bilinear factor (r) assumed in Rahman frame numerical model on maxima of various pounding response values (1mm separation gap). Compliant foundations case. 1940 El Centro earthquake applied left-right.

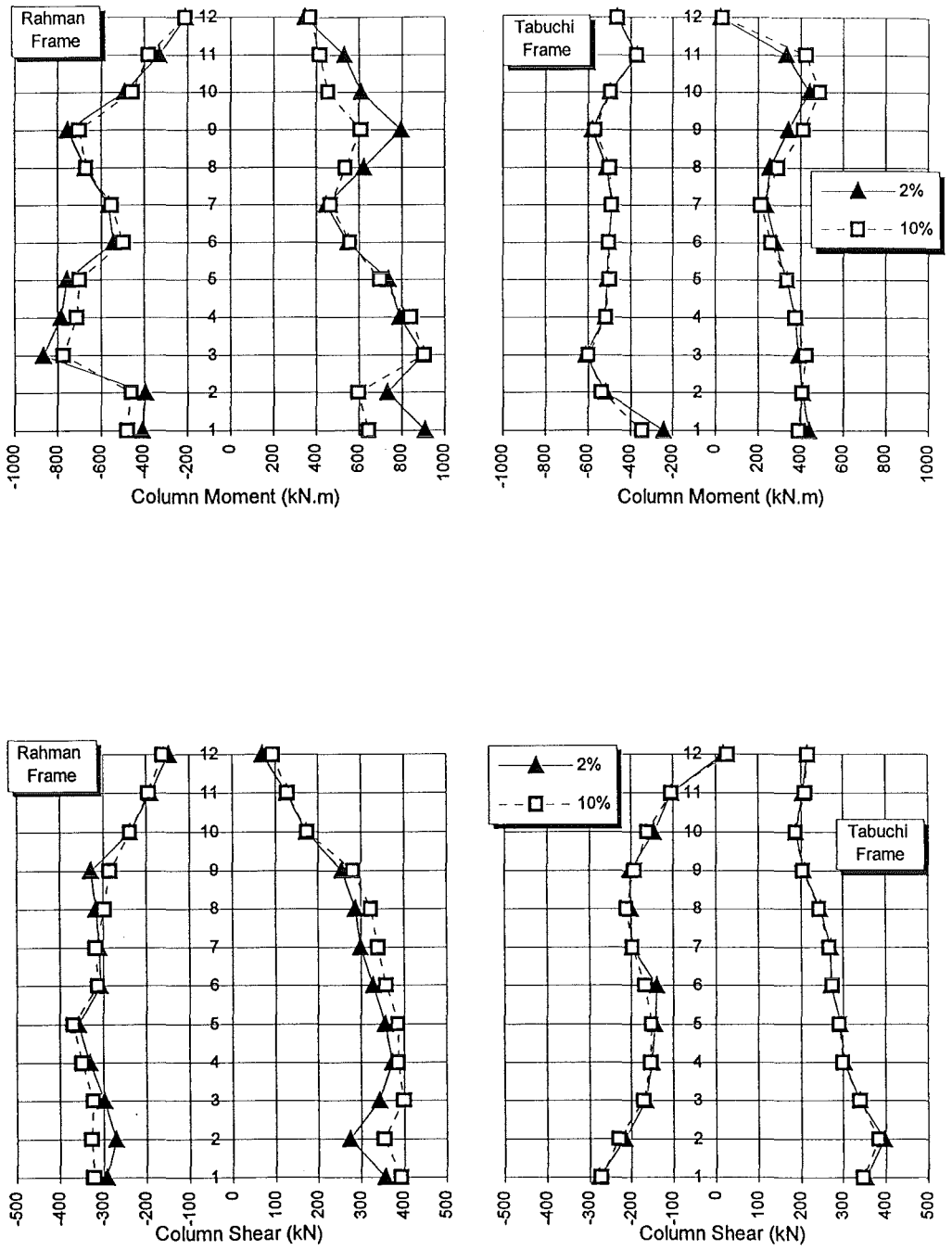

Fig. A.2b: Effect of bilinear factor (r) assumed in Rahman frame numerical model on maxima of various pounding response values (1mm separation gap). Compliant foundations case. 1940 El Centro earthquake applied left-right.

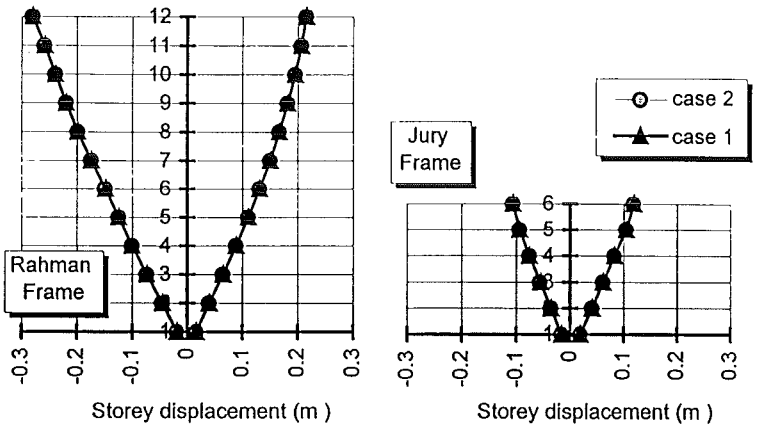

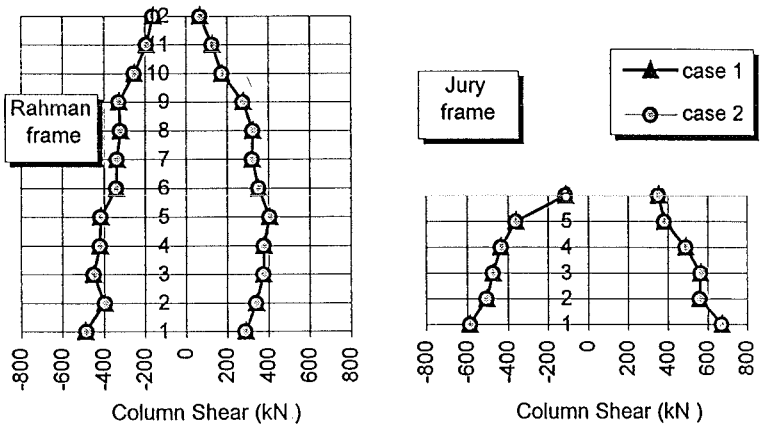

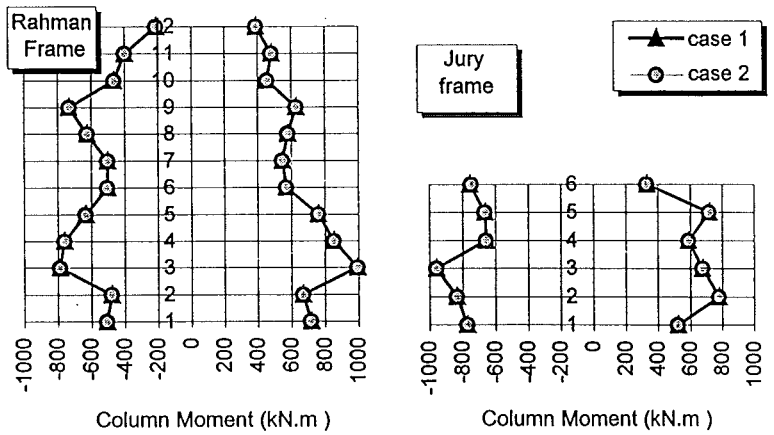

Fig. A.3: Effect of μ coefficient implemented in through-soil interaction model for the different values of foundation widths (B) of the various frames on maxima of various no pounding response values. 1940 El Centro earthquake applied left-right.

Case 1: μ = 0.303 B = 3.5m
Case 2: μ = 0.379 B = 2.8m

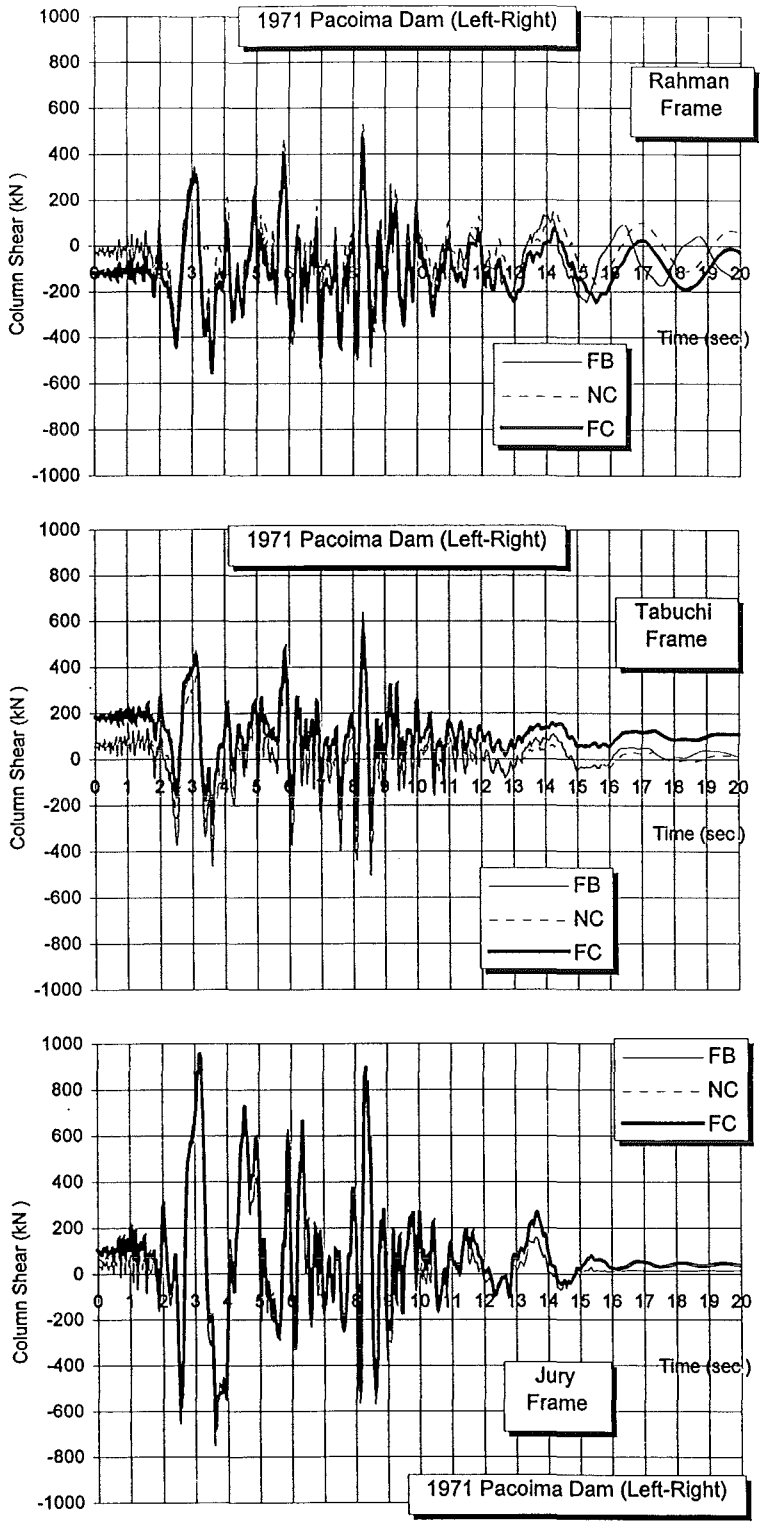

Fig. A.4: Effect of foundation fixity conditions on time-history of impact-side column shear for no pounding case. 1971 Pacoima Dam earthquake applied left-right.

FB = Fixed Base
NC = Non-Coupled (i.e. only soil-structure interaction considered)
FC = Foundations Coupled

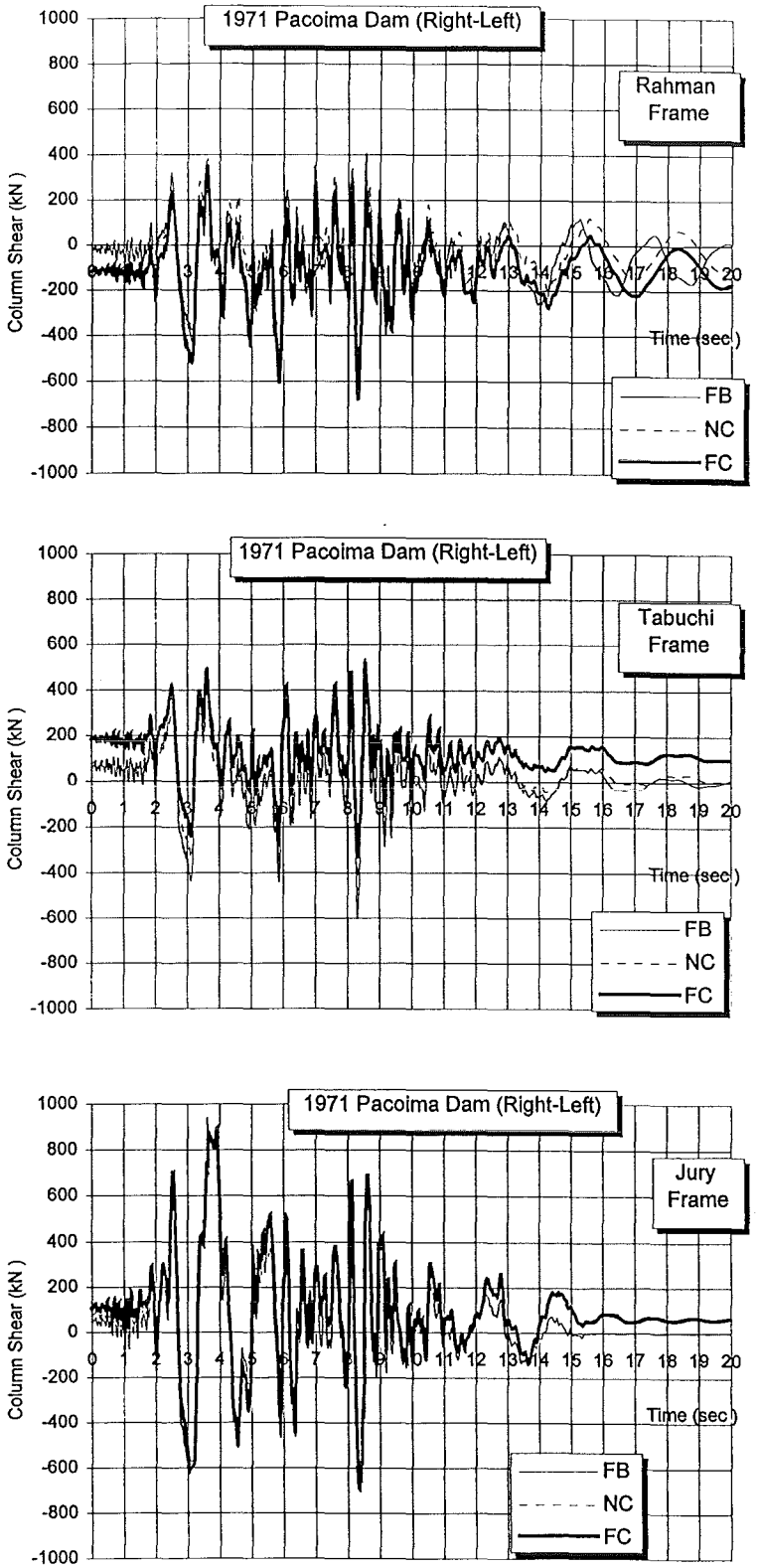

Fig. A.5: Effect of foundation fixity conditions on time-history of impact-side column shear for no pounding case. 1971 Pacoima Dam earthquake applied right-left.

FB = Fixed Base
NC = Non-Coupled (i.e. only soil-structure interaction considered)
FC = Foundations Coupled

APPENDIX B

COMPARISON OF IMPACT FORCE VARIATION FOR THE VARIOUS CASES

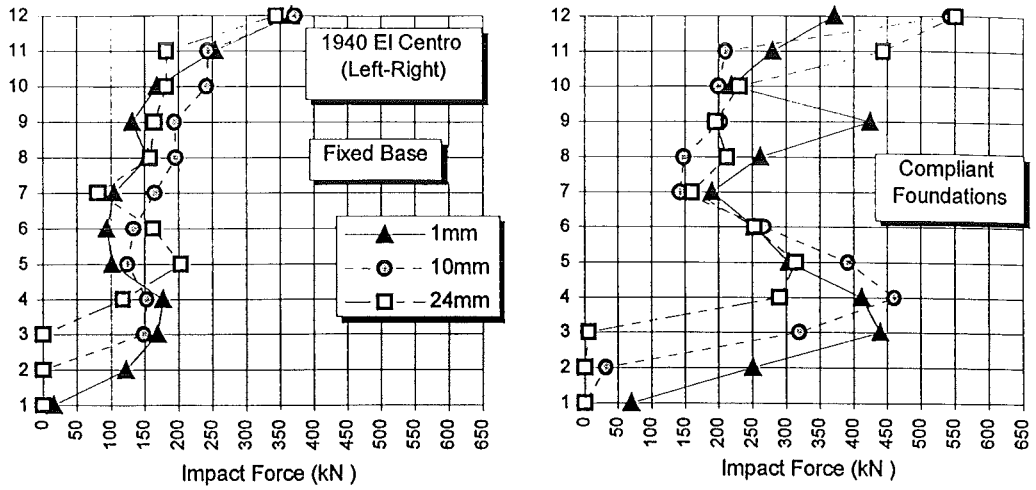

Fig. B.1: Maximum impact forces developed in Configuration 1 fixed base and compliant foundations cases for various separation gaps. 1940 El Centro earthquake applied left-right.

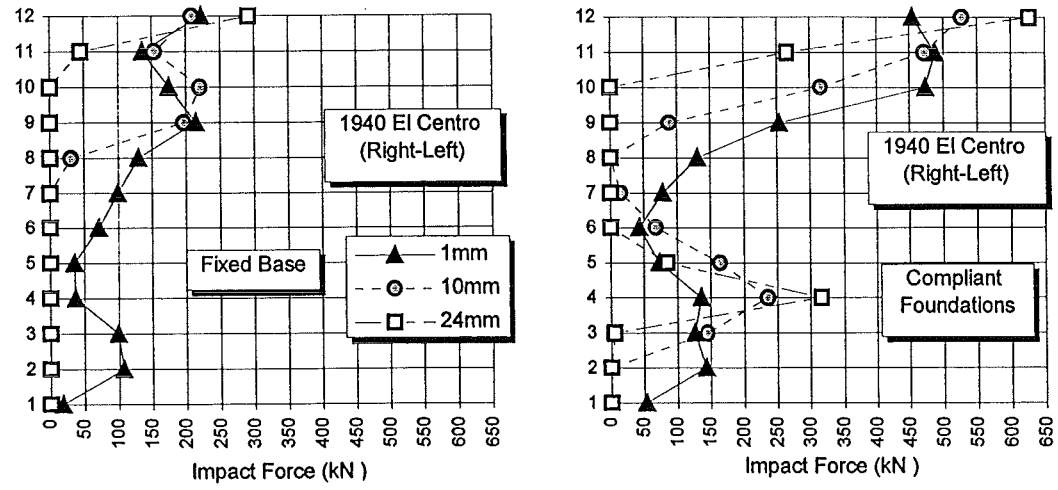

Fig. B.2: Maximum impact forces developed in Configuration 1 fixed base and compliant foundations cases for various separation gaps. 1940 El Centro earthquake applied right-left.

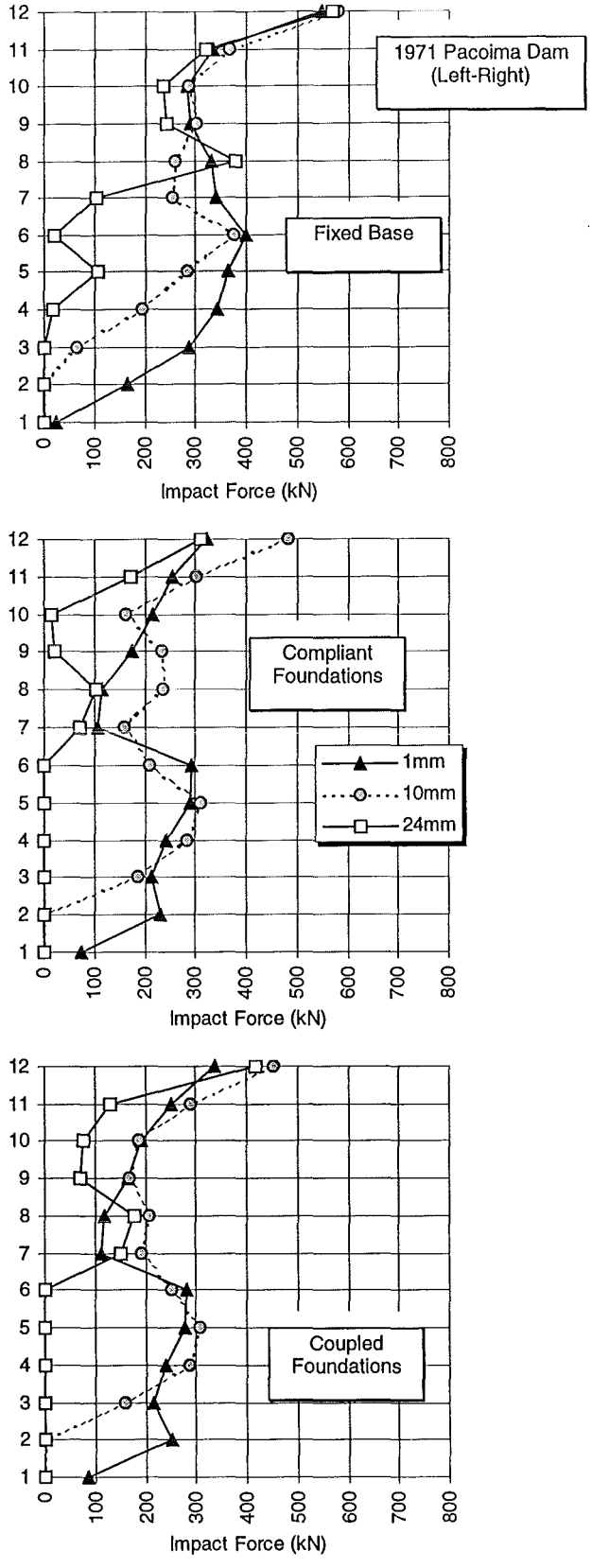

Fig. B.3: Maximum impact forces developed in Configuration 1 for various separation gaps and foundation fixity conditions. 1971 Pacoima Dam earthquake applied left-right.

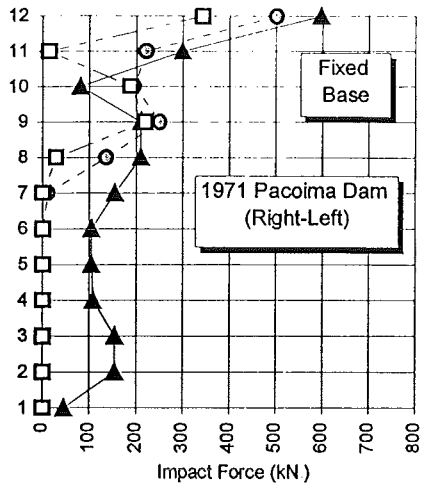

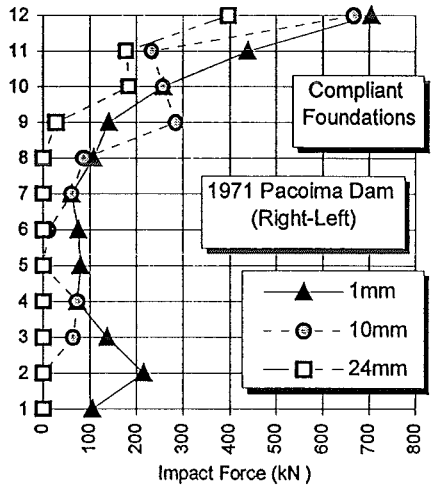

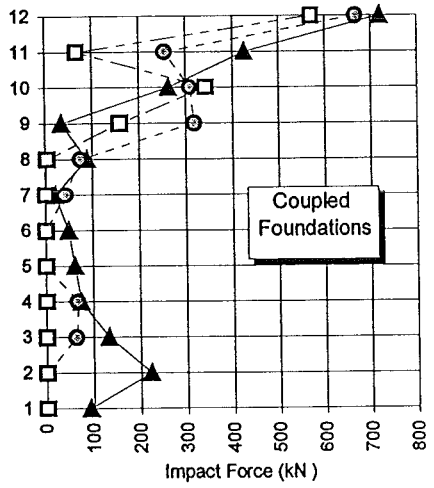

Fig. B.4: Maximum impact forces developed in Configuration 1 for various separation gaps and foundation fixity conditions. 1971 Pacoima Dam earthquake applied right-left.

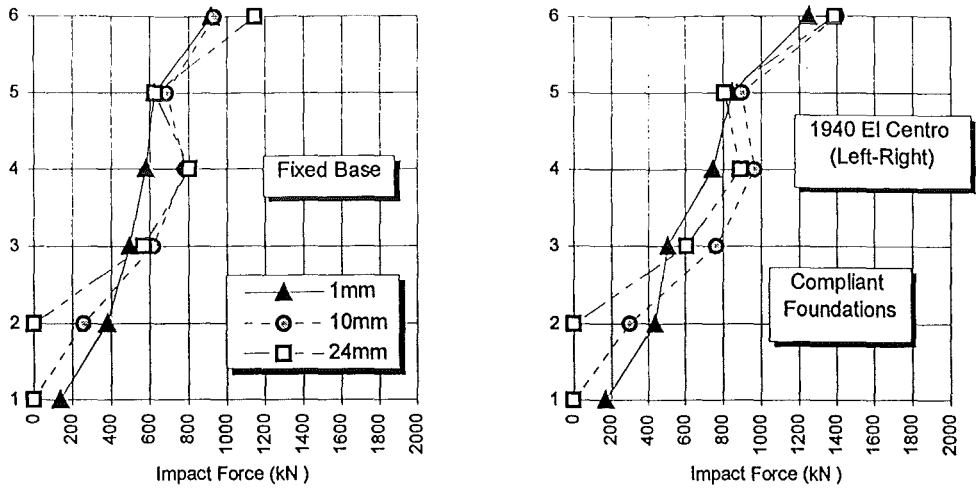

Fig. B.5: Maximum impact forces developed in Configuration 2 in fixed base and compliant foundation cases for various separation gaps. 1940 El Centro earthquake applied left-right.

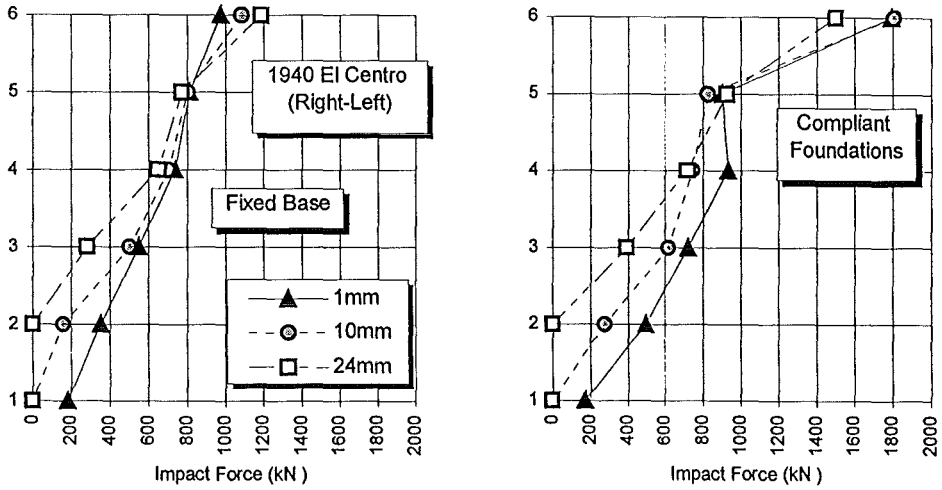

Fig. B.6: Maximum impact forces developed in Configuration 2 in fixed base and compliant foundation cases for various separation gaps. 1940 El Centro earthquake applied right-left.

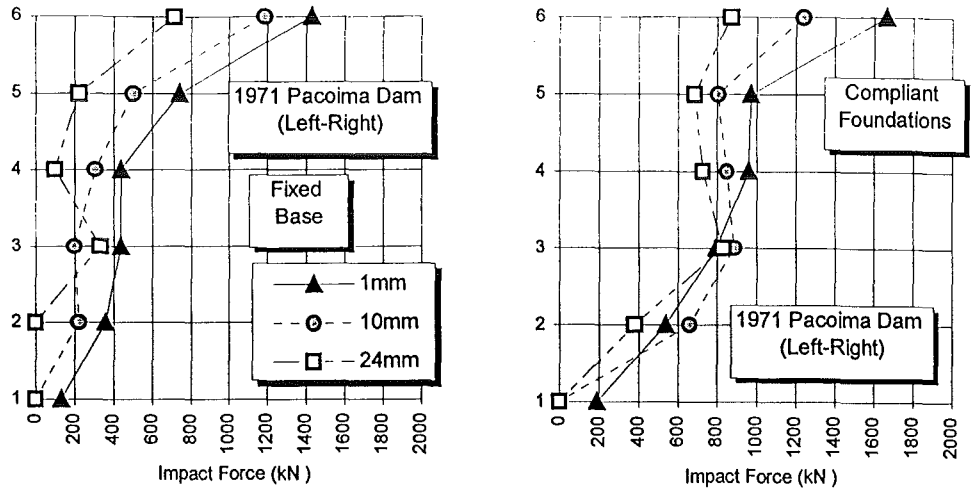

Fig. B.7: Maximum impact forces developed in Configuration 2 in fixed base and compliant foundation cases for various separation gaps. 1971 Pacoima Dam earthquake applied left-right.

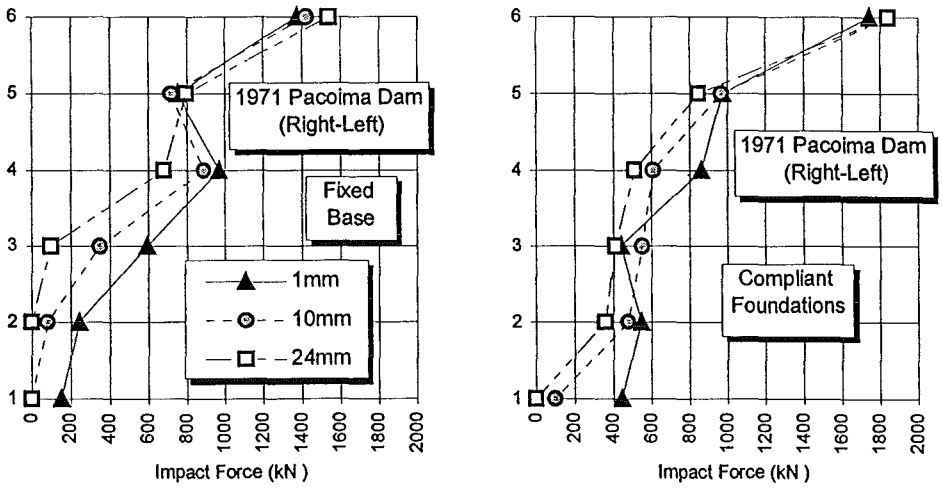

Fig. B.8: Maximum impact forces developed in Configuration 2 in fixed base and compliant foundation cases for various separation gaps. 1971 Pacoima Dam earthquake applied right-left.

APPENDIX C

RESPONSE OF RAHMAN FRAME

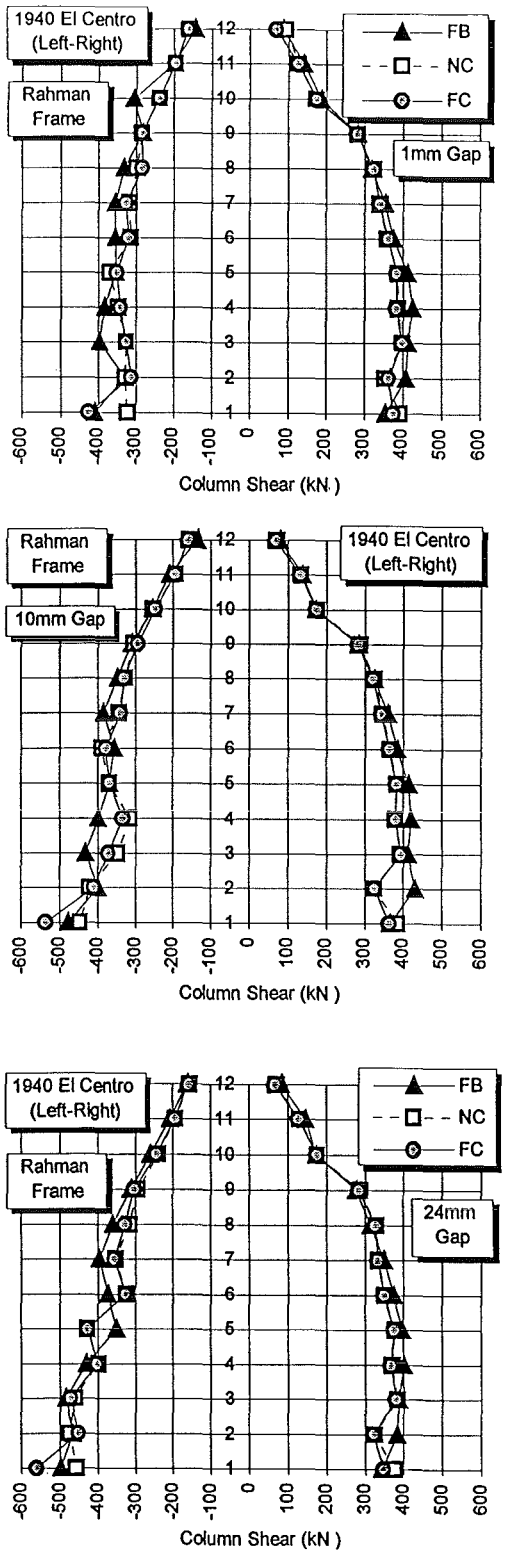

Fig. C.1: Effect of foundation fixity conditions on impact-side column shear of twelve-storey Rahman frame (Configuration 1) for various initial separation gaps. 1940 El Centro earthquake applied left-right.

FB = Fixed Base
NC = Non-Coupled (i.e. only soil-structure interaction considered)
FC = Foundations Coupled

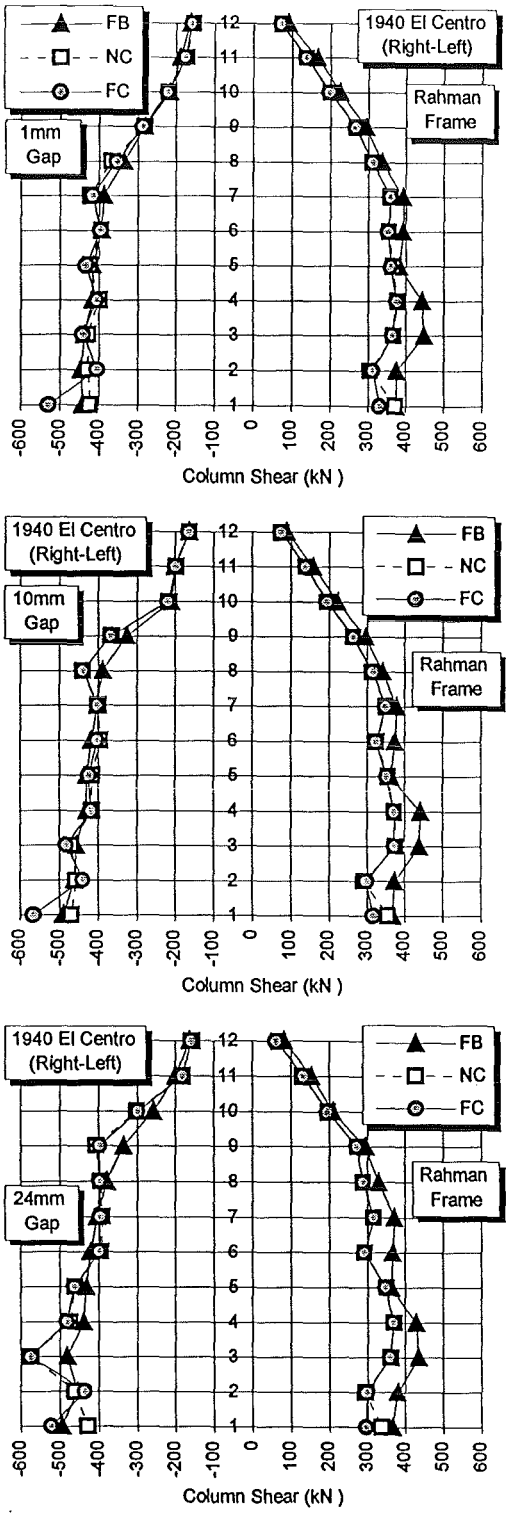

Fig. C.2: Effect of foundation fixity conditions on impact-side column shear of twelve-storey Rahman frame (Configuration 1) for various initial separation gaps. 1940 El Centro earthquake applied right-left.

FB = Fixed Base
NC = Non-Coupled (i.e. only soil-structure interaction considered)
FC = Foundations Coupled

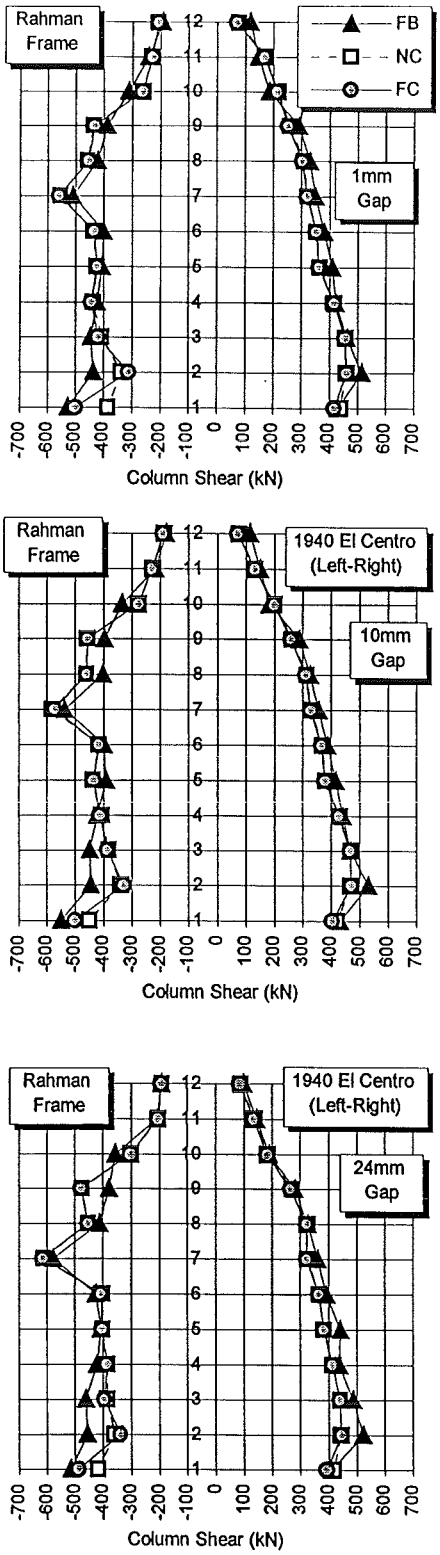

Fig. C.3: Effect of foundation fixity conditions on impact-side column shear of twelve-storey Rahman frame (Configuration 2) for various initial separation gaps. 1940 El Centro earthquake applied left-right.

FB = Fixed Base
NC = Non-Coupled (i.e. only soil-structure interaction considered)
FC = Foundations Coupled

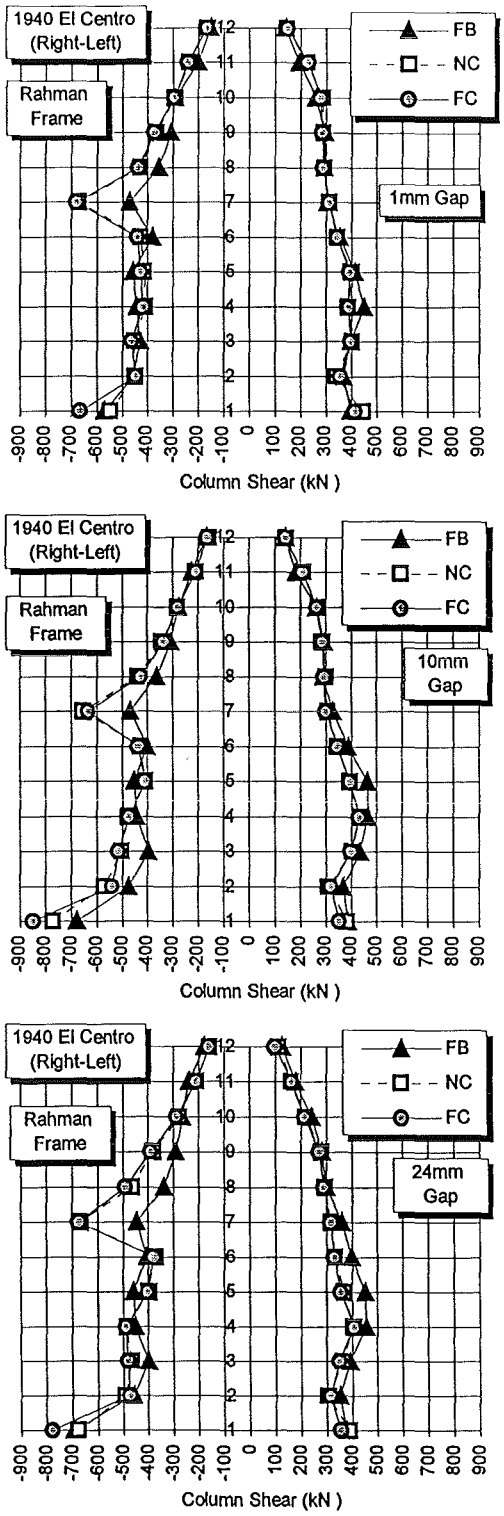

Fig. C.4: Effect of foundation fixity conditions on impact-side column shear of twelve-storey Rahman frame (Configuration 2) for various initial separation gaps. 1940 El Centro earthquake applied right-left.

FB = Fixed Base
NC = Non-Coupled (i.e. only soil-structure interaction considered)
FC = Foundations Coupled

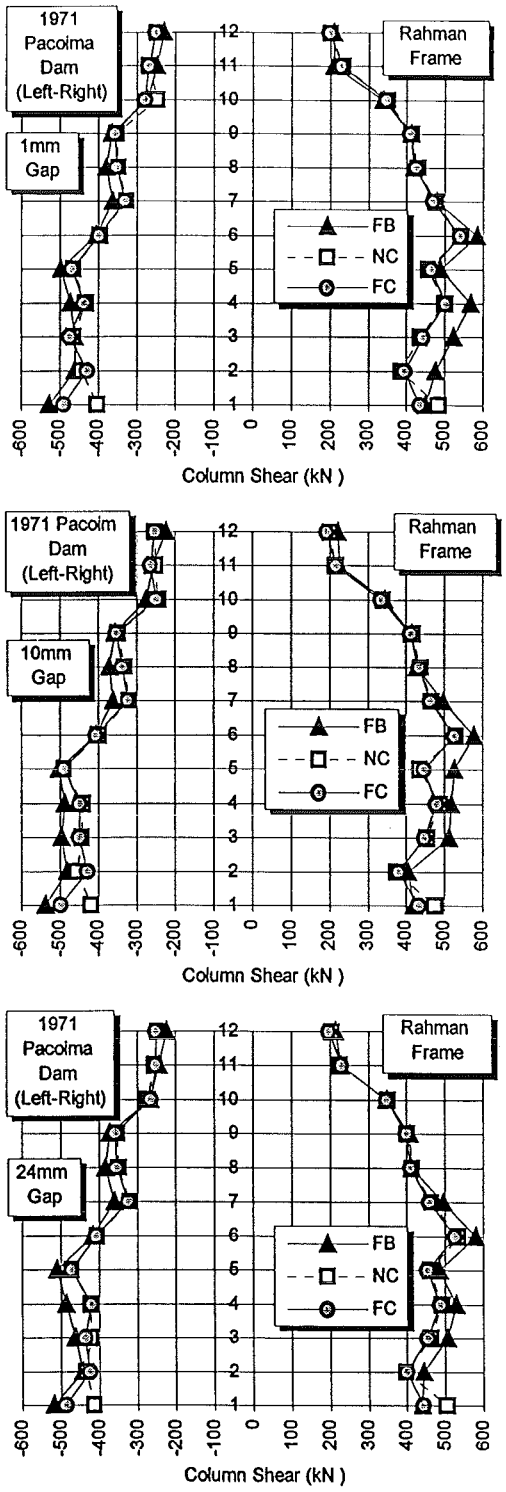

Fig. C.5: Effect of foundation fixity conditions on impact-side column shear of twelve-storey Rahman frame (Configuration 1) for various initial separation gaps. 1971 Pacoima Dam earthquake applied left-right.

FB = Fixed Base
NC = Non-Coupled (i.e. only soil-structure interaction considered)
FC = Foundations Coupled

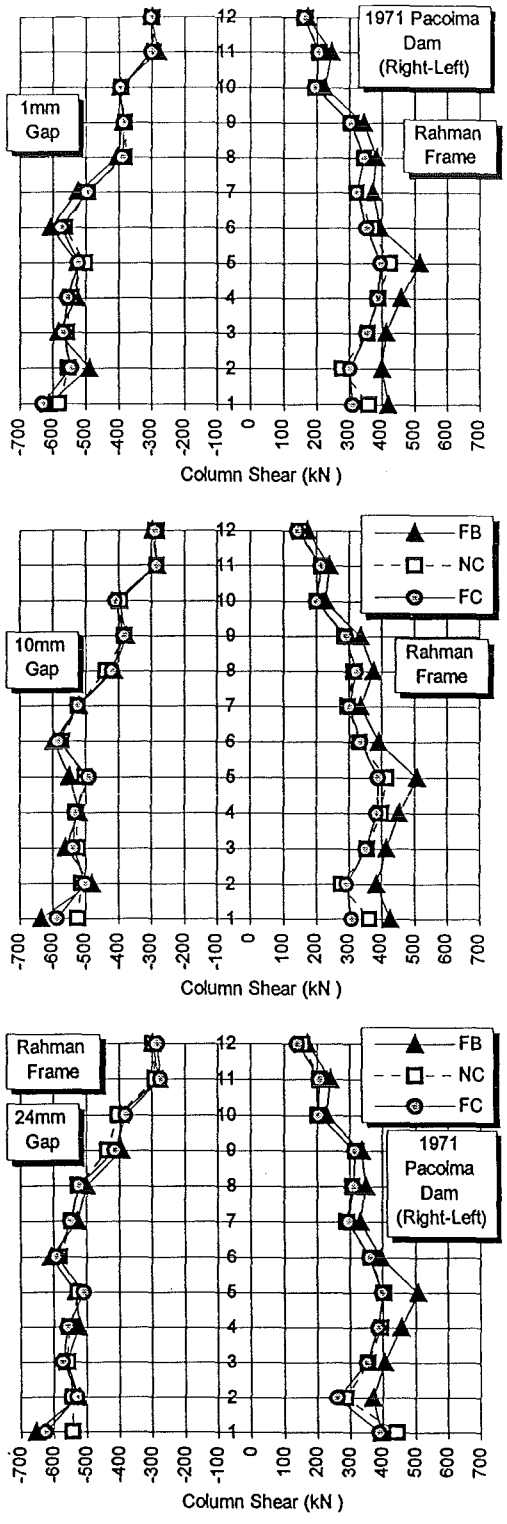

Fig. C.6: Effect of foundation fixity conditions on impact-side column shear of twelve-storey Rahman frame (Configuration 1) for various initial separation gaps. 1971 Pacoima Dam earthquake applied right-left.

FB = Fixed Base
NC = Non-Coupled (i.e. only soil-structure interaction considered)
FC = Foundations Coupled

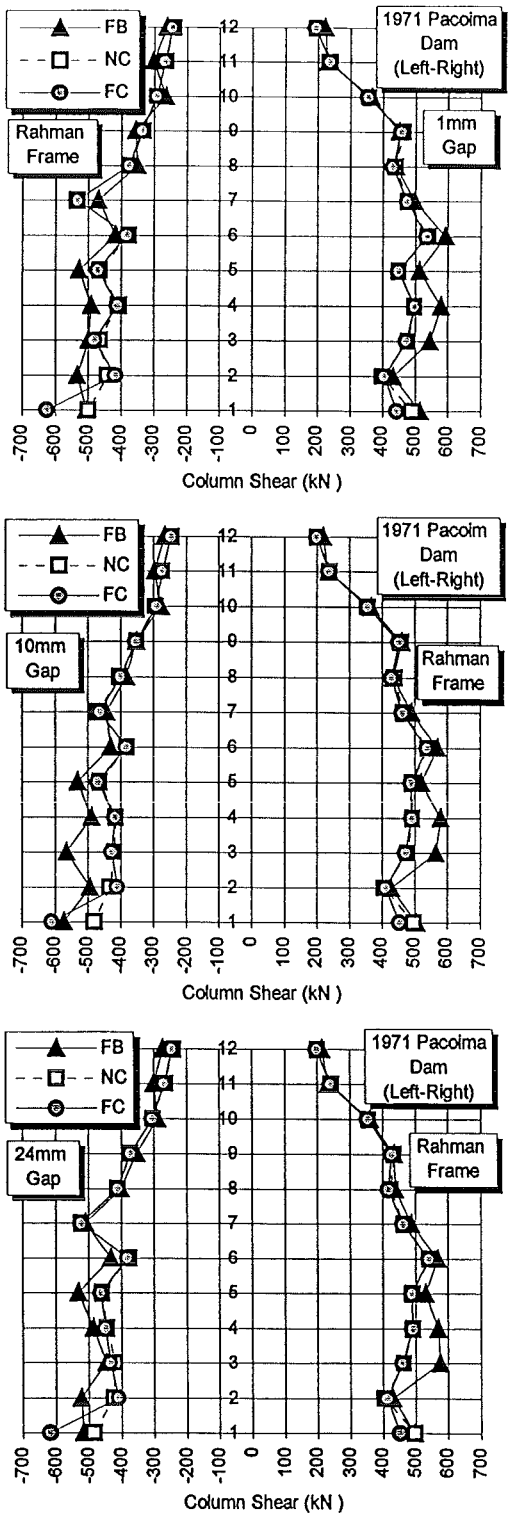

Fig. C.7: Effect of foundation fixity conditions on impact-side column shear of twelve-storey Rahman frame (Configuration 2) for various initial separation gaps. 1971 Pacoima Dam earthquake applied left-right.

FB = Fixed Base
NC = Non-Coupled (i.e. only soil-structure interaction considered)
FC = Foundations Coupled

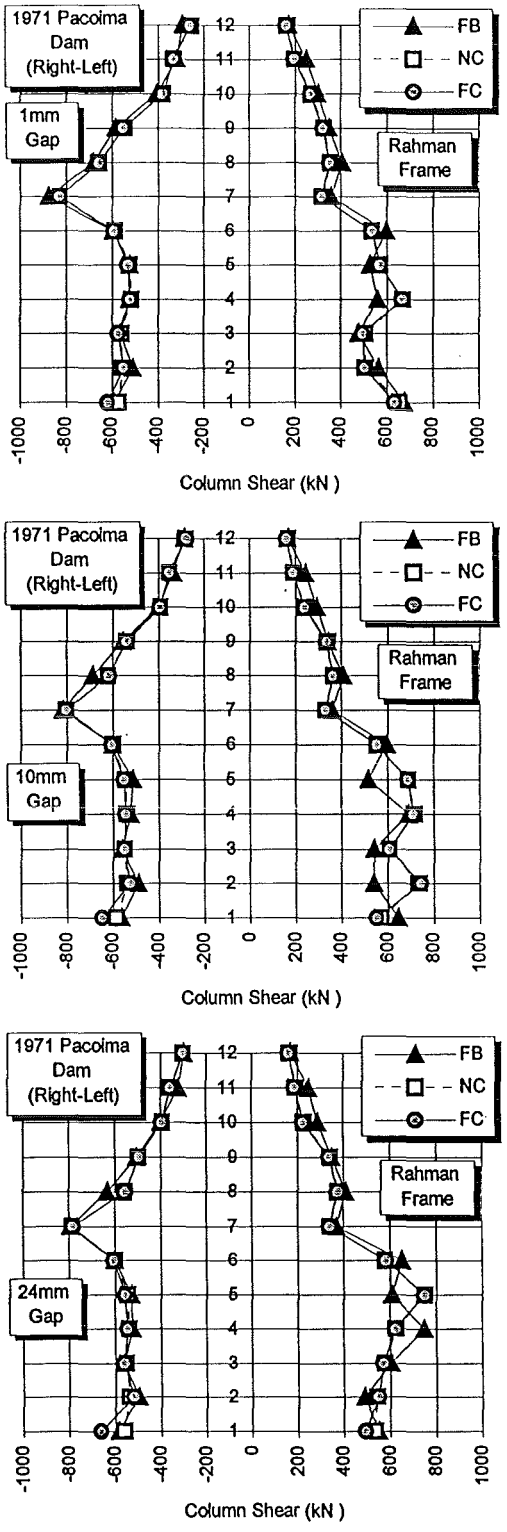

Fig. C.8: Effect of foundation fixity conditions on impact-side column shear of twelve-storey Rahman frame (Configuration 2) for various initial separation gaps. 1971 Pacoima Dam earthquake applied right-left.

FB = Fixed Base
NC = Non-Coupled (i.e. only soil-structure interaction considered)
FC = Foundations Coupled

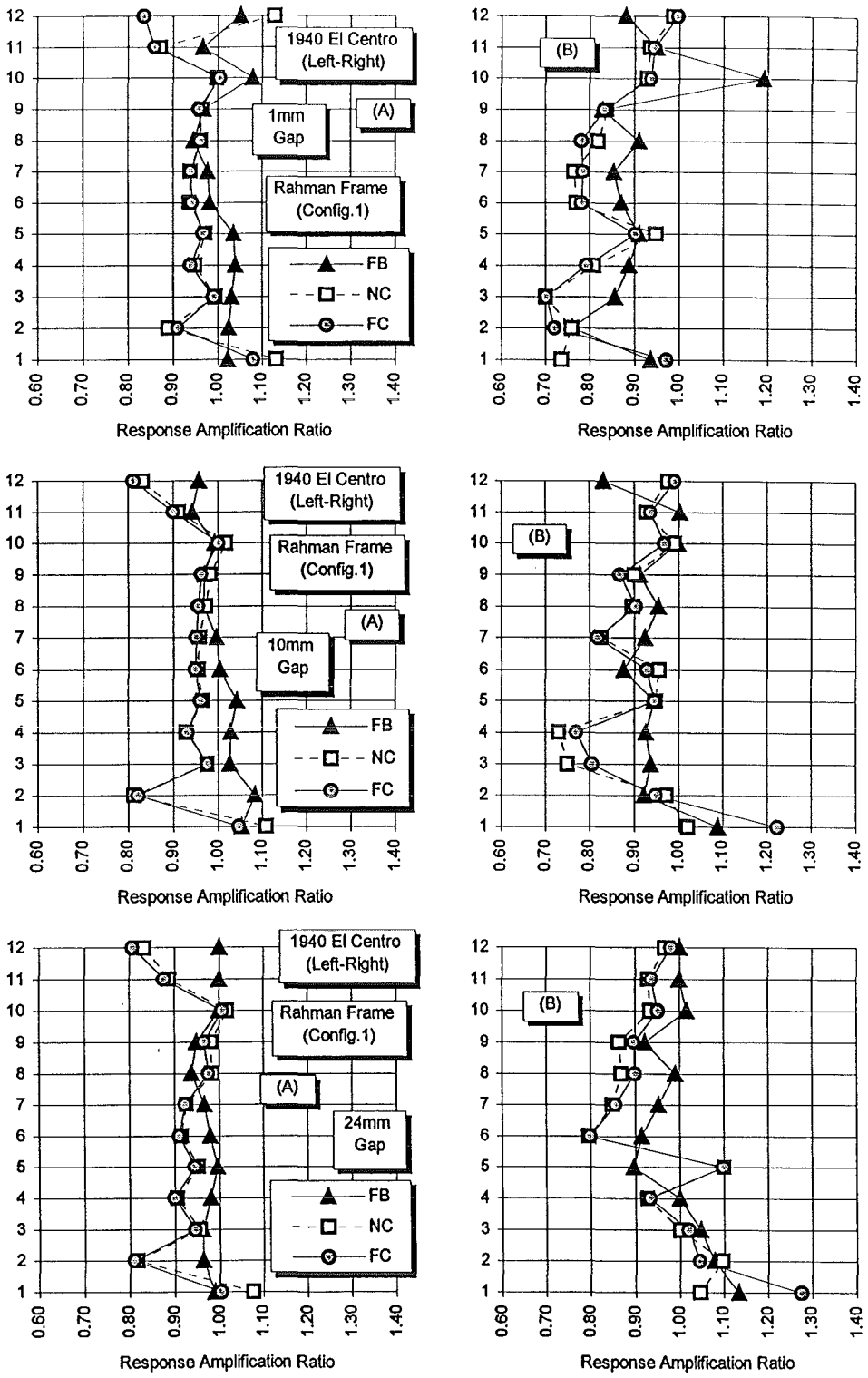

Fig. C.9: Response amplification ratio (from fixed base no pounding case) of impact-side column shear of twelve-storey Rahman frame (Configuration 1) for various initial separation gaps and foundation conditions. 1940 El Centro earthquake applied left-right.

A = Positive Shear B = Negative Shear
FB = Fixed Base
NC = Non-Coupled (i.e. only soil-structure interaction considered)
FC = Foundations Coupled

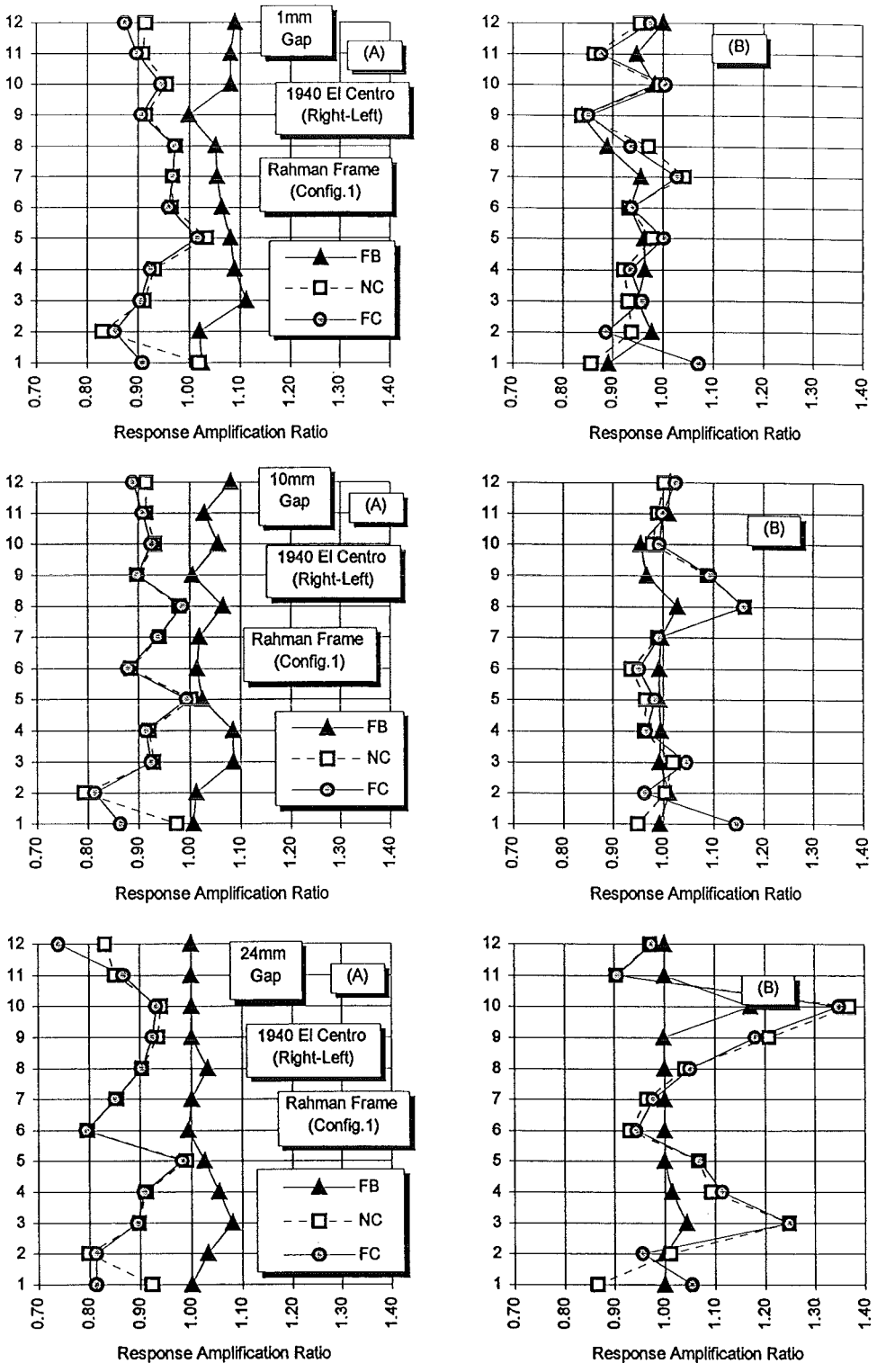

Fig. C.10: Response amplification ratio (from fixed base no pounding case) of impact-side column shear of twelve-storey Rahman frame (Configuration 1) for various initial separation gaps and foundation conditions. 1940 El Centro earthquake applied right-left.

A = Positive Shear B = Negative Shear
FB = Fixed Base
NC = Non-Coupled (i.e. only soil-structure interaction considered)
FC = Foundations Coupled

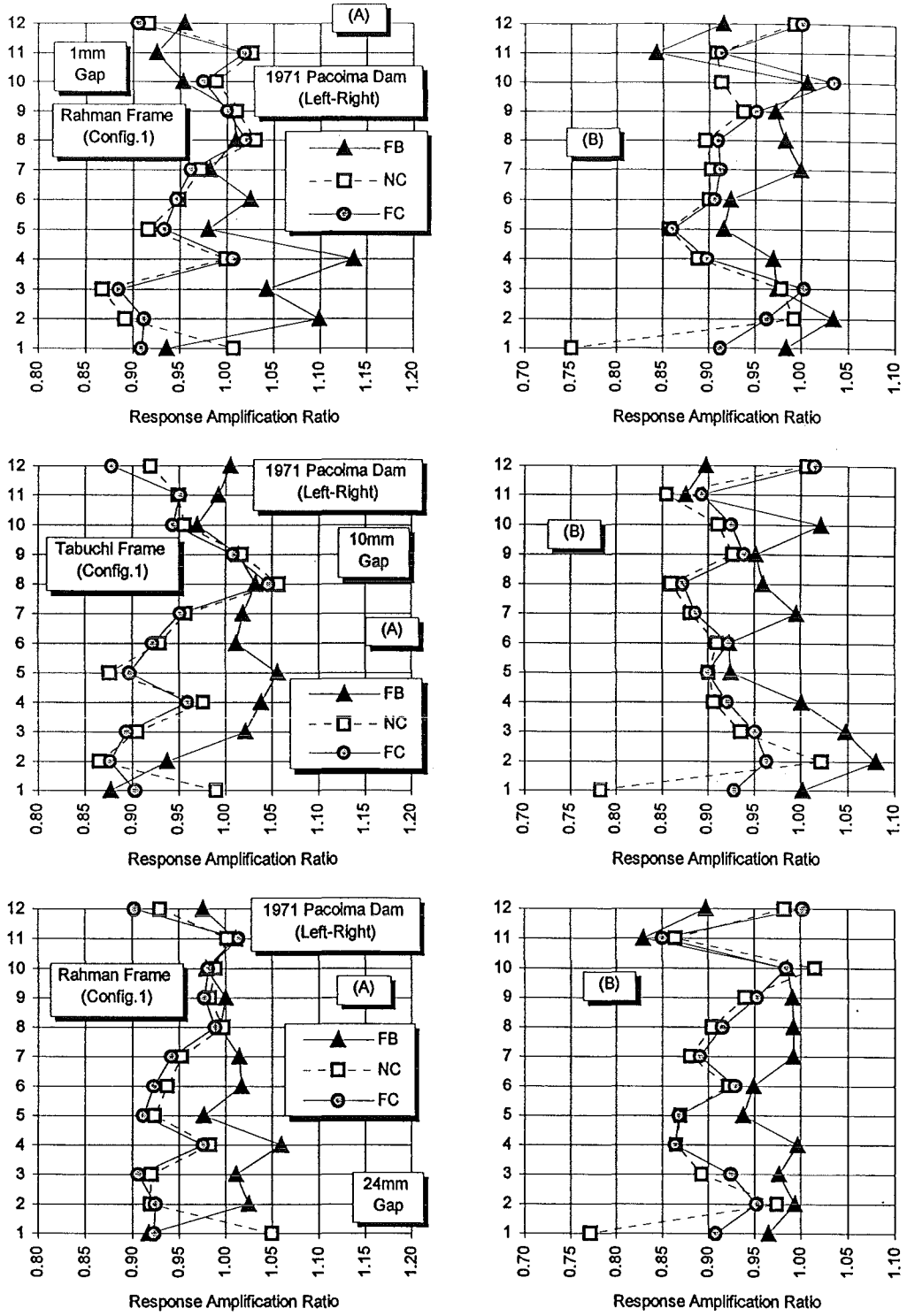

Fig. C.11: Response amplification ratio (from fixed base no pounding case) of impact-side column shear of twelve-storey Rahman frame (Configuration 1) for various initial separation gaps and foundation conditions. 1971 Pacoima Dam earthquake applied left-right.

A = Positive Shear B = Negative Shear
FB = Fixed Base
NC = Non-Coupled (i.e. only soil-structure interaction considered)
FC = Foundations Coupled

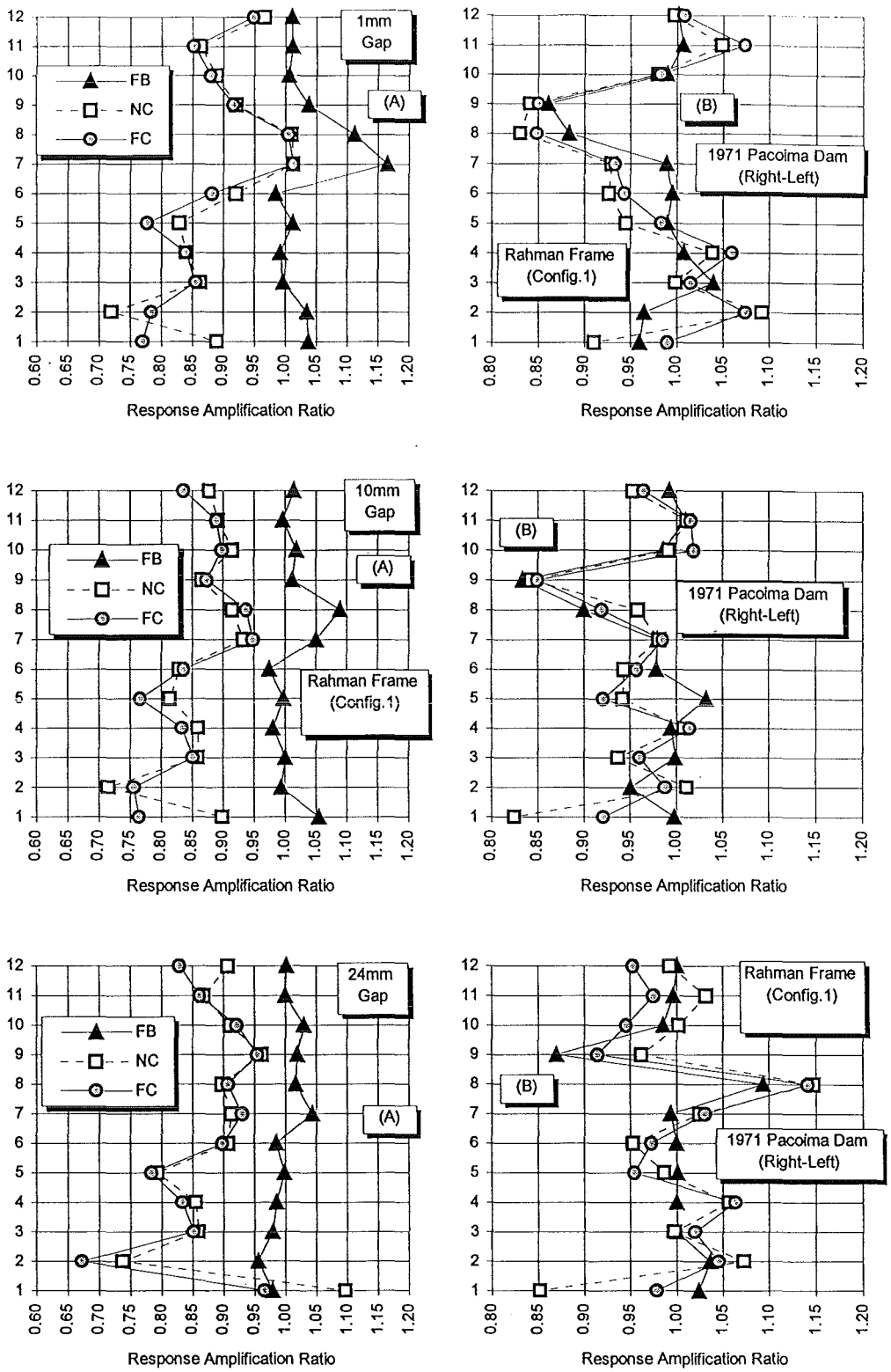

Fig. C.12: Response amplification ratio (from fixed base no pounding case) of impact-side column shear of twelve-storey Rahman frame (Configuration 1) for various initial separation gaps and foundation conditions. 1971 Pacoima Dam earthquake applied right-left.

A = Positive Shear B = Negative Shear
FB = Fixed Base
NC = Non-Coupled (i.e. only soil-structure interaction considered)
FC = Foundations Coupled

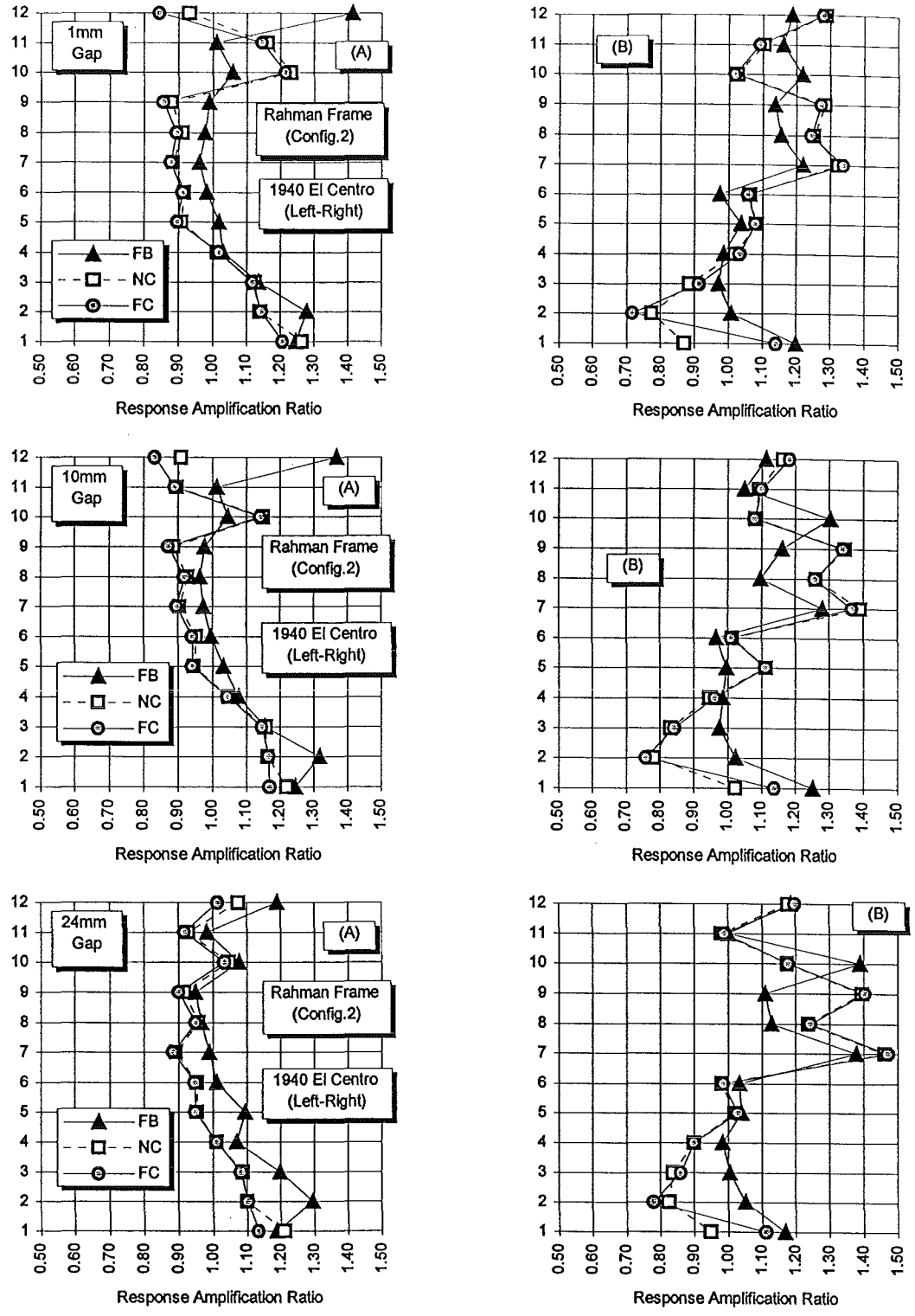

Fig. C.13: Response amplification ratio (from fixed base no pounding case) of impact-side column shear of twelve-storey Rahman frame (Configuration 2) for various initial separation gaps and foundation conditions. 1940 El Centro earthquake applied left-right.

A = Positive Shear B = Negative Shear
FB = Fixed Base
NC = Non-Coupled (i.e. only soil-structure interaction considered)
FC = Foundations Coupled

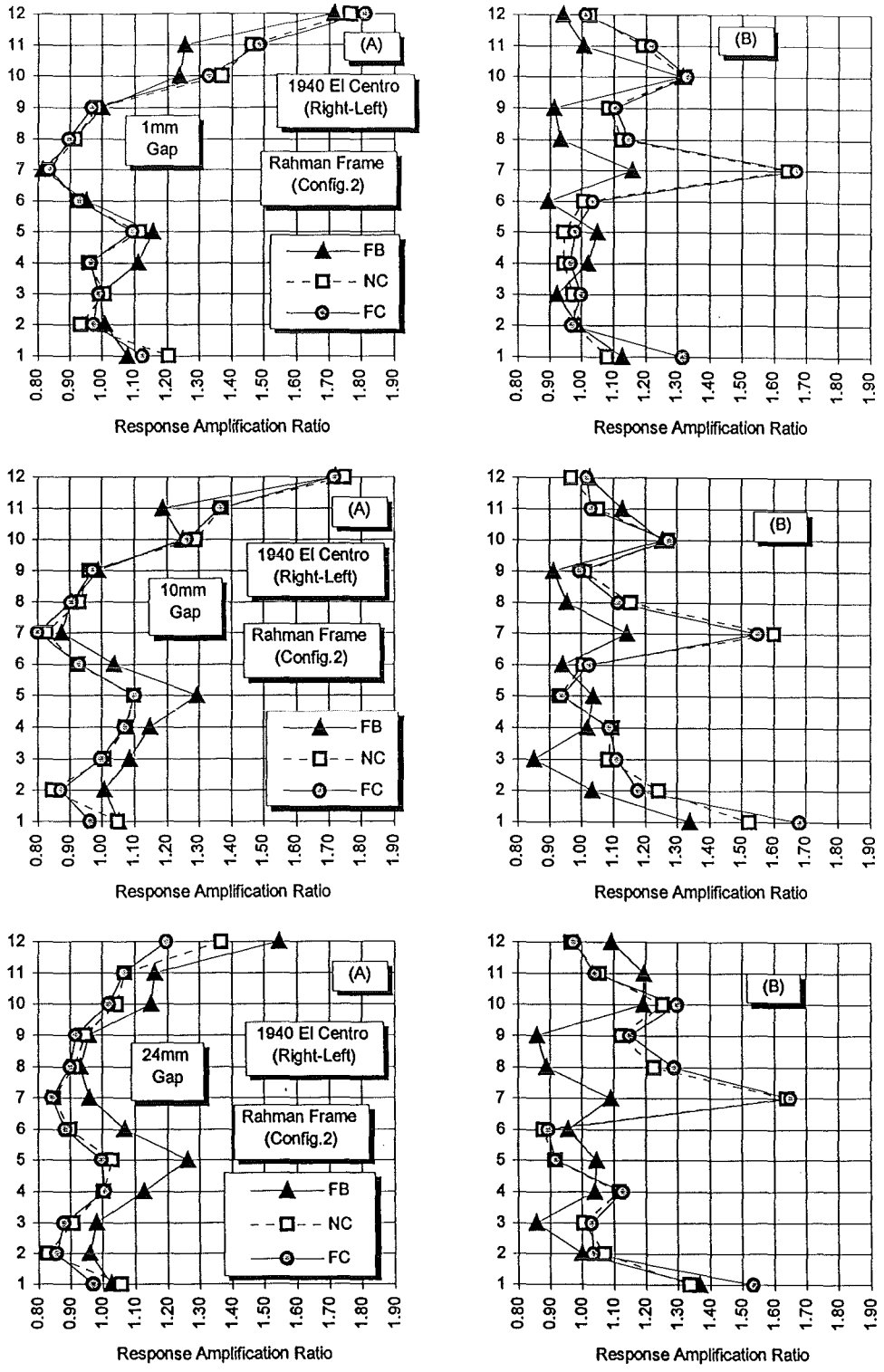

Fig. C.14: Response amplification ratio (from fixed base no pounding case) of impact-side column shear of twelve-storey Rahman frame (Configuration 2) for various initial separation gaps and foundation conditions. 1940 El Centro earthquake applied right-left.

A = Positive Shear B = Negative Shear
FB = Fixed Base
NC = Non-Coupled (i.e. only soil-structure interaction considered)
FC = Foundations Coupled

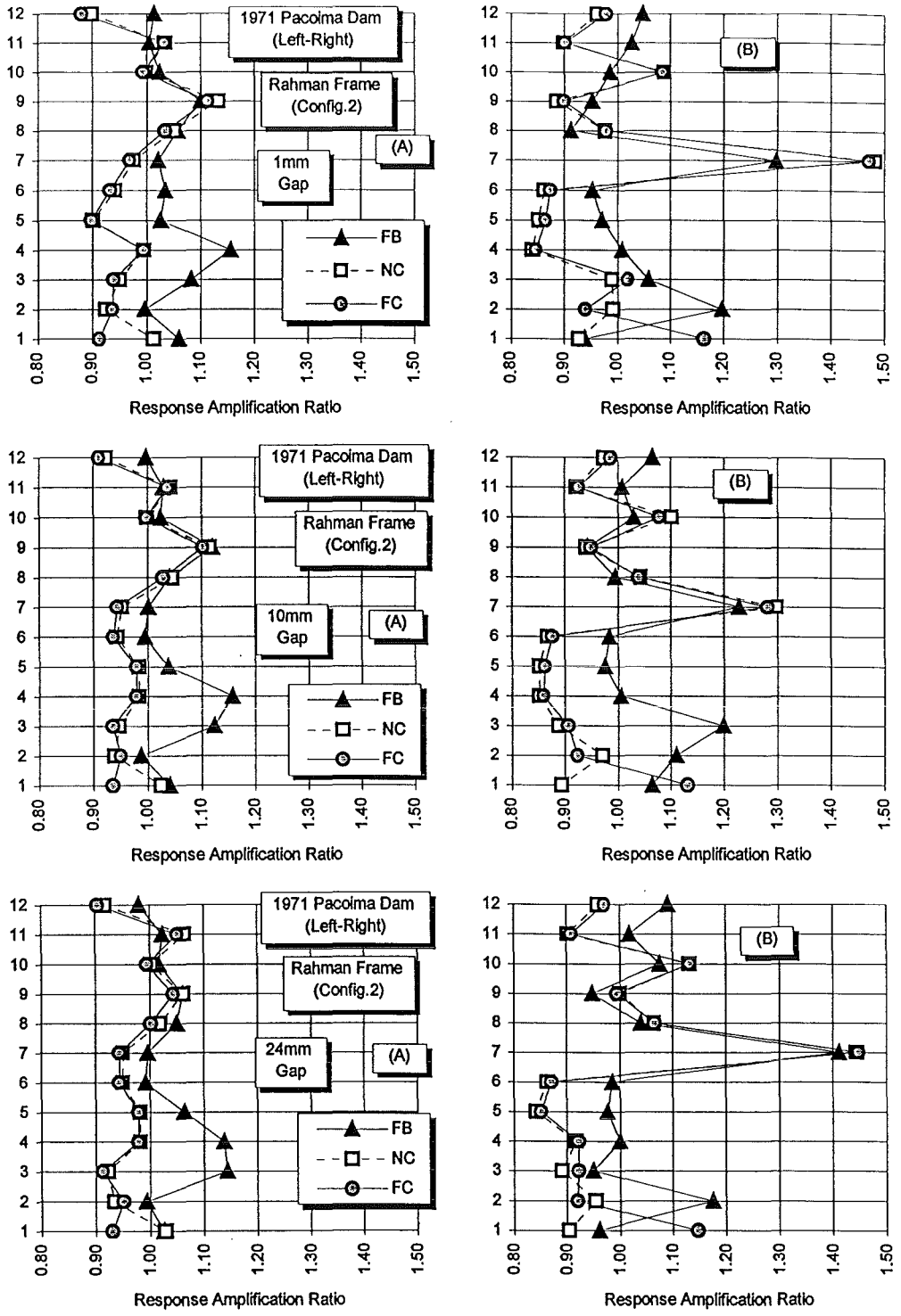

Fig. C.15: Response amplification ratio (from fixed base no pounding case) of impact-side column shear of twelve-storey Rahman frame (Configuration 2) for various initial separation gaps and foundation conditions. 1971 Pacoima Dam earthquake applied left-right.

A = Positive Shear B = Negative Shear
FB = Fixed Base
NC = Non-Coupled (i.e. only soil-structure interaction considered)
FC = Foundations Coupled

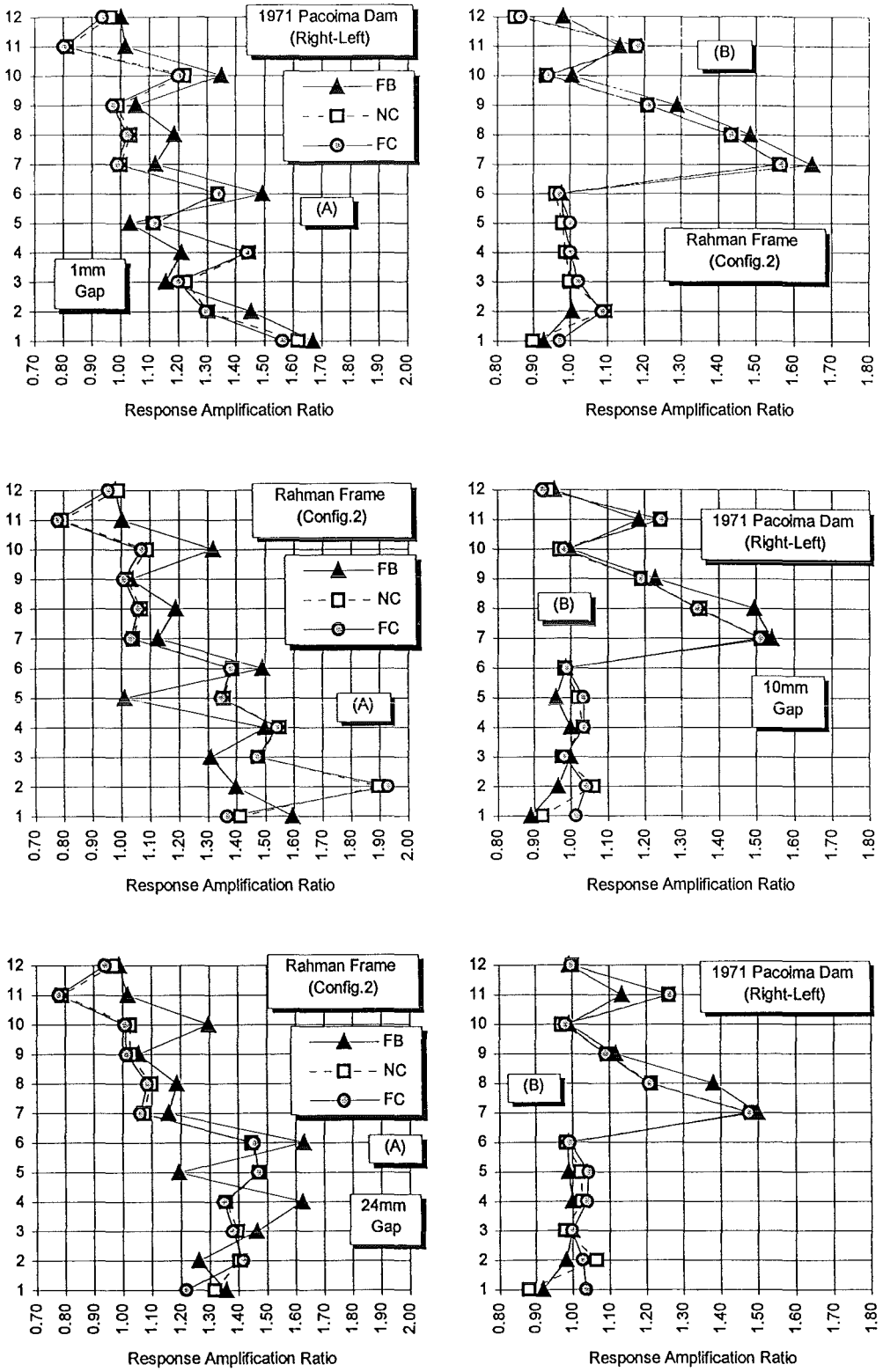

Fig. C.16: Response amplification ratio (from fixed base no pounding case) of impact-side column shear of twelve-storey Rahman frame (Configuration 2) for various initial separation gaps and foundation conditions. 1971 Pacoima Dam earthquake applied right-left.

A = Positive Shear B = Negative Shear
FB = Fixed Base
NC = Non-Coupled (i.e. only soil-structure interaction considered)
FC = Foundations Coupled

APPENDIX D

RESPONSE OF TABUCHI FRAME

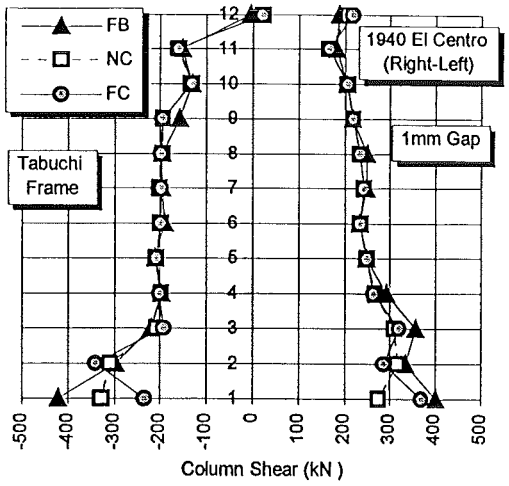

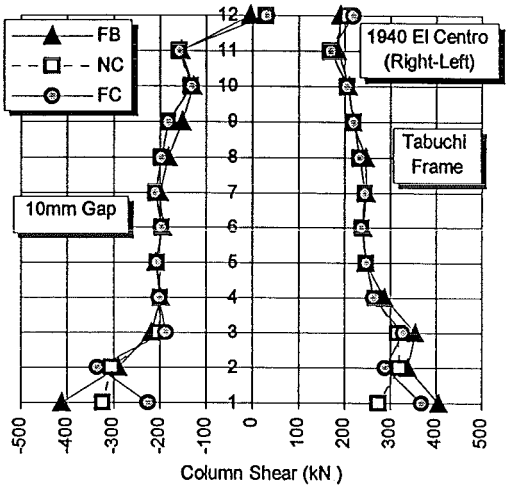

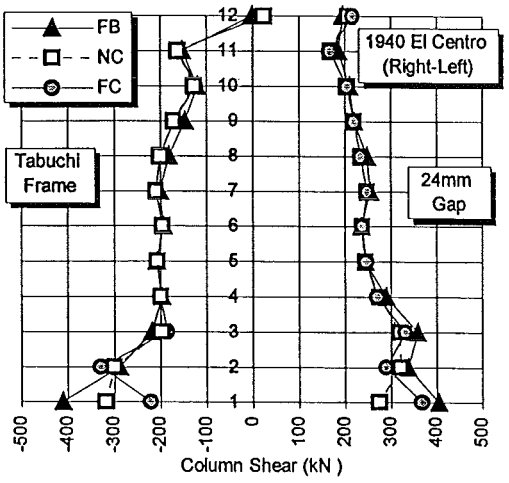

Fig. D.1: Effect of foundation fixity conditions on impact-side column shear of twelve-storey Tabuchi frame (Configuration 1) for various initial separation gaps. 1940 El Centro earthquake applied right-left.

FB = Fixed Base
NC = Non-Coupled (i.e. only soil-structure interaction considered)
FC = Foundations Coupled

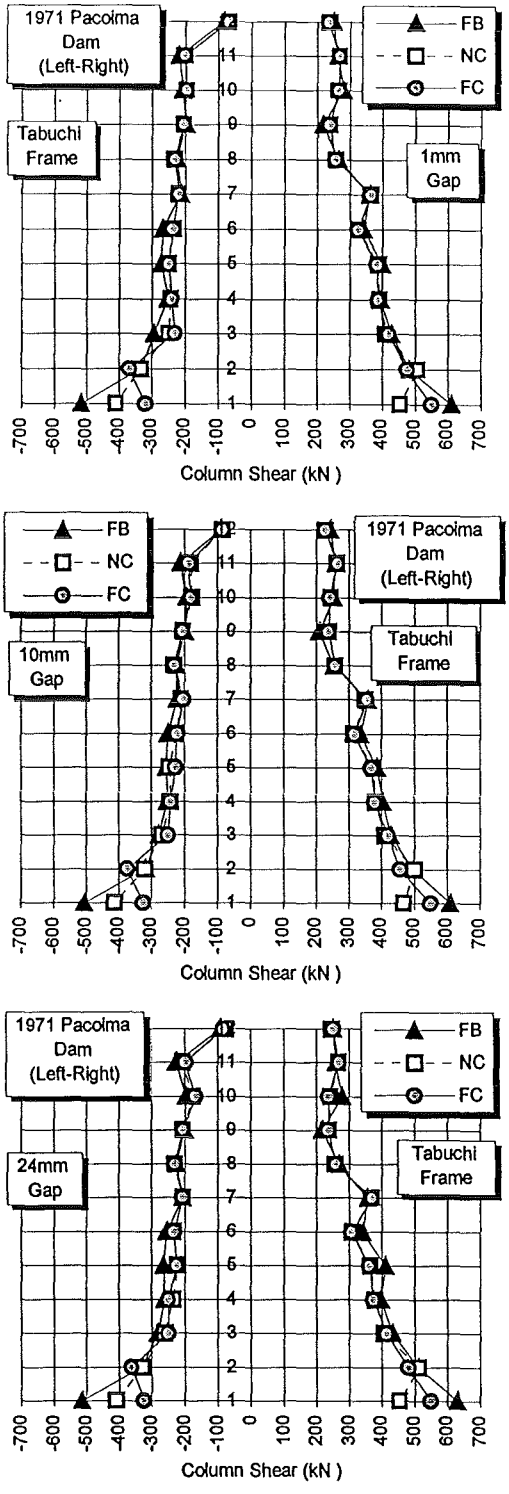

Fig. D.2: Effect of foundation fixity conditions on impact-side column shear of twelve-storey Tabuchi frame (Configuration 1) for various initial separation gaps. 1971 Pacoima Dam earthquake applied left-right.

FB = Fixed Base
NC = Non-Coupled (i.e. only soil-structure interaction considered)
FC = Foundations Coupled

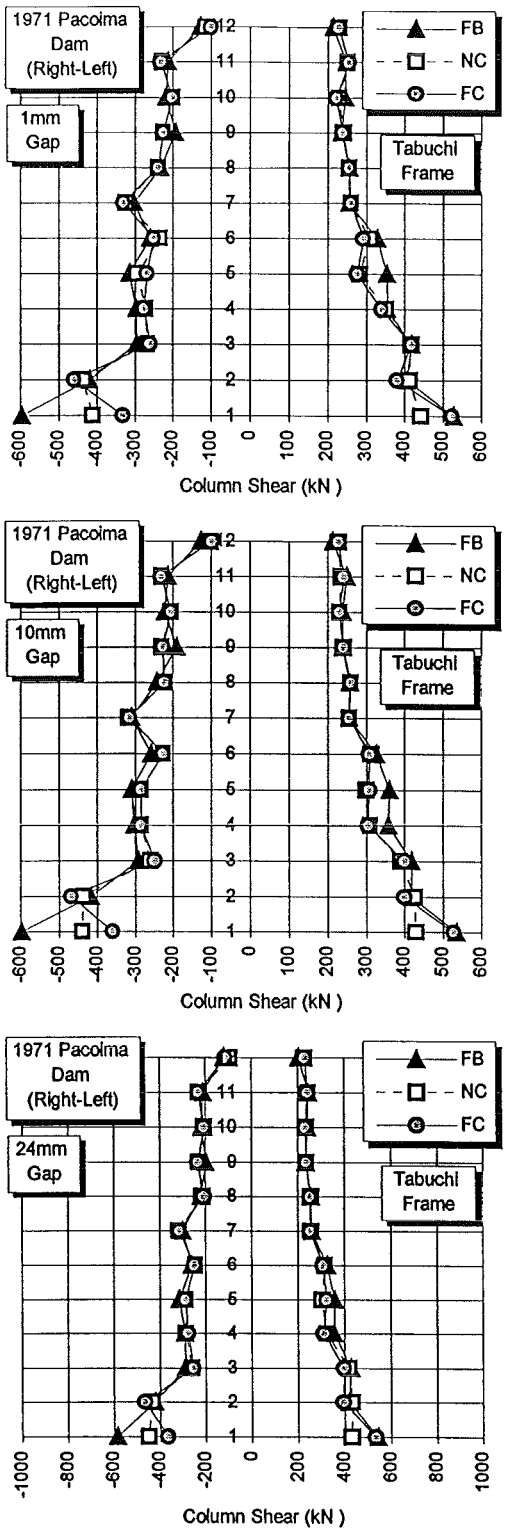

Fig. D.3: Effect of foundation fixity conditions on impact-side column shear of twelve-storey Tabuchi frame (Configuration 1) for various initial separation gaps. 1971 Pacoima Dam earthquake applied right-left.

FB = Fixed Base
NC = Non-Coupled (i.e. only soil-structure interaction considered)
FC = Foundations Coupled

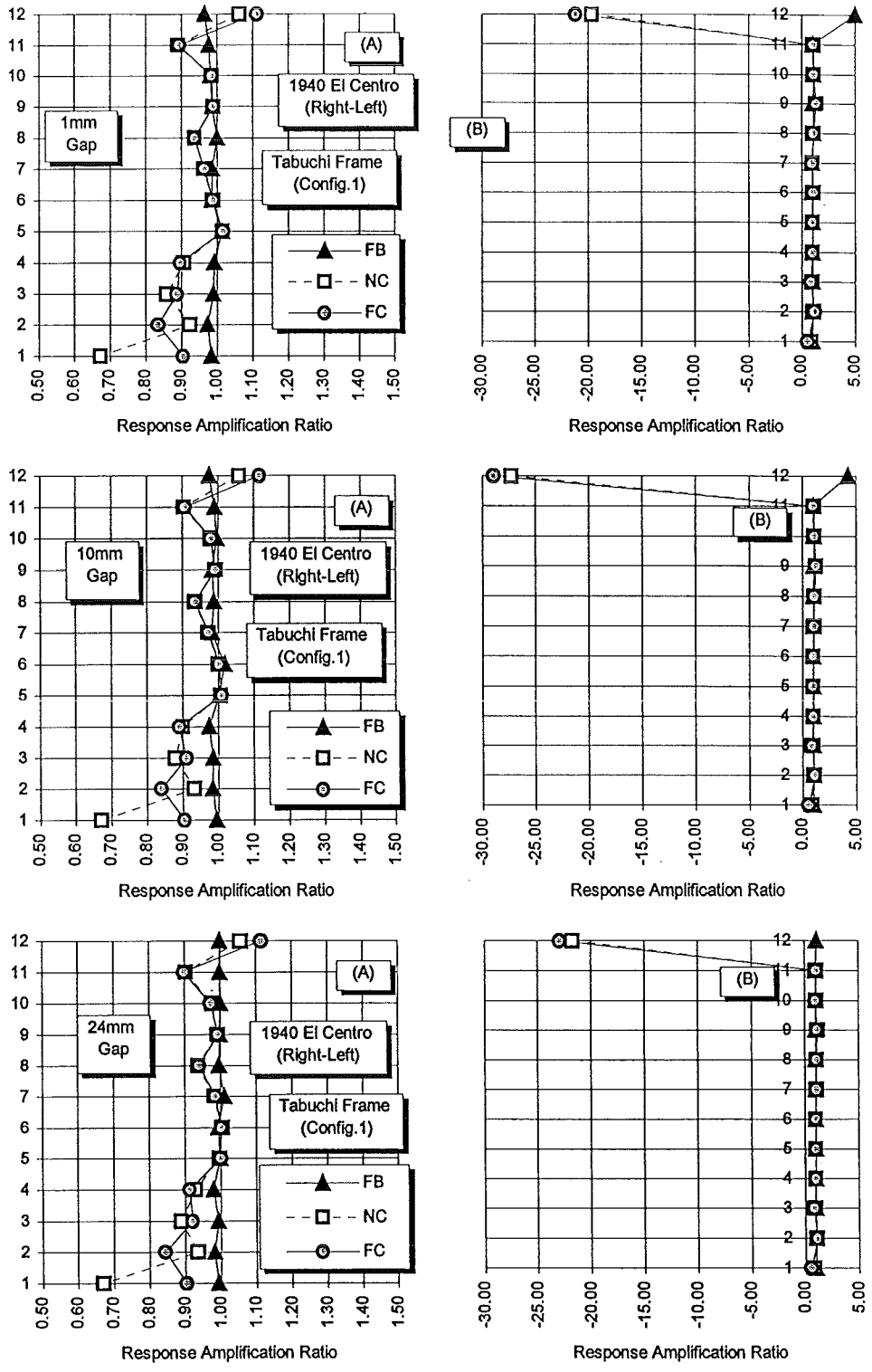

Fig. D.4: Response amplification ratio (from fixed base no pounding case) of impact-side column shear of twelve-storey Tabuchi frame (Configuration 1) for various initial separation gaps and foundation conditions. 1940 El Centro earthquake applied right-left.

A = Positive Shear B = Negative Shear
FB = Fixed Base
NC = Non-Coupled (i.e. only soil-structure interaction considered)
FC = Foundations Coupled

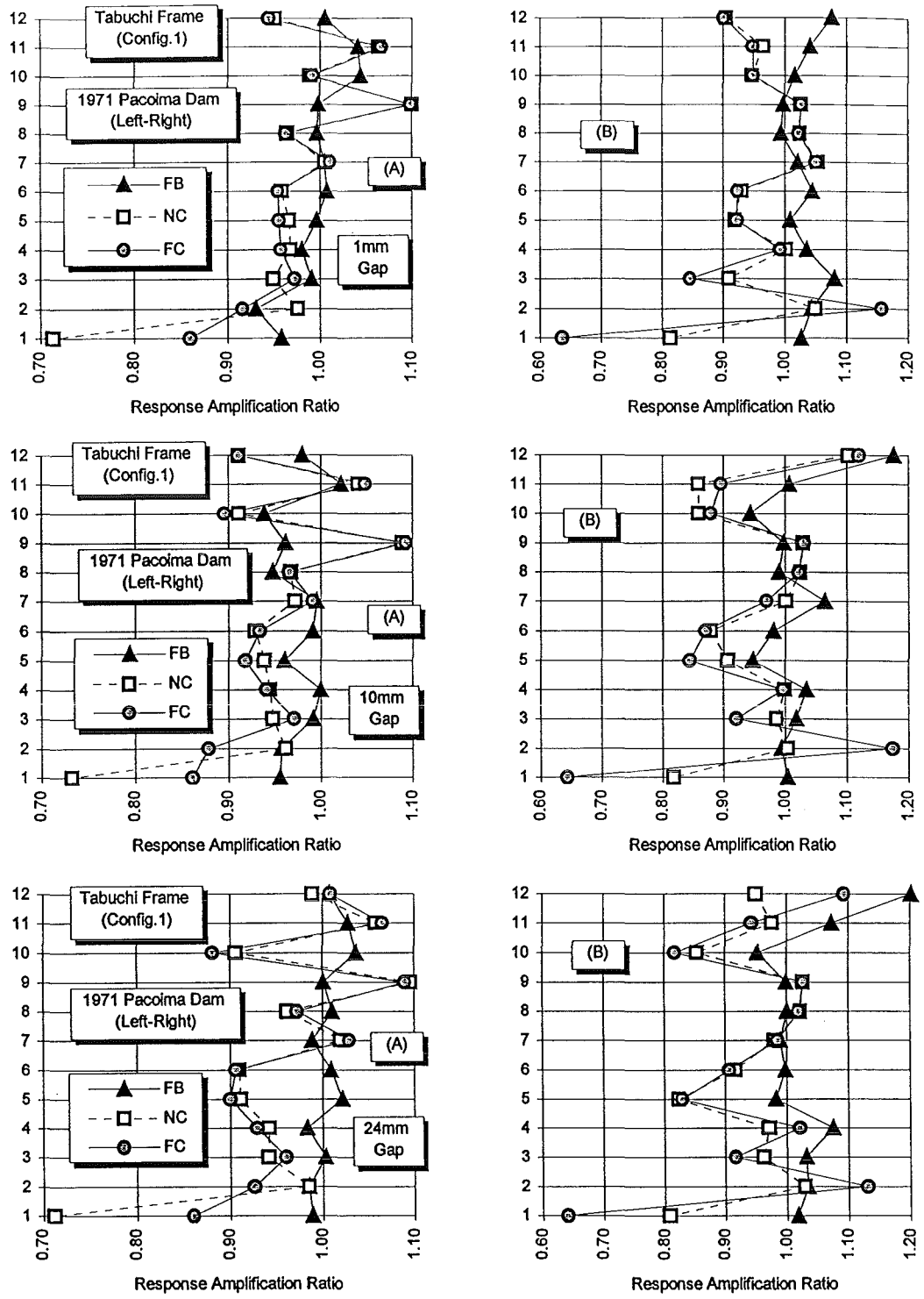

Fig. D.5: Response amplification ratio (from fixed base no pounding case) of impact-side column shear of twelve-storey Tabuchi frame (Configuration 1) for various initial separation gaps and foundation conditions. 1971 Pacoima Dam earthquake applied left-right.

A = Positive Shear B = Negative Shear
FB = Fixed Base
NC = Non-Coupled (i.e. only soil-structure interaction considered)
FC = Foundations Coupled

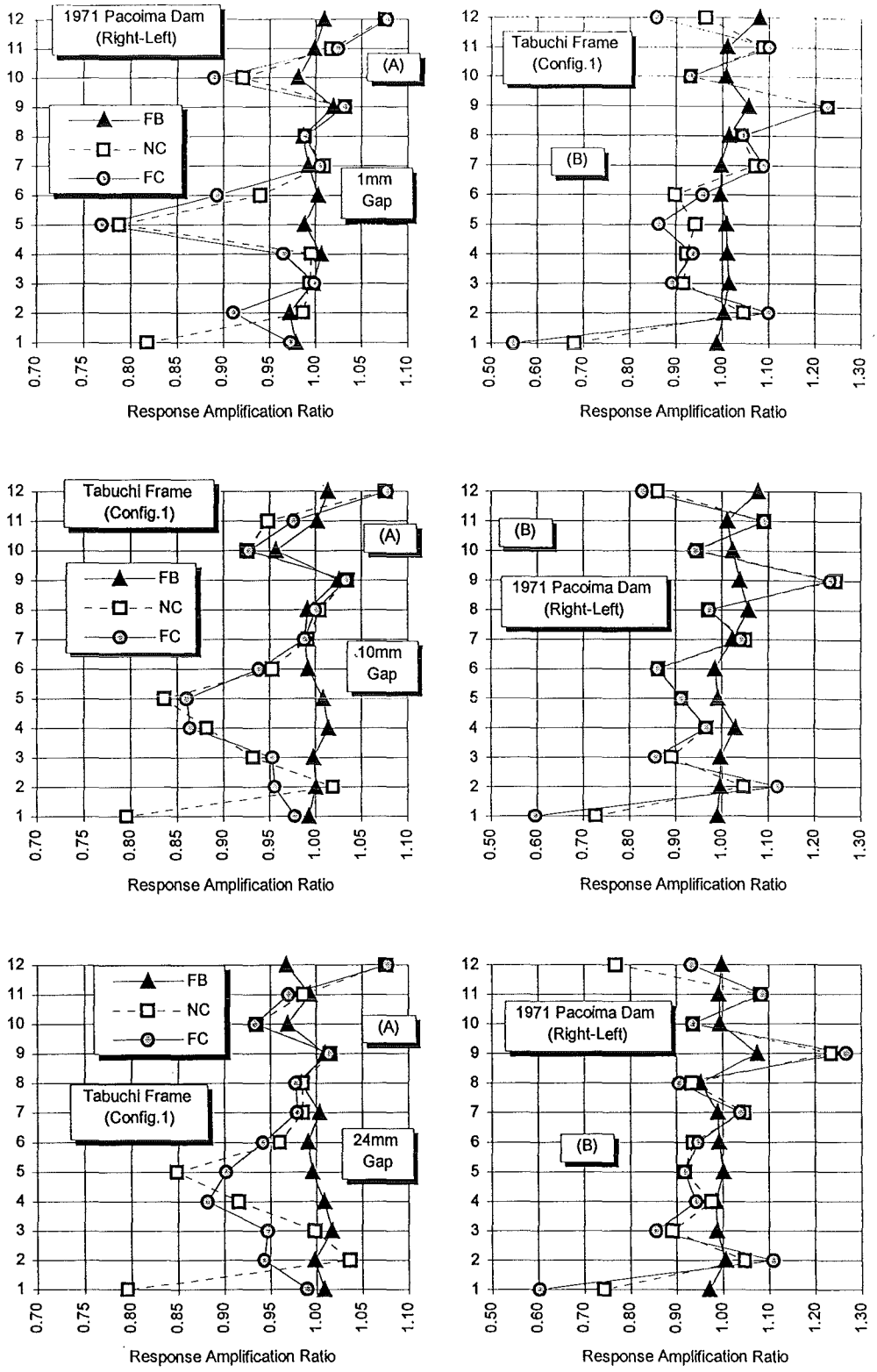

Fig. D.6: Response amplification ratio (from fixed base no pounding case) of impact-side column shear of twelve-storey Tabuchi frame (Configuration 1) for various initial separation gaps and foundation conditions. 1971 Pacoima Dam earthquake applied right-left.

A = Positive Shear B = Negative Shear
FB = Fixed Base
NC = Non-Coupled (i.e. only soil-structure interaction considered)
FC = Foundations Coupled

APPENDIX E

RESPONSE OF JURY FRAME

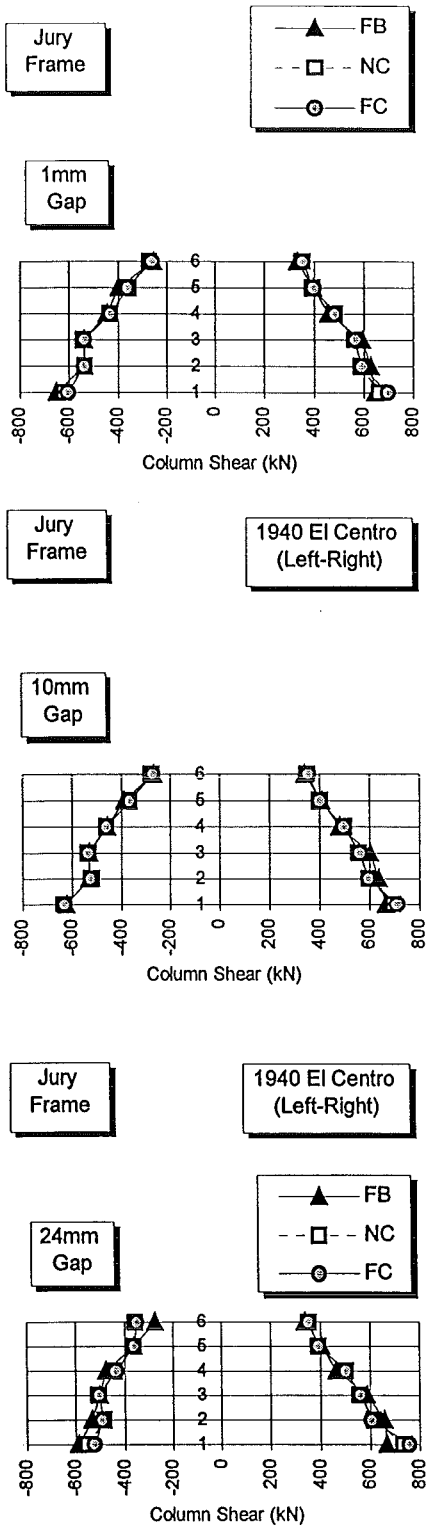

Fig. E.1: Effect of foundation fixity conditions on impact-side column shear of six-storey Jury frame (Configuration 2) for various initial separation gaps. 1940 El Centro earthquake applied left-right.

FB = Fixed Base
NC = Non-Coupled (i.e. only soil-structure interaction considered)
FC = Foundations Coupled

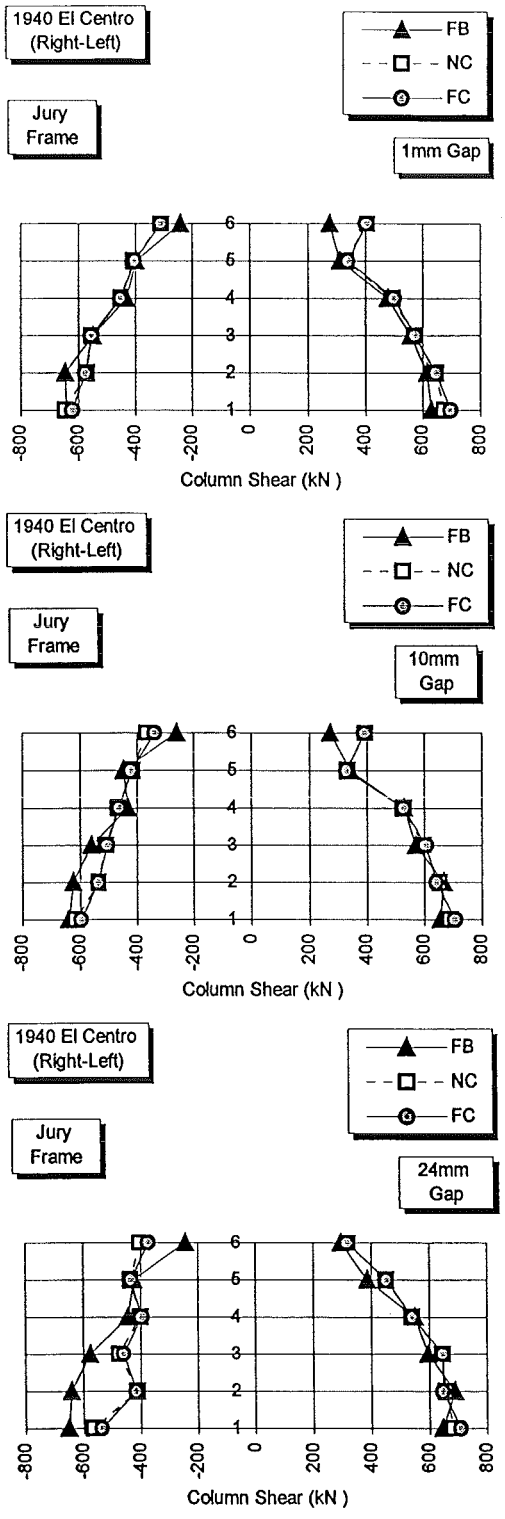

Fig. E.2: Effect of foundation fixity conditions on impact-side column shear of six-storey Jury frame (Configuration 2) for various initial separation gaps. 1940 El Centro earthquake applied right-left.

FB = Fixed Base
NC = Non-Coupled (i.e. only soil-structure interaction considered)
FC = Foundations Coupled

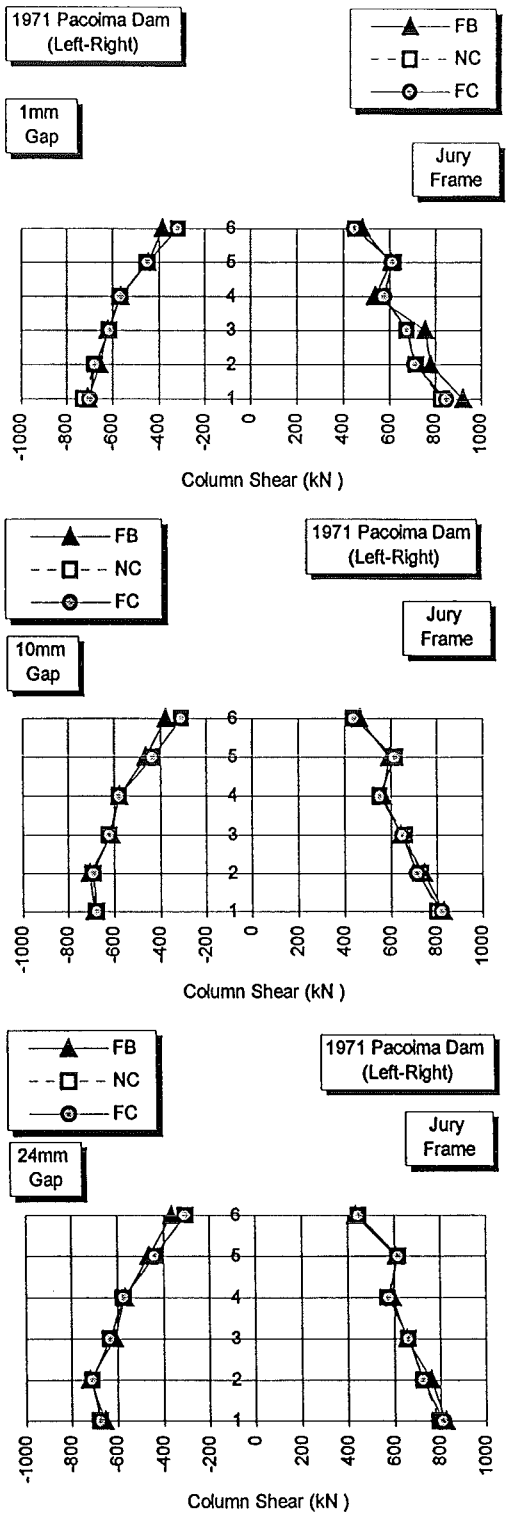

Fig. E.3: Effect of foundation fixity conditions on impact-side column shear of six-storey Jury frame (Configuration 2) for various initial separation gaps. 1971 Pacoima Dam earthquake applied left-right.

FB = Fixed Base
NC = Non-Coupled (i.e. only soil-structure interaction considered)
FC = Foundations Coupled

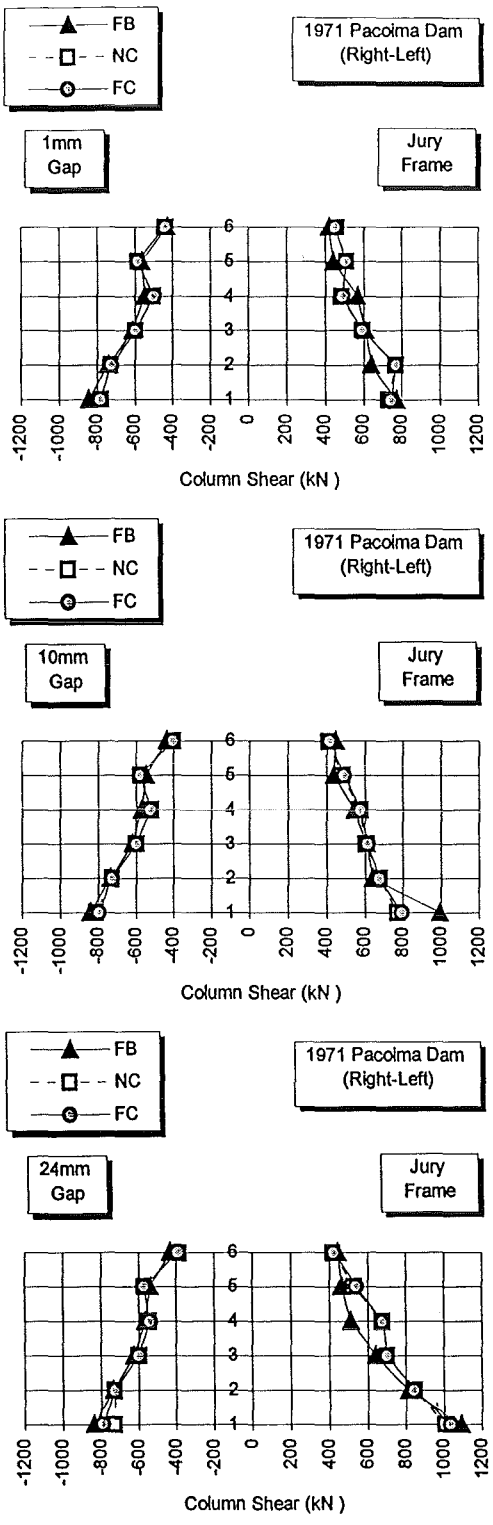

Fig. E.4: Effect of foundation fixity conditions on impact-side column shear of six-storey Jury frame (Configuration 2) for various initial separation gaps. 1971 Pacoima Dam earthquake applied right-left.

FB = Fixed Base
NC = Non-Coupled (i.e. only soil-structure interaction considered)
FC = Foundations Coupled

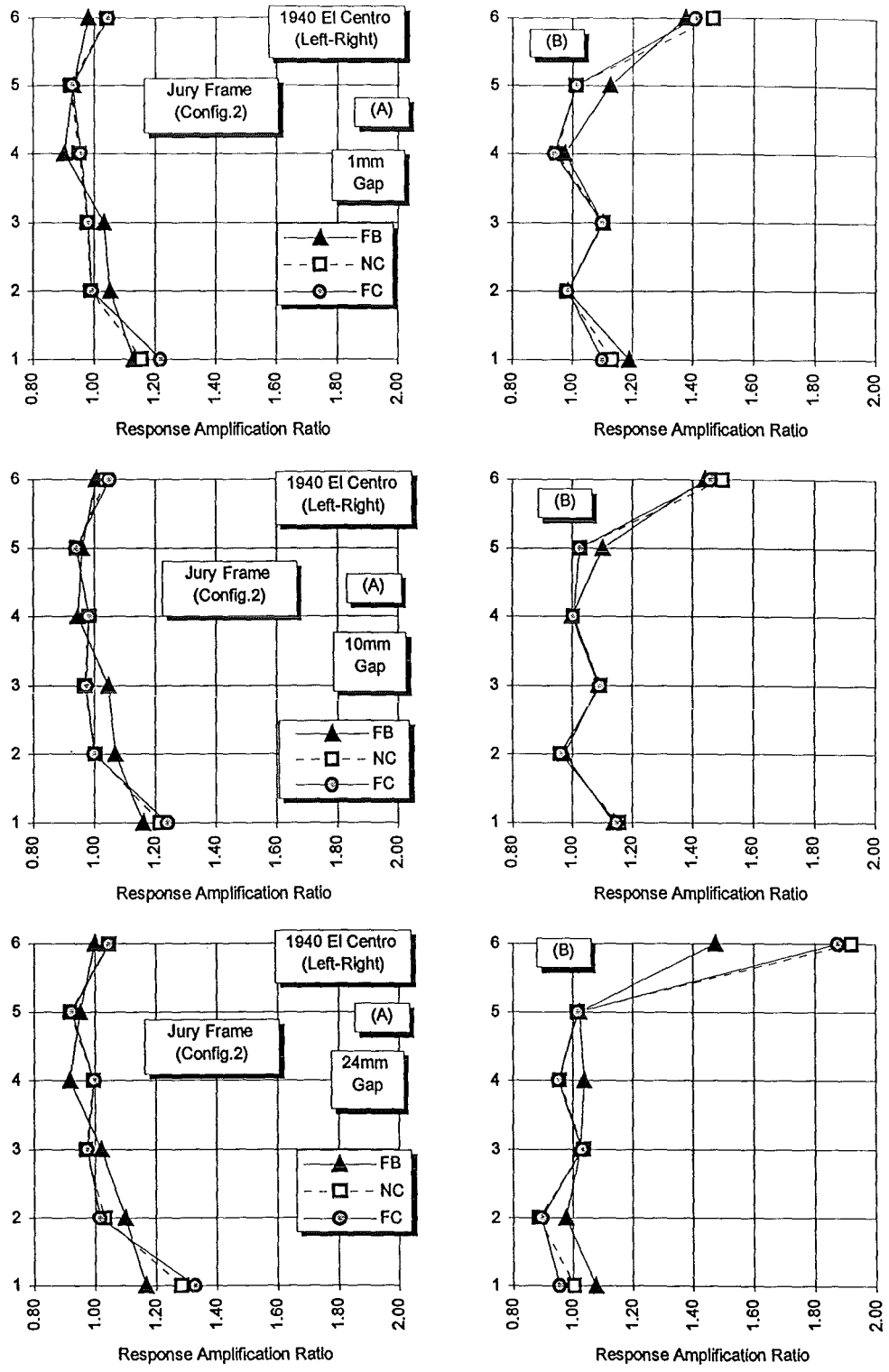

Fig. E.5: Response amplification ratio (from fixed base no pounding case) of impact-side column shear of six-storey Jury frame (Configuration 2) for various initial separation gaps and foundation conditions. 1940 El Centro earthquake applied left-right.

A = Positive Shear B = Negative Shear
FB = Fixed Base
NC = Non-Coupled (i.e. only soil-structure interaction considered)
FC = Foundations Coupled

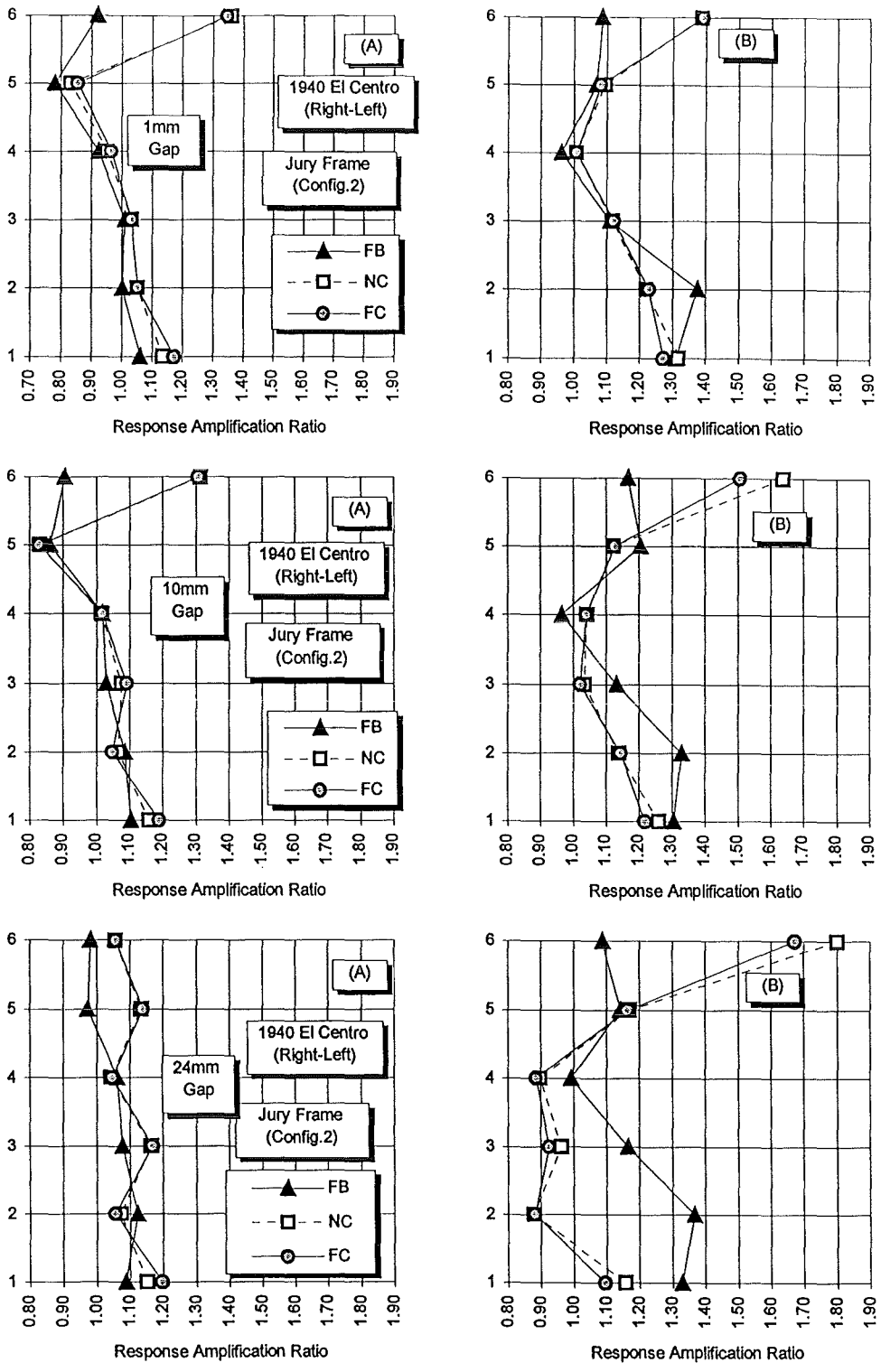

Fig. E.6: Response amplification ratio (from fixed base no pounding case) of impact-side column shear of six-storey Jury frame (Configuration 2) for various initial separation gaps and foundation conditions. 1940 El Centro earthquake applied right-left.

A = Positive Shear B = Negative Shear
FB = Fixed Base
NC = Non-Coupled (i.e. only soil-structure interaction considered)
FC = Foundations Coupled

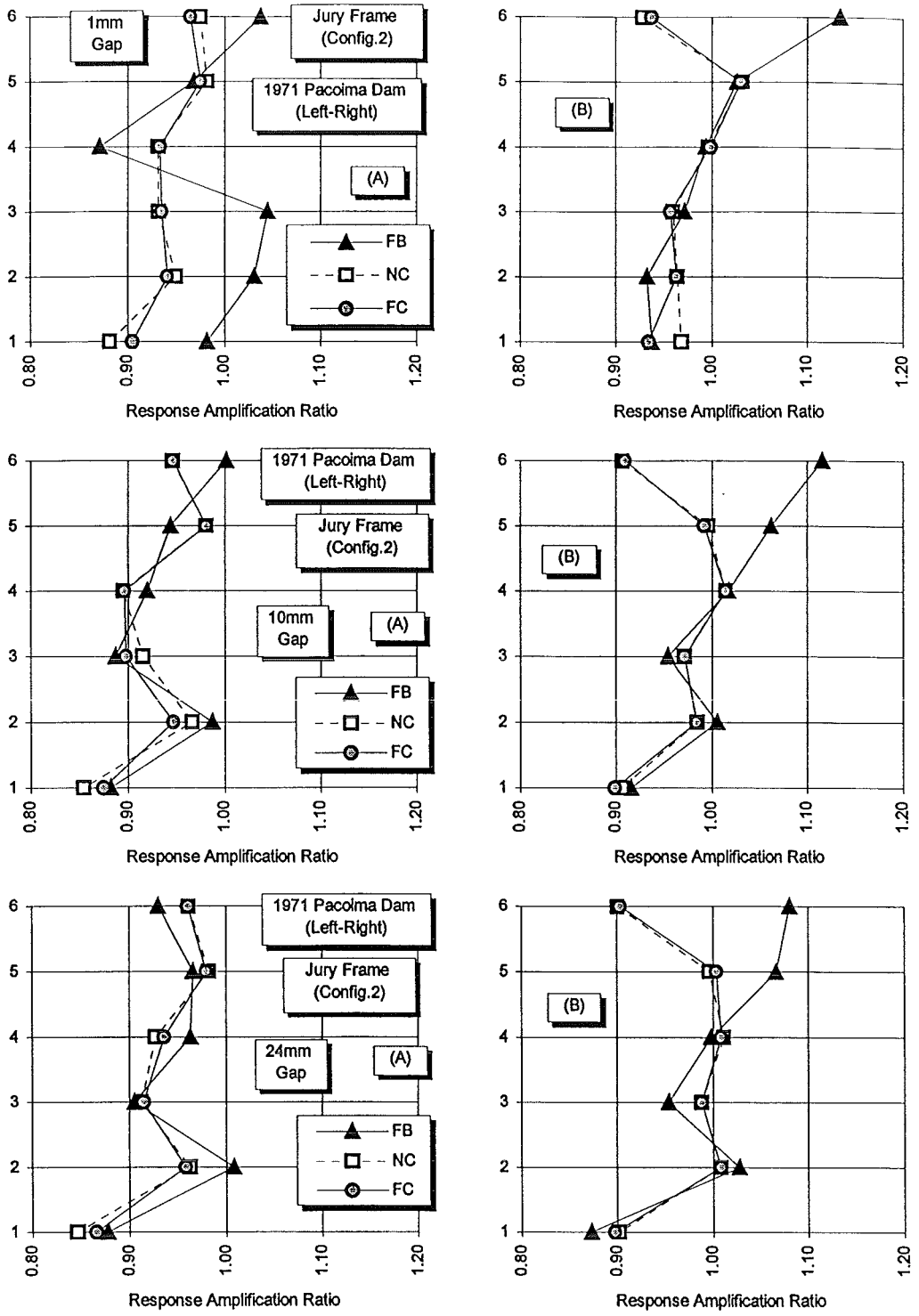

Fig. E.7: Response amplification ratio (from fixed base no pounding case) of impact-side column shear of six-storey Jury frame (Configuration 2) for various initial separation gaps and foundation conditions. 1971 Pacoima Dam earthquake applied left-right.

A = Positive Shear B = Negative Shear
FB = Fixed Base
NC = Non-Coupled (i.e. only soil-structure interaction considered)
FC = Foundations Coupled

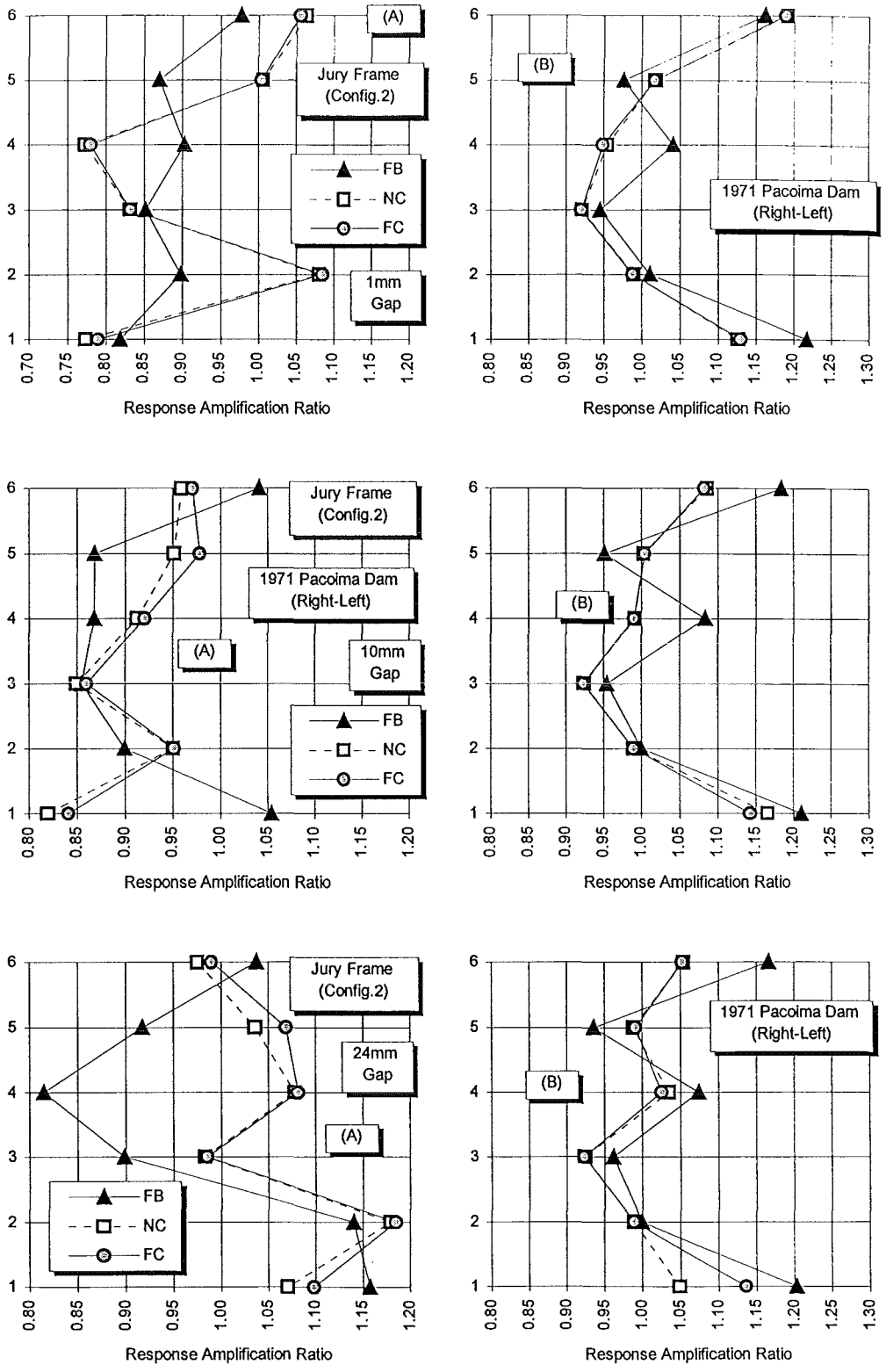

Fig. E.8: Response amplification ratio (from fixed base no pounding case) of impact-side column shear of six-storey Jury frame (Configuration 2) for various initial separation gaps and foundation conditions. 1971 Pacoima Dam earthquake applied right-left.

A = Positive Shear B = Negative Shear
FB = Fixed Base
NC = Non-Coupled (i.e. only soil-structure interaction considered)
FC = Foundations Coupled

APPENDIX F

NUMERICAL MODELS

Rahman Frame (Interior Frame)

COLUMNS

		Geometric Properties					Initial Fixed-End Forces				
No.	Level	Dims.	END1	END2	H1	H2	M1	M2	V1	V2	Axial
1	1	0.65x0.75 (ext.)	0.0	0.2	0.375	0.375	0.0	0.0	0.0	0.0	-585.56
2	2	0.65x0.75 (ext.)	0.2	0.2	Elastic	Elastic	0.0	0.0	0.0	0.0	-585.56
3	3-5	0.65x0.75 (ext.)	0.2	0.2	Elastic	Elastic	0.0	0.0	0.0	0.0	-585.56
4	6-9	0.6x0.7 (ext.)	0.2	0.2	Elastic	Elastic	0.0	0.0	0.0	0.0	-535.96
5	10-11	0.5x0.7 (ext.)	0.2	0.2	Elastic	Elastic	0.0	0.0	0.0	0.0	-472.56
6	12	0.5x0.7 (ext.)	0.2	0.2	Elastic	Elastic	0.0	0.0	0.0	0.0	-412.00
7	1	0.4x0.4 (int.)	0.0	0.2	0.2	0.2	0.0	0.0	0.0	0.0	-560.08
8	2-6 10-11	0.4x0.4 (int.)	0.2	0.2	Elastic	Elastic	0.0	0.0	0.0	0.0	-560.08
9	7-9	0.4x0.4 (int.)	0.2	0.2	Elastic	Elastic	0.0	0.0	0.0	0.0	-560.08
10	12	0.4x0.4 (int.)	0.2	0.2	Elastic	Elastic	0.0	0.0	0.0	0.0	-532.00
BEAMS											
11	1	0.4x0.4	0.375	0.2	0.2	0.2	-216.4	-216.4	-196.8	196.8	0.0
12	1	0.4x0.4	0.2	0.375	0.2	0.2	-216.4	-216.4	-196.8	196.8	0.0
13	2-4	0.4x.04	0.375	0.2	0.2	0.2	-216.4	-216.4	-196.8	196.8	0.0
14	2-4	0.4x0.4	0.2	0.375	0.2	0.2	-216.4	-216.4	-196.8	196.8	0.0
15	5	0.4x0.4	0.375	0.2	0.2	0.2	-216.4	-216.4	-196.8	196.8	0.0
16	5	0.4x0.4	0.2	0.375	0.2	0.2	-216.4	-216.4	-196.8	196.8	0.0
17	6-9	0.4x0.4	0.35	0.2	0.2	0.2	-219.4	-219.4	-198.5	-198.5	0.0
18	6-9	0.4x0.4	0.2	0.35	0.2	0.2	-219.4	-219.4	-198.5	-198.5	0.0
19	10-12	0.4x0.4	0.2	0.35	0.2	0.2	-219.4	-219.4	-198.5	-198.5	0.0
20	10-12	0.4x0.4	0.35	0.2	0.2	0.2	-219.4	-219.4	-198.5	-198.5	0.0

Notes:
(1) Square bays 6.00 x 6.00 m. , 6 bays (2 external and 4 internal).
(2) Storey height = 3.65m.
(3) kN.m.sec units.
(4) Modulus of elasticity of concrete $E = 30 \times 10^6$ kN/m^2.
(5) Shear modulus of concrete $G = 12.5 \times 10^6$ kN/m^2.
(6) Slab length of 0.35m added to each side of beams in calculation of geometric properties.

Rahman Frame (Exterior Frame)

COLUMNS

		Geometric Properties					Initial Fixed-End Forces				
No.	Level	Dims.	END1	END2	H1	H2	M1	M2	V1	V2	Axial
21	1	0.65x0.75 (ext.)	0.0	0.35	0.375	0.375	0.0	0.0	0.0	0.0	-189.10
22	2-5	0.65x0.75 (ext.)	0.35	0.35	Elastic	Elastic	0.0	0.0	0.0	0.0	-189.10
23	6	0.6x0.7 (ext.)	0.35	0.3	Elastic	Elastic	0.0	0.0	0.0	0.0	-170.78
24	7-9	0.6x0.7 (ext.)	0.3	0.3	Elastic	Elastic	0.0	0.0	0.0	0.0	-170.78
25	10	0.5x0.7 (ext.)	0.3	0.225	Elastic	Elastic	0.0	0.0	0.0	0.0	-148.80
26	11	0.5x0.7 (ext.)	0.225	0.225	Elastic	Elastic	0.0	0.0	0.0	0.0	-148.80
27	12	0.5x0.7 (ext.)	0.225	0.225	Elastic	Elastic	0.0	0.0	0.0	0.0	-118.14
28	1	0.65x0.75 (int.)	0.0	0.35	0.375	0.375	0.0	0.0	0.0	0.0	-211.42
29	2-5	0.65x0.75 (int.)	0.35	0.35	Elastic	Elastic	0.0	0.0	0.0	0.0	-211.42
30	6	0.6x0.7 (int.)	0.35	0.3	Elastic	Elastic	0.0	0.0	0.0	0.0	-199.58
31	7-9	0.6x0.7 (int.)	0.3	0.3	Elastic	Elastic	0.0	0.0	0.0	0.0	-199.58
32	10	0.5x0.7 (int.)	0.3	0.225	Elastic	Elastic	0.0	0.0	0.0	0.0	-187.32
33	11	0.5x0.7 (int.)	0.225	0.225	Elastic	Elastic	0.0	0.0	0.0	0.0	-187.32
34	12	0.5x0.7 (int.)	0.225	0.225	Elastic	Elastic	0.0	0.0	0.0	0.0	-156.66

BEAMS

35	1	0.45x0.7	0.375	0.375	0.35	0.35	-83.14	-83.14	-85.02	85.02	0.0
36	2	0.45x0.7	0.375	0.375	0.35	0.35	-83.14	-83.14	-85.02	85.02	0.0
37	3-5	0.45x0.7	0.375	0.375	0.35	0.35	-83.14	-83.14	-85.02	85.02	0.0
38	6	0.45x0.6	0.35	0.35	0.3	0.3	-79.24	-79.24	-79.72	79.72	0.0
39	7-9	0.45x0.6	0.35	0.35	0.3	0.3	-79.24	-79.24	-79.72	79.72	0.0
40	10-12	0.45x0.45	0.35	0.35	0.225	0.225	-71.64	-71.64	-71.14	71.14	0.0

Notes:

(1) Square bays 6.00 x 6.00 m., 6 bays (2 external and 4 internal).
(2) Storey height = 3.65m.
(3) kN.m.sec units.
(4) Modulus of elasticity of concrete E = 30×10^6 kN/m^2.
(5) Shear modulus of concrete G = 12.5×10^6 kN/m^2.
(6) Slab length of 0.25m added to beam (in direction of span) in calculation of geometric properties.

BEAM-COLUMN Yield Surface of Interior Rahman Frame Elements

Element No.	Storey	PYC (kN)	PB (kN)	MB (kN.m)	M1B (kN.m)	M2B (kN.m)	MO (kN.m)	PYT (kN)
1	1	-49 000	-21 892	-5 980	0.0	0.0	2 344	7 024
7	1	-16 519	-6 576	1 072	0.0	0.0	458	2 764
11	1	0.0	0.0	312	-612	224	-612	0.0
12	1	0.0	0.0	224	-612	312	-612	0.0
13	2-4	0.0	0.0	232	-612	292	-612	0.0
14	2-4	0.0	0.0	292	-612	232	-612	0.0
15	5	0.0	0.0	312	-612	224	-612	0.0
16	5	0.0	0.0	224	-612	312	-612	0.0
17	6-9	0.0	0.0	312	-612	224	-612	0.0
18	6-9	0.0	0.0	224	-616	312	-616	0.0
19	10-12	0.0	0.0	164	-560	164	-560	0.0
20	10-12	0.0	0.0	164	-560	164	-560	0.0

BEAM-COLUMN Yield Surface of Exterior Rahman Frame Elements

Element No.	Storey	PYC (kN)	PB (kN)	MB (kN.m)	M1B (kN.m)	M2B (kN.m)	MO (kN.m)	PYT (kN)
21	1	-25 270	-11 130	3 036	0.0	0.0	1 355	4 324
28	1	-24 500	-10 946	2 990	0.0	0.0	1 172	3 512
35	1	0.0	0.0	156.8	-348.0	156.8	-348.0	0.0
36	2	0.0	0.0	316.0	-542.0	316.0	-542.0	0.0
37	3-5	0.0	0.0	986.0	-896.8	986.0	-896.8	0.0
38	6	0.0	0.0	674.0	-664.0	674.0	-664.0	0.0
39	7-9	0.0	0.0	624.0	-606.0	624.0	-606.0	0.0
40	10-12	0.0	0.0	212.0	-313.2	212.0	-313.2	0.0

Nodal Weights of Rahman Frame (kN)

Level	Exterior	Interior
Interior Frame		
1	761.09	957.97
2	761.09	957.97
3	761.09	957.97
4	761.09	957.97
5	761.09	957.97
6	716.93	952.8
7	716.93	952.8
8	716.93	952.8
9	716.93	952.8
10	660.77	959.92
11	660.77	959.92
12	601.97	932.4
Exterior Frame		
1	271.12	385.54
2	271.12	385.54
3	271.12	385.54
4	271.12	385.54
5	271.12	385.54
6	249.1	363.68
7	249.1	363.68
8	249.1	363.68
9	249.1	363.68
10	206.4	336.36
11	206.4	336.36
12	177	306.96

Nodal Weights of Rahman Frame Foundation (kN)

	X-dir.	Y-dir.	Rotational
Interior Frame			
Ext. Node	1104	1104	381.76
Int. Node	1380	1380	381.76
Exterior Frame			
Ext. Node	450	450	190.88
Int. Node	552	552	190.88

Tabuchi Frame (Interior Frame)

COLUMNS

Geometric Properties							BEAM-COLUMN Yield Surface						
Element No.	Level	Total Area	END1	END2	H1	H2	PYC (kN)	PB (kN)	MB (kN.m)	M1B (kN.m)	M2B (kN.m)	MO (kN.m)	PYT (kN)
77	1	2.45	0.4	0.4	0.49	0.49	-73 445	-61 000	3 600	7 065	7 445	3 600	11 660
78-80	2-4	2.45	0.4	0.4	Elastic	Elastic							
81	5	2.113	0.4	0.375	Elastic	Elastic							
82-84	6-8	2.113	0.375	0.375	Elastic	Elastic							
85	9	1.8	0.375	0.35	Elastic	Elastic							
86-88	10-12	1.8	0.35	0.35	Elastic	Elastic							
89	1	2.45	0.4	0.4	0.49	0.49	-73 445	-61 000	3 600	7 065	7 445	3 600	11 660
90-92	2-4	2.45	0.4	0.4	Elastic	Elastic							
93	5	2.113	0.4	0.375	Elastic	Elastic							
94-96	6-8	2.113	0.375	0.375	Elastic	Elastic							
97	9	1.8	0.375	0.35	Elastic	Elastic							
98-100	10-12	1.8	0.35	0.35	Elastic	Elastic							

Tabuchi Frame notes:

(1) Modulus of elasticity = 25×10^6 kN/m^2.
(2) Shear modulus = 10.4×10^6 kN/m^2.
(3) Storey height = 3.65 m.
(4) Modified Takeda hysteresis rule (unloading and reloading stiffnesses equal to zero with reloading stiffness power factor equal to zero and unloading as in *DRAIN-2D)*.
(5) Damage indices computed (positive and negative ductilities equal to 30.0).
(6) All bays 8.00 x 8.00 m.

BEAMS (Interior Tabuchi Frame)

Geometric Properties							Initial Fixed-End Forces					
Element No.	Level	Total Area	END1	END2	H1	H2	M1	M2	V1	V2	Axial	AXPS
101	1	1.4	0.35	0.35	0.56	0.56	-965.0	-965.0	-585.0	585.0	0.0	0.0
102-103	2-3	1.4	0.35	0.35	0.56	0.56	-965.0	-965.0	-585.0	585.0	0.0	0.0
104	4	1.4	0.35	0.35	0.56	0.56	-965.0	-965.0	-585.0	585.0	0.0	0.0
105	5	1.313	0.325	0.325	0.525	0.525	-954.0	-954.0	-577.0	577.0	0.0	0.0
106	6	1.313	0.325	0.325	0.525	0.525	-954.0	-954.0	-577.0	577.0	0.0	0.0
107-108	7-8	1.313	0.325	0.325	0.525	0.525	-954.0	-954.0	-577.0	577.0	0.0	0.0
109-112	9-12	1.225	0.3	0.3	0.49	0.49	-943.0	-943.0	-568.5	568.5	0.0	0.0

BEAM Yield Conditions (Interior Tabuchi Frame)

Element No.	Level	PYT (kN)	PYC (kN)	MY1+ (kN.m)	MY1- (kN.m)	MY2+ (kN.m)	M21- (kN.m)
101	1	0.0	0.0	1 315	-2 195	1 315	-2 195
102-103	2-3	0.0	0.0	1 605	-2 465	1 605	-2 465
104	4	0.0	0.0	1 315	-2 465	1 315	-2 465
105	5	0.0	0.0	1 220	-2 285	1 220	-2 258
106	6	0.0	0.0	1 220	-2 035	1 220	-2 035
107-108	7-8	0.0	0.0	1 155	-1 785	1 155	-1 785
109-112	9-12	0.0	0.0	930	-1 450	930	-1 450

Tabuchi Frame (Exterior Frame)

COLUMNS

Geometric Properties							BEAM-COLUMN Yield Surface						
Element No.	Level	Total Area	END1	END2	H1	H2	PYC (kN)	PB (kN)	MB (kN.m)	M1B (kN.m)	M2B (kN.m)	MO (kN.m)	PYT (kN)
41-44	1-4	0.98	0.4	0.4	0.49	0.49	-29 378	-24 400	1 440	2 826	2 978	1 440	4 664
45	5	0.845	0.4	0.375	0.455	0.455	-25 936	-21 000	1 318	2 372	2 512	1 318	4 664
							-24 596	-21 200	932	2 102	2 222	932	3 240
46-48	6-8	0.845	0.375	0.375	0.455	0.455	-24 596	-21 200	932	2 102	2 222	932	3 240
49	9	0.72	0.375	0.35	0.42	0.42	-21 408	-18 200	848	1 720	1 824	848	3 240
50-52	10-12	0.72	0.35	0.35	0.42	0.42	-21 408	-18 200	848	1 720	1 824	848	3 240
53-56	1-4	0.98	0.4	0.4	0.49	0.49	-29 378	-24 400	1 440	2 826	2 978	1 440	4 664
57	5	0.845	0.4	0.375	0.455	0.455	-25 936	-21 000	1 318	2 372	2 512	1 318	4 664
							-24 596	-21 200	932	2 102	2 222	932	3 240
58-60	6-8	0.845	0.375	0.375	0.455	0.455	-24 596	-21 200	932	2 102	2 222	932	3 240
61	9	0.72	0.375	0.35	0.42	0.42	-21 408	-18 200	848	1 720	1 824	848	3 240
							-22 748	-17 600	1 196	1 974	2 080	1 196	4 664
62-64	10-12	0.72	0.35	0.35	0.42	0.42	-22 748	-17 600	1 196	1 974	2 080	1 196	4 664

Tabuchi Frame Geometric Properties (Contd.)

Element No.	Shear area (m^2)	Moment of inertia (m^4)
41-44	0.49	2.4E-2
45-48	0.423	1.78E-2
49-52	0.36	1.30E-2
53-56	0.49	3.2E-2
57-60	0.423	2.38E-2
61-64	0.36	1.73E-2
65-68	0.28	1.36E-2
69-72	0.263	1.13E-2
73-76	0.245	9.24E-3
77-80	1.225	6.01E-2
81-84	1.056	4.46E-2
85-88	0.9	3.24E-2
89-92	0.225	8.01E-2
93-96	1.056	5.95E-2
97-100	0.9	4.32E-2
101-104	0.7	4.0E-2
105-108	0.656	3.32E-2
109-112	0.613	2.7E-2

BEAMS (Exterior Tabuchi Frame)

Geometric Properties							Initial Fixed-End Forces					
Element No.	Level	Total Area	END1	END2	H1	H2	M1	M2	V1	V2	Axial	AXPS
65-68	1-4	0.56	0.35	0.35	0.56	0.56	-244.4	-244.4	-155.0	155.0	0.0	0.0
69-70	5-6	0.525	0.325	0.325	0.525	0.525	-240	-240	-151.6	151.6	0.0	0.0
71	7	0.525	0.325	0.325	0.525	0.525	-240	-240	-151.6	151.6	0.0	0.0
72	8	0.525	0.325	0.325	0.525	0.525	-240	-240	-151.6	151.6	0.0	0.0
73-76	9-12	0.49	0.3	0.3	0.49	0.49	-237.8	-237.8	-148.4	-148.4	0.0	0.0

BEAM Yield Conditions (Exterior Tabuchi Frame)

Element No.	Level	PYT (kN)	PYC (kN)	MY1+ (kN.m)	MY1- (kN.m)	MY2+ (kN.m)	M21- (kN.m)
65-68	1	0.0	0.0	526.0	-642.0	526.0	-642.0
69-70	5-6	0.0	0.0	488.0	-714.0	488.0	-714.0
71	7	0.0	0.0	462.0	-546.0	462.0	-546.0
72	8	0.0	0.0	462.0	-462.0	462.0	-462.0
73-76	9-12	0.0	0.0	372.0	-454.0	372.0	-454.0

Nodal Weights of Tabuchi Frame (kN)

Level	Exterior	Interior
Interior Frame		
1	1018	2036.5
2	1018	2036.5
3	1018	2036.5
4	1018	2036.5
5	990	1980
6	990	1980
7	990	1980
8	990	1980
9	963.5	1927
10	963.5	1927
11	963.5	1927
12	890.5	1781
Exterior Frame		
1	354.6	709.2
2	354.6	709.2
3	354.6	709.2
4	354.6	709.2
5	344.8	689.6
6	344.8	689.6
7	344.8	689.6
8	344.8	689.6
9	335.6	671.2
10	335.6	671.2
11	335.6	671.2
12	310.2	620.2

Nodal Weights of Tabuchi Frame Foundation (kN)

	X-dir.	Y-dir.	Rotational
Interior Frame			
Exterior	2224.4	2224.4	1671.81
Interior	3055	3055	1671.81
Exterior Frame			
Exterior	528	528	190.88
Interior	698	698	190.88

Nodal Loads of Tabuchi Frame (kN)

Level	Exterior	Interior
Interior Frame		
1	-558.5	-1117
2	-558.5	-1117
3	-558.5	-1117
4	-558.5	-1117
5	-535	-1070
6	-535	-1070
7	-535	-1070
8	-535	-1070
9	-513.5	-1027.5
10	-513.5	-1027.5
11	-513.5	-1027.5
12	-431.5	-863.5
Exterior Frame		
1	-73.8	-147.4
2	-73.8	-147.4
3	-73.8	-147.4
4	-73.8	-147.4
5	-70.8	-141.6
6	-70.8	-141.6
7	-70.8	-141.6
8	-70.8	-141.6
9	-68	-136
10	-68	-136
11	-68	-136
12	-51.6	-103.2

Jury Frame

Member	Levels	Area (m^2)	Shear Area (m^2)	Moment of Inertia (m^4)	Plastic Hinge Length (m)
Beams	1-3	0.1704	0.1050	0.005984	0.3
	4-6	0.1617	0.0963	0.004635	0.28
External Columns	1-3	0.1688	0.1688	0.003516	0.25
	4-6	0.1519	0.1519	0.002563	0.23
Internal Columns	1-3	0.2269	0.2269	0.005719	0.28
	4-6	0.1875	0.1875	0.003906	0.25

Notes:
(a) Modulus of elasticity E = 25×10^6 kN/m^2.
(b) Shear modulus G = 10.4×10^6 kN/m^2.
(c) Bay width = 5.5m with 6 identical bays.
(d) Storey height = 3.65 m.
(e) Column hysteresis is bi-linear elastic (bi-linear factor r = 0.2%)

BEAM-COLUMN Yield Surface of Jury Frame Elements

Level	PYC (kN)	PB (kN)	MB (kN.m)	M1B (kN.m)	M2B (kN.m)	MO (kN.m)	PYT (kN)
Exterior							
1-3	-6290	-3690	435	519	423	197	934
4	-5664	-3353	352	420	342	160	841
	-5747	-3233	352	420	342	176	925
5-6	-5664	-3353	352	420	342	160	841
Interior							
1-3	0.0	0.0	316.0	-542.0	316.0	-542.0	0.0
4	-6992	-4139	484	577	470	219	1038
	-7200	-3900	484	577	470	274	1246
5-6	-6992	-4139	484	577	470	219	1038

Left-Bay Beam Yield Moments of Jury Frame (kN.m)

Level	Left End (Positive)	Left End (Negative)	Right End (Positive)	Right End (Negative)
1-3	262	-262	232	-232
4	173	-184	155	-155
5	115	-131	119	-115
6	115	-115	115	-115

Beam Initial Fixed-End Moments (kN.m) and Shears (kN) of Jury Frame

Level	Moment (Right End)	Moment (Left End)	Shear (Right End)	Shear (Left End)
1-3	-41.25	40.04	-48.33	48.33
4-6	-41.68	40.05	-47.33	47.33

Nodal Loads and Masses in Jury Frame (kN)

	Weight		Loads	
Level	External	Internal	External	Internal
1	134	219	-85.34	-122.5
2	134	219	-85.34	-122.5
3	133	217	-83.34	-118.5
4	129	211	-81.33	-116.5
5	129	211	-81.33	-116.5
6	120	200	-63.33	-94.5

Appendix G

VERIFICATION OF THROUGH-SOIL INTERACTION MODEL

G.1 Summary

A test case was investigated to confirm the validity of the Vlazov-Leontiev [V5] two-parameter model utilized in the GROUND element of RUAUMOKO [C1]. The case that was considered was of a reinforced concrete beam resting on the surface of a deep soil layer subjected to a point load. The length of the beam was chosen such that the vertical deflections at the end of the beam obtained from the numerical solution were negligible (15.00 metres). The properties of the beam and underlying soil are presented in Table G.1. The vertical deformation of the beam at various distances from the point load was obtained numerically and compared with the analytical solution of the lateral deflection of an infinite beam at a point directly beneath the point of load application. The deflection profile of the beam (Figure G.2) demonstrates the ability of the proposed model to transmit shear.

	Dimensions (m)	Modulus of Elasticity (kN/m^2)	Poisson's ratio ν
Beam Properties	Width = 0.50 Height = 1.00	$E = 25 \times 10^{6}$ [1]	ν = 0.2
Soil Properties		$E_o = 30.0 \times 10^{3}$ [1]	$\nu_o = 1/3$

Table G.1: Assumptions incorporated in case study verifying the validity of the numerical model.

NOTES: [1] The shear modulus (G) is calculated from: $G = \frac{E}{2(1+\nu)}$ (kN/m^2).

G.2 Numerical Model

Figure G.1 is a schematic representation of the discretization scheme of the soil surface. Since the case study is symmetric in geometry and loading, the rotation of Nodes 1 and 32 (under the point load and at the end of the specimen) are constrained. Two elements, each one representing the beam and supporting soil, connect consecutive nodal points. These elements are the FRAME and GROUND elements, respectively, of the two-dimensional structural analysis program RUAUMOKO [C1]. The beam is assumed to respond elastically while the coefficients of the two-parameter soil model (GROUND element) are defined through an exponential variation of normal deformations with depth, as expounded by Vlazov and Leontiev [V5]. These coefficients, k and k_1 defined in Equations G.2 and G.5, respectively, are utilized in the cubic shape function of

the finite element model and represent the vertical and shear stiffness coefficients, respectively. The vertical deflections of the 15 metre long concrete beam (width = 0.50 metres) subjected to a point load (P = 1 000 kN) at mid-span are determined and plotted in Figure G.2.

Nodal Point [1]	1	2	3	4	5	6	7	8	9-17	18-32
Distance from Load (m)	0.00	0.001	0.005	0.010	0.015	0.02	0.025	0.050	Equally spaced 0.10 - 0.90	Equally spaced 1.00 – 15.00

Figure G.1: Schematic of numerical model implemented in RUAUMOKO [C1].
Notes: [1] All nodes are unconstrained in translation (vertical and horizontal) and in rotation. The exception to this is Node 1 in which the rotation is constrained as this is a symmetric loading case.

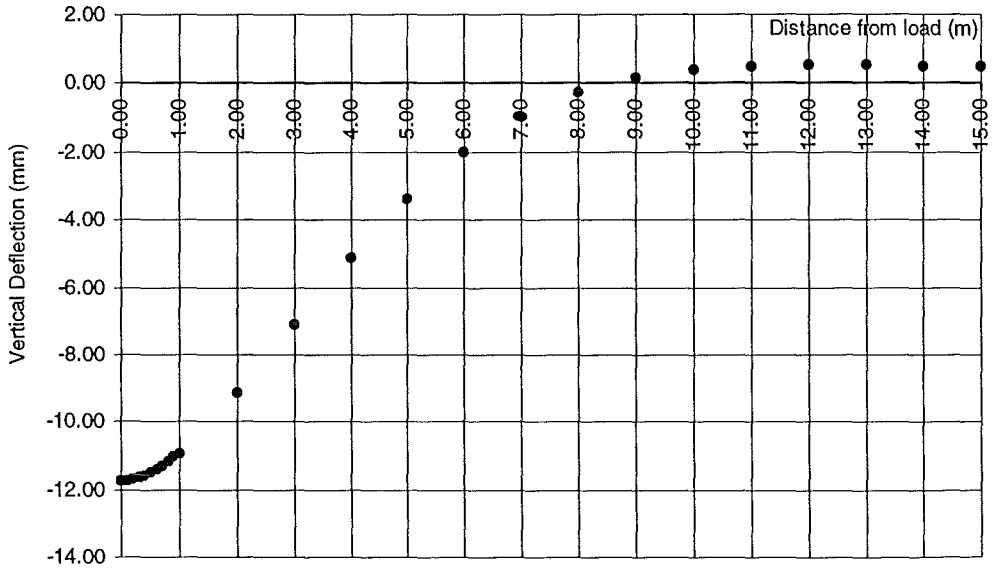

Fig. G.2: Variation of vertical displacement of the surface of a deep soil layer with distance from point of load application.

G.3 Analytical Method

The analytical expression defining the maximum deflection (ω_m) of an elastic beam of infinite length loaded by a vertical point load is given by the following expression [S3]:

$$\omega_m = \frac{P\lambda^2}{2k\alpha} \qquad \text{(G.1)}$$

This deflection occurs directly under the point of application of the load. The parameters of this equation are defined as follows [S3]:

$k = \frac{E_o}{(1-\nu_o^2)}\frac{\mu B}{2}$ = Vertical stiffness coefficient of two-parameter model. (G.2)

P = Point load (kN) = 2 000 kN.

$\lambda = \sqrt[4]{\frac{k}{4EI}}$ = *1/L* where *L* is the characteristic length. (G.3)

$$\alpha = \sqrt{\lambda^2 + \frac{k_1}{4EI}} \qquad \text{(G.4)}$$

$k_1 = \frac{E_o}{(1+\nu_o)}\frac{B}{4\mu}$ = Shear interaction coefficient of two-parameter model (G.5)

As outlined in Chapter 4, the quantity μB appearing in Equation G.2 may be taken equal to *1.06*. The value of the point load *P* is twice the value implemented in the numerical model as the latter represents a symmetric loading case. Substituting the properties assumed in this case study for the beam and soil (Table G.1) into Equations G.2 – G.5 the deflection is found to be:

$\omega_m \cong$ **14mm**

This compares with the value of approximately 12mm obtained from the numerical model. The difference in the result is expected due to the cubic shape function employed in the numerical model to represent the force-deformation response of the soil mass.

Further tests were conducted of beams of various dimensions and the numerical results showed similar levels of convergence with those obtained from the analytical expression (Eq. G.1). These tests are detailed in Table G.2 below.

Beam Dimensions (m)		Numerically Obtained Displacement (mm)	Analytically Obtained Displacement (mm)
Width	Height		
1.0	2.00	5.6	7
0.8	1.5	7.7	9
0.5	1.0	12	14

Table G.2: Comparison of numerical and analytical results for various beam dimensions.